Pipe Conveying Fluid:

a Paradigm of Nonlinear Dynamics

by

Christian Semler

Department of Mechanical Engineering
McGill University
Montréal, Québec, Canada.

April 1996

A Thesis submitted to the Faculty of Graduate Studies and Research
in partial fulfillment of the requirements for the degree of
Doctor of Philosophy.

An meine Oma, die mich lesen gelernt hat,
A mes parents, qui m'ont donné la chance d'étudier,
A France, présente à chaque étape,
Et à mon petit prince, Audran.

Philosopher, c'est penser sa vie, et vivre sa pensée.

André Comte-Sponville

ABSTRACT

This thesis deals with the nonlinear dynamics of a flexible pipe conveying fluid. It consists of a series of seven articles, published or submitted for publication, describing the dynamical behaviour of this generally nonconservative system. It is endeavoured to show that the system of a pipe conveying fluid has become a new paradigm of *nonlinear* dynamics.

In particular, the nonlinear behaviour of (i) a pipe with a spring support, (ii) a pipe impacting on physical constraints, (iii) a pipe fitted with a small end-mass at the free end, and (iv) a pipe conveying unsteady sinusoidal flow is examined.

The equations of motion are obtained by energy and Newtonian methods. Different derivations are made for cantilevered pipes, where the centreline is assumed inextensible, and for pipes with both ends fixed. The resulting equations are compared with those already in existence and the infinite dimensional model discretized by Galerkin's technique.

An in-depth numerical investigation is undertaken. Fourth and eighth-order Runge-Kutta methods and AUTO are used on the set of first-order differential equations, while the Houbolt finite difference scheme and the incremental harmonic balance method are developed to integrate numerically the set of second-order implicit nonlinear differential equations. Using phase portraits, power spectral densities and bifurcation diagrams, the response of the pipe subjected to various conditions is described from a geometrical point of view. Quantitatively, Poincaré and Lorenz maps, Floquet multipliers and Lyapunov exponents are used to explain, confirm and validate the changes of the dynamical behaviour and the emergence of chaotic dynamics.

Furthermore, to simplify the analysis, the tools of modern dynamics theory are exploited. In particular, centre manifold, normal form and codimension-one and -two bifurcation theories are used extensively; pitchfork, Hopf and double degeneracy bifurcations are analyzed, local and global behaviour are examined in detail, as well as the effects of various parameters and of the nonlinear terms.

In most cases, experiments conducted with elastomer pipes conveying water corroborate the theoretically predicted behaviour.

SOMMAIRE

Cette thèse traite de la dynamique non linéaire d'un tube flexible parcouru par un fluide. Elle consiste en une série de sept articles publiés ou soumis pour publication et décrivant le comportement dynamique de ce système généralement nonconservatif. Le but de la thèse est de montrer que le tube parcouru par un fluide est devenu un nouveau paradigme de la dynamique non linéaire.

En particulier, plusieures configurations différentes et le comportement non linéaire sont étudiés: (i) un tube supporté par un ressort, (ii) un tube heurtant des contraintes physiques, (iii) un tube auquel une petite masse est ajoutée au bout, et (iv) un tube soumis à un écoulement sinusoidal non constant.

Les équations du mouvement sont obtenus par des considérations énergétiques et par la méthode de Newton. La dérivation est différente dans le cas du tube encastré-libre, que l'on suppose inextensible, et du tube fixe aux deux extrémités. Ces équations sont ensuite comparées avec celles déjà connues, et le modèle de dimension infinie est discrétisé par la méthode de Galerkin.

Une étude numérique en profondeur est ensuite entreprise. Les méthodes de Runge-Kutta d'ordre quatre et huit ainsi que AUTO sont utilisés pour résoudre le système d'équations différentielles d'ordre un, tandis que le schémas par différences finies de Houbolt et la méthode des harmoniques par incrémentation sont développés pour intégrer numériquement le système de second ordre d'équations différentielles non linéaires implicites. En utilisant des diagrammes de phase, des analyses spectrales et des diagrammes de bifurcation, la réponse du tube soumis à diverses conditions est décrite d'un point de vue géometrique. Quantitativement, les cartes de Poincaré et de

Lorenz et les exposants de Floquet et de Lyapunov sont utilisés dans le but d'expliquer, de confirmer et de valider les variations du comportement dynamique, et l'émergence du chaos.

De plus, pour simplifier l'analyse, les principes de la théorie de la dynamique non linéaire moderne sont exploités. En particulier, les théories des variétés centrales, des formes normales et de bifurcation de codimension une et deux ont été utilisées de manière extensive. Ainsi, les bifurcations d'ordre un, de Hopf, et de double dégénérescence, le comportement local et global, les effets de nombreux paramètres et des termes non linéaires ont été examinés en détail.

Dans la plupart des cas, les expériences conduites avec des tubes en élastomère parcourus par de l'eau et construits en laboratoire confirment les prédictions théoriques.

ACKNOWLEDGEMENTS

The author wishes to thank Professor M.P. Païdoussis for his guidance and advice he offered throughout the course of this work. He would like to thank him also for providing him with an exceptional work environment as well as for giving him the opportunity to attend numerous conferences and to teach several courses.

The helpful suggestions and constructive discussions with fellow colleagues in the fluid-structure interaction group were invaluable to this research. I would like to thank more particularly Dr Hekmatollah Alighanbari, Dr Guang-Xuan Li and Dr Njuki Mureithi for their many suggestions and help, and Ms Wendy Gentleman, for her work and her literature review on numerical methods for solving second-order implicit non-linear differential equations.

Many thanks to Scott Manktelow for his advice and help with the construction of the experimental apparatus. Merci également à mes collègues et amis de l'ENSMA, Fabienne Grosshans, Héloise Hugot, Frédéric Milcent et Bertrand Petermann, pour leur aide dans la construction des tubes, pour les nombreuses heures de travail passées à mener des expériences, et pour leur soutien moral, les jours où rien ne semblait vouloir marcher.

Special thanks are due to Professor S. C. Sinha for his suggestion to use the Picard iteration method with Chebyshev series, to Professor E.J. Doedel for giving freely his time and his wonderful software AUTO, and to Professor D.H. van Campen for trying the incremental harmonic balance on DIANA.

I wish to thank also Mrs Mary Fiorilli St-Germain for helping me navigate in the world of Latex, as well as for her patience with all the administrative tasks.

Many thanks are due to the chairman of the department of Mechanical Engineering, Professor A.M. Ahmed, and to the chairman of the department of Civil Engineering, Professor A.P.S. Selvadurai, for giving me the opportunity to teach while conducting this research.

In these times of budget cuts, the financial support of the Natural Sciences and Engineering Research Council of Canada (NSERC), Le Fonds pour la Formation de Chercheurs et l'Aide à la Recherche du Québec (FCAR), Hydro-Québec and McGill University, through the fellowship program, is acknowledged with gratitude.

Je voudrais aussi remercier tous mes amis, ici à Montréal, Gilles et Anne, Bertrand et Isabelle, Stéphane et Josiane, Eric et Anne-Catherine, Hekmat et Wadood, et outre Atlantique, Christophe, Michel, Jean-Philippe, Christine, Brigitte et Fabien, pour leur amitié et leur soutien moral.

Un gros merci à toute ma famille et celle de France, pour leur aide et encouragements.

Finalement, merci à toi, France, pour avoir été présente tout au long de ces longues et belles années.

STATEMENT OF CONTRIBUTION TO ORIGINAL KNOWLEDGE

The system of a pipe conveying fluid has received considerable attention during the last few decades, and does so still, mainly because of the variety of interesting dynamical behaviour it is able to display. The analysis of the nonlinear dynamics of this system is the subject of the study presented here and to the author's best knowledge, this is the first time that a systematic and unified investigation is undertaken, covering various aspects of the problem and various approaches, and proposing various methods of solution (analytical, numerical and experimental). Below is a summary of the main contributions of the thesis to original knowledge.

- The in-depth nonlinear analysis of the dynamical behaviour of a pipe conveying fluid is undertaken. The identification of chaotic motion, as well as the detailed bifurcation analysis of the pipe under various conditions — with a spring support, impacting on physical constraints, fitted with both positive and negative end-masses, and subjected to pulsating flow — is believed to be a first.

- A detailed derivation of a nonlinear model of the system is undertaken, as well as a comparison of existing different, or different-looking, models; in the case of a pipe with both ends fixed, the equations of motion derived here are considered to be the most complete and correct.

- The numerical problems associated with the presence of nonlinear inertial terms (i.e., the inability of conventional methods to solve such problems) has been "forgotten" by the nonlinear dynamics community; two numerical methods are proposed and developed here to treat this unusual case (second-order implicit nonlinear differential equations). Particular attention is paid throughout to the effects of the nonlinear inertial terms on the dynamics.

- The tools of modern nonlinear dynamics theory, usually restricted to "simple" dynamical system, are used here on a high-dimensional system, and the results provided by the simplified normal forms are compared with those obtained numerically and experimentally, showing therefore the utility of such tools. The three-fold pursuit and comparison of numerical, analytical and experimental methods for such a high-dimensional system is unusual, if not unique.

CONTRIBUTIONS BY CO-AUTHORS

In the papers, published or submitted to be published, that make up this Thesis, Professor Païdoussis appears as co-author in several papers. The extent of his contribution to the work is what is normal for a supervisor and a co-author; in all papers, therefore, the principal author is the Thesis candidate. This also applies to the other papers with additional co-authors (Dr Guang-Xuan Li and Ms Wendy Gentleman).

Contents

List of Figures

List of Tables

Chapter 1

INTRODUCTION

Over the last two decades, scientists and mathematicians have developed new tools in the field of dynamics, especially in the field of nonlinear dynamics. With these tools, the study of relatively simple nonlinear oscillators, such as described by van der Pol's equation or Duffing's equation, and of simple sets of nonlinear equations, such as the Lorenz equations, has demonstrated that very complex, "rich" dynamical behaviour is possible (Guckenheimer & Holmes 1983); for these simple equations at least, the dynamics is now fairly well understood, and the implications of the complex behaviour observed have been elucidated.

In real situations, as in engineering, economics or physiology, nonlinearity is commonplace, and in many cases essential in the proper description of the phenomena of interest; these fields of study, thus, provide a wide spectrum of problems in which these new dynamical tools can be applied. Of particular interest, especially to engineers, is the domain of fluid-structure interaction, in which system behaviour is very often complicated and difficult to understand (Païdoussis 1987). Indeed, structures subjected to either internal or external flows can be found in many engineering constructions. These include steam generator tube bundles, other pressure vessel internals, turbine blades, highway bridges and power transmission lines. It is well known that depending on the characteristics of the structure and the flow field, these structures may be subject to flow-induced vibrations or *fluidelastic instabilities* of different types, involving various mechanisms (Blevins 1977; Païdoussis 1980, 1981). Almost ten years ago, Païdoussis (1987) reviewed in detail flow-induced instabilities of *cylindrical* structures and reported a wide diversity in the subject. For simplicity, he divided the problem into four different classes depending on the disposition of the flow *vis-à-vis* the structure: (i) axial flow within tubular structures; (ii) axial flow outside the cylindrical structures, i.e. along the long axes of the cylinders; (iii) annular flow in systems of coaxial cylinders and (iv) cross-flow about arrays of cylinders, i.e. normal to the long axes of the cylinders. To that must be added the class in which most of the work to-date has been done: that of a solitary cylinder subjected to cross-flow.

The present investigation is mainly concerned with the first class. More specifically, it is concerned with the study of the ***post-instability behaviour of slender tubes conveying fluid***, which necessarily needs the inclusion of the nonlinearities in the analysis. As shown by Païdoussis (1991), the model of a pipe conveying fluid has become "a paradigm in the study of fluid-structure interaction", as most types of fluidelastic instability can be illustrated and studied both theoretically and experimentally with this system.

Divergence and flutter are the most common types of instability in this physically simple system, and were usually only investigated from a linear point of view, thereby preventing any prediction beyond the instability point. However, with (i) the proper description of the nonlinearities, (ii) the new tools of nonlinear dynamics and (iii) the knowledge and understanding of the aforementioned simple oscillators, it is now possible to gain a better understanding of the post-instability behaviour and of even more complex phenomena. However, before considering these aspects, it is of interest to recall first why "Pipes Conveying Fluid (have become): *a Model Dynamical Problem*",[†] and what are their major characteristics.

[†]This corresponds to the title of the recent literature review by Païdoussis & Li (1993).

1.1 PIPES CONVEYING FLUID: THE FUNDAMENTALS

In the past, most of the theoretical studies were concerned with stability and were based on linearized analytical models. Bourrières (1939) was one of the first to study the dynamics of flexible pipes conveying fluid. The interest in vibration of pipelines served as the initial inspiration to many subsequent studies, such as those by Housner (1952), Niordson (1953) and Benjamin (1961).

The particularly interesting problem of the dynamics of a cantilevered pipe conveying fluid was studied further by Gregory & Païdoussis (1966) and Païdoussis (1970), in the case of steady flow, and by Païdoussis & Issid (1974) for flow with a pulsating component; these references are representative of what has become an extensive body of literature. Excellent bibliographical surveys undertaken by Païdoussis & Issid (1974) for the study of the linearized equations and by Païdoussis & Li (1993) for a selective and updated review illustrate the constant growth of the literature, and help to explain how and why the system of a pipe conveying fluid has become a new paradigm in dynamics, the main reasons being summarized as follows:[§]

(i) "it is a physically simple system, easily modelled by simple equations;

(ii) it is a fairly easily realizable system, which affords the possibility of theoretical and experimental investigation in parallel;

(iii) this being a more general problem than that of the column and in some ways of the rotating shaft, yet including their essential characteristics, may be thought as complementing them;

(iv) it is a problem in the larger category of dynamical systems involving momentum transport, such as travelling chains and bands, chain-saw blades, etc. (Mote 1968)".

To understand the dynamics of fluid-conveying pipes, let us consider first the

[§]Taken from Païdoussis (1991)

most simple case, i.e. when gravity, internal damping, externally imposed tension and pressurization effects are either absent or neglected. Figure 1.1 illustrates schematically such a case.

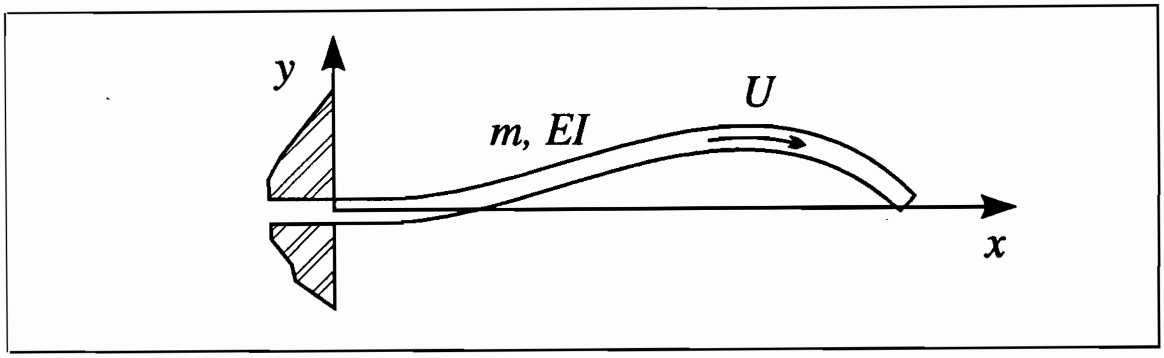

Figure 1.1: The horizontal pipe conveying fluid.

Assuming small lateral displacements, the linear equation for planar motion takes the particularly simple form

$$EI\frac{\partial^4 y}{\partial x^4} + M(\frac{\partial}{\partial t} + U\frac{\partial}{\partial x})^2 y + m\frac{\partial^2 y}{\partial t^2} = 0, \tag{1.1}$$

in which the three terms correspond, respectively, to bending, fluid inertia and pipe inertia. The pipe is assumed to respond as an Euler-Bernoulli beam with stiffness EI, internal cross-sectional area A, mass per unit length m, length L and lateral displacement y. The conveyed fluid of mass per unit length M is assumed to flow through the pipe as a steady plug flow (flat velocity profile) at a constant velocity U, which is the simplest possible form of the slender body approximation for the problem at hand (Niordson 1953). The independent variables are time t, and the axial coordinate along the undeformed axis of the tube, x. Expanding the fluid-inertial term in equation (1.1) yields

$$EI\frac{\partial^4 y}{\partial x^4} + MU^2\frac{\partial^2 y}{\partial x^2} + 2MU\frac{\partial^2 y}{\partial x \partial t} + (M+m)\frac{\partial^2 y}{\partial t^2} = 0, \tag{1.2}$$

which may in fact be considered as the standard, simplest version of equation of motion. The various terms in (1.2) may be identified, sequentially, as the flexural restoring force, the centrifugal force associated with the axial velocity U and the curvature of the structure, the Coriolis force associated with the axial flow velocity and the angular velocity of the pipe, and the inertia forces. Equation (1.2) may be compared to the equation of motion of a beam subjected to a compressive load, P (Bolotin 1964),

$$EI\frac{\partial^4 y}{\partial x^4} + P\frac{\partial^2 y}{\partial x^2} + m\frac{\partial^2 y}{\partial t^2} = 0. \tag{1.3}$$

It is then clear that the centrifugal force in (1.2) acts in the same manner as a compressive load. In this way, it is easy to see and to understand physically that, with increasing U, the effective stiffness of the system is diminished.

To gain a better understanding of the mechanism that leads to instability, it is instructive to look into the energy transfer between the structure and the fluid. To do that, Benjamin (1961) found the rate of work done on the pipe by the fluid-dynamic forces,

$$\frac{\mathrm{d}W}{\mathrm{d}t} = -\int_0^L \frac{\partial y}{\partial t} M\left[\frac{\partial}{\partial t} + U\frac{\partial}{\partial x}\right]^2 y\,\mathrm{d}x, \tag{1.4}$$

and hence, also, the work done over a cycle of oscillation of period T

$$\Delta W = -MU\int_0^T \left[\left(\frac{\partial y}{\partial t}\right)^2 + U\left(\frac{\partial y}{\partial t}\right)\left(\frac{\partial y}{\partial x}\right)\right]\Bigg|_0^L \mathrm{d}t. \tag{1.5}$$

To simplify the analysis, two different cases may be distinguished: when the pipe is free to move at the outlet or when it is fixed at both ends. For a pipe ***supported at both ends***, it is clear that $\partial y/\partial t = 0$ at $x = 0$ and $x = L$, so that

$$\Delta W = 0. \tag{1.6}$$

This shows that the system is conservative in this case. It is then well known that it might be subjected to *static* instabilities (Bolotin 1963, 1964). Indeed, recalling the analogy between (1.2) and (1.3), it is obvious that for sufficiently large U, the destabilizing centrifugal force may overcome the restoring flexural force, resulting in ***divergence***, known also as ***buckling*** or, as will be seen later, as a ***pitchfork bifurcation*** in nonlinear dynamics. Therefore the procedure to find the static instabilities becomes straighforward, since it is necessary to consider only the time-independent terms in equation (1.2). For example, for the case of a simply-supported pipe, the nondimensional critical flow velocity u_{cr}, related to the dimensional quantities by $u_{cr} = \sqrt{M/EI}\, U_{cr} L$, can be obtained easily and is simply given by

$$u_{cr} = \pi. \tag{1.7}$$

Païdoussis & Issid (1974) showed that the dynamical behaviour of pipes with one or both ends clamped, rather than simply supported, is similar. They proved also that according to linear theory, coupled-mode flutter may follow divergence, at a higher flow velocity. This is due to the fact that the system is not only conservative but also *gyroscopic*, by virtue of the presence of the Coriolis terms, which may lead to the coalescence of two modes in the complex-frequency plane (Ziegler 1968). However, the physical existence of this post-divergence flutter instability is questionable, as linear theory cannot be used to provide reliable information once the system becomes unstable, i.e. once it leaves the vicinity of the undeflected state, and this issue has to be decided by nonlinear theory. This question was definitively addressed, almost simultaneously, by Holmes (1978) and by Ch'ng & Dowell (1979) [see also Ch'ng (1978)]: they both proved that amplified oscillatory motions do exist near the origin, but divergence is the ultimate steady-state.

For the case of a *cantilevered pipe*, the stability analysis is somewhat more difficult, because, as will be seen, it is a *nonconservative* system. Considering again the work done on the pipe over a cycle of oscillation, equation (1.5), it is possible to explain in simple terms what is the mechanism that leads the system to *flutter* of the single-degree-of-freedom type, i.e. flutter arising from a *Hopf bifurcation.* This also was first elucidated by Benjamin (1961). The work done over a cycle of oscillation in this case is not zero but equal to

$$\Delta W = -MU \int_0^T \left[\left(\frac{\partial y}{\partial t}\right)^2 + U \left(\frac{\partial y}{\partial t}\right)\left(\frac{\partial y}{\partial x}\right) \right]_{x=L} \mathrm{d}t, \tag{1.8}$$

for a pipe fixed at $x = 0$ and free at $x = L$. The first term on the right-hand side of (1.8) represents the energy dissipation in the flowing fluid, while the second one represents the supply of energy from the nonconservative loading at the free end. For $U > 0$ and sufficiently small, it is clear that $\Delta W < 0$, and free motions of the pipe are damped — an effect due to the Coriolis forces, which, unlike the case of supported ends, in this case *do* work. If, however, U is sufficiently large, while over most of the cycle $\partial y/\partial x$ and $\partial y/\partial t$ have opposite signs at the free end ($x = L$), then $\Delta W > 0$, i.e. the pipe will gain energy from the flow, and free motions will be amplified. These signs of the free-end velocity and slope mean that the free end of the tube must slope backwards *vis-à-vis* the direction of motion during most of the cycle of vibration; therefore the motion of the free end resembles the sort of dragging/lagging motion that one would obtain when laterally oscillating a long flexible blade in water. This characteristic has been remarked by Bourrières (1939), Benjamin (1961) and Gregory & Païdoussis (1966).

The stability of the cantilevered pipe can be linked to the classical problem of a column subjected to a tangential follower-type load at the free end (the direction and/or magnitude of loading being determined by the configuration of the structure and changes as the structure is deformed), i.e. Beck's problem (Bolotin 1963; Ziegler 1968), as demonstrated by Nemat-Nasser *et al.* (1966), Herrmann (1967) and Herrmann & Nemat-Nasser (1967). The cantilevered pipe being not only nonconservative but also gyroscopic helps to explain why it has received so much attention during the last forty years and why it exhibits many "strange" or unexpected features of behaviour. For example, (i) the addition of structural damping in some cases *destabilizes* an otherwise stable system (Gregory & Païdoussis 1966; Nemat-Nasser *et al.* 1966); (ii) by supporting the downstream end of the cantilever by a finger or a pencil, the system can become unstable by divergence, which means that the addition of a support causes instability (Thompson 1982; Sugiyama *et al.* 1985); or (iii) the study of the dynamics of the continuous system by means of discretized models, at least for a small number of degrees of freedom, may lead to qualitatively wrong results (Païdoussis & Deksnis 1970).

Many variants of the system have been studied in detail as well. For example, the pipe with added masses along its length (Hill & Swanson 1970), with a translational spring (Chen 1971), with an elastic foundation (Becker *et al.* 1978) or with flow jets exiting at either end (Wiley & Furkert 1972; Hannoyer & Païdoussis 1979). Other work involved also articulated pipes (see, for instance, Païdoussis & Deksnis 1970), curved pipes (Misra *et al.* 1988), thin shell-like cylindrical pipes (e.g. Païdoussis *et al.* 1984), short pipes requiring a Timoshenko beam theory (Païdoussis & Laithier 1976), and so forth. All these interesting studies, and even a much wider variety, are summarized by Païdoussis & Li (1993) and will be reported soon in a detailed review by Païdoussis (1996).

1.2 NONLINEAR ASPECTS

Over the past twenty years or so, interest has grown in the nonlinear dynamical aspects of the problem of a pipe conveying fluid; this involves more interesting but also more complex analysis and will be the main subject of this Thesis. First of all, a nonlinear analysis has the advantage of being able to predict the behaviour of the system beyond the critical values, while linear models predict exponential increase in amplitude after bifurcation. Experimental evidence suggests that limit-cycle motion or a stable buckled state arise (Dodds & Runyan 1965; Païdoussis 1966), so that the inclusion of nonlinear contributions is of particular interest, in order to improve agreement between theoretical prediction and experimental observation. Secondly, the nonlinear approach enables classification in a parameter space of the different possible types of qualitative behaviour of the system, by generating so-called bifurcation diagrams. Finally, although Rousselet & Herrmann's theoretical work (1981), as well as some experimental work (Païdoussis 1970), proved that the system was only weakly nonlinear, in some other cases very interesting features were observed (Sethna & Shaw 1987; Bajaj 1987; Li & Païdoussis 1994; to name but a few). To simplify the overall picture, let us divide the review on the nonlinear dynamics of this system into three categories: continuous cantilevered pipes, articulated cantilevered ones, and pipes fixed at both ends.

1.2.1 Continuous cantilevered pipes

For the cantilevered pipe, a number of papers presenting a nonlinear analysis are of particular interest, and will be discussed briefly in what follows. In all cases, the centreline of the pipe is assumed to be inextensible.

Bourrières (1939), more than fifty years ago, was the first to derive the nonlinear equations of planar motion. He utilized the Newtonian force-balance method and wrote down the full and exact nonlinear relationships, such as the expression of the curvature for example. "Unfortunately", he then proceeded to simplify the system by linearization to obtain analytically some very interesting results, without undertaking any nonlinear analysis. Although he could not find the critical flow velocity, he explained many of the characteristics of the system.

Subsequent research on the nonlinear dynamics of this system has been conducted by Rousselet & Herrmann (1977, 1981). They derived the equations in two different ways, the force balance and the energy methods, following closely Bourrières' work in the former case. They also took into account the friction force acting between the fluid and the deformed pipe and the resultant nonlinear pressure loss, and so had to derive another equation for the fluid itself. The equations were then solved by the Krylov-Bogoliubov averaging method (Minorsky 1962), yielding the limit-cycle amplitude as a function of the mass parameter $\beta = M/(m+M)$. They showed that there are regions of β where nonlinearities stabilize the system ($0.02 < \beta < 0.21$ and $0.42 < \beta < 0.66$), and others where they destabilize it.

A second set of equations was derived by Lundgren *et al.* (1979), resulting in a set of integrodifferential equations which appears to be absolutely correct. No major approximation was made, except for the assumption of zero gravity effects (which is perfectly valid for horizontal pipes undergoing motions in a horizontal plane in any case); apart from that, the derivation is complete and correct. Like Bourrières, they kept the two equations in a general form without interconnecting them. These equations were subsequently used by Bajaj *et al.* (1980), Edelstein *et al.* (1986) and Steindl

& Troger (1988).

Lundgren *et al.* (1979) studied a pipe fitted with an inclined terminal nozzle, causing sinusoidal static deformations of the tube which were obtained through the nonlinear equations. The stability of the new static equilibria was then investigated for both in-plane and out-of-plane motions with respect to the plane of the inclined nozzle. Bajaj *et al.* (1980), like Rousselet & Herrmann (1977), considered a parameter related to the pressure loss of the pipe. Using centre manifold theory (Carr 1981) and the method of averaging, they studied the nonlinear dynamics of a horizontal cantilevered pipe. After finding the critical flow velocity, which was not an easy task, their major contribution was to reconstruct the periodic solution after the bifurcation. This was done by following the fundamental methods developed earlier by Joseph & Sattinger (1972) and Chow & Mallet-Paret (1977). They found also that depending on the pressure loss in the pipe, the Hopf bifurcation may be either subcritical or supercritical. Steindl & Troger (1988) extended their work by adding a rotationally symmetric elastic support in order to examine even more complicated situations for loss of stability. Using the Lyapunov-Schmidt method (Golubitsky & Schaeffer 1985) for reducing the governing partial differential equation into a set of ordinary differential equations, and normal form theory (Guckenheimer & Holmes 1983; Rand & Armbruster 1987), they obtained the bifurcation equations exhibiting both planar and rotary motions as well as bifurcation diagrams for cases where two unfolding parameters were necessary.

Finally, Li & Païdoussis (1994) studied a vertical standing system near the double degeneracy where the buckled pipe regains stability through a pitchfork bifurcation and simultaneously loses it by flutter through a Hopf bifurcation. By using the theories of centre manifold and normal forms, they showed that heteroclinic cycles exist in the reduced system, which is an indication of the possible existence of chaotic oscillations for small perturbations; these were indeed found to exist numerically for harmonically perturbed flow velocities.

1.2.2 Articulated cantilevered pipes

Articulated cylinders received considerable attention also. Rousselet & Herrmann (1977) were the first to consider the system of two rigid pipes flexibly interconnected from a nonlinear viewpoint. The equations of motion were a modified form of Benjamin's (1961) and Païdoussis & Deksnis' (1970), but with the upstream pressure remaining constant instead of the flow velocity (which again may vary with motions through a frictional loss factor). By means of the Krylov-Bogoliubov method, they showed that the Hopf bifurcation could be either subcritical or supercritical depending on the value of β and this was confirmed qualitatively by experiment.

Bajaj & Sethna (1982) conducted an analysis on three-dimensional motions of two articulated pipes in the neighbourhood of the critical flow velocity for the Hopf bifurcation. The joints in this case did not have torsional rigidity and therefore permitted both motions transverse to the long axis of symmetry and rotary ones about it. Periodic solutions of the nonlinear equations were determined by the method of Alternate Problems (Hale 1969; Bajaj 1982), which transforms a set of ordinary differential equations into a set of algebraic ones. Two independent sets of periodic solutions were found to exist, corresponding to clockwise or counterclockwise rotary motions, and planar transverse motions. The stability of these periodic motions was determined by computing the Floquet exponents of the corresponding variational equations.

The foregoing analysis was restricted to solutions in the neighbourhood of the straight vertical equilibrium. This restriction was removed later by Sethna & Gu (1985). Many configurations were examined and investigated using either a linear approach or the centre manifold theory, and analytical results were complemented by numerical simulations. Sethna & Shaw (1987) studied also codimension-three bifurcations of a two-segment articulated system vibrating in a plane, near a point of double degeneracy [unlike the continuously flexible system, the articulated one can lose stability either by divergence or flutter (Païdoussis & Deksnis 1970)]. Using centre manifold reduction and the averaging method, the original system was transformed into a simplified three-dimensional subsystem, and a very complete bifurcation analysis was undertaken. An extensive classification of possible dynamical behaviour was presented with the aid of appropriate phase portraits.

1.2.3 Pipes fixed at both ends

Other researchers have also studied the case of a pipe fixed at both ends. Thurman & Mote (1969) were mainly concerned with the oscillations of bands of moving materials, such as saw blades or conveyor belts, which are in the same general dynamical family as pipes supported at both ends. Unlike the cantilevered system, the centreline in this case was not considered inextensible, so that the essential nonlinearity was associated with the axial tube elongation and the extension-induced tension in the tube, both of which are dependent on lateral deformation. All the other relationships (such as that for moment/curvature for example) were assumed to be linear. Their major results, obtained by the Krylov-Bogoliubov method, showed the effects of the nonlinear terms on the fundamental period of oscillation.

Holmes (1977) was one of the first to use the tools of modern nonlinear dynamics in the study of a pipe conveying fluid with both ends supported. The only nonlinear term considered was associated with the deflection-induced tension in the pipe that was added to the linear equation derived by Païdoussis & Issid (1974). After discretization of the equation, Holmes was able to find many characteristics of the system, and he discussed the existence of local as well as global bifurcations. He also studied the panel flutter problem, which is qualitatively similar to that of a cantilevered pipe conveying a fluid (loss of stability via a Hopf bifurcation). In a subsequent paper, he proved that sustained flutter motion is impossible with these equations, by studying the local and global stability of the equilibrium positions which emerge after the first instability (Holmes 1978). The same conclusion was reached by Ch'ng & Dowell (1979).

Yoshizawa *et al.* (1986) considered the case of a clamped-pinned vertical pipe conveying fluid with a pulsating upstream pressure. Both the two equations of motion utilized and the physical system followed Rousselet & Herrmann's (1981) work. After a one-mode Galerkin projection, the two resulting equations were solved by the method of multiple scales (Nayfeh & Mook 1979) for the principal primary region of parametric resonance. They showed that the nonlinear inertial terms are important at low flow velocities, but that hardening-spring effects associated with the nonlinear centrifugal forces predominate at higher flows. Finally, Namachchivaya (1989) and Namachchivaya & Tien (1989) were among the last to deal with nonlinear behaviour of supported pipes conveying pulsatile fluid. They found some interesting bifurcations near the subharmonic and the combination resonances, using the method of averaging, and hardening-spring effects were obtained in the amplitude versus frequency plane.

1.2.4 Chaos

The study of chaos, usually associated with strong nonlinearities, has become more and more popular in recent dynamics research. Therefore, it is not surprising to see a certain number of papers on the subject in the area of fluid-structure interaction. Thus, Païdoussis & Moon (1988) and Païdoussis *et al.* (1989) introduced strong nonlinearities by the addition of motion-limiting constraints and Tang & Dowell (1988) used two equispaced permanent magnets on either side of a pipe fitted with a steel strip. In all cases, experiments as well as theoretical results indicate that there exist regions of chaos beyond the Hopf bifurcation, i.e. once the amplitudes of motion become large. Chaotic responses were found to occur after the instability of the limit cycle, followed by a cascade of *period-doubling* bifurcations, which is one of the well-known routes to chaos (Feigenbaum 1983). Fractal dimension calculations were undertaken via delay embedding techniques by Païdoussis *et al.* (1992), showing that an analytical model capable of capturing the qualitative dynamics of the system is required to have a least two and up to four degrees of freedom. An excellent treatment of fractal geometry is given by Mandelbrot (1983), and of fractal dimensions, as applied to dynamical systems, as well as numerical procedures for their determination by Parker & Chua

(1989) and Moon (1992). Païdoussis *et al.* (1991) considered the effects of the number of degrees of freedom, and, with the use of improved theoretical models, obtained even better agreement with the experiments. The same problem was also studied by Makrides & Edelstein (1992) using the finite element method, and agreement with the experimental results of Païdoussis & Moon (1988) was found to be reasonably good, and by Miles *et al.* (1992), using bispectral analysis techniques.

It is well known that the perturbation of a homoclinic orbit leading to a "horseshoe" may lead to chaos. This has been explained from a fundamental point of view by Smale (1963, 1967) and is treated in detail in Guckenheimer & Holmes (1983) and Devaney (1987). This concept was applied to the case of fluid-conveying pipes by several authors: Sethna & Shaw (1987) in the case of an articulated system, Bajaj (1987) in the case of a pulsating flow, and Steindl & Troger (1988) in the case of continuous system with a linear spring, who found situations where homoclinic or heteroclinic orbits exist. For an articulated cantilevered system, Champneys (1991, 1993), using AUTO (Doedel & Kernevés 1986) and direct numerical integration, found chaos arising from a complicated bifurcation structure, also involving homoclinic bifurcations; he also observed chaos following cascades of period-doubling bifurcations within certain narrow ranges of the flow velocity. Li & Païdoussis (1994) found cases where double degeneracy conditions exist (two types of instabilities arising simultaneously) and, by perturbation of these orbits, were able to find chaotic oscillations.

Finally, Copeland (1992) and Copeland & Moon (1992), both theoretically and experimentally, found that a *three-dimensional* cantilevered system with a mass added at the free end is capable of developing chaotic motions through a *quasiperiodic* route to chaos, using power spectra, delay-embedding reconstruction of the orbit, and measurements of correlation dimensions.

Consequently, it becomes obvious that slight modifications or variants of the original system tend to enrich the dynamical behaviour, and that chaotic responses emerge through different routes.

1.3 OBJECTIVES AND THESIS OUTLINE

From the literature review, it is obvious that the system of a pipe conveying fluid has received considerable attention during the last four decades. The present study aims to build on the knowledge of the *nonlinear* dynamics of a cantilevered pipe and to describe its fascinating behaviour by introducing and using many of the new concepts of nonlinear dynamics theory developed in the last few years. It also aims to discuss, clarify and prove the existence of complicated motions, such as quasiperiodic or chaotic oscillations, in this rather simple physical system.

The Thesis consists of eight chapters. In order to explore the widest and most interesting range of situations, the original system, as described in Figure 1.1, is modified throughout the following chapters, to indeed describe variants of the original system. To gain a better understanding of the structure of the Thesis, the diagram in Figure 1.2 illustrates schematically the links and relationships between the different studies undertaken. After the introduction of the basic system and a general literature review, presented in this chapter, a nonlinear model is developed (Chapter 2). Then, four distinct configurations (modifications) are examined: the pipe with a spring support (Chapter 3), the pipe with impact constraints (Chapter 4), the pipe with an end-mass (Chapter 6) and the pipe with a pulsating fluid (Chapter 7). In parallel, an experimental investigation is undertaken, and some numerical methods, necessary to solve the nonlinear equations, developed (Chapter 5). With this unified approach, the present study aims to extend the work undertaken by numerous researchers in the field, hoping to convince the reader that this system has also become "*a paradigm of nonlinear dynamics*".

Because of the diversity of the subject matter, the various configurations chosen here are of course selective, rather than exhaustive. One justification is that the different chapters of the Thesis (except for the present and the final ones) have been taken from seven studies undertaken during the last five years and that have either been published or submitted for publication in various Journals. For the same reason,

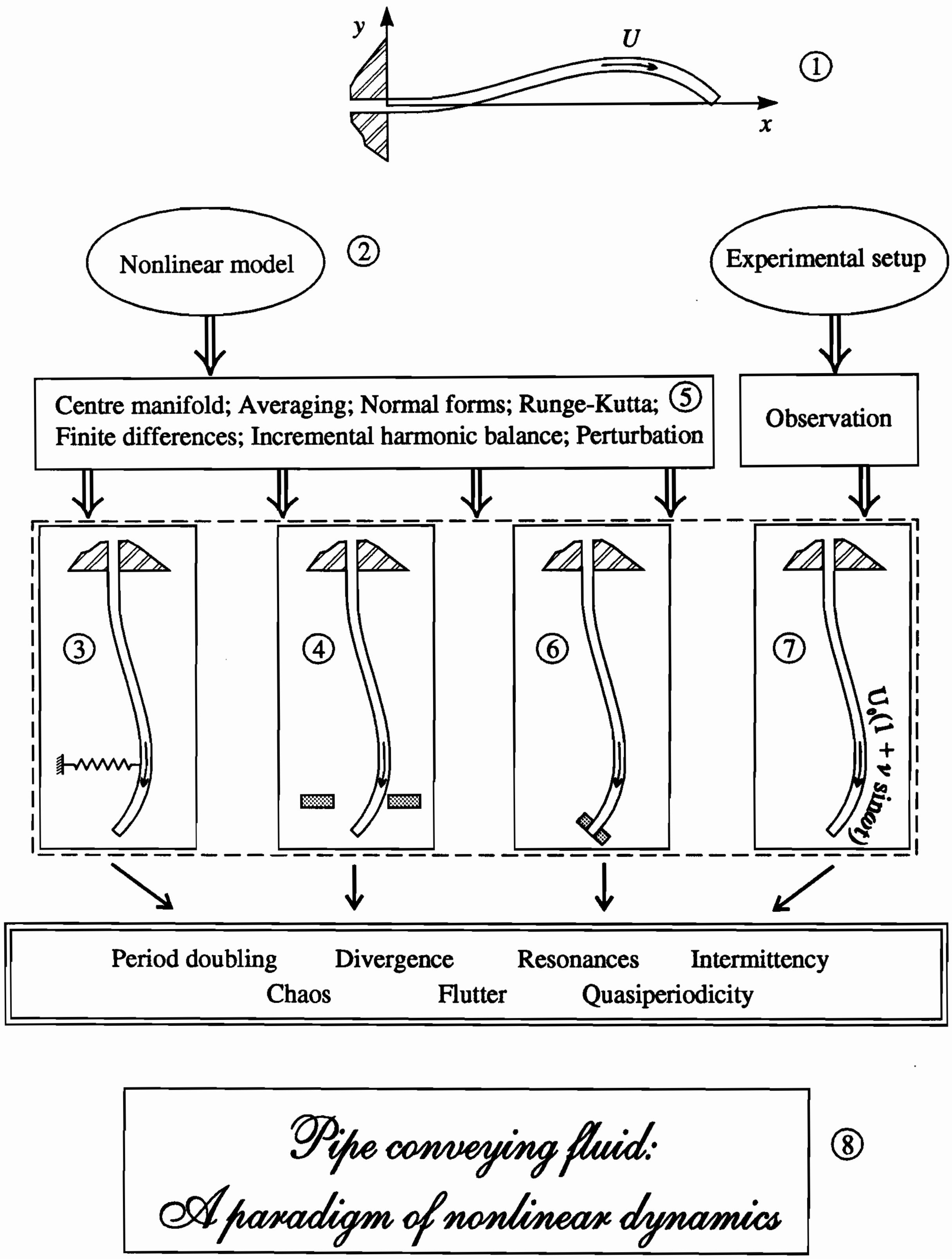

Figure 1.2: Structure of the Thesis; encircled numbers refer to corresponding chapters.

there may exist in some cases some redundancies that the reader may skip over easily. For example, the description of the system and the equations of motion is very similar in all chapters, and there is some repetition in the literature review in the different introductions. Also, it will become obvious that the degree of "exactness" and "completeness" increases throughout the Thesis; for example, the number of degrees of freedom is higher in Chapter 4 than in Chapter 3, the numerical methods involved are more sophisticated after Chapter 5, and the approximation of the centre manifold in the presence of a pulsating fluid is more accurate in Chapter 7 than in Chapter 3. Nevertheless, this structure has been preferred because it corresponds to the evolution of the understanding gained by the author and to his search of constant improvement. Moreover, the different chapters may be read independently, enabling the interested reader to grasp just the information he or she needs. The detailed outline of the different chapters may be summarized as follows.

In Chapter 2, the complete theoretical model is presented.[†] As shown in Section 1.2, various equations of motion had been derived and used by a certain number of "schools", but no systematic comparison of these equations was ever made theretofore. This, incidentally, is not a trivial task, in view of the different approaches adopted and assumptions made, the different notations and final form of the equations, as well as the relative obscurity of some of the derivations. Consequently, the first task in this Thesis is to rederive the nonlinear equations of motion of fluid-conveying pipes in simple and accessible terms. Different derivations are made for cantilevered pipes, where the centreline is assumed inextensible, and for pipes with both ends fixed; it is shown that the derivations, the origin of the various terms and the structure of the equations are distinctly different in these two cases of end support. The equations of motion are then compared with those already in existence, e.g. by Bourrières (1939), Rousselet & Herrmann (1981), and Lundgren, Sethna & Bajaj (1979), at the same time clarifying the derivations and assumptions made, and discussing the validity and completeness

[†]This corresponds to the article by Semler, Li & Païdoussis 1994 The nonlinear equations of motion of a pipe conveying a fluid. *Journal of Sound and Vibration* **169**, 577-599.

of the final equations.

In Chapter 3, the nonlinear planar dynamics of a vertical cantilevered pipe conveying fluid are explored, in the presence of an intermediate spring support, by means of a two-degree-of-freedom Galerkin discretization of the flexible system.‡ The stability of the original equilibrium is examined, and the regions in the parameter space where the system is stable or loses stability by divergence or flutter are determined. Then, by examining the nonlinear equations of motion, the stability of the other fixed points that emerge with increasing flow velocity is studied, for various system parameters, revealing a very rich bifurcational behaviour. The nonlinear dynamics is also studied in the vicinity of various bifurcations by means of centre manifold theory and normal form reduction, as well as by numerical simulation, in the vicinity of pitchfork, Hopf and double degeneracy bifurcations; local and global behaviour are explored. Finally, the dynamics in the presence of harmonic perturbations in the flow is investigated numerically in the neighbourhood of the double degeneracy, where heteroclinic orbits arise.

In Chapter 4, the planar dynamics of a nonlinearly constrained pipe conveying fluid is examined numerically, by considering the full nonlinear equation of motions and a refined trilinear-spring model for the impact constraints§ — completing therefore the circle of studies on the subject undertaken by Païdoussis & Moon (1988) and Païdoussis *et al.* (1989,1991,1992). The effect of varying system parameters is investigated for the two-degree-of-freedom ($N = 2$) model of the system, followed by less extensive similar investigations for $N = 3$ and 4. Phase portraits, bifurcation diagrams, power spectra and Lyapunov exponents are presented for a selected set of system parameters, showing some rather interesting, and sometimes unexpected, results; the numerical results are compared with experimental ones obtained previously.

‡Païdoussis & Semler 1993 Nonlinear dynamics of a fluid-conveying cantilevered pipe with an intermediate spring support. *Journal of Fluids and Structures* 7, 269-298.

§Païdoussis & Semler 1993 Nonlinear and chaotic oscillations of a constrained cantilevered pipe conveying fluid: a full nonlinear analysis. *Nonlinear Dynamics* 4, 655-670.

In Chapter 5, because the nonlinear equations of motion of a pipe conveying fluid contain *strong* nonlinear inertial terms that cannot be removed, numerical schemes for solving second order *implicit* nonlinear differential equations are elaborated and investigated.[†] Three specific methods are examined. Two of them are based on series expansions: Picard iteration using Chebyshev series, and Incremental Harmonic Balance (IHB) in which the nonlinear differential equation is transformed into a set of algebraic ones that are solved iteratively. The third method is based on a 4th-order (Houbolt's scheme) and an 8th-order backward finite difference method (FDM). Each method is presented, and then applied to specific examples. It is shown how the combination of IHB and FDM can be a powerful tool for the analysis of nonlinear vibration problems defined by implicit differential equations (including also explicit ones), since bifurcation diagrams of stable and unstable periodic solutions can be computed easily with IHB, while periodic and non-periodic stable oscillations may be obtained with FDM.

Chapter 6 can be regarded an extension of Copeland's (1992) thesis and Copeland & Moon's (1992) work, but in a simplified configuration, i.e. a pipe fitted with an end-mass with the motion restricted to *a plane*. Both cases of a positive and negative end-mass are considered. One of the objectives is to see if the case with no end-mass is singular as was found in the study of the three-dimensional system (in the sense that only the Hopf bifurcation is present, with no other qualitative changes as the flow is increased), to investigate the possible existence of chaotic oscillations and to elucidate how and why they arise. In the first part of Chapter 6,[‡] the dynamics of the system is examined when the added mass is negative (a *mass defect*), by means of standard numerical methods and the software package AUTO. Loss of stability of the periodic solutions are determined by computing the Floquet multipliers, and chaotic

---

[†]Semler, Gentleman & Païdoussis 1996 Numerical solutions of second-order implicit ordinary differential equations. Accepted in *Journal of Sound and Vibration.*

[‡]Semler & Païdoussis 1995 Intermittency route to chaos of a cantilevered pipe conveying fluid fitted with an end-mass. *Journal of Applied Mechanics* **62**, 903-908.

oscillations are investigated through Poincaré return maps and Lyapunov exponents. In the second part of the chapter, the more "realistic" case of a *positive* end-mass is investigated, both numerically and experimentally;[§] the assumption of a small end-mass is removed in this case and the numerical methods developed in Chapter 5 are used, and finally a comparison with the results obtained experimentally is undertaken.

Chapter 7 deals with the fourth and last system of Figure 1.2, and is concerned with the nonlinear dynamics and stability of cantilevered pipes when the fluid has a harmonic component superposed on a constant mean value.[†] The mean flow velocity is near the critical value for which the pipe becomes unstable by flutter through a Hopf bifurcation. Again, the full nonlinear equations of motion containing nonlinear inertial terms are considered and various approaches are adopted to tackle the problem: (a) the centre manifold theory applied on the set of *non-autonomous* equations, followed by the normal form method, yielding both the principal and the fundamental resonances; (b) a perturbation method via which the nonlinear inertial terms are removed by finding an equivalent term using the linear equation; (c) a finite difference method (FDM) based on Houbolt's scheme and (d) an incremental harmonic balance (IHB) method, as in Chapter 5. Using the four methods, the dynamics of the fluid-conveying pipe is investigated in detail. In particular, the effects of the forcing frequency, the perturbation amplitude, and the constant flow velocity are considered, and attention is paid to the effects of the nonlinear terms. Again, these results are compared with experiments undertaken in the laboratory, utilizing elastomer pipes conveying water.

Finally, Chapter 8 is a retrospective summary of this series of studies, and possible directions for future work are presented.

[§] Païdoussis & Semler 1996 Nonlinear dynamics of a fluid-conveying cantilevered pipe with a small mass attached at the free end. Submitted to the *International Journal of Non-Linear Mechanics*.

[†] Semler & Païdoussis 1996 Nonlinear analysis of the parametric resonances of a planar fluid-conveying cantilevered pipe. Submitted to the *Journal of Fluids and Structures*.

Chapter 2

THE NONLINEAR EQUATIONS OF MOTION§

2.1 INTRODUCTION

The dynamics of pipes conveying fluid has been studied very extensively in the past few decades. The conclusion of a recent surveys of the subject, undertaken by Païdoussis (1991) and Païdoussis & Li (1993) and involving more than two hundred references, was that this topic has now become a new paradigm of dynamics, superseding the classical problem of a column subjected to various types of end load, because its dynamics is much richer and because of a very distinct advantage: experiments with a pipe conveying fluid are relatively simple in all cases, whereas the nonconservative system of a column subjected to a follower load, for instance, is rather difficult to realize.

The linear dynamics of the system have been understood for quite some time; see, for instance, Païdoussis & Issid's (1974) review of work up to 1974. Thus, a pipe with supported ends loses stability by divergence at sufficiently high flow velocity, and its nonconservative cantilevered counterpart by single-degree-of-freedom flutter, i.e. via a Hopf bifurcation giving rise to limit-cycle motion. Agreement between theoretical

§This corresponds to the article by Semler, Li & Païdoussis 1994 The nonlinear equations of motion of a pipe conveying a fluid. *Journal of Sound and Vibration* **169**, 577-599.

and experimental values of the critical flow velocities is quite good; see, for instance, Païdoussis (1966, 1970) and Jendrzejczyk & Chen (1985).

In recent years, more and more effort has been devoted to the study of the nonlinear dynamics of the system, starting with Holmes' (1977) benchmark paper on the subject. Among many notable papers in this area, those by Holmes (1978), Ch'ng & Dowell (1979), Rousselet & Herrmann (1981), Lundgren *et al.* (1979), Bajaj *et al.* (1980), Bajaj & Sethna (1991) might be mentioned. With the help of the modern tools of dynamical theory (e.g., centre manifold reduction, bifurcation-unfolding techniques, the Lyapunov-Schmidt method, and so on), extremely rich bifurcational sets, illustrating a veritable kaleidoscope of phenomena, have been revealed for the basic system and its many variants: a pipe with pulsating flow, cantilevered pipes with an end-mass, pipes with unequal stiffness in two perpendicular planes, and so on.

In many of the early papers on nonlinear dynamics, the equations of motion were derived *ab initio*. As a result, several sets of different or different-looking equations came into existence. To the author's knowledge no systematic comparison of these equations was ever made. This, incidentally, is not a trivial task, in view of the different approaches adopted and assumptions made, the different notations and final form of the equations, as well as the relative obscurity of some of the derivations. The current situation is that a number of "schools" may be identified, each group and their followers using a different set of basic equations. Consequently, a thorough discussion, comparison and demystification of the various equations of motion appear particularly interesting and useful for the research community.

This, in fact, is the goal of the present chapter. In the first part, the equations of motion are derived, using a simple set of assumptions and a very accessible level of derivation. Since both energy and Newtonian approaches have been used in the past, the equations are derived in both ways and are shown to be identical. In the second part (Section 2.6), previous derivations and the resulting equations are discussed, together with their validity, completeness, added sophistication, and their similarities and differences to one another and to the equations derived here.

Thus, it is shown that not all of the equations available are correct: some are correct and consistent to the assumptions made but less complete than others, and so on. It is also shown that the equations of motion of pipes with both ends fixed and cantilevered pipes are fundamentally different, in terms of assumptions made, their derivation and their final structure. This and several other important points on this subject are clarified here.

2.2 SOME BASIC ASSUMPTIONS AND CONCEPTS

The system under consideration consists of a tubular beam of length L, internal cross-sectional area A, mass per unit length m and flexural rigidity EI, conveying a fluid of mass M per unit length with an axial velocity U, which may vary with time (Figure 2.1). The pipe is assumed to be initially lying along the X-axis (in the direction of gravity) and to oscillate in the (X, Y) plane.

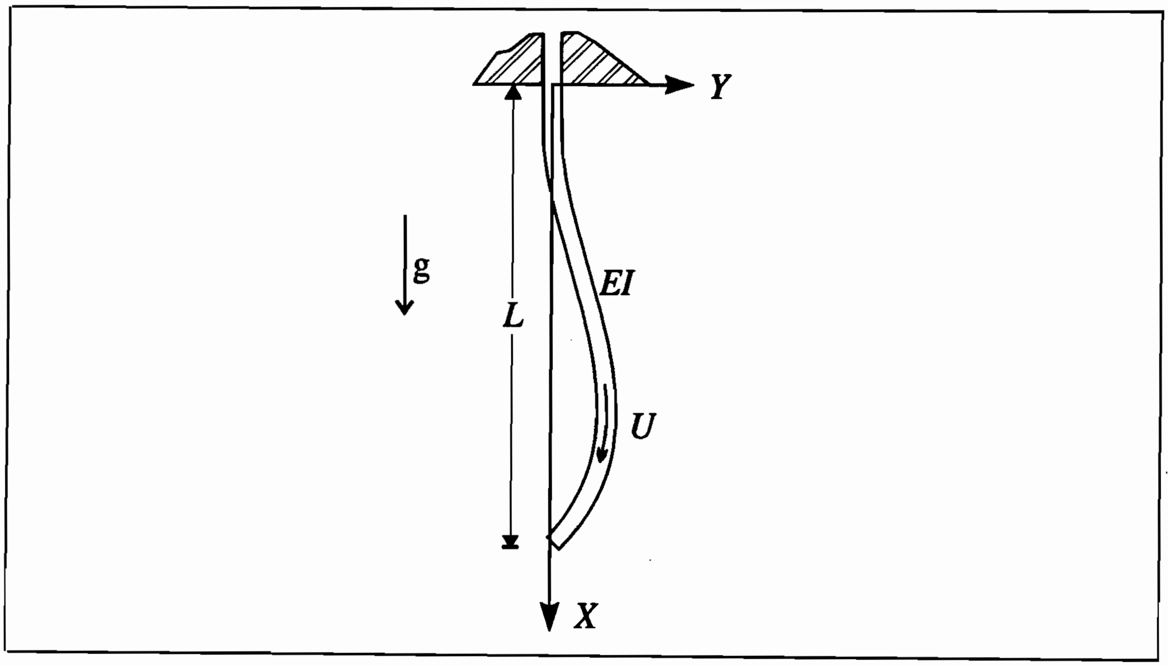

Figure 2.1: Schematic of the system.

The basic assumptions made for the pipe and the fluid are as follows: (i) the fluid is incompressible; (ii) the velocity profile of the fluid is uniform (plug-flow approximation for a turbulent-flow profile); (iii) the diameter of the pipe is small compared to its length, so that the pipe behaves like an Euler-Bernoulli beam; (iv) the motion is planar; (v) the deflections of the pipe are large, but the strains are small; (vi) rotatory inertia and shear deformation are neglected; (vii) *in the case of a cantilevered pipe*, the pipe centreline is inextensible.

2.2.1 Notation and coordinate systems

In order to correctly define some intermediate physical quantities, essential for deriving the nonlinear governing equations (nonlinear curvature for example), some words concerning the choice of the coordinates may be useful. In continuum mechanics, to describe the position of material points, one usually has the choice between two sets of coordinate systems: one for the undeformed body (Lagrangian coordinates) and another for the deformed body (Eulerian coordinates). The deformation of a point is described by the relation of the coordinates of the same material point in the undeformed and deformed states (Eringen 1987). Let (X, Y, Z) represent the position of a material point P in its original state, and (x, y, z) the position of the same material point in the deformed state. Then, the displacement of that material point is defined as $u = x - X$, $v = y - Y$ and $w = z - Z$ (Figure 2.2); these may be expressed wholly in either set of coordinates. Other quantities, such as the deformation gradients and strain tensors, can also be expressed in either set of coordinates, and hence the problem may be formulated in terms of one or the other coordinate system. In infinitesimal deformation theory, the distinction between the Lagrangian and Eulerian strains disappears (Eringen 1987); however, this distinction must absolutely be made when nonlinear relationships are sought.

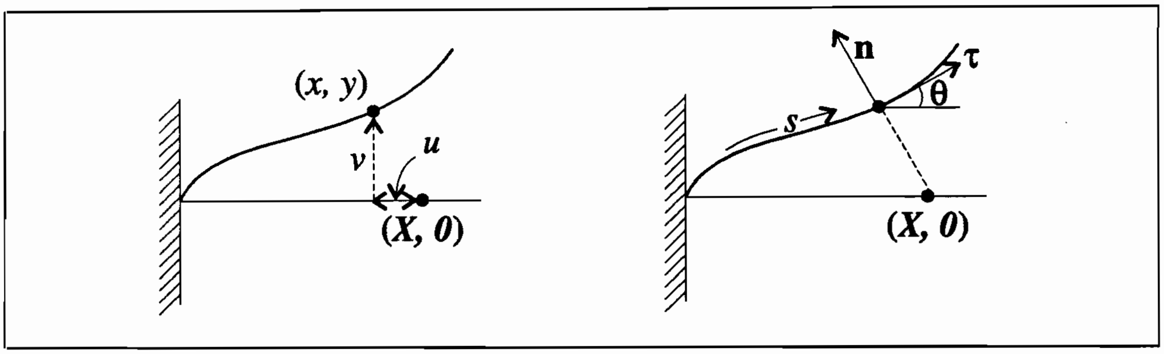

Figure 2.2: Coordinate systems for the physical system.

For a slender pipe with its initially undeformed state along the X-axis and undergoing motions in the (X, Y) plane, we have $Y = 0$, so that y is identical to the displacement v. Here, the Lagrangian representation is chosen, so that the coordinate of a point always refers to the undeformed body which is represented by X. However, when the pipe is inextensible, it is customary to introduce a curvilinear coordinate, s, along the centreline of the pipe (see Figure 2.2). In such a case, all other physical quantities and the final governing equation can be expressed in terms of (s, t).

2.2.2 Inextensibility condition

In the case of a *cantilevered pipe*, one may assume the pipe to be inextensible. This condition of inextensibility is very important and will thus be discussed in some detail.

Let P and Q be two distinct points in an elastic body, and P' and Q' be the same two material points after deformation. Denoting by ds_0 the distance between P and Q, and by ds that between P' and Q', then, by definition

$$\begin{aligned} (ds_0)^2 &= (dX)^2 + (dY)^2 , \\ (ds)^2 &= (dx)^2 + (dy)^2 ; \end{aligned}$$

hence the relative change of this distance is obtained from

$$(ds)^2 - (ds_0)^2 = (dx)^2 + (dy)^2 - dX^2 - dY^2 . \tag{2.1}$$

For a pipe system initially lying along the X-axis and undergoing planar motions in the (X, Y) plane, equation (2.1) becomes

$$(ds)^2 - (ds_0)^2 = \left[\left(\frac{dx}{dX}\right)^2 + \left(\frac{dy}{dX}\right)^2 - 1\right](dX)^2 . \tag{2.2}$$

When the pipe is inextensible, $ds = ds_0$ by definition, and dX can be identified with ds, as they both represent an infinitesimal displacement of the *undeformed* body; hence,

$$\left(\frac{\partial x}{\partial X}\right)^2 + \left(\frac{\partial y}{\partial X}\right)^2 = 1 . \tag{2.3}$$

The inextensibility condition can also be expressed in terms of the displacement components (u, v) as follows:

$$\left(1 + \frac{\partial u}{\partial X}\right)^2 + \left(\frac{\partial v}{\partial X}\right)^2 = 1 . \tag{2.4}$$

For a pipe *fixed at both ends*, however, dX and ds are no longer identically equal; by using equation (2.2) and defining ε as the axial strain along the centreline of the pipe, one may nevertheless still relate one to the other through the condition

$$\frac{\partial X}{\partial s} = \frac{1}{1+\varepsilon} , \tag{2.5}$$

with

$$1 + \varepsilon(X) = \sqrt{\left(1 + \frac{\partial u}{\partial X}\right)^2 + \left(\frac{\partial v}{\partial X}\right)^2} .$$

Hence, $\varepsilon = 0$ for an inextensible pipe, and generally $\varepsilon \neq 0$ for a pipe fixed at both ends.

2.2.3 Expression for curvature

An exact expression for the curvature, κ, is useful in the derivations that follow, and is thus presented here. Depending on the choice of the coordinate system and the assumptions concerning the inextensibility of the pipe, the expression for κ varies.

Let θ be the angle between the position of the pipe and the X-axis (Figure 2.2) and s the curvilinear coordinate along the pipe. For a pipe undergoing a planar motion, extensible or inextensible, the curvature is given by

$$\kappa = \frac{\partial \theta}{\partial s} \,. \tag{2.6}$$

For simply supported pipes, θ is defined by

$$\cos\theta = \frac{1 + \partial u/\partial X}{1 + \varepsilon\,(X)} \,, \qquad \sin\theta = \frac{\partial v/\partial X}{1 + \varepsilon\,(X)} \,. \tag{2.7}$$

In terms of the X-coordinate, equation (2.6) becomes

$$\kappa = \frac{\partial \theta}{\partial X}\,\frac{\partial X}{\partial s} = \frac{1}{1+\varepsilon}\,\frac{\partial \theta}{\partial X} \,. \tag{2.8}$$

The derivative in the above expression may be obtained from (2.7),

$$\frac{\partial \theta}{\partial X} = \frac{\dfrac{\partial^2 v}{\partial X^2}\left(1 + \dfrac{\partial u}{\partial X}\right) - \dfrac{\partial v}{\partial X}\dfrac{\partial^2 u}{\partial X^2}}{(1+\varepsilon)^2} \,, \tag{2.9}$$

thus, yielding the curvature (2.8) for pipes whose centreline may be extensible.

On the other hand, for cantilevered pipes whose centreline is assumed inextensible, expressions (2.6) and (2.7) still hold, except that $\varepsilon = 0$. In this case, $s = X$, and hence $\partial\theta/\partial X$ becomes

$$\frac{\partial \theta}{\partial X} = \frac{\partial x}{\partial s}\,\frac{\partial^2 y}{\partial s^2} - \frac{\partial y}{\partial s}\,\frac{\partial^2 x}{\partial s^2} \,. \tag{2.10}$$

Application of the inextensibility condition (2.3) leads to the following expression of the curvature

$$\kappa = \frac{\partial^2 y/\partial s^2}{\sqrt{1 - (\partial y/\partial s)^2}} \,. \tag{2.11}$$

Alternatively, the curvature may also be defined as a vector,

$$\mathbf{b} = \frac{\partial^2\,\mathbf{r}}{\partial s^2} \equiv \kappa\,\mathbf{n} \,,$$

where $\mathbf{n}$ is the normal unit vector which is always perpendicular to the tangent direction of the pipe and $\mathbf{r} = (x, y)$ is the position vector along the pipe. Hence,

$$\kappa = \left|\frac{\partial^2 \mathbf{r}}{\partial s^2}\right| = \sqrt{\left(\frac{\partial^2 x}{\partial s^2}\right)^2 + \left(\frac{\partial^2 y}{\partial s^2}\right)^2} \,.$$

If the inextensibility condition is once again applied to the expression above, one obtains an expression identical to (2.11).

Note that for a curve defined by $y(x)$ (Eulerian description) rather than $y(s)$, one has the familiar expression of curvature,

$$\kappa = \frac{\partial^2 y/\partial x^2}{\left[1 + (\partial y/\partial x)^2\right]^{3/2}} \, . \tag{2.12}$$

Care must be taken as to which expression of κ is used, depending on the physical problem.

2.3 EQUATIONS OF MOTION BASED ON THE ENERGY METHOD

2.3.1 Introduction

2.3.1.1 Hamilton's principle

The energy method is based on Hamilton's principle, written usually as

$$\delta \int_{t_1}^{t_2} \mathcal{L}\, \mathrm{d}t + \int_{t_1}^{t_2} \delta\, \mathcal{W}\, \mathrm{d}t = 0\, , \tag{2.13}$$

where $\mathcal{L}$ is the Lagrangian of the system ($\mathcal{L} = \mathcal{T}_F + \mathcal{T}_P - \mathcal{V}_F - \mathcal{V}_P$, $\mathcal{T}_P$ and $\mathcal{V}_P$ being the kinetic and potential energies associated with the pipe, and $\mathcal{T}_F$ and $\mathcal{V}_F$ the corresponding quantities for the enclosed fluid), and $\delta\mathcal{W}$ is the virtual work due to nonconservative forces not included in the Lagrangian.

Even if there are no explicit external forces applied to the pipe conveying fluid, $\delta\mathcal{W}$ in equation (2.13) would not vanish if one or both ends of the pipe were not fixed. For example, for a cantilevered pipe which discharges fluid at its free end, the fluid does transfer energy to the pipe due to motion at the free end. The virtual work done by the discharged fluid is thus equal to the product of the virtual displacement and the change of momentum of the fluid. In this case, statement (2.13) may be written as

$$\delta \int_{t_1}^{t_2} \mathcal{L}\, \mathrm{d}t = \int_{t_1}^{t_2} \left[MU \left(\frac{\partial \mathbf{r}_L}{\partial t} + U\, \boldsymbol{\tau}_L \right) \cdot \delta\, \mathbf{r}_L \right] \mathrm{d}t\, , \tag{2.14}$$

where $\mathbf{r}_L$ and $\boldsymbol{\tau}_L$ represent, respectively, the position vector and the tangential unit vector at the end of the pipe. This was done by Benjamin (1961) for an Euler-Bernoulli beam conveying fluid. It was also rederived in a more general way by McIver (1973) who considered, more generally, systems of changing mass.

As was elucidated by Benjamin (1961), the right-hand term of (2.14) is also directly related to the mechanism of instability; indeed, he proved that

$$\Delta W = -\int_0^T MU\left(\dot{r}_L^2 + U\,\boldsymbol{\tau}_L \cdot \dot{\mathbf{r}}_L\right)\mathrm{d}t$$

represents the energy gained by the pipe in a period T. If the pipe is fixed at both ends, then $\Delta W = 0$, and the system is conservative; however, if one end is free to move, then $\Delta W \neq 0$ and the system becomes nonconservative (Païdoussis 1970). In the latter case, when U is small enough, it is clear that $\Delta W < 0$, which means that the system is stable (effect of the Coriolis force). However, for positive and sufficiently large U, ΔW could become positive, i.e. energy might be extracted from the flow, and the system would thus become unstable.

As discussed by Benjamin (1961), the operative force responsible for loss of stability (by divergence) of a pipe with both ends supported is the centrifugal (or compressive) force, proportional to MU^2. On the other hand, for cantilevered pipes, which lose stability by flutter (Hopf bifurcation), both centrifugal and Coriolis forces, the latter proportional to MU, are involved. In what follows, special attention is paid to the provenance of the centrifugal terms.

2.3.1.2 Order of magnitude considerations

Although the deflection of the pipe can be considered to be large, only cubic nonlinear terms will be retained in the final equations; thus, an order of magnitude analysis will be useful. For planar motions, the lateral displacement may be supposed to be "small", relative to the length of the pipe, i.e.

$$y = v \sim \mathcal{O}(\epsilon)\,, \tag{2.15}$$

where $\epsilon \ll 1$. Large motions imply that terms of higher order than the linear ones have to be kept in the equation. Consequently, and because of the symmetry of the system itself, the nonlinear equations will necessarily be of odd order, which means that terms of $\mathcal{O}(\epsilon^3)$ have to be present in the equations. However, the variational technique always requires one order higher than the one sought, so that all expressions under the integrand in statement (2.14) have to be at least of $\mathcal{O}(\epsilon^4)$. Therefore, the various expressions, $\mathcal{V}$ and $\mathcal{T}$ for example, have to be exact to $\mathcal{O}(\epsilon^4)$ before any simplification is undertaken.

By applying the inextensibility condition, one can easily see that the longitudinal displacement u is

$$u \sim \mathcal{O}(\epsilon^2)\,, \tag{2.16}$$

i.e., one order higher than v.

2.3.1.3 Kinetic and potential energies

The total kinetic energy of the system is the sum of the kinetic energy of the pipe, $\mathcal{T}_p$, plus the kinetic energy of the fluid, $\mathcal{T}_F$, defined by

$$\mathcal{T} = \mathcal{T}_P + \mathcal{T}_F = \frac{m}{2}\int_0^L V_P^2 \,\mathrm{d}X + \frac{M}{2}\int_0^L V_F^2 \,\mathrm{d}X\,. \tag{2.17}$$

The potential energy comprises gravitational and strain energy components. In general, the gravitational energy depends on the distribution of mass (Fung 1969), and is written as

$$\mathcal{G} = \int \rho\,\phi(\xi)\,dV\,,$$

where ϕ is the gravitational potential per unit mass; in a uniform gravitational field, it becomes

$$\mathcal{G} = \int \rho\,g\,\xi\,dV\,,$$

where g is the gravitational acceleration and ξ is a distance measured from a reference plane in a direction opposite to the gravitational field. Consequently, with the notation used in this paper,

$$\mathcal{G} = -(m+M)\,g\int_0^L x\,\mathrm{d}X\,. \tag{2.18}$$

It is very important to define an exact form of the strain energy in the case of large deflections, correct to $\mathcal{O}(\epsilon^4)$. This problem was solved by Stoker (1968), with only one major (but not drastic) assumption: the strain is small even though the deflection can be large. His analysis finally led to

$$\mathcal{V} = \frac{E}{2} \int_0^L \left[A\,\varepsilon^2 + I(1+\varepsilon)^2\,\kappa^2\right] \mathrm{d}X\,, \tag{2.19}$$

where X represents the Lagrangian coordinate, A the cross-sectional area, I the moment of inertia and ε the axial strain.

2.3.1.4 Relationship between δx and δy

Finally, a relationship between the virtual displacement δx and δy is derived, which is necessary in the process of carrying out the variational analysis in the case of a cantilevered pipe. By applying the variational operator δ to the inextensibility condition, one obtains

$$\delta x' = -\frac{y'\,\delta y'}{\sqrt{1-y'^2}} = -y'\left(1+\tfrac{1}{2}\,y'^2\right)\delta y' + \mathcal{O}(\epsilon^4)\,;$$

hence,

$$\delta x = -\int_0^s \left[y'\,\delta y' + \tfrac{1}{2}\,y'^3\,\delta y'\right] \mathrm{d}s\,. \tag{2.20}$$

After integrating the right-hand side of (2.20) by parts and noting that $\delta y = 0$ at $s = 0$, one obtains

$$\delta x = -\left(y' + \tfrac{1}{2}\,y'^3\right)\delta y + \int_0^s \left(y'' + \tfrac{3}{2}\,y'^2\,y''\right)\delta y\;\mathrm{d}s + \mathcal{O}(\epsilon^4)\,. \tag{2.21}$$

One can also prove quite easily that (Appendix A)

$$\int_0^L g(s)\left(\int_0^s f(s)\,\delta y\,\mathrm{d}s\right)\mathrm{d}s = \int_0^L \left(\int_s^L g(s)\,\mathrm{d}s\right) f(s)\,\delta y\,\mathrm{d}s\,. \tag{2.22}$$

Equation (2.22) is important, since terms of that form will arise from (2.21) in the process of relating δx to δy.

2.3.2 The equation of motion for a cantilevered pipe

In this subsection, kinetic and potential energies are first derived for a cantilevered pipe conveying fluid. Then, variational procedures are employed in conjunction with equation (2.14) to yield the governing differential equation of motion.

2.3.2.1 Kinetic energy

Consider a small segment of the pipe and the fluid. By definition, the velocity of the pipe element is

$$\mathbf{V}_P = \frac{\partial \mathbf{r}}{\partial t} = \dot{x}\,\mathbf{i} + \dot{y}\,\mathbf{j}\,, \tag{2.23}$$

and the velocity of the fluid element is

$$\mathbf{V}_F = \mathbf{V}_P + U\,\boldsymbol{\tau}\,,$$

where $U\,\boldsymbol{\tau}$ is the relative velocity of the fluid element with respect to the pipe element, $\boldsymbol{\tau}$ being the unit vector along s. For the cantilevered pipe, where the inextensibility condition is assumed to hold true, $\boldsymbol{\tau}$ has the form

$$\boldsymbol{\tau} = \frac{\partial x}{\partial s}\mathbf{i} + \frac{\partial y}{\partial s}\mathbf{j}\,.$$

Consequently,

$$\mathbf{V}_F = \left(\frac{\partial}{\partial t} + U\,\frac{\partial}{\partial s}\right)(x\mathbf{i} + y\mathbf{j}) \equiv \frac{D\mathbf{r}}{Dt}\,, \tag{2.24}$$

where D/Dt is the material derivative of the fluid element. By analogy, the accelerations of the pipe and of the fluid are, respectively,

$$\mathbf{a}_P = \frac{\partial^2 \mathbf{r}}{\partial t^2}\,, \quad \mathbf{a}_F = \frac{D^2 \mathbf{r}}{Dt^2}\,. \tag{2.25}$$

Hence, the total kinetic energy, $\mathcal{T}$, may be written as

$$\mathcal{T} = \frac{m}{2}\int_0^L (\dot{x}^2 + \dot{y}^2)\,\mathrm{d}s + \frac{M}{2}\int_0^L \left[(\dot{x} + U\,x')^2 + (\dot{y} + U\,y')^2\right]\mathrm{d}s\,. \tag{2.26}$$

where the dots and primes denote $\partial(\;)/\partial t$ and $\partial(\;)/\partial s$, respectively.

One important remark that ought to be made is that no variable term proportional to U^2 arises from the above expression since, by expanding the integrand and by virtue of the inextensibility condition, one obtains only a constant term:

$$U^2\, x'^2 + U^2\, y'^2 = U^2\,.$$

This illustrates the importance of the right-hand side of statement (2.14), which will provide both linear and nonlinear components of the centrifugal force proportional to MU^2.

The variational operations on $\mathcal{T}$ lead to

$$\begin{aligned}\delta \int_{t_1}^{t_2} \mathcal{T}\,\mathrm{d}t = \quad & m \int\!\!\int (\dot{x}\,\delta\dot{x} + \dot{y}\,\delta\dot{y})\,\mathrm{d}s\,\mathrm{d}t + M \int\!\!\int [(\dot{x} + U\,x')(\delta\dot{x} + U\,\delta x') \\ & + (\dot{y} + Uy')(\delta\dot{y} + U\,\delta y')]\;\mathrm{d}s\,\mathrm{d}t\,.\end{aligned}$$

Integrating by parts and noting that $x'\,\delta x' + y'\,\delta y' = 0$, one obtains

$$\begin{aligned}\delta \int_{t_1}^{t_2} \mathcal{T}\,\mathrm{d}t = & - \int\!\!\int \left[(m+M)\ddot{x} + M\,\dot{U}\,x' + 2\,MU\,\dot{x}'\right]\delta x\,\mathrm{d}s\,\mathrm{d}t \\ & - \int\!\!\int \left[(m+M)\ddot{y} + M\,\dot{U}\,y' + 2\,MU\,\dot{y}'\right]\delta y\,\mathrm{d}s\,\mathrm{d}t \\ & + \; MU \int_{t_1}^{t_2} [\dot{x}_L\,\delta x_L + \dot{y}_L\,\delta y_L]\,\mathrm{d}t\,,\end{aligned} \tag{2.27}$$

where $x_L = x(L)$, $y_L = y(L)$ are the displacements of the free end of the pipe. The limits for the double integrals, although not explicitly written, are understood to be from 0 to L for s, and from t_1 to t_2 for t.

2.3.2.2 Potential energy

In this case, two components have to be derived. Considering first the strain energy expression (2.19) with $\varepsilon = 0$, one can write

$$\delta \int_{t_1}^{t_2} \mathcal{V}\,\mathrm{d}t = \frac{EI}{2} \int\!\!\int \delta\,(\kappa^2)\,\mathrm{d}s\,\mathrm{d}t\,.$$

Utilization of the curvature expression (2.11) leads to

$$\begin{aligned}\delta \int_{t_1}^{t_2} \mathcal{V}\,\mathrm{d}t &= \frac{EI}{2}\int\int \delta\left(y''^2(1+y'^2)\right)\mathrm{d}s\mathrm{d}t + \mathcal{O}(\epsilon^5)\\ &= EI\int\int\left[(y''+y''\,y'^2)''-(y''^2\,y')'\right]\delta y\;\mathrm{d}s\mathrm{d}t + \mathcal{O}(\epsilon^5)\\ &= EI\int\int\left[y''''+4y'\,y''\,y'''+y''^3+y''''\,y'^2\right]\delta y\;\mathrm{d}s\mathrm{d}t + \mathcal{O}(\epsilon^5).\end{aligned} \tag{2.28}$$

Similarly, by the use of equations (2.21) and (2.22), the variational of the gravitational energy (2.18),

$$\delta \int_{t_1}^{t_2} \mathcal{G}\mathrm{d}t = -(m+M)g\int\int\left[-\left(y'+\tfrac{1}{2}\,y'^3\right)\delta y+(L-s)\left(y''+\tfrac{3}{2}\,y''\,y'^2\right)\delta y\right]\mathrm{d}s\mathrm{d}t+\mathcal{O}(\epsilon^5) \tag{2.29}$$

is obtained.

2.3.2.3 The nonconservative forces

Application of the variational procedure to the right-hand side (rhs) of Hamilton's principle leads to

$$\begin{aligned}\text{rhs} &= MU\int_{t_1}^{t_2}\left[(\dot{x}_L+U\,x'_L)\,\delta x_L+(\dot{y}_L+U\,y'_L)\delta y_L\right]\mathrm{d}t\\ &= MU\int_{t_1}^{t_2}(\dot{x}_L\,\delta x_L+\dot{y}_L\,\delta y_L)\,\mathrm{d}t+MU^2\int_{t_1}^{t_2}(x'_L\,\delta x_L+y'_L\,\delta y_L)\,\mathrm{d}t\\ &= A+B\,.\end{aligned} \tag{2.30}$$

The first term, A, cancels the last term in equation (2.27), while, with the use of equations (2.3) and (2.21), B is found to be

$$B = MU^2\int\int\left[y''+y'^2\,y''-y''\int_s^L(y'\,y'')\mathrm{d}s\right]\delta y\;\mathrm{d}s\mathrm{d}t\,, \tag{2.31}$$

and hence contributes all the centrifugal-force terms.

2.3.2.4 The final equation of motion

After many transformations and manipulations, the general equation of motion is found to be

$$
\begin{aligned}
& (m+M)\,\ddot{y} + 2\,MU\,\dot{y}'(1+y'^2) + (m+M)\,g\,y'\left(1+\tfrac{1}{2}\,y'^2\right) \\
+ \;& y''\left[MU^2\left(1+y'^2\right) + \left(M\dot{U} - (m+M)\,g\right)(L-s)\left(1+\tfrac{3}{2}\,y'^2\right)\right] \\
+ \;& EI\left[y''''(1+y'^2) + 4\,y'\,y''\,y''' + y''^3\right] \\
- \;& y''\left[\int_s^L \int_0^s (m+M)(\dot{y}'^2 + y'\,\ddot{y}')\,\mathrm{d}s\,\mathrm{d}s\right. \\
& \qquad \left. + \int_s^L \left(\tfrac{1}{2}M\dot{U}\,y'^2 + 2MU\,y'\,\dot{y}' + MU^2\,y'\,y''\right)\mathrm{d}s\right] \\
+ \;& y' \int_0^s (m+M)(\dot{y}'^2 + y'\,\ddot{y}')\,\mathrm{d}s = 0\,.
\end{aligned}
\tag{2.32}
$$

This equation will be discussed in detail after it has been derived by the force balance method.

2.3.3 The equation of motion for a pipe fixed at both ends

Here, as the inextensibility condition can no longer be applied, two equations are necessary: one in the x- and the other in the y-direction. Moreover, since both ends of the pipe are fixed, the right-hand side of expression (2.14) is now zero; hence, Hamilton's principle simply becomes

$$\delta \int_{t_1}^{t_2} \mathcal{L}\,\mathrm{d}t = 0\,.$$

2.3.3.1 Kinetic energy

As the right-hand side in the statement of Hamilton's principle vanishes for a pipe fixed at both ends, it is clear that the contribution of the fluid forces is not the same as in the case of the cantilevered pipe. Hence, the derivation of the kinetic energy is very important. Although the inextensibility condition is no longer true, one basic assumption still holds — the incompressibility of the fluid.

When a bar is subjected to tension, the axial elongation is accompanied by a lateral contraction. Within the elastic range, the Poisson ratio ν is constant (Timoshenko & Gere 1961) and, for rubber-like materials, $\nu \simeq 0.5$. In the case where only a uniaxial load is applied to an elastic body, the change of unit volume is proportional to $1 - 2\,\nu$. Consequently, for rubber-like materials, the volume change due to uniaxial stress can be considered zero, i.e., they are incompressible. In the case of a pipe, this conservation of volume leads, for any initial volume of length dX, to

$$dX\, S_0 = dX(1+\varepsilon)\, S_1,$$

where S_1 represents the cross-sectional area of the pipe after elongation. For the incompressible fluid inside the pipe, one also has

$$U_0\, S_0 = U_1\, S_1,$$

with U_0 and U_1 being the flow velocities before and after elongation. Thus,

$$U_1(X) = U_0\,(S_0/S_1) = U_0\,(1+\varepsilon)\,. \tag{2.33}$$

This shows that the ***velocity of the fluid with respect to the pipe is no longer constant.*** Hence, the absolute velocity is

$$\begin{aligned} \mathbf{V}_F &= \mathbf{V}_P + U(X)\,\boldsymbol{\tau} \\ &= (\dot{x}\,\mathbf{i} + \dot{y}\,\mathbf{j}) + U(1+\varepsilon)\left(\frac{x'}{1+\varepsilon}\,\mathbf{i} + \frac{y'}{1+\varepsilon}\,\mathbf{j}\right), \end{aligned}$$

where the prime denotes the derivative with respect to X. Consequently,

$$\mathbf{V}_F = \left(\frac{\partial}{\partial t} + U\,\frac{\partial}{\partial X}\right)\mathbf{r}\,. \tag{2.34}$$

Relationship (2.24) derived for the case of the cantilevered pipe still holds, with the difference that the inextensibility condition is not valid here, so that U^2 terms in this case survive in the kinetic energy and are therefore not associated with the right-hand side of (2.14). The total kinetic energy is given by

$$\mathcal{T} = \frac{m}{2}\int_0^L (\dot{u}^2 + \dot{v}^2)\mathrm{d}X + \frac{M}{2}\int_0^L \left[(\dot{u} + U(1+u'))^2 + (\dot{v} + U\,v')^2\right]\mathrm{d}X\,. \tag{2.35}$$

For the case of non-rubber like materials ($\nu \neq 0.5$), some additional words are necessary. The change of volume is no longer equal to zero, and $S_0/S_1 = 1/(1 - 2\,\nu\,\varepsilon)$.

The fluid being incompressible, one obtains

$$\begin{aligned} U(X) &= U_0\,(1 + 2\,\nu\,\varepsilon) \\ &= U_0(1+\varepsilon) + U_0\,\varepsilon\,(2\,\nu - 1) \\ &= U_1(X) + U_0\,\varepsilon\,(2\,\nu - 1)\,, \end{aligned}$$

i.e.

$$[U(X) - U_1(X)]\,/U_0 = \varepsilon\,(2\,\nu - 1)\,. \tag{2.36}$$

To fourth order, the strain ε is given by

$$\varepsilon = u' + \tfrac{1}{2}\,v'^2 + \mathcal{O}(\epsilon^4)\,, \tag{2.37}$$

so that for a pipe of length $L = 1$, with $|u| \sim 0.01$, and $|v| \sim 0.1$, one obtains $|\epsilon| < 1.5 \times 10^{-2}$. For $\nu = 0.4$, the error in the flow velocity is 0.3% which is of same order of magnitude as the error made by assuming the velocity profile to be uniform. Hence, equation (2.35) may still be considered valid.

2.3.3.2 Potential energy component

Again, the potential energy comprises two components. To derive the strain energy, the axial strain is itself decomposed into two components: a steady-state strain due to an externally applied tension T_0 and pressurization P, and an oscillatory strain due to pipe oscillation. By reference to equation (2.19), this strain energy may be expressed as

$$\mathcal{V} = \frac{EA}{2}\int_0^L \left(\frac{T_0 - P}{EA} + \varepsilon\right)^2 \mathrm{d}X + \frac{EI}{2}\int_0^L (1+\varepsilon)^2\,\kappa^2\,\mathrm{d}X\,.$$

By using (2.8), this can be simplified to

$$\mathcal{V} = \frac{EA}{2}\int_0^L \left(\frac{T_0 - P}{EA} + \varepsilon\right)^2 \mathrm{d}X + \frac{EI}{2}\int_0^L \left(\frac{\partial\theta}{\partial X}\right)^2 \mathrm{d}X\,. \tag{2.38}$$

Recalling that $u \sim \mathcal{O}(\epsilon^2)$, $v \sim \mathcal{O}(\epsilon)$, and using (2.9),

$$(\partial\theta/\partial X)^2 = v''^2 - 2\,v''^2\,u' - 2\,v''^2\,v'^2 - 2\,v'\,v''\,u'' + \mathcal{O}(\epsilon^5)$$

is obtained. Moreover, ε is given by equation (2.37).

The expression for gravitational energy is the same as in the case of the cantilevered pipe, i.e.

$$\mathcal{G} = -(m+M)\,g \int_0^L (X+u)\mathrm{d}X\,. \tag{2.39}$$

2.3.3.3 Final equation

Variational techniques are applied again, with two independent variants, δu and δv. After many integrations by parts, one finally obtains

$$\begin{aligned}(m+M)\,\ddot{u} + M\dot{U} \;&+\; 2\,MU\,\dot{u}' + MU^2\,u'' + M\dot{U}\,u' - EAu'' \\ -EI(v''''\,v' + v''\,v''') \;&+\; (T_0 - P - EA)v'\,v'' - (m+M)g = 0\,,\end{aligned} \tag{2.40a}$$

$$\begin{aligned}&(m+M)\ddot{v} + M\dot{U}\,v' + 2\,MU\,\dot{v}' + MU^2\,v'' - (T_0 - P)v'' + EI\,v'''' \\ &\quad-\;\; EI\left(3\,u'''\,v'' + 4\,u''\,v''' + 2\,u'\,v'''' + v'\,u'''' + 2\,v'^2\,v'''' + 8\,v'\,v''\,v''' + 2\,v''^3\right) \\ &\quad+\;\; (T_0 - P - EA)\left(u''\,v' + u'\,v'' + \tfrac{3}{2}\,v'^2\,v''\right) = 0\,,\end{aligned} \tag{2.40b}$$

where one now has two independent equations, instead of the one obtained for a cantilevered pipe.

2.3.4 Boundary conditions

Using variational methods, it is straightforward to derive boundary conditions for the different cases considered. For the cantilevered pipe, the boundary conditions are the same as for the linear case: $y(0) = y'(0)$ and $y''(L) = y'''(L) = 0$. For the pipe fixed at both ends, it is obvious that $u(0) = v(0) = u(L) = v(L) = 0$; in addition, if the pipe is simply supported, one obtains $v''(0) = v''(L) = 0$, while for the clamped-clamped pipe, $v'(0) = v'(L) = 0$. It is noted that only two boundary conditions are necessary for u.

2.4 EQUATIONS OF MOTION BASED ON THE FORCE BALANCE METHOD

2.4.1 Cantilevered pipe

This derivation is based on Lundgren's *et al.* (1979) work, but has been further developed into a single equation suitable for further analysis. It consists of equating the forces and moments acting on an element of the pipe.

Consider an element of the pipe of length ds (Figure 2.3). Let $\mathbf{Q}$ and $\mathbf{M}$ represent the resultant force and bending moment on the left cross section, and $\mathbf{Q} + \mathbf{dQ}$ and $\mathbf{M} + \mathbf{dM}$ on the right cross section. A force balance leads to

$$\frac{\partial \mathbf{Q}}{\partial s} + (m+M)\, g\, \mathbf{i} = m\, \frac{\partial^2 \mathbf{r}}{\partial t^2} + M\, \frac{D^2 \mathbf{r}}{D t^2}\,, \tag{2.41}$$

and a moment balance to

$$\frac{\partial \mathbf{M}}{\partial s} + \boldsymbol{\tau} \times \mathbf{Q} = 0\,. \tag{2.42}$$

As the effect of rotary motion is neglected, and due to the assumptions associated with Euler-Bernoulli beam theory, the following moment-curvature relation holds:

$$\mathbf{M} = EI\, \boldsymbol{\tau} \times \frac{\partial \boldsymbol{\tau}}{\partial s} = EI\, \boldsymbol{\tau} \times \boldsymbol{\kappa}\,. \tag{2.43}$$

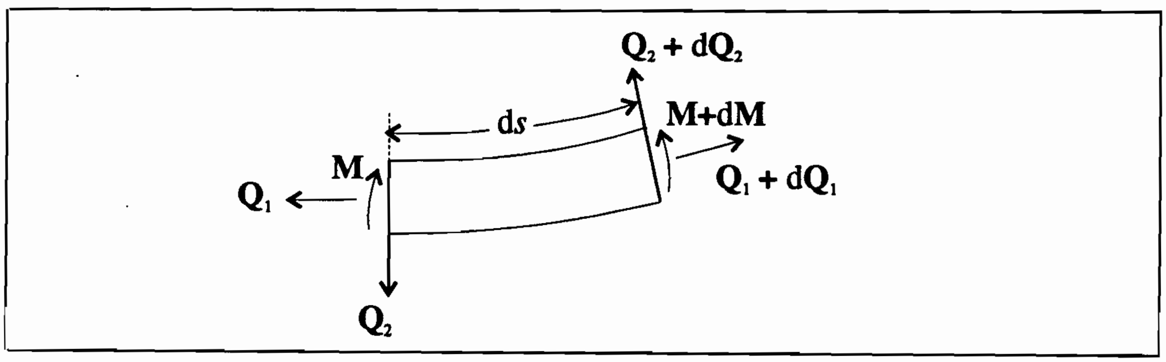

Figure 2.3: Free-body diagram of an element of the pipe; for clarity, velocity-dependent forces are not included.

Decomposing $\mathbf{Q}$ along $\boldsymbol{\tau}$ and $\mathbf{n}$ (Figure 2.2) gives

$$\mathbf{Q} = (T_0 - P)\,\boldsymbol{\tau} + \boldsymbol{\tau} \times \frac{\partial \mathbf{M}}{\partial s}\,, \tag{2.44}$$

where $(T_0 - P)$ is the axial force due to tension and fluid pressure. By combining (2.43) with (2.44) one obtains

$$\begin{aligned} \mathbf{Q} &= (T_0 - P)\,\boldsymbol{\tau} + EI\,\boldsymbol{\tau} \times \frac{\partial}{\partial s}\left(\boldsymbol{\tau} \times \frac{\partial \boldsymbol{\tau}}{\partial s}\right) \\ &= (T_0 - P)\,\boldsymbol{\tau} + EI\left[\left(\boldsymbol{\tau} \cdot \frac{\partial^2 \boldsymbol{\tau}}{\partial s^2}\right)\boldsymbol{\tau} - \frac{\partial^2 \boldsymbol{\tau}}{\partial s^2}\right]. \end{aligned} \tag{2.45}$$

After some further manipulations, involving the use of properties of $\boldsymbol{\tau}$ and its derivatives (Appendix B), and projecting along x and y, one obtains the following equations (corresponding to equations (2.17) and (2.18) in the paper by Lundgren's *et al.* (1979)):

$$(m+M)g - EI\,\frac{\partial^4 x}{\partial s^4} + \frac{\partial}{\partial s}\left[(T_0 - P - EI\,\kappa^2)\,\frac{\partial x}{\partial s}\right] = m\,\frac{\partial^2 x}{\partial t^2} + M\,\frac{D^2 x}{Dt^2}\,, \tag{2.46a}$$

$$-\,EI\,\frac{\partial^4 y}{\partial s^4} + \frac{\partial}{\partial s}\left[(T_0 - P - EI\,\kappa^2)\,\frac{\partial y}{\partial s}\right] = m\,\frac{\partial^2 y}{\partial t^2} + M\,\frac{D^2 y}{Dt^2}\,. \tag{2.46b}$$

These two equations are coupled through the curvature κ and the axial force $(T_0 - P)$. In order to derive a single equation of motion in terms of y, the first equation is integrated from s to L, divided by $\partial x/\partial s$ to yield $(T_0 - P - EI\,\kappa^2)$, and x is eliminated through the inextensibility condition. After many straightforward but tedious manipulations, one finally finds the same equation as that obtained by the energy method, equation (2.32). Note that, in this derivation, the terms need to be correct to $\mathcal{O}(\epsilon^3)$ only, and higher order terms have been neglected.

2.4.2 Pipe fixed at both ends

Equations (2.46a,b) and the results obtained from the derivation of the previous section are no longer valid for pipes fixed at both ends. The problem being planar, two equations in scalar form are derived. Recalling that the forces and moments are also defined in terms of the original coordinate X, equation (2.41) becomes

$$\frac{\partial \mathbf{Q}}{\partial X} + (M+m)\,g\,\mathbf{i} = m\,\frac{\partial^2 \mathbf{r}}{\partial t^2} + M\,\frac{D^2 \mathbf{r}}{Dt^2}\,, \tag{2.47}$$

where the material derivative is defined as in (2.34). By taking into account the force due to $(T_0 - P)$ and the extensibility of the pipe, the force $\mathbf{Q}$ may be expressed as

$$\mathbf{Q} = \mathbf{Q}_1 + \mathbf{Q}_2\,. \tag{2.48}$$

From expression (2.38), the axial force $\mathbf{Q}_1$ is

$$\mathbf{Q}_1 = (T_0 - P + EA\,\varepsilon)\,\boldsymbol{\tau}\,, \tag{2.49a}$$

while the shear force $\mathbf{Q}_2$, perpendicular to $\mathbf{Q}_1$, (see Figure 2.3) is given by

$$\mathbf{Q}_2 = -\frac{\partial M}{\partial s}\,\mathbf{n} = -\frac{1}{1+\varepsilon}\,\frac{\partial M}{\partial X}\,\mathbf{n}\,. \tag{2.49b}$$

As the effect of rotatory motion is neglected, the moment due to bending has a contribution only in the $\mathbf{n}$ direction. Moreover, the moment in its scalar form becomes simply

$$M = EI(1+\varepsilon)\,\frac{\partial \theta}{\partial s} = EI\,\frac{\partial \theta}{\partial X}. \tag{2.50}$$

Therefore, decomposing $\mathbf{Q}$ along $\boldsymbol{\tau}$ and $\mathbf{n}$, one obtains

$$\mathbf{Q} = \mathbf{Q}_1 + \mathbf{Q}_2 = (T_0 - P + EA\,\varepsilon)\,\boldsymbol{\tau} - \frac{EI}{1+\varepsilon}\,\frac{\partial^2 \theta}{\partial X^2}\,\mathbf{n}\,. \tag{2.51}$$

By decomposing these two components along the x and y direction, recalling the expressions of the accelerations obtained in (2.25), extending the results of (2.34) and introducing again the angle θ, one obtains

$$(m+M)g + \frac{\partial}{\partial X}(Q_1 \cos\theta) - \frac{\partial}{\partial X}(Q_2 \sin\theta) = m\,\frac{\partial^2 u}{\partial t^2} + M\,\frac{D^2(X+u)}{Dt^2} \tag{2.52a}$$

$$\frac{\partial}{\partial X}(Q_1 \sin\theta) + \frac{\partial}{\partial X}(Q_2 \cos\theta) = m\,\frac{\partial^2 v}{\partial t^2} + M\,\frac{D^2 v}{Dt^2}\,. \tag{2.52b}$$

where $\sin\theta$ and $\cos\theta$ are defined by (2.7).

Here, an order of magnitude analysis is useful, so as to simplify the algebra as much as possible. The first equation (in the X-direction) is of second order, and the second (in the Y-direction) of third order. Hence, all the terms have to be exact up to third order. For example,

$$\begin{aligned}
\sin\theta &= v'\left(1 - u' - \tfrac{1}{2}\,v'^2\right) + \mathcal{O}(\epsilon^4)\,, \\
\cos\theta &= 1 - \tfrac{1}{2}\,v'^2 + \mathcal{O}(\epsilon^4)\,, \\
\varepsilon &= u' + \tfrac{1}{2}\,v'^2 + \mathcal{O}(\epsilon^4)\,.
\end{aligned}$$

Finally, after some manipulations, the governing equations obtained are found to be the same as those derived by the energy method, equations (2.40a,b).

It can be shown that equations (2.52a,b) are equivalent to equations (2.46a,b) simply by letting $\varepsilon = 0$ and by replacing X by s. In other words, the equations of the cantilevered pipe can be obtained from the equations of a pipe fixed at both ends by imposing the inextensibility condition.

2.4.3 Dissipative terms

Dissipative terms have to be added to complete the equations. This can be done by assuming that the internal dissipation of the pipe material is viscoelastic and of the Kelvin-Voigt type (Snowdon 1968), i.e. that it is represented by

$$\sigma = E\,\varepsilon + E^*\,\dot{\varepsilon},$$

where σ is the stress and ε the strain. Following then the approach used by Stoker (1968), the strain energy is then modified, providing additional terms that can be written as

$$E \rightarrow E\left(1 + a\,\frac{\partial}{\partial t}\right)\,, \tag{2.53}$$

where a is the coefficient of Kelvin-Voigt damping in the material. Therefore, in equations (2.32) and (2.40a,b), EI may be replaced by $EI(1 + a\,\partial/\partial t)$ and EA by $EA(1 + a\,\partial/\partial t)$. Moreover, for reasons of simplicity, and because, in any case, the

Kelvin-Voigt dissipation is only an approximation, the dissipative terms are usually assumed to be linear.

The damping associated with frictional forces due to surrounding air is neglected.

2.5 DIMENSIONLESS EQUATIONS

2.5.1 Cantilevered pipe

Introducing next the same nondimensional quantities as in the linear case,

$$\begin{aligned} \xi = \frac{s}{L}, \quad \eta &= \frac{y}{L}, \quad \tau = \left(\frac{EI}{m+M}\right)^{\frac{1}{2}} \frac{t}{L^2}, \quad \alpha = \left(\frac{EI}{m+M}\right)^{1/2} \frac{a}{L^2}, \\ \mathcal{U} &= \left(\frac{M}{EI}\right)^{\frac{1}{2}} U\,L, \quad \gamma = \frac{m+M}{EI} L^3 g, \quad \beta = \frac{M}{m+M} \end{aligned} \tag{2.54}$$

one may rewrite equation (2.32), with (2.53) taken into account, in dimensionless form as follows:

$$\begin{aligned} \alpha\ \ & \dot\eta'''' + \eta'''' + \ddot\eta + 2\,\mathcal{U}\,\sqrt{\beta}\,\dot\eta'(1+\eta'^2) \\ + \ \ & \eta''\left[\mathcal{U}^2(1+\eta'^2) + \left(\dot{\mathcal{U}}\,\sqrt{\beta} - \gamma\right)(1-\xi)\left(1+\tfrac{3}{2}\,\eta'^2\right)\right] \\ + \ \ & \gamma\,\eta'\left(1+\tfrac{1}{2}\,\eta'^2\right) + \left(1+\alpha\,\frac{\partial}{\partial t}\right)\left[\eta''''\,\eta'^2 + 4\,\eta'\,\eta''\,\eta''' + \eta''^3\right] \\ - \ \ & \eta''\left[\int_\xi^1 \int_0^\xi (\dot\eta'^2 + \eta'\,\ddot\eta')\,\mathrm{d}\xi\,\mathrm{d}\xi + \int_\xi^1 \left(\tfrac{1}{2}\dot{\mathcal{U}}\sqrt{\beta}\,\eta'^2 + 2\,\mathcal{U}\,\sqrt{\beta}\,\eta'\,\dot\eta' + \mathcal{U}^2\,\eta'\,\eta''\right)\mathrm{d}\xi\right] \\ + \ \ & \eta' \int_0^\xi (\dot\eta'^2 + \eta'\,\ddot\eta')\,\mathrm{d}\xi = 0\,. \end{aligned} \tag{2.55}$$

Of particular interest is the appearance in (2.55) of some nonlinear inertial terms which render the equations non-standard and which create difficulties in its solution. In order to eventually obtain a solution by means of dynamical system theory, the nonlinear inertial terms must be eliminated or replaced. This can be accomplished through a perturbation technique. To this end, equation (2.55) is written as

$$L(\eta) + [N_1(\eta) + N_2(\eta)] = 0\,,$$

in which $L(\eta)$ represents the linear terms and N_i the nonlinear ones:

$$L(\eta) = \ddot{\eta} + 2\,\mathcal{U}\,\sqrt{\beta}\,\dot{\eta}' + \eta''\left[\mathcal{U}^2 + (\dot{\mathcal{U}}\,\sqrt{\beta} - \gamma)(1-\xi)\right] + \gamma\,\eta' + \eta'''' \,, \tag{2.56a}$$

$$\begin{aligned} N_1(\eta) \;&=\; 2\,\mathcal{U}\,\sqrt{\beta}\dot{\eta}'\,\eta'^2 + \eta''\left[\mathcal{U}^2 + \tfrac{3}{2}(\dot{\mathcal{U}}\,\sqrt{\beta} - \gamma)(1-\xi)\right]\eta'^2 \\ &\quad + \tfrac{1}{2}\gamma\eta'^3 + \eta''''\,\eta'^2 + 4\,\eta'\,\eta''\,\eta''' + \eta''^3 \,, \end{aligned} \tag{2.56b}$$

$$\begin{aligned} N_2(\eta) \;&=\; \eta' \int_0^\xi (\dot{\eta}'^2 + \eta'\,\ddot{\eta}')\mathrm{d}\xi - \eta''\left[\int_\xi^1 \int_0^\xi (\dot{\eta}'^2 + \eta'\,\ddot{\eta}')\mathrm{d}\xi\,\mathrm{d}\xi \right. \\ &\quad \left. + \int_\xi^1 \left(\tfrac{1}{2}\dot{\mathcal{U}}\,\sqrt{\beta}\,\eta'^2 + 2\,\mathcal{U}\,\sqrt{\beta}\,\eta'\,\dot{\eta}' + \mathcal{U}^2\,\eta'\,\eta''\right)\mathrm{d}\xi\right] \,, \end{aligned} \tag{2.56c}$$

in which, for simplicity, α is omitted for the present. Again, η corresponds to the lateral displacement divided by the length L and can therefore be assumed to be "small", i.e. $\eta \sim \mathcal{O}(\epsilon)$. Hence, in equations (2.56a,b,c), $L(\eta') \sim \mathcal{O}(\epsilon)$ and $N(\eta) \sim \mathcal{O}(\epsilon^3)$. $L(\eta)$ being linear, $L(\eta') = [L(\eta)]'$, so that

$$\int_0^\xi \eta'\,L(\eta')\,\mathrm{d}\xi = \mathcal{O}(\epsilon^2)\,. \tag{2.57}$$

Consequently, after some manipulations in (2.56a), one obtains

$$\begin{aligned} \int_0^\xi \eta'\,\ddot{\eta}'\,\mathrm{d}\xi = \;&-\; \int_0^\xi \left[2\,\mathcal{U}\,\sqrt{\beta}\,\eta'\,\dot{\eta}'' + \eta'\,\eta'''\left(\mathcal{U}^2 + (\dot{\mathcal{U}}\,\sqrt{\beta} - \gamma)(1-\xi)\right)\right. \\ &+\; \left.\eta'\,\eta''\,(2\,\gamma - \dot{\mathcal{U}}\,\sqrt{\beta} + \eta'\,\eta'''''\right]\mathrm{d}\xi + \mathcal{O}(\epsilon^2)\,. \end{aligned} \tag{2.58}$$

Integration of (2.58) from ξ to 1 yields the other nonlinear inertial term. The two nonlinear inertial terms are replaced in $N_2(\eta)$, to obtain, after some long but straightforward algebra,

$$\ddot{\eta} + 2\,\mathcal{U}\,\sqrt{\beta}\,\dot{\eta}' + \eta''\left(\mathcal{U}^2 + (\dot{\mathcal{U}}\,\sqrt{\beta} - \gamma)(1-\xi)\right) + \gamma\,\eta' + \eta'''' + N(\eta) = 0\,, \tag{2.59}$$

where

$$
\begin{aligned}
N(\eta) &= 2\mathcal{U}\sqrt{\beta}\,\dot{\eta}'\,\eta'^2 + \eta''\left[\mathcal{U}^2 + \tfrac{3}{2}(\dot{\mathcal{U}}\sqrt{\beta} - \gamma)(1-\xi)\right]\eta''^2 \\
&+ \tfrac{1}{2}(\dot{\mathcal{U}}\sqrt{\beta} - \gamma)\eta'^3 + 3\,\eta'\,\eta''\,\eta''' + \eta''^3 \\
&+ \eta' \int_0^\xi \left\{\dot{\eta}'^2 - 2\mathcal{U}\sqrt{\beta}\,\eta'\,\dot{\eta}'' - \eta'\,\eta'''\left[\mathcal{U}^2 + (\dot{\mathcal{U}}\sqrt{\beta} - \gamma)(1-\xi)\right] + \eta''\,\eta''''\right\} \mathrm{d}\xi \\
&- \eta'' \int_\xi^1 \int_0^\xi \left\{\dot{\eta}'^2 - 2\mathcal{U}\sqrt{\beta}\,\eta'\,\dot{\eta}'' - \eta'\,\eta'''\left[\mathcal{U}^2 + (\dot{\mathcal{U}}\sqrt{\beta} - \gamma)(1-\xi)\right]\right. \\
&\qquad\qquad\qquad \left. + \eta''\,\eta''''\right\} \mathrm{d}\xi\,\mathrm{d}\xi \\
&- \eta'' \int_\xi^1 \left\{(\dot{\mathcal{U}}\sqrt{\beta} - \gamma)\eta'^2 + 2\mathcal{U}\sqrt{\beta}\,\eta'\,\dot{\eta}' + \mathcal{U}^2\,\eta'\,\eta'' + \eta''\,\eta'''\right\} \mathrm{d}\xi\,. \qquad (2.60)
\end{aligned}
$$

Hence, the transformed nonlinear equation of motion is correct to $\mathcal{O}(\epsilon^3)$.

In physical terms, $\mathcal{U}$ in (2.55) is the nondimensional fluid velocity, γ represents the relative measure of gravity to flexural forces, and β is the ratio of the fluid mass to the total mass per unit length. For positive γ, the pipe is hanging downwards, while for negative γ, the pipe is "standing", with the free end above the fixed one.

2.5.2 Pipe fixed at both ends

In the case of a pipe with the two ends fixed, some additional nondimensional quantities have to be introduced, the dimensionless initial tension Π_0, flexibility Π_1 and initial pressure Π_2,

$$
\Pi_0 = \frac{T_0\,L^2}{EI}\,, \quad \Pi_1 = \frac{EA\,L^2}{EI}\,, \quad \Pi_2 = \frac{P\,L^2}{EI}\,. \qquad (2.61)
$$

Moreover, the lateral and longitudinal displacements are simply replaced by

$$
u \to \frac{u}{L}\,, \qquad v \to \frac{v}{L}\,.
$$

Thus, equations (2.40a,b) are written in dimensionless form as follows:

$$
\begin{aligned}
\ddot{u} &+ \dot{\mathcal{U}}\sqrt{\beta} + 2\mathcal{U}\sqrt{\beta}\,\dot{u}' + \mathcal{U}^2\,u'' + \dot{\mathcal{U}}\sqrt{\beta}\,u' - \Pi_1\,u'' \\
&- (v''''\,v' + v''\,v''') + (\Pi_0 - \Pi_1 - \Pi_2)v'\,v'' - \gamma = 0\,, \qquad (2.62a)
\end{aligned}
$$

$$
\begin{aligned}
&\ddot{v} + \dot{\mathcal{U}}\sqrt{\beta}\, v' + 2\,\mathcal{U}\sqrt{\beta}\,\dot{v}' + \mathcal{U}^2\, v'' - (\Pi_0 - \Pi_2) v'' + v'''' \\
&- \left[3\, u'''\, v'' + 4\, u''\, v''' + 2\, u'\, v'''' + v'\, u'''' + 2\, v'^2\, v'''' + 8\, v'\, v''\, v''' + 2\, v''^3\right] \\
&+ (\Pi_0 - \Pi_1 - \Pi_2)(u''\, v' + u'\, v'' + \tfrac{3}{2}\, v'^2\, v'') = 0\,. \qquad (2.62b)
\end{aligned}
$$

Note that the dissipative terms have been omitted for clarity, and that the nonlinear inertial terms are not present in the current form of the equations. In fact, the real penalty for the absence of nonlinear inertial terms is the additional equation governing the small axial motion of the pipe.

2.6 COMPARISON WITH PREVIOUS DERIVATIONS

In this section, the nonlinear equations of motion obtained by different researchers are described and compared in some detail. In order to get a more "comparable" set of equations, a standardization of the notation has been imposed.

2.6.1 Case of a cantileved pipe

2.6.1.1 Bourrières' work

This work is very original, all the more so since it was written in 1939 (Bourrières 1939). Bourrières studied the case of planar motion of two interacting strings, one of them moving with respect to the other. The pipe and the fluid represented by the strings are assumed to be inextensible, and the string representing the fluid is supposed to be infinitely flexible. Using the force balance method, Bourrières obtained the equations of motion of the tube and the fluid. The relationship between the shearing force Q and the bending moment M, together with the condition of inextensibility, provides the nonlinear terms. Seven equations with nine parameters were obtained, two of which are independent, with coordinate s and time t as two independent variables. After some algebraic manipulations, Bourrières eliminated the fluid friction force and found the following five equations:

$$
\begin{aligned}
((\Theta &+ T)x')' - (Qy')' - (m+M)\ddot{x} - 2\,M\,U\,\dot{x}' - M\,U^2\,x'' = 0\,,\\
((\Theta &+ T)y')' - (Qx')' - (m+M)\ddot{y} - 2\,M\,U\,\dot{y}' - M\,U^2\,y'' = 0\,,\\
x'^2 &+ y'^2 = 1\,,\\
Q &= -M'\,,\\
M &= EI(x'\,y'' - y'\,x'')\,,
\end{aligned}
\tag{2.63}
$$

where Θ and T represent the tension in the tube and in the fluid, respectively, and $()' = \partial()/\partial s$.

Bourrières considered only the linear case for his study. However, his approach, if carried out far enough, would have led him eventually to expressions similar to those derived in Section 2.3. Consequently, without approximation, the only difference between the equations derived here and (2.63) lies in the $\mathrm{d}U/\mathrm{d}t$ term, which is not surprising, since Bourrières had not taken into account any effect of unsteadiness in the flow. The expression for Q and M is correct, as well as the expression of the curvature. That makes Bourrières' work irreproachable.

The remaining task is to combine all the five equations of (2.63) into one, and to compare it with equation (2.55). This will not be done here since it has effectively already been done by Rousselet & Herrmann (1981).

2.6.1.2 Rousselet and Herrmann's work

Rousselet & Herrmann (1981) derived the equations of motion in two different ways: by the force balance method and the energy method. They obtained a set of equations, fairly close to the one found in Section 2.3, but with some minor differences.

Their first method follows closely Bourrières' work, and thus, it is not surprising to find equations which are very similar to (2.63). Two differences are simply due to the addition of gravity forces and the assumption that unsteady flow velocity effects may be present.

Considering an element of the system (Figure 2.3), the application of Newton's law led to

$$
\begin{aligned}
\frac{\partial}{\partial s} & \quad [(T-P)\cos\theta] - \frac{\partial}{\partial s}(Q\,\sin\theta) + (m+M)g \\
= & \quad (m+M)\,\frac{\partial^2 x}{\partial t^2} + M\,\dot{U}\,\cos\theta - \frac{M\,U^2}{R}\,\sin\theta - 2\,M\,U\,\frac{\mathrm{d}\theta}{\mathrm{d}t}\,\sin\theta\,, \qquad (2.64a)
\end{aligned}
$$

$$
\begin{aligned}
\frac{\partial}{\partial s} & \quad [(T-P)\sin\theta] + \frac{\partial}{\partial s}(Q\,\cos\theta) \\
= & \quad (m+M)\,\frac{\partial^2 y}{\partial t^2} + 2\,M\,U\,\frac{\mathrm{d}\theta}{\mathrm{d}t}\,\cos\theta + \frac{M\,U^2}{R}\,\cos\theta + M\,\dot{U}\,\sin\theta\,. \qquad (2.64b)
\end{aligned}
$$

In these equations, $(T-P)$ represents the tangential forces and Q the shear force, and $\sin\theta$ and $\cos\theta$ are related to x and y by

$$
\sin\theta = \frac{\partial y}{\partial s}\,, \qquad \cos\theta = \frac{\partial x}{\partial s}\,. \qquad (2.65)
$$

Using the inextensibility condition and the definition of the curvature κ, one can also prove that

$$
\frac{1}{R}\,\frac{\partial x}{\partial s} = \frac{\partial^2 y}{\partial s^2}\,, \qquad -\frac{1}{R}\,\frac{\partial y}{\partial s} = \frac{\partial^2 x}{\partial s^2}\,. \qquad (2.66)
$$

Substituting (2.65) and (2.66) into (2.64a,b), one obtains

$$
\begin{aligned}
\frac{\partial}{\partial s} & \quad \left((T-P)\,\frac{\partial x}{\partial s}\right) - \frac{\partial}{\partial s}\left(Q\,\frac{\partial y}{\partial s}\right) + (m+M)\,g \\
= & \quad (m+M)\,\frac{\partial^2 x}{\partial t^2} + 2\,M\,U\,\frac{\partial^2 x}{\partial s \partial t} + M\,U^2\,\frac{\partial^2 x}{\partial s^2} + M\,\dot{U}\,\frac{\partial x}{\partial s}\,, \qquad (2.67a)
\end{aligned}
$$

$$
\begin{aligned}
\frac{\partial}{\partial s} & \quad \left((T-P)\,\frac{\partial y}{\partial s}\right) + \frac{\partial}{\partial s}\left(Q\,\frac{\partial x}{\partial s}\right) \\
= & \quad (m+M)\,\frac{\partial^2 y}{\partial t^2} + 2\,M\,U\,\frac{\partial^2 y}{\partial s \partial t} + M\,U^2\,\frac{\partial^2 y}{\partial s^2} + M\,\dot{U}\,\frac{\partial y}{\partial s}\,. \qquad (2.67b)
\end{aligned}
$$

In this form, the similarity with Bourrières' equations is self-evident. Note that κ and the condition of inextensibility have already been used implicitly. At this stage, Rousselet and Herrmann have reduced this set of equations into one. With the different relationships defined in Rousselet (1975), it was possible to convert that equation into standard notation. After some manipulations, the nondimensional equation found is

$$\begin{aligned} \ddot{\eta} \; & +2\mathcal{U}\sqrt{\beta}\,\dot{\eta}'(1+\eta'^2) + \eta''\left[\mathcal{U}^2(1+\eta'^2) - \gamma(1-\xi)\left(1+\tfrac{3}{2}\eta'^2\right) + \dot{\mathcal{U}}\sqrt{\beta}\,(1-\xi)\right] \\ + & \;\; \gamma\,\eta'(1+\tfrac{1}{2}\eta'^2) + \eta''''(1+\eta'^2) + 4\,\eta'\,\eta''\,\eta''' + \eta''^3 + \eta' \int_0^\xi (\dot{\eta}'^2 + \eta'\,\ddot{\eta}')\mathrm{d}\xi \\ - & \;\; \eta''\left[\int_\xi^1 \int_0^\xi (\dot{\eta}'^2 + \eta'\,\ddot{\eta}')\,\mathrm{d}\xi\,\mathrm{d}\xi + \int_\xi^1 (2\,\mathcal{U}\sqrt{\beta}\,\eta'\,\dot{\eta}' + \mathcal{U}^2\,\eta'\,\eta'')\,\mathrm{d}\xi\right] = 0\,. \qquad (2.68) \end{aligned}$$

Compared to (2.55), two differences may be noticed in the nonlinear terms of the unsteady velocity; they arise from an error in the use of the following relationship:

$$\int_0^L F(x)\left(\int_0^x (\tan\theta)'\right)\delta w\,\mathrm{d}x\mathrm{d}x = \int_0^L \left(\int_x^L F(x)\,\mathrm{d}x\right)(\tan\theta)'\,\delta w\,\mathrm{d}x\,. \qquad (2.69)$$

This relationship is true, but in the order analysis, if F is of order 0, then $\tan\theta$ must be approximated to the third order. This was not considered by Rousselet and Herrmann. As explained in Section 3.1.2, this relationship (derived in Section 3.1.4, equation (2.22)) had to be rigorous up to order $\mathcal{O}(\epsilon^4)$. Except for these two differences, (2.55) and (2.68) are the same.

Rousselet and Herrmann also considered the effects on the fluid of the friction or of the related pressure drop, and derived a flow equation,

$$P_0 - \alpha\,MU^2 + \int_0^L (M\,g\,x' - M\,\dot{U})\,\mathrm{d}s - \int_0^L M(\ddot{x}\,x' + \ddot{y}\,y')\,\mathrm{d}s = 0\,, \qquad (2.70)$$

where P_0 is the compressive force acting on the fluid cross-section at $s = 0$, and $\alpha\,MU^2$ is the sum of the friction forces between the fluid and the pipe (α is a constant which depends on the roughness of the pipe). The two partial differential equations are coupled through the nonlinear terms. Thus, instead of considering the flow velocity as constant, the upstream pressure (in a large reservoir) is assumed constant instead. This idea was first proposed by Roth (1964).

2.6.1.3 Sethna, Bajaj and Lundgren's work

Lundgren *et al.* (1979) derived equations of motion by the force balance method. The assumptions made are the same as in other work, but, from a mathematical point of view, they tried to be as rigorous as possible. The force balance method in Section 2.4.1 follows the same procedure, so that all their equations were checked very carefully and appear to be exact. They used the condition of inextensibility and the exact expression for curvature. All the nonlinearities come from the terms $(T_0 - P)$ and $EI\,\kappa^2$.

Lundgren *et al.* stopped their derivation at an early stage, without taking further advantage of the inextensibility condition. In their subsequent paper (Bajaj *et al.* 1980), some nonlinear terms are ***apparently*** missing, especially nonlinear velocity-dependent terms. Under the form of an integrodifferential set of equations and neglecting, for the moment, the unsteady flow velocity, one may read (equation (5) in Bajaj *et al.* (1980))

$$\begin{aligned}(\partial x/\partial s)^2 \;&+\; (\partial y/\partial s)^2 = 1\,,\\ EI\,y'''' \;&+\; 2\,M\,U\,\dot{y}' + M\,U^2\,y'' + (m+M)\ddot{y} = \mathrm{NL}\,,\end{aligned} \tag{2.71}$$

where

$$\mathrm{NL} = -\tfrac{3}{2}\,EI\,\frac{\partial}{\partial s}\left(y'(x''^2 + y''^2)\right) - (m+M)\,\frac{\partial}{\partial s}\left(y'\int_s^L (x'\,\ddot{x} + y'\,\ddot{y})\mathrm{d}s\right).$$

At first glance these equations seem wrong (as no nonlinear velocity-dependent terms are present); however, if further simplification is carried out, equation (2.71) will yield the correct form of governing equation in terms of y. The U and U^2 terms are actually hidden in the nonlinear inertial term. Indeed, eliminating x through the condition of inextensibility leads to

$$\begin{aligned}&(m+M)\,\ddot{y}(1-y'^2) + 2\,M\,U\,\dot{y}' + M\,U^2\,y'' + EI\left(y'''' + 3\,y'\,y''\,y''' + \tfrac{3}{2}\,y''^3\right)\\ &+\; y'\int_0^s (m+M)\,(\dot{y}'^2 + y'\,\ddot{y}')\,\mathrm{d}s\\ &-\; y''\left(\int_s^L\int_0^s (m+M)(\dot{y}'^2 + y'\,\ddot{y}')\mathrm{d}s\mathrm{d}s - \int_s^L (m+M)\,\ddot{y}\,y'\mathrm{d}s\right) = 0\,.\end{aligned} \tag{2.72}$$

By multiplying by $(1+y'^2)$ throughout, keeping cubic nonlinear terms and replacing nonlinear inertial terms, one may bring equation (2.72) into the same form as (2.32).

In conclusion, this equation of motion is irreproachable. No nonlinear terms are missing, except for the gravity terms that have been neglected. However, the different steps from one equation to another were not very clear in the original derivation; hence, verification was not easy. Bajaj *et al.* (1980) used some implicit relationships of the curvature (Appendix B) and the procedure used to eliminate nonlinear inertial terms was not fully explained.

Finally, like Rousselet and Herrmann, Bajaj *et al.* also found an equation for the flow, by considering a force balance on a fluid element, yielding

$$M\,\alpha(U_0^2 - U^2) - M\int_0^L (\ddot{x}\,x' + \ddot{y}\,y')\mathrm{d}s - M\,\dot{U}\,L = 0\,, \tag{2.73}$$

where U_0 is the constant flow velocity when the tube is not in motion, α represents the resistance to the fluid motion (proportional to a friction factor) and $\alpha\,MU_0^2$ represents the constant pressure force at the fixed end $s = 0$ of the tube. Bajaj *et al.* (1980) found that α plays a determining role on whether the system loses stability by sub– or supercritical Hopf bifurcation.

2.6.1.4 Ch'ng and Dowell's work

Ch'ng & Dowell (1979) obtained nonlinear equations of motion of a pipe conveying fluid by the energy method based on Hamilton's principle. They used an Eulerian approach to describe the dynamics of the system, and assumed the flow to be steady. Using first only linear relationships, they found the well-known linear equation:

$$EI\,y'''' + 2\,M\,U\,\dot{y}' + M\,U^2\,y'' - (M+m)g\,[(L-x)y']' + (m+M)\,\ddot{y} = 0\,. \tag{2.74}$$

Ch'ng and Dowell then considered the nonlinear effects due to tension associated with the axial elongation of the pipe:

$$\int_0^L \mathrm{d}s = \int_0^L \sqrt{1+y'^2}\,\mathrm{d}x. \tag{2.75}$$

This relationship implicitly means that the cantilevered pipe is extensible, which is an unusual but by no means erroneous assumption. By assuming the tube to be Hookean, the axial nonlinear force T is added to (2.74), giving rise to

$$-\left(\frac{EA}{2L}\int_0^L y'^2\,\mathrm{d}x\right)y''\,. \tag{2.76}$$

Because of the extensibility assumption, this equation cannot be compared with any of the previous ones. However, it should be mentioned that the strain was approximated to the second order only, which does not fulfill the order considerations discussed in Section 3.1.2.

Additionally, Ch'ng and Dowell also considered a nonlinear relationship for the curvature. They used expression (12) for the curvature κ and the elastic strain energy

$$\mathcal{V} = \tfrac{1}{2} \int_0^L EI\, \kappa^2 \, \mathrm{d}x \,, \tag{2.77}$$

and obtained additional terms

$$-\, EI \left(3\, y'^2\, y'''' + 12\, y'\, y''\, y''' + 3\, y''^3\right) . \tag{2.78}$$

It is seen that expression (2.77) is not fully consistent with the strain energy derived by Stoker (1968) because the pipe is implicitly assumed to be extensible ($\varepsilon \neq 0$). Therefore, comparison cannot be made with other versions of the governing equations.

2.6.2 Case of a pipe fixed at both ends

In this section, two papers are discussed, representative of all the derivations for tubes fixed at both ends. Again, a standardization of the notation has been undertaken.

2.6.2.1 Thurman and Mote's work

Thurman & Mote (1969) were mainly concerned with the oscillations of bands of moving materials. They considered an axially-moving strip, simply supported at its ends, in order to show how the axial motion could significantly reduce the applicability of the linear analysis. They then extended this work to deal with pipes conveying fluid. The centreline being extensible, nonlinearities are associated with the axial tube elongation and the extension-induced tension in the tube. Therefore, the strain and the tension become

$$\begin{aligned} \varepsilon &= \frac{T_0}{EA} + \sqrt{(1+u')^2 + v'^2} - 1 \,, \\ T &= T_0 + EA\left(\sqrt{(1+u')^2 + v'^2} - 1\right) . \end{aligned} \tag{2.79}$$

Since a linear moment-curvature relationship and a linear approximation for the velocities were considered, the equations of motion obtained are

$$\begin{aligned} EI \quad & v'''' - (T_0 - M\,U^2)v'' + 2\,M\,U\,\dot{v}' + (m+M)\ddot{v} \\ = \quad & (EA - T_0)\left(\tfrac{3}{2}v'^2\,v'' + u'\,v'' + u''\,v'\right)\,, \end{aligned} \tag{2.80a}$$

$$M\,\ddot{u} - EA\,u'' = (EA - T_0)\,v'\,v''\,. \tag{2.80b}$$

These are actually a simplified set of (2.40a,b). The differences come from the assumptions made: (i) no gravity forces, (ii) steady flow velocity, (iii) linear moment-curvature relationship, (iv) simple approximation of the fluid velocity.

Consequently, on the basis of the assumptions made, the equations derived are correct.

2.6.2.2 Holmes' work

Holmes (1977) was one of the first to develop the new tools of modern dynamics, and to introduce them in the study of fluid-structure dynamical systems. He was less concerned with the derivation of the equations and he considered only the major nonlinear terms associated with the deflection-induced tension in the pipe.

Starting from the linear equation obtained by Païdoussis & Issid (1974), Holmes added the effect of the axial extension. To a first order approximation, the axial tension induced by lateral motions is

$$T = \sigma\,A = (E\,\varepsilon + \eta\,\dot{\varepsilon})A\,,$$

in which a Kelvin-Voigt viscoelastic material has been considered and where ε is the averaged axial strain defined by

$$\varepsilon = \frac{1}{2L}\int_0^L (y')^2\,\mathrm{d}s\,.^{\S}$$

Thus, an axial force T is added to the linear equation, where

$$T = -\frac{EA}{2L}\int_0^L (y'^2)\mathrm{d}s - \frac{\eta A}{L}\int_0^L (y'\,\dot{y}')\mathrm{d}s\,. \tag{2.81}$$

[§] There are some errors in sign in a few intermediate steps in Holmes' derivation (1977); the final equation, however, is correct.

The addition of this extra deflection-dependent axial force leads to one equation with two cubic nonlinear terms. Subsequently, a fairly complete bifurcation analysis based on a discretized two-mode model was carried out.

This axial force T (with $\eta = 0$) has also been obtained by Ch'ng & Dowell (1979) and by Namachchivaya & Tien (1989b) through the energy method. In this case, however, attention must be paid to the order approximation, as was already mentionned in Section 3.1.2.

It is noticed that Holmes' version of the nonlinear equation is a single scalar one, as compared to the two equations derived in this paper and also by others. The implication in Holmes' work is that axial motion of the pipe is negligible and also symmetric *vis-à-vis* the underformed position.

2.7 CONCLUSIONS

The nonlinear equations of motion of a pipe conveying fluid have been derived in a simple manner, by both the energy and the Newtonian method. It was shown that the equations of motion of a cantilevered pipe and of a pipe fixed at both ends are fundamentally different. In the first case the pipe may be considered to be inextensible and nonlinearities are mainly geometric, related to the large curvature in the course of arbitrary motions. In the case of a pipe fixed at the ends, nonlinearities are mainly associated with stretching of the pipe and the nonlinear forces generated thereby.

Of the anterior derivations, some were found to be absolutely correct, some correct for the purposes to which they were used, and some to contain errors or inconsistencies. Of the equations derived for *cantilevered pipes*, those by Lundgren *et al.* (1979) and Bajaj *et al.* (1980) were found to be absolutely correct, while those by Rousselet & Herrmann (1981) to be correct, except for a small order-of-magnitude inconsistency. Furthermore, both sets contain a distinct refinement *vis-à-vis* those derived here: the flow velocity is not assumed to be constant; instead the upstream pressure is taken to be constant, while the flow velocity generally varies with deformation. Of the equations derived for *pipes with fixed ends*, the set derived here is considered to be the only one available, correct to the same order as that for the cantilevered pipes. On the other hand, the simpler equation derived originally by Holmes (1977) is correct as far as it goes and may be preferred in some cases because of its simplicity. It is of interest that the origin of the terms in the equations — even some of the linear terms — as well as the structure of the equations are distinctly different for pipes with both ends fixed as compared to cantilevered pipes.

Chapter 3

THE PIPE WITH AN INTERMEDIATE SPRING SUPPORT[§]

3.1 INTRODUCTION

Ever since the early work on the dynamics of a pipe conveying fluid, e.g. by Bourrières (1939), Feodos'ev (1951) and Housner (1952), well over 200 papers have been written on the subject (Païdoussis 1991); indeed, the problem has become a new paradigm in dynamics, on a par with, for instance, the classical problem of a column subjected to various types of axial loading, but much richer.

It is well known that a pipe positively supported at both ends loses stability, for sufficiently high flow velocities, by divergence (Feodos'ev 1951; Housner 1952); a cantilevered pipe, on the other hand, loses stability by flutter (Bourrières 1939; Benjamin 1961). The case of a pipe with a clamped upstream end and a spring at the other was first considered by Chen (1971), who found that stability is lost by

[§]This corresponds to the article by Païdoussis & Semler 1993 Nonlinear dynamics of a fluid-conveying cantilevered pipe with an intermediate spring support. *Journal of Fluids and Structures* **7**, 269-298.

divergence or flutter, depending on the stiffness of the spring. The same system, but with the spring at some point intermediate between the fixed and free ends was studied by Sugiyama *et al.* (1985), Edelstein & Chen (1985) and others. More complex behaviour can be obtained in this case, as expected; the dynamics depends both on spring location and stiffness.

All of the studies mentioned so far explored the linear dynamics, whereas the present one deals with aspects of nonlinear dynamics of the system. Some key contributions to the study of the nonlinear dynamics of pipes conveying fluid have been made by Holmes (1977, 1978) for pipes supported at both ends, by Bajaj, Sethna and associates, e.g. Bajaj *et al.* (1980), for the cantilevered system, and more recently by Steindl & Troger (1988) for a pipe with an elastic support; in these studies, the tools of modern dynamical theory are utilized to explore analytically the qualitative dynamics of the system. An extensive literature review may be found in a review paper by Païdoussis (1991).

In the present study, an interesting variant of the system is considered: a cantilevered pipe with an intermediate (between the fixed and free ends) spring support; this renders possible the occurrence of a double degeneracy, i.e., the simultaneous occurrence of divergence and flutter for appropriately chosen parameter values. The analytical model studied is a two-degree-of-freedom system obtained by Galerkin discretization of the original. The stability of the original and new fixed points that emerge as the flow velocity is varied, the periodic orbits, and more generally the bifurcational behaviour of the system, are investigated. In the analytical component of the study of the nonlinear system, centre manifold, normal form and bifurcation techniques are used to obtain complete bifurcation sets, which define the qualitative dynamics of the system. The thus predicted dynamical behaviour is compared to that obtained by numerical simulation of the full nonlinear equations. In the last part of the chapter, special attention is given to the dynamics in the vicinity of the double degeneracy, and the possibility of chaotic oscillations in the perturbed system is explored.

3.2 THE ANALYTICAL MODEL

The system under consideration consists of a tubular beam of length L, internal cross-sectional area A, mass per unit length m and flexural rigidity EI conveying a fluid of mass M per unit length with an axial velocity U which may vary with time (Figure 3.1). The pipe is assumed to be initially along the x-axis (in the direction of gravity) and to oscillate in the (x, y) plane. The curvilinear coordinate along the centreline of the pipe is denoted by s. A linear spring of constant stiffness k is attached to the pipe at a distance s_s from the fixed end.

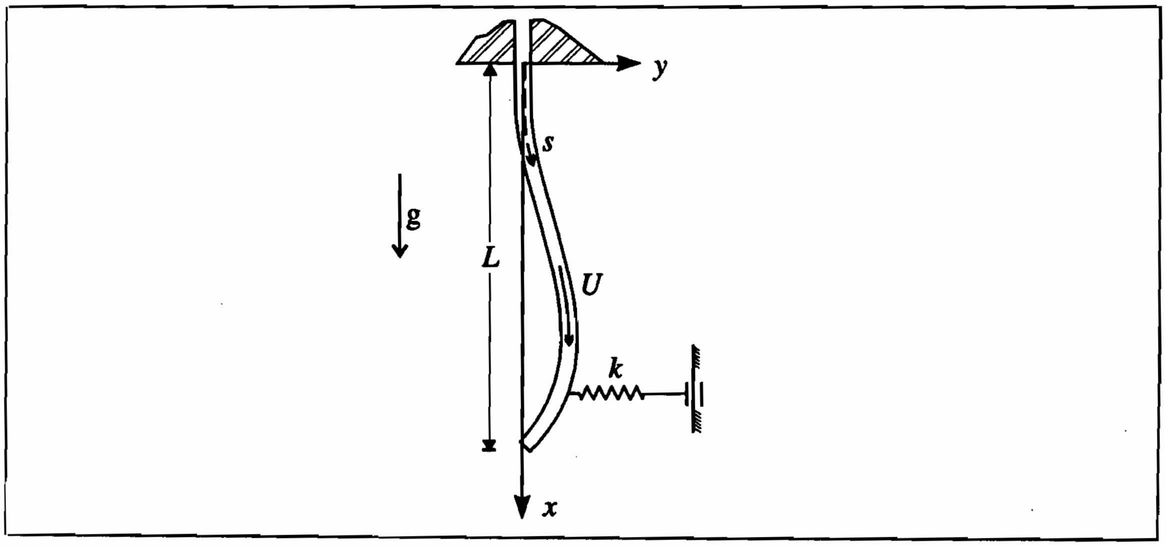

Figure 3.1: Schematic of the system.

The equation of motion, obtained by either the Hamiltonian method or the Newtonian method may be written as follows (see Chapter 2, equation (2.32) or Semler *et al.* 1994):

$$
\begin{aligned}
& (m+M)\,\ddot{y} + 2\,MU\,\dot{y}'(1+y'^2) + (m+M)\,g\,y'\left(1+\tfrac{1}{2}\,y'^2\right) + k\,y\,\delta(s-s_s) \\
+ \;& y''\left[MU^2\left(1+y'^2\right) + \left(M\dot{U} - (m+M)\,g\right)(L-s)\left(1+\tfrac{3}{2}\,y'^2\right)\right] \\
+ \;& EI\left[y''''(1+y'^2) + 4\,y'\,y''\,y''' + y''^3\right] \\
- \;& y''\left[\int_s^L \int_0^s (m+M)(\dot{y}'^2 + y'\,\ddot{y}')\,\mathrm{d}s\,\mathrm{d}s\right. \\
& \qquad \left. + \int_s^L \left(\tfrac{1}{2}M\dot{U}\,y'^2 + 2MU\,y'\,\dot{y}' + MU^2\,y'\,y''\right)\mathrm{d}s\right] \\
+ \;& y'\int_0^s (m+M)(\dot{y}'^2 + y'\,\ddot{y}')\,\mathrm{d}s = 0\,.
\end{aligned}
\tag{3.1}
$$

This equation is very similar to nonlinear equations derived for this problem by Lundgren *et al.* (1979) and Rousselet & Herrmann (1981).

To derive equation (3.1), the following assumptions for the pipe and the fluid were made: (i) the fluid is incompressible; (ii) the velocity profile of the fluid is uniform (plug-flow approximation for a turbulent-flow profile); (iii) the diameter of the pipe is small compared to its length, so that the pipe behaves like a Euler-Bernoulli beam; (iv) the motion is planar; (v) the deflections of the pipe may be large, but the strains remain small; (vi) rotatory inertia and shear deformation are neglected; (vii) the pipe centreline is inextensible; (viii) the spring is attached to a sliding support (Figure 3.1), so that, for a reasonable range of extensions, it has only a linear contribution in the equations of motion. The linear part of equation (3.1) corresponds to the equation obtained by Païdoussis & Issid (1974). The nonlinearities are obtained by considering all the nonlinear relationships up to the third order (for the force balance method) and up to the fourth order (in the derivation by the energy method) of the different components; the kinetic energy, the strain and the gravitational energy, for example.

Dissipative terms have to be added to complete the equation. This is done by assuming that the internal dissipation of the pipe material is viscoelastic and of the Kelvin-Voigt type (Snowdon 1968). The dissipation is further assumed to be small and that it may be lumped into a single term associated with the linear restoring force, thus providing an additional term in the equation:

$$E^* I \frac{\partial}{\partial t} \left(\frac{\partial^4 y}{\partial s^4} \right),$$

where E^* is the viscoelastic coefficient (assuming a linearly viscoelastic material). The damping associated with frictional forces due to the surrounding air is neglected in comparison to internal dissipation.

Introducing next the same nondimensional quantities as have been used in the past for the analysis of the linear system,

$$\begin{aligned}
\xi &= \frac{s}{L}, \quad \eta = \frac{y}{L}, \quad \tau = \left(\frac{EI}{m+M}\right)^{1/2} \frac{t}{L^2}, \quad \alpha = \left(\frac{I}{E(m+M)}\right)^{1/2} \frac{E^*}{L^2}, \\
u &= \left(\frac{M}{EI}\right)^{\frac{1}{2}} U\,L, \quad \gamma = \frac{m+M}{EI} L^3 g, \quad \beta = \frac{M}{m+M}, \quad \kappa = \frac{kL^3}{EI},
\end{aligned} \tag{3.2}$$

equation (3.1) may be rewritten in dimensionless form as follows:

$$\begin{aligned}
&\alpha \quad \dot{\eta}'''' + \eta'''' + \ddot{\eta} + 2u\sqrt{\beta}\,\dot{\eta}'\left(1+\eta'^2\right) + \kappa\,\eta\,\delta(\xi-\xi_s) \\
&+ \quad \eta''\left[u^2\left(1+\eta'^2\right) + (\dot{u}\sqrt{\beta}-\gamma)(1-\xi)\,\left(1+\tfrac{3}{2}\eta'^2\right)\right] \\
&+ \quad \gamma\,\eta'\left(1+\tfrac{1}{2}\eta'^2\right) + \eta''''\,\eta'^2 + 4\,\eta'\,\eta''\,\eta''' + \eta''^3 \\
&- \quad \eta''\left[\int_\xi^1 \int_0^\xi \left(\dot{\eta}'^2 + \eta'\,\ddot{\eta}'\right)\,\mathrm{d}\xi\,\mathrm{d}\xi + \int_\xi^1 \left(\tfrac{1}{2}\dot{u}\sqrt{\beta}\,\eta'^2 + 2\,u\sqrt{\beta}\,\eta'\,\dot{\eta}' + u^2\,\eta'\,\eta''\right)\mathrm{d}\xi\right] \\
&+ \quad \eta' \int_0^\xi \left(\dot{\eta}'^2 + \eta'\,\ddot{\eta}'\right)\,\mathrm{d}\xi = 0\,.
\end{aligned} \tag{3.3}$$

Of particular interest is the appearance in (3.3) of nonlinear inertial terms, which render the equation non-standard and which create difficulties in its solution. These terms are replaced by equivalent velocity and displacement terms by using a perturbation method, as follows. Equation (3.3) may be written as

$$\mathcal{L}(\eta) + [\mathcal{N}_1(\eta) + \mathcal{N}_2(\eta)] = 0\,, \tag{3.4}$$

in which $\mathcal{L}(\eta)$ represents the linear terms and $\mathcal{N}_i$ the nonlinear terms:

$$\mathcal{L}(\eta) = \ddot{\eta} + 2\,u\sqrt{\beta}\,\dot{\eta}' + \eta''\left[u^2 + (\dot{u}\sqrt{\beta}-\gamma)\,(1-\xi)\right] + \gamma\,\eta' + \eta''''\,, \tag{3.5a}$$

$$\begin{aligned}\mathcal{N}_1(\eta) &= 2\,u\,\sqrt{\beta}\,\dot{\eta}'\,\eta'^2 + \eta''\left[u^2 + \tfrac{3}{2}\,(\dot{u}\,\sqrt{\beta} - \gamma)\,(1-\xi)\right]\eta'^2 \\ &\quad + \tfrac{1}{2}\,\gamma\eta'^3 + \eta''''\,\eta'^2 + 4\,\eta'\,\eta''\,\eta''' + \eta''^3\,,\end{aligned} \tag{3.5b}$$

$$\begin{aligned}\mathcal{N}_2(\eta) = \quad & \eta' \int_0^{\xi} \left(\dot{\eta}'^2 + \eta'\,\ddot{\eta}'\right) \mathrm{d}\xi - \eta''\Big[\int_{\xi}^{1} \int_0^{\xi} \left(\dot{\eta}'^2 + \eta'\,\ddot{\eta}'\right) \mathrm{d}\xi\,\mathrm{d}\xi \\ & + \int_{\xi}^{1} \left(\tfrac{1}{2}\,\dot{u}\,\sqrt{\beta}\,\eta'^2 + 2\,u\,\sqrt{\beta}\,\eta'\,\dot{\eta}' + u^2\,\eta'\,\eta''\right) \mathrm{d}\xi\Big]\,,\end{aligned} \tag{3.5c}$$

in which, for simplicity, the terms involving α and κ are omitted for the present. Although the deflection of the pipe can be considered to be large, an order of magnitude analysis may nevertheless be usefully undertaken: η corresponds to the lateral displacement which can still be expressed as being "small" and may be written as $\eta = \mathcal{O}(\varepsilon)$. Looking for large deflection motions means that, in the equation, terms of higher order than the linear ones have to be kept. Hence, in equation (3.5), $\mathcal{L}(\eta) = \mathcal{O}(\varepsilon)$ and $\mathcal{N}(\eta) = \mathcal{O}(\varepsilon^3)$. $\mathcal{L}$ being linear, $\mathcal{L}\,(\eta')$ is clearly defined, so that

$$\int_0^{\xi} \eta'\,\mathcal{L}(\eta')\,\mathrm{d}\xi = \mathcal{O}(\varepsilon^2)\,. \tag{3.6}$$

Consequently, after some manipulations in equation (3.5a), one obtains

$$\begin{aligned}\int_0^{\xi} \eta'\,\ddot{\eta}'\,\mathrm{d}\xi = \; & -\int_0^{\xi} \Big\{2\,u\,\sqrt{\beta}\,\eta'\,\dot{\eta}'' + \eta'\,\eta'''\left[u^2 + (\dot{u}\,\sqrt{\beta} - \gamma)(1-\xi)\right] \\ & + \eta'\,\eta''\left(2\,\gamma - \dot{u}\,\sqrt{\beta}\right) + \eta'\,\eta''''\Big\}\mathrm{d}\xi + \mathcal{O}(\varepsilon^2)\,.\end{aligned} \tag{3.7}$$

Integration of (3.7) from ξ to 1 yields the other nonlinear inertial term. The two nonlinear inertial terms are replaced in $\mathcal{N}_2(\eta)$, to obtain, after some long but straightforward algebra:

$$\ddot{\eta} + 2u\sqrt{\beta}\dot{\eta}' + \eta''\left[u^2 + (\dot{U}\,\sqrt{\beta} - \gamma)(1-\xi)\right] + \gamma\eta' + \kappa\eta\,\delta(\xi - \xi_s) + \alpha\dot{\eta}'''' + \eta'''' + \mathcal{N}(\eta) = 0, \tag{3.8}$$

where

$$
\begin{aligned}
\mathcal{N}(\eta) \;=\;& 2\,u\,\sqrt{\beta}\,\dot{\eta}'\,\eta'^2 + \eta''\left[u^2 + \tfrac{3}{2}(\dot{u}\,\sqrt{\beta} - \gamma)(1-\xi)\right]\eta'^2 \\
&+\; \tfrac{1}{2}(\dot{u}\,\sqrt{\beta} - \gamma)\,\eta'^3 + 3\,\eta'\,\eta''\,\eta''' + \eta''^3 \\
&+\; \eta' \int_0^{\xi} \left\{\dot{\eta}'^2 - 2\,u\,\sqrt{\beta}\,\eta'\dot{\eta}'' - \eta'\,\eta'''\left[u^2 + (\dot{u}\,\sqrt{\beta} - \gamma)(1-\xi)\right] + \eta''\,\eta''''\right\} \mathrm{d}\xi \\
&-\; \eta'' \int_{\xi}^{1} \int_0^{\xi} \left\{\dot{\eta}'^2 - 2\,u\,\sqrt{\beta}\,\eta'\,\dot{\eta}'' - \eta'\,\eta'''\left[u^2 + (\dot{u}\,\sqrt{\beta} - \gamma)(1-\xi)\right]\right. \\
&\qquad\qquad\qquad\qquad \left. + \eta''\,\eta''''\right\}\mathrm{d}\xi\,\mathrm{d}\xi \\
&-\; \eta'' \int_{\xi}^{1} \left\{(\dot{u}\,\sqrt{\beta} - \gamma)\,\eta'^2 + 2\,\sqrt{\beta}\,\eta'\,\dot{\eta}' + u^2\,\eta'\,\eta'' + \eta''\,\eta'''\right\}\mathrm{d}\xi\,.
\end{aligned}
\tag{3.9}
$$

Hence, the transformed nonlinear equation of motion is correct to $\mathcal{O}(\varepsilon^3)$. From now on, in order to simplify the notation, ε will represent "a small quantity", and the nonlinear terms will simply be represented by $\varepsilon\,\mathcal{N}(\eta)$.

The infinite-dimensional model is discretized by Galerkin's technique, with the cantilever beam eigenfunctions $\phi_r(\xi)$ being used as a suitable set of base functions and $q_r(\tau)$ being the corresponding generalized coordinates; thus,

$$
\eta(\xi,\tau) = \sum_{r=1}^{N} \phi_r(\xi)\,q_r(\tau)\,. \tag{3.10}
$$

Gregory & Païdoussis (1966) proved that the approximation $N = 2$ is reasonably good for $\beta < 0.3$, although Païdoussis *et al.* (1991) highlighted some quantitative differences with the experiments. For our purposes here and in light of modern dynamics, pursuing the analysis with $N = 2$ is considered to be valid, as the main purpose is to find the *qualitative* characteristics of the system.

Substituting expression (3.10) into (3.9), multiplying by $\phi_i(\xi)$ and integrating from 0 to 1, leads to

$$
\ddot{q}_i + c_{ij}\,\dot{q}_j + k_{ij}\,q_j + \varepsilon\left(\alpha_{ijkl}\,q_j\,q_k\,q_l + \beta_{ijkl}\,q_j\,q_k\,\dot{q}_l + \gamma_{ijkl}\,q_j\,\dot{q}_k\,\dot{q}_l\right) = 0, \tag{3.11}
$$

where c_{ij}, k_{ij}, α_{ijkl}, β_{ijkl} and γ_{ijkl} are coefficients computed from the integrals of the eigenfunctions $\phi_i(\xi)$, analytically (Païdoussis & Issid 1974) or numerically (Appendix C; the linear coefficients are defined in Appendix G). The repeated indices in equation (3.11) implicitly follow the summation convention.

In the case where the fluid flow can have small sinusoïdal fluctuations,

$$u \rightarrow u + \varepsilon\, \nu\, \sin \omega \tau\,, \tag{3.12}$$

certain new terms appear in (3.11), namely

$$+\,\varepsilon \left(2\sqrt{\beta}\, \nu\, \sin \omega t\; a_{ij}\, \dot{q}_j + 2\, u\, \nu\, \sin \omega t\; b_{ij}\, q_j + \sqrt{\beta}\, \nu\, \omega\, \cos \omega t\; d_{ij}\, q_j\right)\,.$$

In order to use the available tools of dynamics theory, the second-order equation is transformed into a set of first-order ordinary differential equations. Introducing the generalized coordinates $p_i = \dot{q}_i$, equation (3.11) may be written in the matrix form

$$\left\{ \begin{array}{c} \dot{q} \\ \dot{p} \end{array} \right\} = \left[\begin{array}{cc} 0 & I \\ -K & -C \end{array} \right] \left\{ \begin{array}{c} q \\ p \end{array} \right\} + \varepsilon \left\{ f(q,p) \right\} + \varepsilon\, \nu \left\{ g(q,p,\tau) \right\}\,, \tag{3.13}$$

i.e.

$$\dot{y} = [A]\, y + \varepsilon\, f(y) + \varepsilon\, \nu\, g(y,\tau)\,, \tag{3.14}$$

where q, p and y are understood to be vectors; f is a third order polynomial function, g is a time-dependent function, and $[A] \equiv [A\,(u,\, \gamma,\, \beta,\, \kappa,\, \xi_s)]$ is a $2N \times 2N$ matrix.

3.3 STABILITY ANALYSIS

Local bifurcations occur when some eigenvalue of the linearized system at a fixed point crosses the imaginary axis. It is therefore interesting to study the behaviour of the linearized system about its equilibrium position as a function of the system parameters. Consequently, the matrix $[A]$ found previously is studied in detail. Since only two modes are considered, $[A]$ is a 4×4 matrix.

Some classical bifurcations are sought by analyzing the eigenvalues of the matrix $[A]$: the Hopf bifurcation, where $[A]$ has a pair of purely imaginary eigenvalues; a pitchfork or a saddle-node bifurcation, where $[A]$ has a zero eigenvalue; and a doubly-degenerate bifurcation, where $[A]$ satisfies both of the foregoing. For a low-dimensional problem, two different methods may be applied: Routh's criteria and a direct eigenvalue analysis.

3.3.1 Routh's criteria

The characteristic equation is a fourth order polynomial in λ,

$$a_4\,\lambda^4 + a_3\,\lambda^3 + a_2\,\lambda^2 + a_1\,\lambda + a_0 = 0\,. \tag{3.15}$$

Routh (1960) showed that the conditions for dynamic instability ($\lambda = \pm\, i\,\omega$) can be written as

$$T_3 = a_1\,a_2\,a_3 - a_0\,a_3^2 - a_4\,a_1^2 = 0 \;\text{ and }\; a_1/a_3 > 0\,,$$

and the condition for a static instability simply becomes

$$a_0 = 0\,.$$

For the matrix [A], a_4 is equal to unity. The coefficients a_0 to a_3 can then be computed analytically as functions of the main parameters u, γ, β, κ and ξ_s using MACSYMA (Rand 1984), then solved numerically and plotted in the parameter space (Appendix D). Here, only a few results are given; for a complete investigation, see Semler (1991). It should be mentioned that the location of the spring is kept constant here, $\xi_s = 0.8$, for simplicity. When this value was modified, no qualitative change in the results was observed.

Divergence is represented by the curve $a_0 = 0$. This condition is a second-order equation in γ (for fixed u), leading consequently to two, one or no value(s) of γ as a solution (see Appendix D). The solution curves can be divided into two classes, exemplified by the cases $\kappa = 0$ and $\kappa = 100$ in Figure 3.2. For low values of κ, divergence occurs only for negative γ (i.e., for an upside-down pipe under the effect of gravity), while for large values of κ divergence becomes possible for positive γ. Hence, for a given positive γ (hanging pipe), divergence occurs only if the stiffness is greater than a critical value κ_{cr}. For example, in Figure 3.2, $\kappa_{cr} = 75$ for $\gamma = 17$. However, this critical value can be modified by changing the location of the spring: the larger ξ_s, the smaller is κ_{cr}.

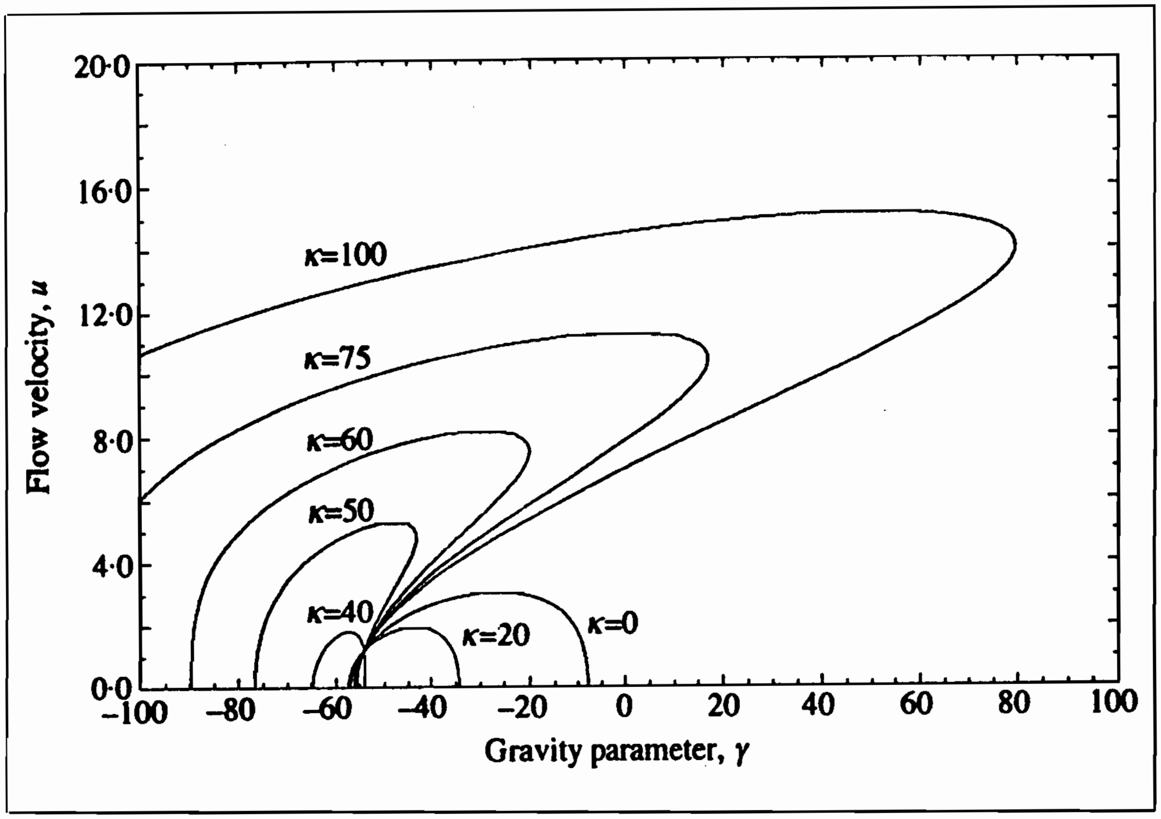

Figure 3.2: Static stability boundaries for different values of κ [$a_0 = 0$ in equation(2.15)] in terms of the dimensionless flow velocity, u, and the gravity parameter, γ. The location of the spring is constant, $\xi_s = 0.8$.

For *flutter*, Figure 3.3 illustrates the influence of some of the pertinent parameters. The projection of the condition $T_3 = 0$ in various planes illuminates the influence of the parameters on the dynamic stability boundaries. For example, for a constant γ,the critical flow velocity increases with β; also, for small β, there is a minimum γ below which flutter does not take place (cf. Païdoussis & Deknis 1970). Only $\beta < 0.3$ has been considered for the reasons given in Section 3.2. It should be emphasized that the results (i) agree very well with those given by Sugiyama *et al.* (1985) for the same number of degrees of freedom, and (ii) are within 1% for divergence and 10% for flutter, at $\beta = 0.25$, of the values obtained with an infinite-dimensional model (Sugiyama *et al.* 1985).

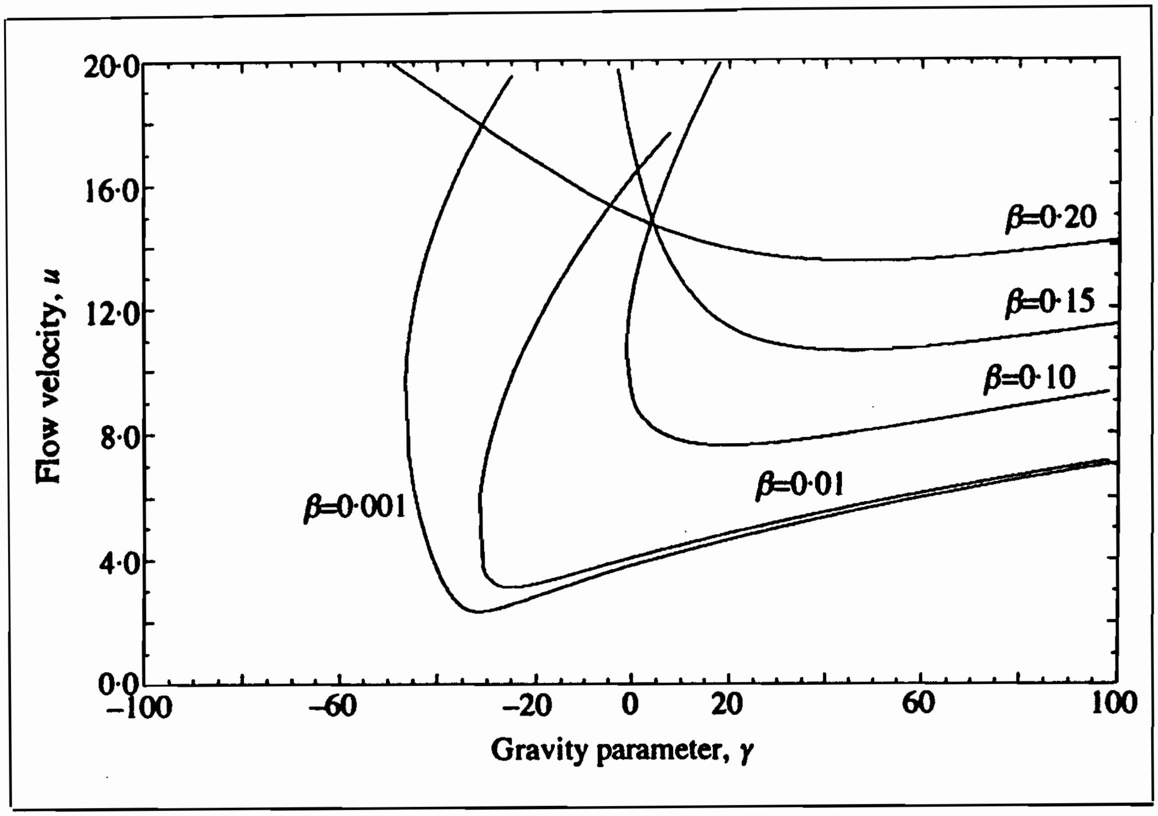

Figure 3.3: Dynamic stability boundaries [$T_3 = 0$ in equation following equation(2.15)]; $\kappa = 100$, $\xi_s = 0.8$.

The *double degeneracy conditions* were also found. These conditions are satisfied when $a_0 = 0$ and $a_1 = a_2\, a_3$, written as

$$f_i(u,\, \gamma,\, \beta,\, \kappa) = 0\,, \qquad i = 1,\, 2\,.$$

From a numerical point of view, three of the four parameters are kept constant, and the fourth varied until the two conditions are satisfied, although solutions do not always exist. Again, two different types of solution are found.

When $\kappa < 45$, $u_{cr} = f(\gamma,\, \beta)$ is a curve which retraces its path; Figure 3.4 represents a projection of these curves in the $(\gamma,\, u)$ plane, for different values of κ, when β is varied as a control parameter $(0 < \beta < 0.3)$. These "closed" curves are explained by the fact that the curve $a_0 = 0$ is independent of β, while the curve

$a_1 = a_2\,a_3$ is not single-valued as a function of β, in the $(\beta,\,u)$ or $(\beta,\,\gamma)$ plane. For example, for $\kappa = 0$ and $\gamma = -45$, $u_{cr} = 2.344$ for both $\beta = 0.003$ and $\beta = 0.176$.

For small values of κ, to achieve a double degeneracy condition, the range of γ is rather small, and $\gamma < 0$. This is not surprising, since the static instability is due only to the effect of gravity, when the stiffness of the spring is small.

When $\kappa > 45$, all the curves, which no longer retrace their paths, have the same qualitative shape. The range for γ is much larger, and double degeneracy can occur for positive values of γ.

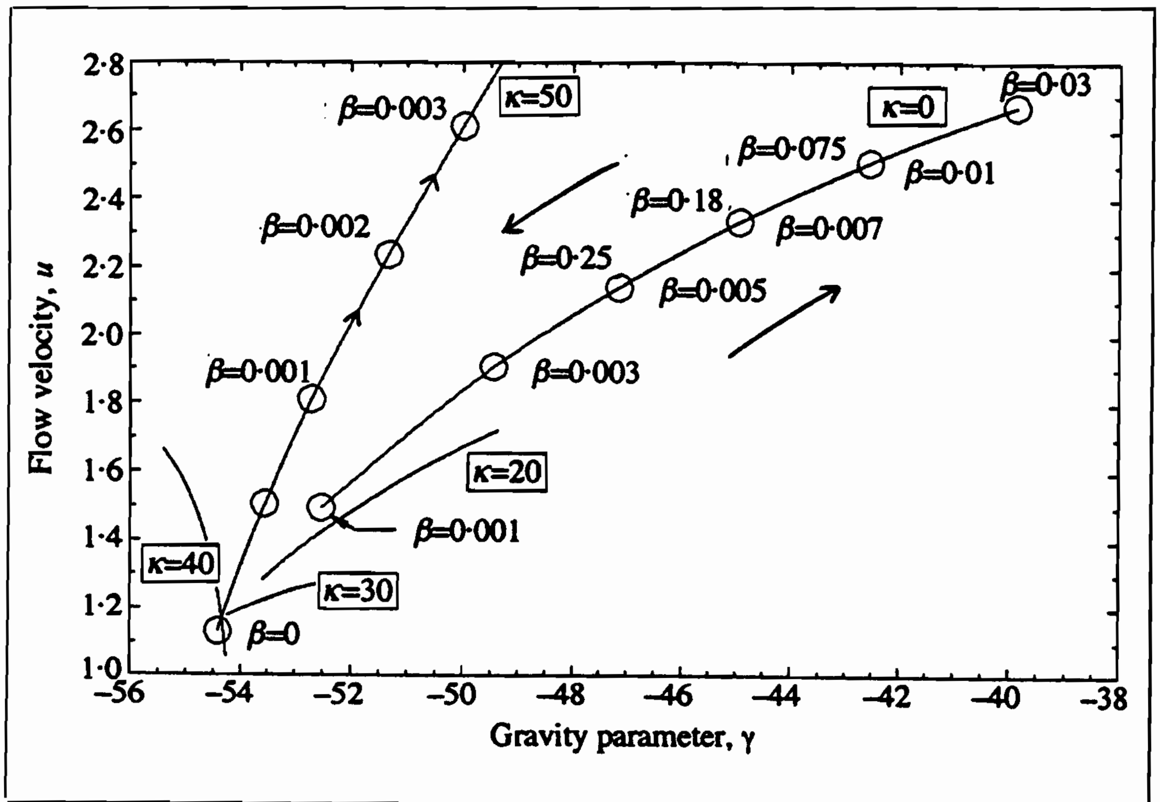

Figure 3.4: Double degeneracy conditions for different values of κ. The control parameter varied is β. It is noted that for $\kappa = 0$ essentially the same curve is retraced as β is incremented past $\beta = 0.03$; this is not the case for higher κ, e.g. $\kappa = 50$, where the curve continues on to positive values of γ.

For an investigation of the qualitative behaviour of the pipe, this linear analysis is sufficient to provide a complete set of parameters (u, γ, β, κ) to study all types of bifurcation. Indeed, this study is more concerned with the post-bifurcation behaviour than with the actual critical parameters where instability occurs.

3.3.2 Direct eigenvalue analysis

The analysis by Routh's criteria can only provide the boundaries of the instabilities, and in order to check the meaning of the results previously obtained, a direct eigenvalue analysis is undertaken. The case with $\beta = 0.18$ and a spring, $\kappa = 100$ at $\xi_s = 0.8$, is chosen to explore the nature of the instability boundaries found previously. To investigate the stability of the origin, the four eigenvalues are sought and plotted in the form of an Argand diagram (the imaginary part of the eigenvalue versus the real part), with the dimensionless flow velocity u as a parameter. All the results are summarized in Figure 3.5(a-d), for different values of γ. Each value of γ has been chosen to represent a qualitatively different phenomenon.

3.3.2.1 Behaviour for $\gamma > 80$; $\gamma = 100$ in Figure 3.5(a)

For low dimensionless flow velocity u, the four eigenvalues are in two complex conjugate pairs, $\lambda_2 = \lambda_1^*$ and $\lambda_4^* = \lambda_3$ with negative real parts, in which the asterisk denotes the complex conjugate; thus, the origin is stable (the negative real part at $u = 0$ results from the effect of the viscoelastic dissipation, $\alpha = 0.005$). For $u = 13.0$, the real part of the first pair, $\mathrm{Re}(\lambda_{1,2})$, becomes zero, while $\mathrm{Im}(\lambda_{1,2}) \neq 0$. This situation corresponds to the well-known Hopf bifurcation, $u = u_H$, represented physically by flutter-type, or in the nonlinear domain by limit-cycle, motions.

The real parts of the other two eigenvalues λ_3, λ_4 remain negative with increasing u, and, hence, play no role in the stability of the system. For high values of γ, the spring simply modifies the behaviour that would exist without it (Païdoussis 1970).

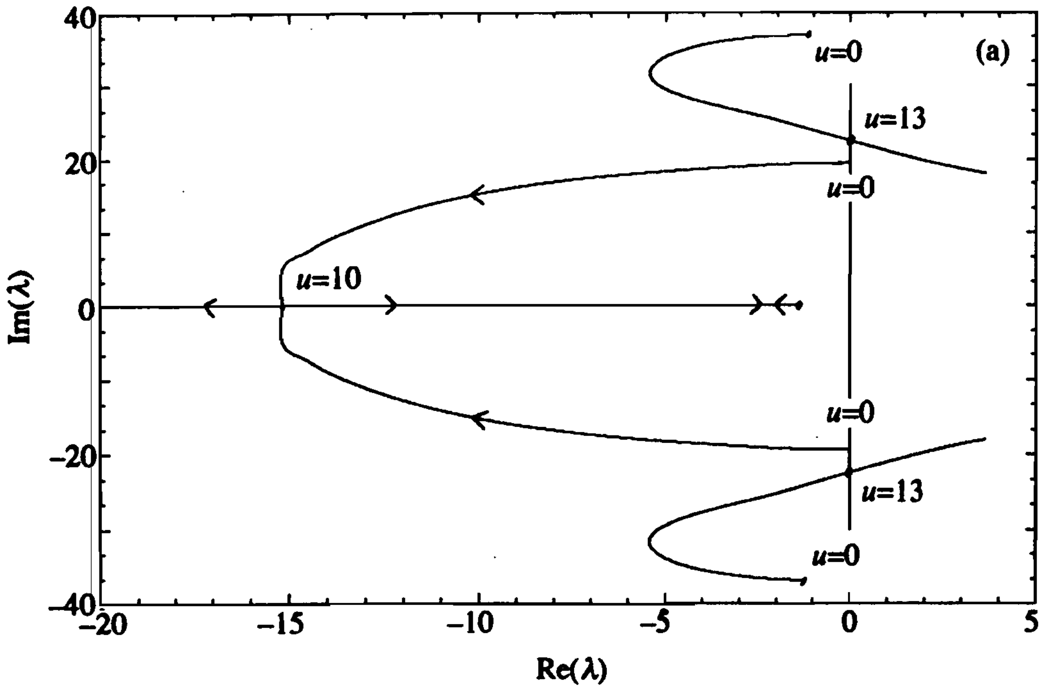

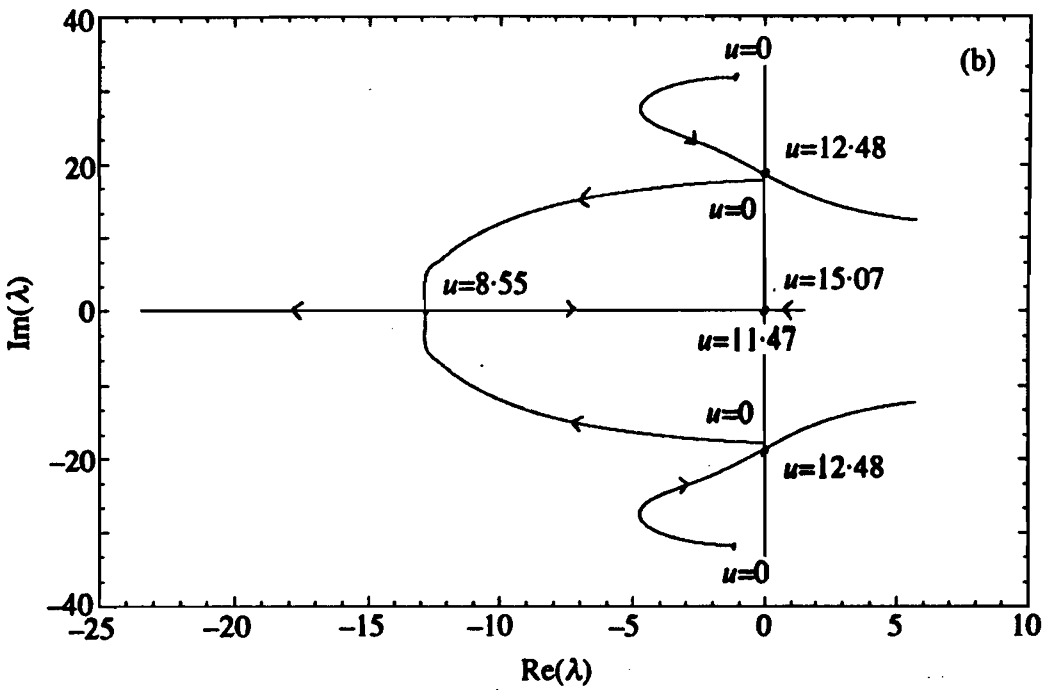

Figure 3.5: The eigenvalues of the linearized system plotted as Argand diagrams, for $\beta = 0.18$, $\kappa = 100$, $\alpha = 5 \times 10^{-3}$, $\xi_s = 0.8$, and for different values of γ. (a) $\gamma = 100$; (b) $\gamma = 60$; (c) $\gamma = 75$; (d) $\gamma = -40$.

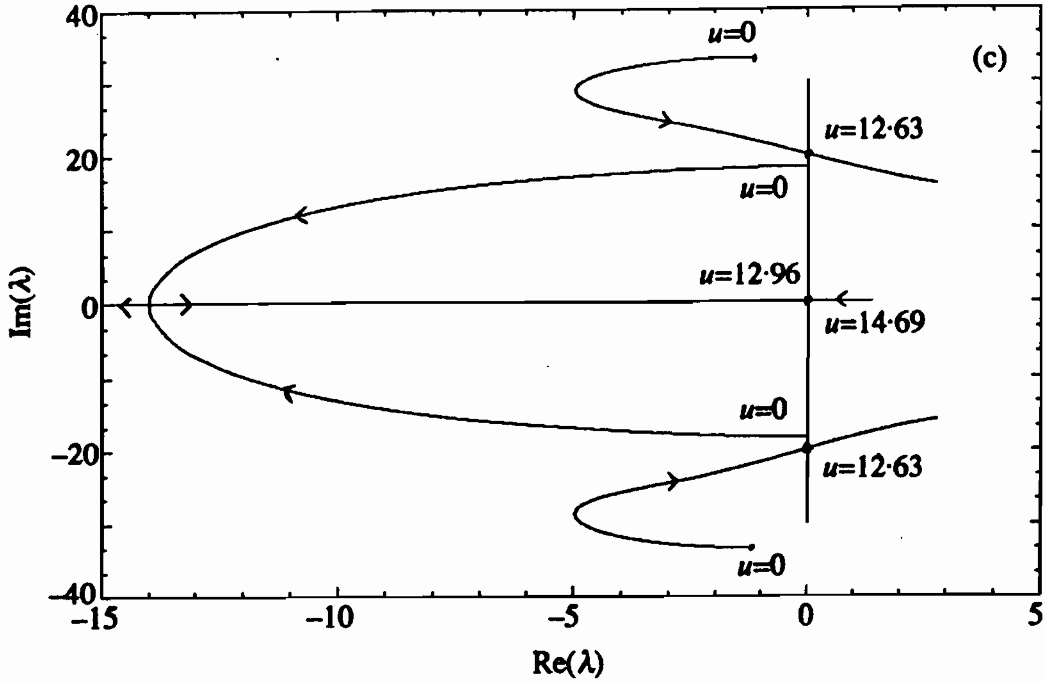

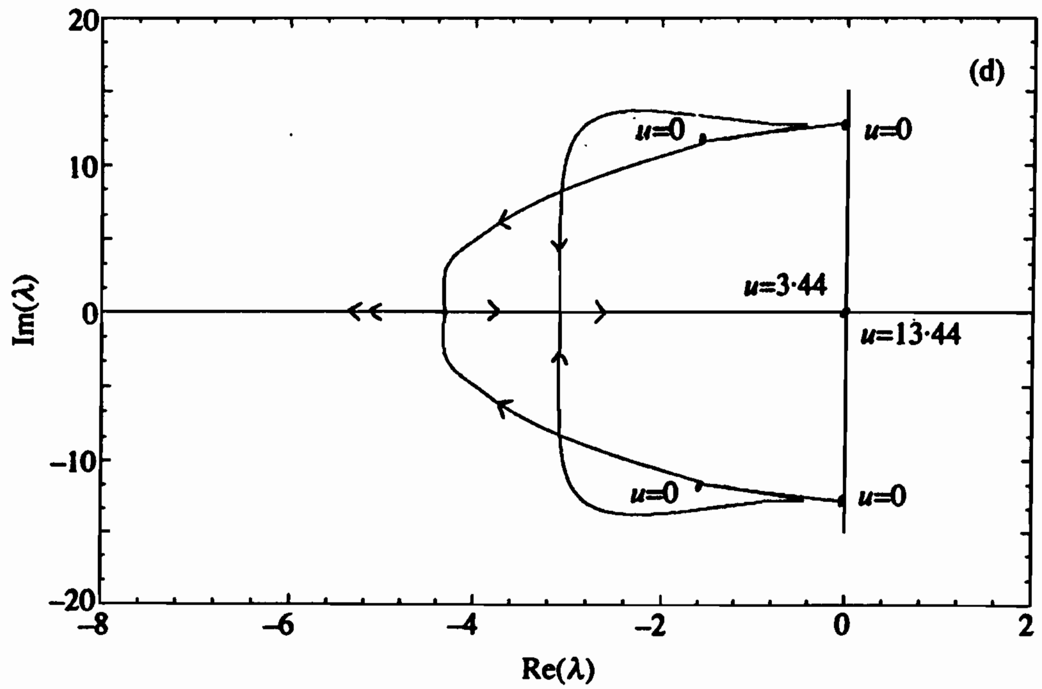

Figure 3.5: Continued.

3.3.2.2 Behaviour for $4.96 < \gamma < 71.94$; $\gamma = 60$ in Figure 3.5(b)

Different types of instability may occur in this case. For low u, the origin is stable. For higher u, one conjugate pair of eigenvalues becomes wholly real ($u = 8.55$), and one of them eventually becomes positive ($u = 11.47$). This point corresponds to static instability, or divergence. For still higher u (namely $u = 12.48$), the system loses stability through a Hopf bifurcation, as the other pair of eigenvalues crosses the imaginary axis. Finally, at $u = 15.07$, the first eigenvalue crosses the imaginary axis again, but from right to left, meaning that the system regains static stability; this value has no real physical meaning, since the system has lost stability dynamically prior to this. However, the boundaries found by Routh's criteria (Figure 3.2) are now clearly explained.

The two extreme cases, $\gamma = 4.96$ and $\gamma = 71.94$ are qualitatively different: in the first case, a double zero eigenvalue occurs; the second corresponds to double degeneracy conditions.

3.3.2.3 Behaviour for $71.94 < \gamma < 80$; $\gamma = 75$ in Figure 3.5(c)

This case corresponds to a hybrid form of the previous two: a Hopf bifurcation occurs first ($u = 12.63$) followed by static instability ($u = 12.96$), and by a restabilization at $u = 14.69$. Again, only the flutter-type motions, representing the first loss of stability, are physically meaningful.

3.3.2.4 Behaviour for $\gamma < 4.96$; $\gamma = -40$ in Figure 3.5(d)

It is obvious that no dynamic instability occurs in this case. The system loses stability through a pitchfork bifurcation at $u = 3.44$; with increasing flow velocity, a second static instability occurs at $u = 13.44$. No restabilization is found. From a physical point of view, two different static equilibria may be observed. Consequently, for $\gamma < 4.96$, the top curve $a_0 = 0$ in Figure 3.2 no longer represents a restabilization, but rather a second static instability.

3.3.2.5 Remarks on the linear stability boundaries

With this direct eigenvalue analysis, it is now possible to distinguish more precisely the different regions of stability. Indeed, the upper branch of the $a_0 = 0$ curves (Figure 3.2) may represent either static restabilization or instability in the second mode, depending on the value of γ; it is important to note that Routh's criteria are unable to distinguish between these two physically distinct phenomena. However, with the aid of the foregoing analysis, the complete stability map obtained from the linearized equations may now be drawn, as shown in Figure 3.6 in which the dashed line and the zone marked "global oscillations", to be discussed in Section 3.4.3, should be ignored for now.

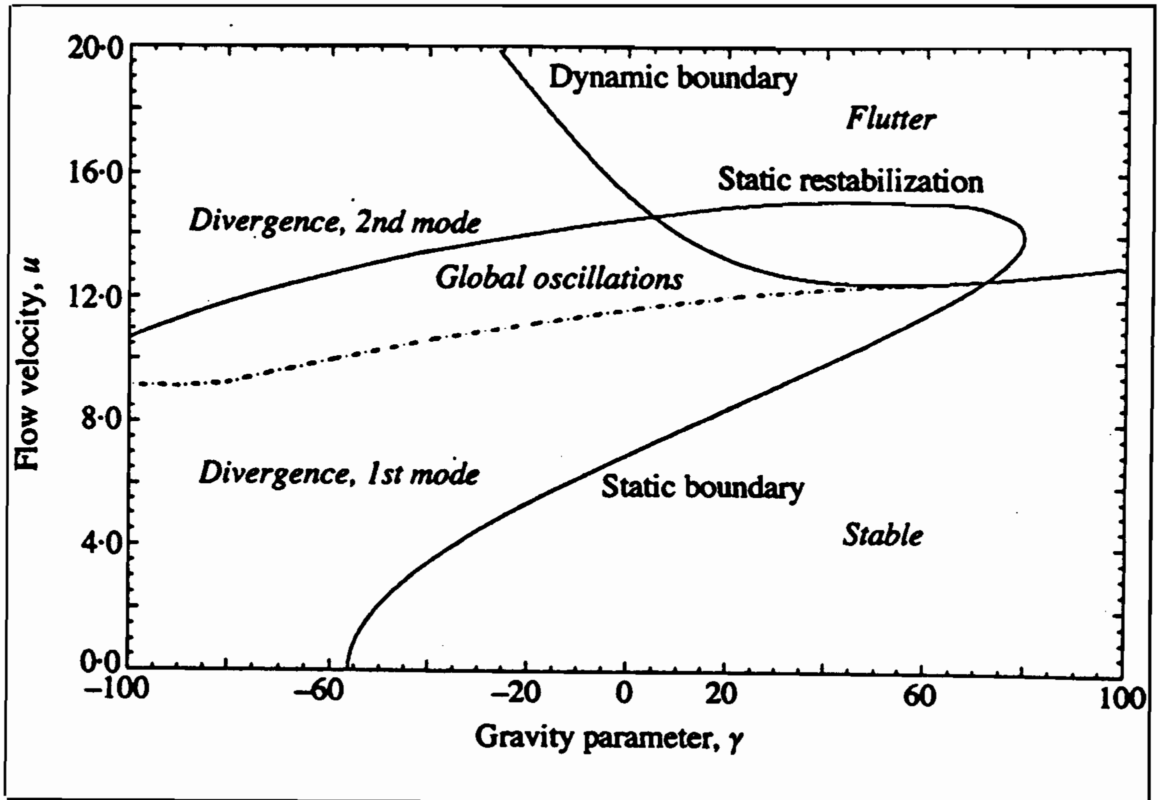

Figure 3.6: Stability boundaries obtained by the direct eigenvalue analysis of Section 3.3.2, for for $\beta = 0.18$, $\kappa = 100$, $\alpha = 5 \times 10^{-3}$ and $\xi_s = 0.8$; also shown is the zone of global oscillations obtained in Section 3.4.

Finally, it should be recalled that the study of the linearized system near the origin has limitations. Theoretically, it is not possible to study the behaviour of the system after a bifurcation. Thus, the study of the linearized system is only valid for the first instability. Concerning the restabilization (and other bifurcations), this also strictly applies to systems that are linearly unstable at $u = 0$, as u is increased. When static instability occurs, a new analysis can be undertaken near the new fixed point which, from a topological point of view, takes the place of the origin. This will be done in the next section, since the inclusion of the nonlinear terms is necessary to find the position of the new "origin".

3.4 NONLINEAR ANALYSIS AND STABILITY OF THE FIXED POINTS

Whereas the linear approximation of the system can predict only the instabilities of the origin, the nonlinear analysis may provide a deeper and more interesting insight into the problem.

One usually starts the study of a nonlinear system $dx/dt = f(x)$, where generally x is a vector and f a vector function, by finding the zeros of f,

$$f(x) = 0\,. \tag{3.16}$$

These zeros, x_0, are referred to as fixed points, equilibria or stationary solutions. Linearization at these points can characterize the behaviour of solutions near x_0. This is done by studying the linear system

$$\frac{d\xi}{dt} = Df(x_0)\xi, \qquad \xi \in \mathcal{R}^n\,, \tag{3.17}$$

where $Df = [\partial f_i/\partial x_j]$ is the Jacobian matrix of the function f at the fixed point x_0, and $\xi = x - x_0\,, \quad |\xi| << 1$.

Actually, the study of the linearized system defined by (3.17) can only provide qualitative information on the nonlinear system in some cases, namely when $Df(x_0)$

has no zero or no purely imaginary eigenvalues (Hartman-Grobman theorem). When $Df(x_0)$ has no eigenvalues with a zero real part, x_0 is called a hyperbolic or nondegenerate fixed point. Hence, from a practical point of view, the interesting problem is to find the degenerate fixed points. This was done partially in the previous section, since the origin $\{0\}$ is a "natural" fixed point; the stability of the origin was investigated through the eigenvalues of the linearized matrix $[A]$.

The approach to be followed here is similar to that used in Section 3.3, but the fixed points other than $\{0\}$ have to be determined first, and then their stability investigated.

3.4.1 Methodology

Recalling that the equations of motion are

$$\begin{aligned} \dot{q}_i &= p_i\,, \\ \dot{p}_i &= -\,k_{ij}\,q_j - c_{ij}\,p_j - \alpha_{ijkl}\,q_j\,q_k\,q_l - \beta_{ijkl}\,q_j\,q_k\,p_l - \gamma_{ijkl}\,q_j\,p_k\,p_l\,, \end{aligned}$$

the fixed points are given by

$$k_{ij}\,q_j^0 + \alpha_{ijkl}\,q_j^0\,q_k^0\,q_l^0 = 0\,. \tag{3.18}$$

For the two-mode model, $i = 2$, two nonlinear equations with two unknowns q_1 and q_2 are solved. Since the coefficients α_{ijkl} are computed numerically, it is impossible to find analytic solutions to the problem. Once $(q_1^0,\, q_2^0)$ are found, the stability of that new fixed point is investigated through a perturbation

$$q_i = q_i^0 + u_i\,, \qquad p_i = v_i\,,$$

which leads to

$$\begin{aligned} &\dot{u}_i = v_i\,, \\ &\dot{v}_i = -k_{ij}\,u_j - c_{ij}\,v_j \quad -\left(\alpha_{ijkl} + \alpha_{ikjl} + \alpha_{ilkj}\right) q_k^0\,q_l^0\,u_j - \ \beta_{ijkl}\,q_j^0\,q_k^0\,v_l\,. \end{aligned} \tag{3.19}$$

To a first order approximation, system (3.19) can be transformed into matrix form,

$$\left\{ \begin{array}{c} \dot{u}_i \\ \dot{v}_i \end{array} \right\} = \left[A^0\right] \left\{ \begin{array}{c} u_i \\ v_i \end{array} \right\}, \tag{3.20}$$

$[A^0]$ being a function of k_{ij}, c_{ij}, α_{ijkl}, β_{ijkl} and q_j^0.

Depending on the parameters, different qualitative and quantitative behaviour may be found. As in the linear analysis near the origin, κ, ξ_s and β are kept constant: $\kappa = 100$, $\xi_s = 0.8$ and $\beta = 0.18$. Depending on the values of γ and u, none, two or four fixed points may exist in addition to the zero fixed point (see Section 3.3 and Figure 3.6). Hence, an Argand diagram for the new fixed points is not relevant, and another notation (Holmes 1977) is used here to present the results. The fixed point $\{0\}$ corresponds to the pipe lying along the x-axis (initial position). Due to the symmetry of the problem, the first new pair of fixed points can be represented by $\{\pm 1\}$, and the second pair by $\{\pm 2\}$. The stability of each point depends on the four eigenvalues of the matrix $[A^0]$ defined by equation (3.20). The four eigenvalues are represented by the quartet $\lambda = (\pm, \pm \pm \pm)$, where "+" stands for an eigenvalue with a positive real part, "−" for one with a negative real part, and "0" for one with zero real part. For example, a stable fixed point is represented by $\lambda = (-, -, -, -)$, and if it undergoes a Hopf bifurcation, it becomes $\lambda = (+, +, -, -)$. Hence, *at* the critical point, the fixed point is $\lambda = (0, 0, -, -)$. Similarly, a saddle-node or a pithfork bifurcation is characterized by $\lambda = (0, \pm, \pm, \pm)$, and a doubly-degenerate fixed point by $\lambda = (0, 0, 0, \pm)$.

Some cases are discussed separately in Section 3.4.2, for different values of γ.

3.4.2 Results

3.4.2.1 Case of $\gamma = 76$; Figure 3.7(a)

The origin $\{0\} = (-, -, -, -)$ is stable for small flow velocities. It undergoes a Hopf bifurcation $(+, +, -, -)$ at $u = 12.65$ and a pitchfork bifurcation at $u = 13.10$, where an unstable fixed point, $\{\pm 1\} = \{+, +, -, -\}$, appears. The fixed points $\{0\}$ and $\{\pm 1\}$ coalesce at $u = 14.72$, the velocity at which a saddle-node bifurcation occurs,

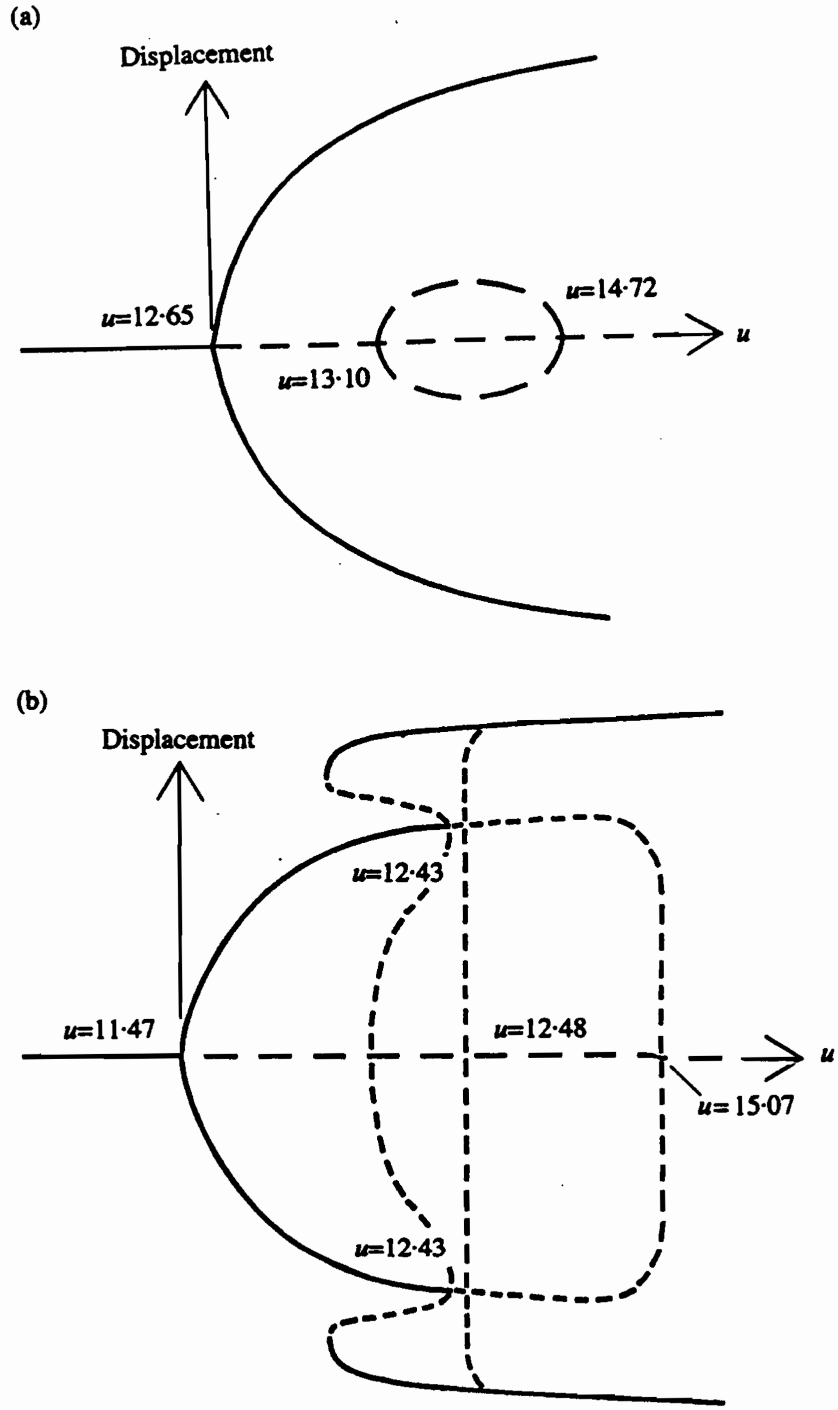

Figure 3.7: Bifurcation diagrams for the tip displacement of the nonlinear system for $\beta = 0.18$, $\kappa = 100$, $\alpha = 5 \times 10^{-3}$, and $\xi_s = 0.8$, and (a) $\gamma = 76$; (b) $\gamma = 60$; (c) $\gamma = 20$; (d) $\gamma = -60$. Dotted lines denote unstable equilibria or limit cycles.

(c)

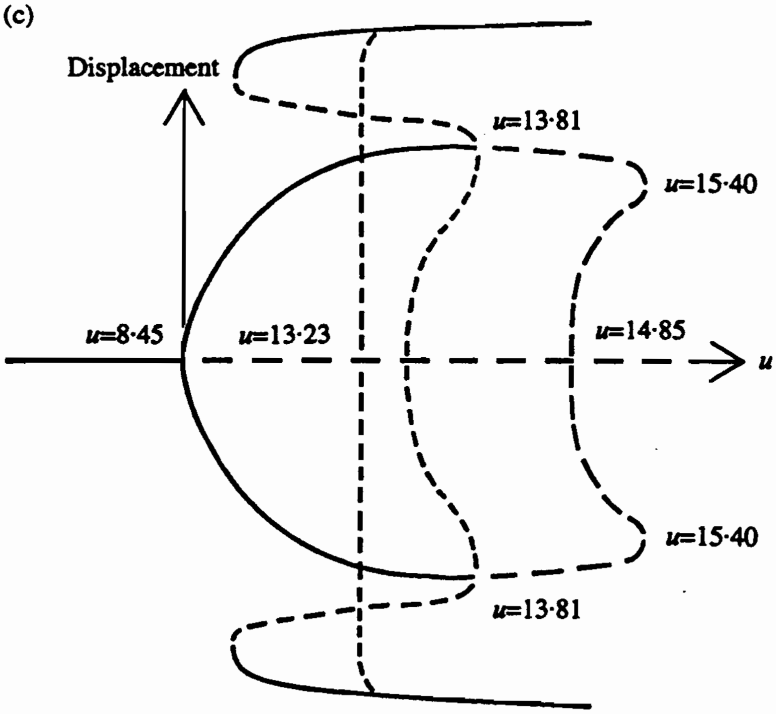

(d)

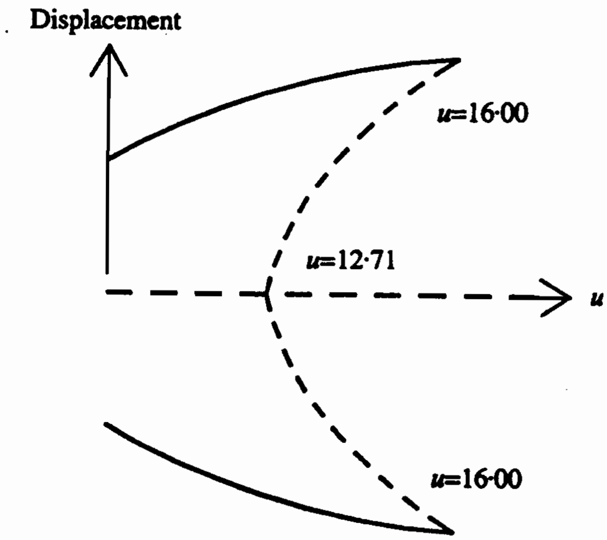

Figure 3.7: Continued.

$\{0\} = \{\pm 1\} = (+, +, 0, -)$. Physically, this means that there exists one unstable static equilibrium position in the velocity range $12.65 < u < 13.10$, and three unstable static equilibrium positions when $13.10 < u < 14.72$; flutter type motion is predominant for $u > 12.65$.

3.4.2.2 Case of $\gamma = 60$; Figure 3.7(b)

The stable origin $\{0\}$ becomes unstable through a pitchfork bifurcation $(+, -, -, -)$ at $u = 11.47$. Two stable static equilibria appear, $\{\pm 1\} = (-, -, -, -)$, until $u = 12.43$ where subcritical Hopf bifurcations occur $(+, +, -, -)$. Again, limit-cycle motion may be present, since no stable equilibrium exists. At $u = 12.48$, it is the origin $\{0\}$ that undergoes a Hopf bifurcation. The three fixed points $\{0\}$ and $\{\pm 1\}$ coalesce at $u = 15.07$ [$\lambda = (+, +, 0, -)$]. A numerical investigation confirms the results found: limit-cycle oscillations are found to exist before the first Hopf bifurcation occurs at $u = 12.43$; these oscillations are due to the subcritical bifurcation of $\{\pm 1\}$. For u a little less than 12.43, e.g. at $u = 12.35$, the orbit can be attracted either by one of the stable fixed points or by the attracting periodic limit-set.

3.4.2.3 Case of $\gamma = 20$; Figure 3.7(c)[§]

The origin $\{0\}$, initially stable for small flow velocities, undergoes a pitchfork bifurcation $(+, -, -, -)$ at $u = 8.45$. The unstable origin $\{0\}$ undergoes another bifurcation at $u = 13.23$, a Hopf bifurcation. Thus, it becomes unstable from a dynamic point of view [$\lambda = (+, +, +, -)$]. At $u = 13.81$, the two static equilibria also become unstable through a subcritical Hopf bifurcation $(+, +, -, -)$. For still higher flow velocities ($u = 14.85$), a static bifurcation occurs at the origin $\{0\}$ which is restabilized in one mode $(+, +, -, -)$ (but $\{0\}$ is still unstable); a second pair of equilibria $\{\pm 2\}$ exists, $(+, +, +, -)$ which is also unstable. Hence, five unstable fixed points coexist in the system. Finally, the two pairs $\{\pm 1\}$ and $\{\pm 2\}$ coalesce at $u = 15.40$ through a

---

[§]See also Appendix E.

saddle-node bifurcation $(+, +, 0, -)$, and disappear for higher flow velocities.

From a physical point of view, one may observe limit-cycle motions for $u > 13.81$, both static equilibrium and limit-cycle oscillations in the velocity range $13.23 < u < 13.81$, and oscillatory motion for $u > 15.4$. Qualitatively, this was also found by Holmes (1977) in the panel flutter problem.

3.4.2.4 Case of $\gamma = -60$; Figure 3.7(d)

This case corresponds to a "standing" pipe; the origin $\{0\}$ is a saddle for small velocities $(+, -, -, -)$, and two stable equilibria $\{\pm 1\} = (-, -, -, -)$ exist. At $u = 12.71$, the origin undergoes another static bifurcation $(+, +, -, -)$, and the second pair $\{\pm 2\}$ of equilibria appears $(+, -, -, -)$, until $u = 16.00$ where the two pairs coalesce. Physically, one should only see one equilibrium. Some flutter-type motions have, however, been observed numerically (see Section 3.4.3).

3.4.3 Physical implications

The results found in the previous section are quite interesting. For a given flow velocity, different steady-states may exist in the system: stable equilibria, unstable equilibria and periodic limit-sets coexist. To better understand the bifurcation diagrams obtained, it is helpful to examine the phase flow portraits for some special parameter values.

For $\gamma = -60$ and $u = 7.5$, $\{0\}$ is a saddle-point and two stable equilibria exist [cf. Figure 3.7(d)]. Figure 3.8(a) illustrates the stable and unstable manifolds of the origin $\{0\}$; all solutions tend to one of the stable equilibria. The pipe is unstable from a static point of view, i.e. it is buckled.

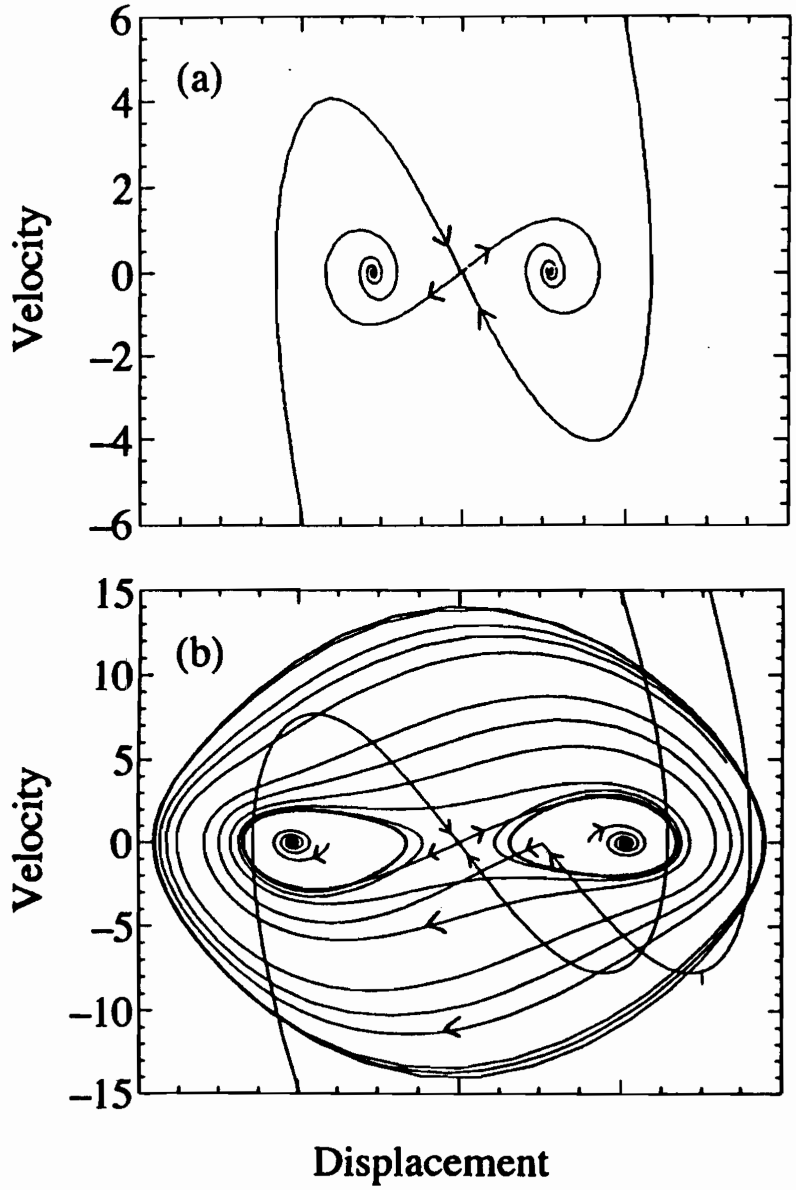

Figure 3.8: Phase portraits representing (a) the saddle node $\{0\}$ and the two stable equilibria $\{\pm 1\}$ at $u = 7.5$ and $\gamma = -60$; (b) three saddles $\{0\}$ and $\{\pm 2\}$, two stable equilibria $\{\pm 1\}$ and oscillatory motions at $u = 13.1$ and $\gamma = -60$ (where, for clarity, not all the manifolds are represented); (c) close to the onset of oscillatory motions at $u = 8.76$, $\gamma = -80$. In all cases, $\beta = 0.18$, $\kappa = 100$, $\alpha = 5 \times 10^{-3}$, $\xi_s = 0.8$.

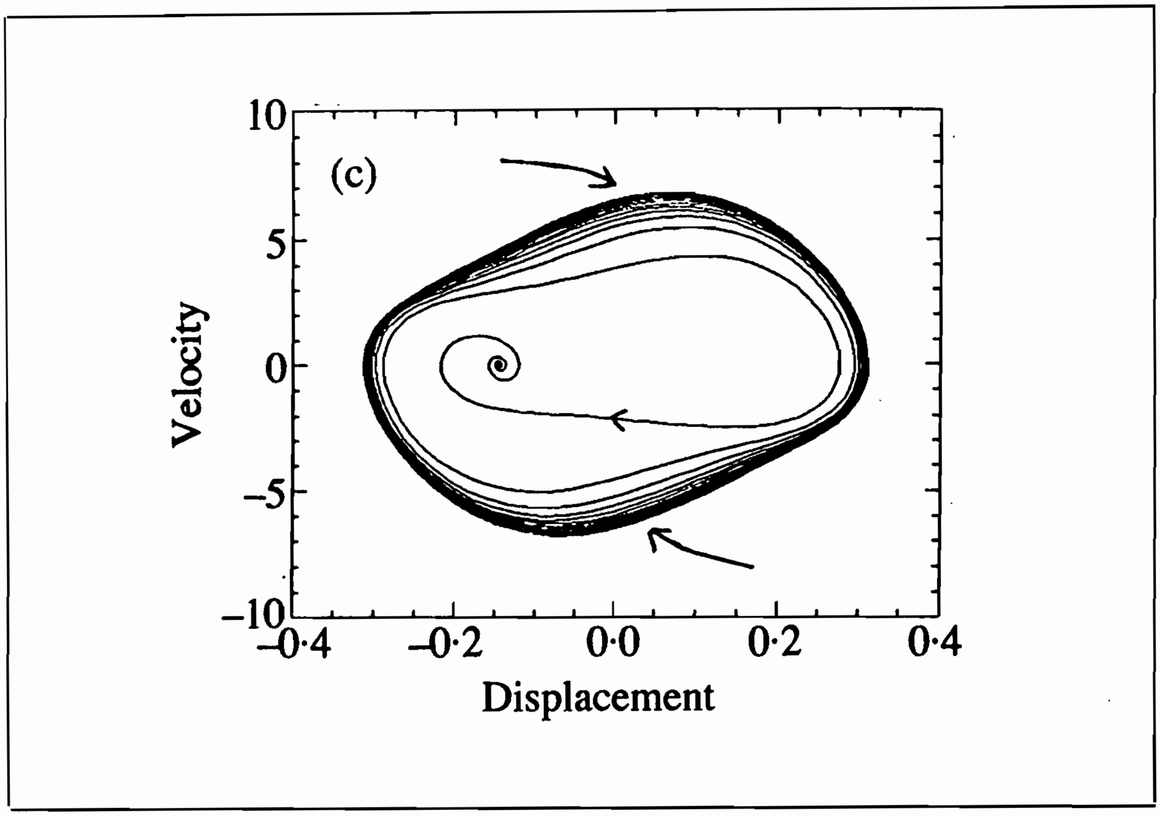

Figure 3.8: Continued.

For $\gamma = -60$ and $u = 13.1$ the dynamics are more complicated: five equilibria exist [Figure 3.8(b)]. The origin $\{0\}$ is a saddle, as well as the second pair $\{\pm 2\}$; (not all the stable and unstable manifolds have been drawn for clarity, and only one fixed point of the second pair). The first pair $\{\pm 1\}$, shown in Figure 3.8(b) at ± 0.2, is "weakly" attracting. Flows with initial conditions close to the equilibrium are attracted by one of the fixed point $\{\pm 1\}$. However, other attracting sets also exist: one may observe either oscillations around one of the equilibria or global oscillations around the five equilibria. Those oscillations do not come from local bifurcations; as in the case of the pendulum, they represent an energy state for which the oscillations do not die out. For Duffing's equation for example, solutions lie on level curves of the Hamiltonian energy, H, of the system. These solutions are closed orbits representing a global stability state (Guckenheimer & Holmes 1983).

The case $\gamma = -80$ and $u = 8.76$ in Figure 3.8(c) depicts the boundary between two states: for $u < 8.76$, no closed orbit can be found, even with very large initial conditions, whereas for $u > 8.76$ it can. The limit-set tracks flows with big initial conditions, but it is not "sufficiently attracting". The flow is finally attracted by one of the stable equilibria.

Numerically, this process of finding the critical velocity, u, can be repeated for different values of γ. In this way, the stability map of Figure 3.6 can then be completed, by the addition of the boundary (shown as a dashed line) for global oscillations.

3.5 STANDARD FORMS, CENTRE MANIFOLD, NORMAL FORMS

The main purpose of this section is to describe qualitatively the dynamics of the autonomous system. The idea is to reduce the dimension of the system at the degenerate fixed points, so as to be able to study it in a clearer, simpler way.

The asymptotic behaviour of the solution near a hyperbolic or nondegenerate fixed point is determined by linearization. Hence, in this case, there exist locally stable and unstable manifolds, W^s_{loc} and W^u_{loc}, of the same dimensions, n_s and n_u, as those of the eigenspaces (E^s, E^u) of the linearized system, and tangent to (E^s, E^u) at the fixed point (Guckenheimer & Holmes 1983). The local dynamical behaviour of the system on those stable or unstable manifolds is relatively simple, since it is controlled by exponentially contracting or expanding flows.

In the case of a degenerate fixed point (i.e., one with at least one eigenvalue with zero real part), a third component, the centre manifold W^c_{loc}, tangent to the centre eigenspace E^c, has to be taken into account. The stability properties of the dynamical system along the stable and unstable manifolds are known, so that one can restrict the study of the dynamics near the degenerate point to the study of the flow on the centre manifold. This is the main idea of centre manifold theory (Carr 1981). For example, if the fixed point contains a single zero eigenvalue, the dimension of the centre space is one, and if the degenerate fixed point has a pair of purely imaginary eigenvalues, the dimension of the centre space becomes two.

Centre manifold theory is especially important in the case of high- or infinite-dimensional problems, since one thereby extracts an essential model on a low dimensional space that captures the local bifurcational behaviour. Consequently, after putting the system in its standard form, one determines the centre manifold and the subsystem on this manifold. Combined with bifurcation theory, i.e. when the system has variable parameters, the method is particularly powerful. Indeed, for low-dimensional problems, a complete classification of most of the "famous" bifurcations was undertaken twenty years ago (Takens 1974) and can be applied directly here. The resulting "simplified" subsystems are called normal forms.

3.5.1 Standard forms

In this section, the standard forms are formulated. Depending on the degree of degeneracy of the fixed point, different situations may arise. In dynamics, a bifurcation problem is usually described by the following equation

$$\dot{x} = f_\mu(x)\,, \qquad x \in \mathcal{R}^n\,, \qquad \mu \in \mathcal{R}^k\,; \tag{3.21}$$

one wants to find a value μ_0 for which the flow of (3.21) is not structurally stable, and draw the qualitative aspects of the flow for small changes in μ. The classification of the bifurcations mentioned in the previous section is based on the theory of transversality in differential topology.

Many possibilities can be listed, depending on the Jacobian derivatives $D_x f_\mu$ evaluated at the bifurcation point $(x_0,\ \mu_0)$. Thus, for a simple zero eigenvalue,

$$[D_x f_\mu] = \begin{bmatrix} 0 & 0 \\ 0 & [M] \end{bmatrix}\,; \tag{3.22}$$

for a simple pure imaginary pair,

$$[D_x f_\mu] = \begin{bmatrix} \begin{bmatrix} 0 & -\omega_0 \\ \omega_0 & 0 \end{bmatrix} & 0 \\ 0 & [M] \end{bmatrix} ; \tag{3.23}$$

for a double zero, nondiagonalizable,

$$[D_x f_\mu] = \begin{bmatrix} \begin{bmatrix} 0 & 1 \\ 0 & 0 \end{bmatrix} & 0 \\ 0 & [M] \end{bmatrix} ; \tag{3.24}$$

and for a simple zero plus a pure imaginary pair,

$$[D_x f_\mu] = \begin{bmatrix} \begin{bmatrix} 0 & -\omega_0 & 0 \\ \omega_0 & 0 & 0 \\ 0 & 0 & 0 \end{bmatrix} & 0 \\ 0 & [M] \end{bmatrix} . \tag{3.25}$$

In each case, $[M]$ is a matrix of appropriate dimension, in which all eigenvalues have nonzero real parts. The "0" are not necessarily scalar zeros, but rather the appropriately sized blocks consisting of zeros.

Consequently, starting from the original equation

$$\dot{y} = [A]\, y + \varepsilon\, f(y)\,, \tag{3.26}$$

evaluated at the critical values, the system may be brought into one of the standard forms cited above (Semler 1991), by constructing the modal matrix $[P]$ and by letting $y = [P]\, x$,

$$\dot{x} = [A']\, x + \varepsilon\, [P^{-1}]\, f([P]\, x)\,, \tag{3.27}$$

with $[A']$ taking one of the forms (3.22)- (3.25), depending on the degeneracy of the fixed point.

3.5.2 Centre manifold

Starting from the standard form (3.27), the centre manifold can be computed. In general, this can be a complicated task. However, it may be found more easily with an order analysis. This was developed by Sethna & Shaw (1987) and Li & Païdoussis (1994). Equation (3.27) can be rewritten as

$$\begin{aligned} \dot{x} &= [A]\, x + \varepsilon\, f(x,y)\,, \qquad & x &\in \mathcal{R}^n\,, \\ \dot{y} &= [B]\, y + \varepsilon\, g(x,y)\,, \qquad & y &\in \mathcal{R}^m\,, \end{aligned} \tag{3.28}$$

where $[A]$ contains either zero or purely imaginary eigenvalues, $[B]$ contains eigenvalues with non-zero real parts, both f and g are homogeneous cubic nonlinear polynomials, and n and m represent the appropriate dimensions.

Considering ε as a variable (with $d\varepsilon/dt = 0$), the centre manifold can be written as

$$y = h(x,\, \varepsilon)\,, \tag{3.29}$$

with the boundary conditions

$$h(0,\,0) = 0, \quad \frac{\partial h}{\partial x}(0,\,0) = 0, \quad \frac{\partial h}{\partial \varepsilon}(0,\,0) = 0\,. \tag{3.30}$$

After various differentiations, substitutions and an order analysis, the flow on the centre manifold is found to be

$$\dot{x} = [A]\, x + \varepsilon\, f(x,\, 0) + \mathcal{O}(\varepsilon^2)\,. \tag{3.31}$$

It is obvious that equation (3.31) can be obtained by neglecting the stable (or unstable) components in (3.28). Practically, these operations are straightforward.

Consequently, the analysis is now restricted to the centre manifold, which is of dimension 1, 2 or 3 depending on the eigenvalues of the fixed point.

3.5.3 Normal forms

After using centre manifold theory, which enables the reduction of the dimension of the problem to its minimum value, the subsystem defined on the centre manifold itself can still be very complicated. The idea of normal form theory is to reduce, to the simplest form, the vector field $f_\mu(x)$ which defines the flow on the centre manifold,

$$\dot{x} = f_\mu(x)\,; \tag{3.32}$$

In the vocabulary of dynamics, "as simple as possible" means in some sense "irreducible" (Guckenheimer & Holmes 1983). Note that (3.32) is similar to (3.21), but does not represent the same problem, the flow here being restricted to the centre manifold. The idea of normal forms begins with finding a near-identity coordinate transformation P,

$$x = y + P(y)\,, \tag{3.33}$$

where P is a polynomial. Therefore, (3.32) becomes

$$\dot{y} = (I + DP(y))^{-1}\; f_\mu\,(y + P(y))\;. \tag{3.34}$$

In terms of power series, one tries to find a sequence of coordinate transformations, P, which removes terms of increasing degree from the Taylor series expansion of (3.34) at the fixed point $\{0\}$. Hence, all inessential terms are removed up to some degree from the Taylor series (Guckenheimer & Holmes 1983). For the simplest cases, a general normal form has already been derived.

Here, as many methods as possible are used in the different examples: (i) the standard normal form in the case of one zero eigenvalue; (ii) the method of averaging yielding the normal form in the case of a pair of purely imaginary eigenvalues; (iii) the use of available normal forms in the doubly-degenerate case.

3.5.4 Results

In this section, centre manifold theory has been utilized to obtain the flows in the neighbourhood of some of the critical parameters associated with specific bifurcations. These solutions are stricly valid very near the bifurcation points (small μ in what follows) — although, as will be seen, the results work for significantly large values of μ.

3.5.4.1 Zero eigenvalue bifurcation

As proved in the linear analysis, a zero eigenvalue occurs for a standing pipe (represented by negative gravity $\gamma < 0$) when $\kappa = 0$. For $\gamma = -25$ for example, this occurs at $u_c = 3.05$.

Processing the system according to centre manifold theory allows the reduction of the dimension of the full system, in the neighbourhood of $u_c = 3.05$, to a one-dimensional subsystem.

The calculations are performed using the computer algebra system MACSYMA, accomplishing the following steps: (i) computation of the linear matrix $[A]$, as a function of the control parameter $\mu = u - u_c$; (ii) calculation of the eigenvalues of $[A]$ at u_c; (iii) construction of the modal matrix $[P]$, evaluated at the critical parameters; (iv) computation of the nonlinear terms; (v) computation of the standard form; (vi) evaluation of the flow on the centre manifold through equation (3.31).

For the system parameters considered ($u_c = 3.05,\ \gamma = -25,\ \beta = 0.2,\ \kappa = 0$), this procedure yields

$$\dot{x} = \left(-4.44\,\mu - 10.85\,x^2\right) x\,. \tag{3.35}$$

From (3.35), it is clear that the bifurcation occurring at the critical parameter is a supercritical pitchfork bifurcation.

When $\mu < 0$ ($u < u_c$), the origin is unstable, and solutions diverge to one or the other (depending on the initial conditions) of the stable equilibria.

When $\mu > 0$ ($u > u_c$), the origin becomes stable, and the two symmetric equilibrium positions disappear; the system regains stability. This was also found through the numerical integration of the complete equations (3.14) and is shown in Figure 3.9(a,b), for $u < u_c$ and $u > u_c$ respectively.

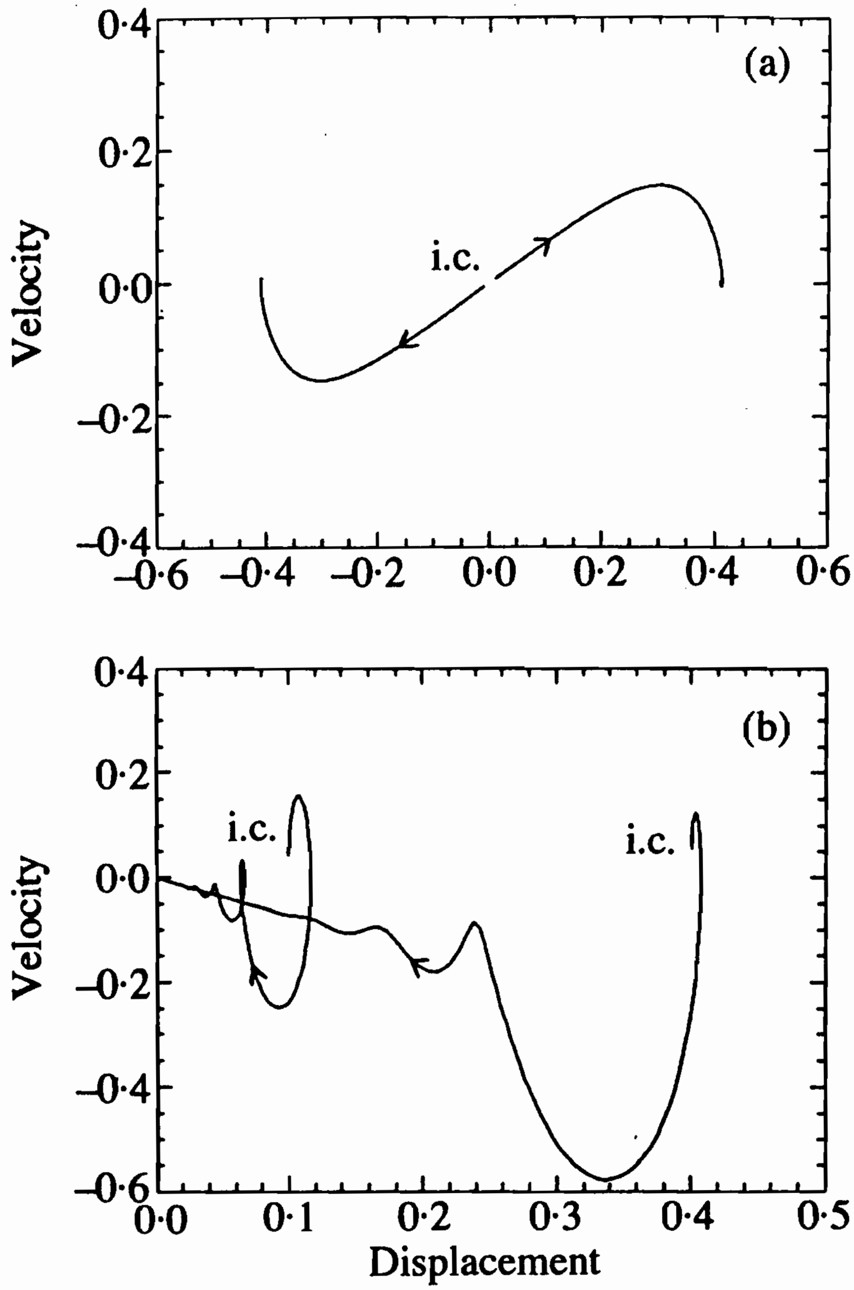

Figure 3.9: Phase and bifurcation diagrams showing the transition of stability of the origin through a pitchfork bifurcation; $u_{cr} = 3.05$ for $\gamma = -25$, $\beta = 0.2$, $\kappa = 0$ and $\alpha = 5 \times 10^{-3}$. Phase diagrams for (a) $u = 2.99$, (b) $u = 3.20$; i.c. stands for initial condition. (c) bifurcation diagram: — , centre manifold approximation; o , numerical integration.

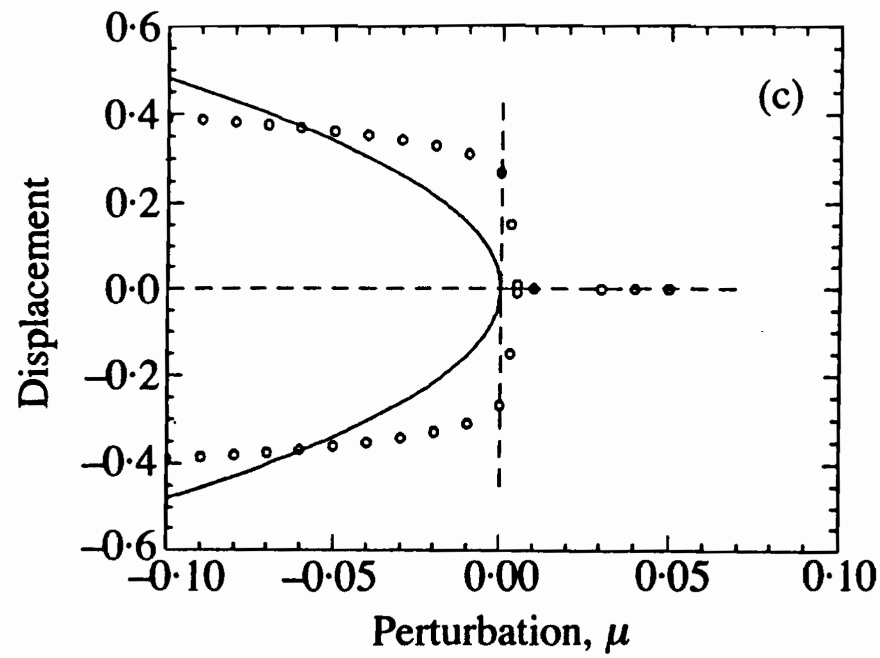

Figure 3.9: Continued.

These results are of course familiar, since the system and the equations have some symmetry properties [the differential equation (3.21) is symmetric or equivariant with respect to the transformation $x \to -x$; thus $f_\mu(-x) = -f_\mu(x)$]; in this case, some transversality conditions cannot be satisfied, and hence, neither saddle-node nor transcritical bifurcations can occur.

Moreover, the equilibrium positions can be evaluated very easily from equation (3.35). Letting $dx/dt = 0$ yields

$$x_{eq} = \pm\sqrt{\frac{-4.44\,\mu}{10.85}} = \pm\,0.64\,\sqrt{-\mu}\,. \tag{3.36}$$

Using the modal matrix $[P]$, one can reconstruct the stationary solution

$$q_{1eq} = x_{eq}\,, \quad q_{2eq} = -0.192\,x_{eq}\,, \tag{3.37}$$

and through the Galerkin transformation, obtain the deflection of any point on the beam. For $\mu = -0.05$ for example, the position of the fixed point is found equal to $y = \pm 0.37$ by numerical integration, and equal to ± 0.35 by reconstruction of the flow.

The results shown in Figure 3.9(c) prove that (i) there is qualitative and quantitative agreement between the solutions of the complete and the reduced systems for small values of μ $(-0.10 \leq \mu \leq 0)$ for the set of parameters chosen, and that (ii) a parabolic shape is obtained. However, before closing this section, it should be remarked that simpler methods can be used to find static solutions.

3.5.4.2 The Hopf bifurcation

This has been studied extensively, physically and mathematically, by many authors (e.g., Marsden & McCracken 1976). In this case, $D_x f_\mu$ takes the form (3.23), and the normal form is given by

$$\dot{r} = \left(d\,\mu + a\,r^2\right) r, \quad \dot{\phi} = \left(\omega_0 + c\,\mu + b\,r^2\right) , \tag{3.38}$$

in which μ is directly related to the change of the parameters (the flow velocity in this case), and a, b, c and d are coefficients to be computed from normal form theory. For example, if the flow on the centre manifold is defined by

$$\dot{x}_1 = -\omega_0\, x_2 + \varepsilon\, f_1(x_1\, x_2)\,, \quad \dot{x}_2 = \omega_0\, x_1 + \varepsilon\, f_2(x_1\, x_2)\,, \tag{3.39}$$

a is simply obtained by

$$a = \frac{1}{8}\, \left(f_{1,12} + 3\, f_{1,30} + 3\, f_{2,03} + f_{2,21}\right)\,, \tag{3.40}$$

where

$$f_i = f_{i,30}\, x_1^3 + f_{i,21}\, x_1^2\, x_2 + f_{i,12}\, x_1\, x_2^2 + f_{i,03}\, x_2^3\,, \qquad i = 1,2.$$

In the case of an autonomous system, the normal form and the averaging methods yield the same results. The second one is used here. Starting from (3.32), one seeks solutions of the form

$$x_1 = r\, \cos(\omega_o\tau + \phi) = r\, C\,, \quad x_2 = r\, \sin(\omega_o\tau + \phi) = r\, S\,, \tag{3.41}$$

where C stands for $\cos(\omega_0\tau+\phi)$ and S for $\sin(\omega_0\tau+\phi)$. Considering the left- and right-hand sides of (3.32), and equating the two sets of expressions leads, after integration, to

$$(\dot{r})_{\mathrm{av}} = \frac{\omega}{2\pi} \int_0^{\frac{2\pi}{\omega}} (f_1\, C + f_2\, S)\,\mathrm{d}\tau\,, \qquad (r\dot{\phi})_{\mathrm{av}} = \frac{\omega}{2\pi} \int_0^{\frac{2\pi}{\omega}} (f_2\, C - f_1\, S)\,\mathrm{d}\tau\,, \tag{3.42}$$

in which integrals r and ϕ are assumed to be constant (Sanders & Verhulst 1985). The advantage of the averaging method is that it is based on several basic comparison theorems which compare solutions of (3.32)and the averaged equations (3.42) (Chow & Mallet-Paret 1977). For solutions valid for time of $\mathcal{O}(\varepsilon^{-1})$, any solutions of (3.42) can be shown to be close to those of (3.32) for sufficiently small ε.

The algebra involved in carrying out these calculations can become tedious; however, it is easily handled on a computer with a symbolic manipulation program, such as MACSYMA. For $\gamma = 25$, $\beta = 0.2$, and $\kappa = 0$; $u_c = 7.093$, and one obtains

$$\dot{r} = 2.277\,\mu\, r - 89.663\, r^3\,, \qquad \dot{\phi} = 16.16 - 0.903\,\mu + 106.529\, r^2\,. \tag{3.43}$$

The nonlinear coefficient a equals $-89.663 < 0$ showing that the corresponding Hopf bifurcation is supercritical. Moreover, under this normal form, the radius of the limit cycle (in the new coordinates) can be obtained, by letting $dr/dt = 0$, or

$$r_{\ell c} = \pm\sqrt{\frac{2.77}{-a}\,\mu}\,, \tag{3.44}$$

where the ℓc subscript stands for 'limit cycle'.

From a physical point of view, for $\mu < 0$ ($u < u_c$), and the origin is stable (no limit cycle); it becomes unstable for $\mu > 0$. These results are familiar. Of more interest is the use of these results in the original coordinates. Letting

$$r = r_{\ell c} = 0.176\,\sqrt{\mu}\,, \qquad \dot{\phi} = \dot{\phi}_{\ell c} = 16.16 + 1.802\,\mu\,, \tag{3.45}$$

one can easily reconstruct the original equation on the centre manifold: from

$\{y\} = [P]\{x\}$, and by approximating $\{x\}$ as

$$\{x\} = \left\{ \begin{array}{c} r_{\ell c} \cos(\phi_{1c}\tau) \\ r_{\ell c} \sin(\phi_{1c}\tau) \\ 0 \\ 0 \end{array} \right\},$$

one obtains

$$\{y\} = \left\{ \begin{array}{c} y_1 \\ y_2 \\ y_3 \\ y_4 \end{array} \right\} = \left\{ \begin{array}{c} r_{\ell c} \cos(\phi_{\ell c}\tau) \\ -0.3421\, r_{\ell c} \sin(\phi_{\ell c}\tau) \\ -16.16\, r_{\ell c} \sin(\phi_{\ell c}\tau) \\ -5.53\, r_{\ell c} \cos(\phi_{\ell c}\tau) \end{array} \right\},$$

Of course, $y_3 = dy_1/dt$ and $y_4 = dy_2/dt$ as they should be. The displacements and velocities at the end of the pipe are computed through the Galerkin approximation

$$\begin{aligned} x(1,\tau) &= y_1(\tau)\, \phi_1(1) + y_2(\tau)\, \phi_2(1)\,, \\ \dot{x}(1,\tau) &= y_3(\tau)\, \phi_1(1) + y_4(\tau)\, \phi_2(1)\,. \end{aligned} \tag{3.46}$$

The phase plots for $\mu = 0.3$ are compared with those obtained by numerical integration, in Figure 3.10(a,b). Considering the fact that μ is not very small (as required in the theory), the approximations of the flow on the centre manifold are excellent. The comparison is also made for the bifurcation diagram in Figure 3.10(c) and confirms all these results. Again, the bifurcation type is clearly defined, and agreement for a large range of μ is obtained.

Consequently, not only the qualitative aspect of the bifurcation has been found, but also the quantitative behaviour after the bifurcation. This is of great interest: by utilizing the normal-form reduction, the type of bifurcation has been clarified, the post-bifurcation behaviour has been predicted, and complicated equations have been transformed into a much simpler system.

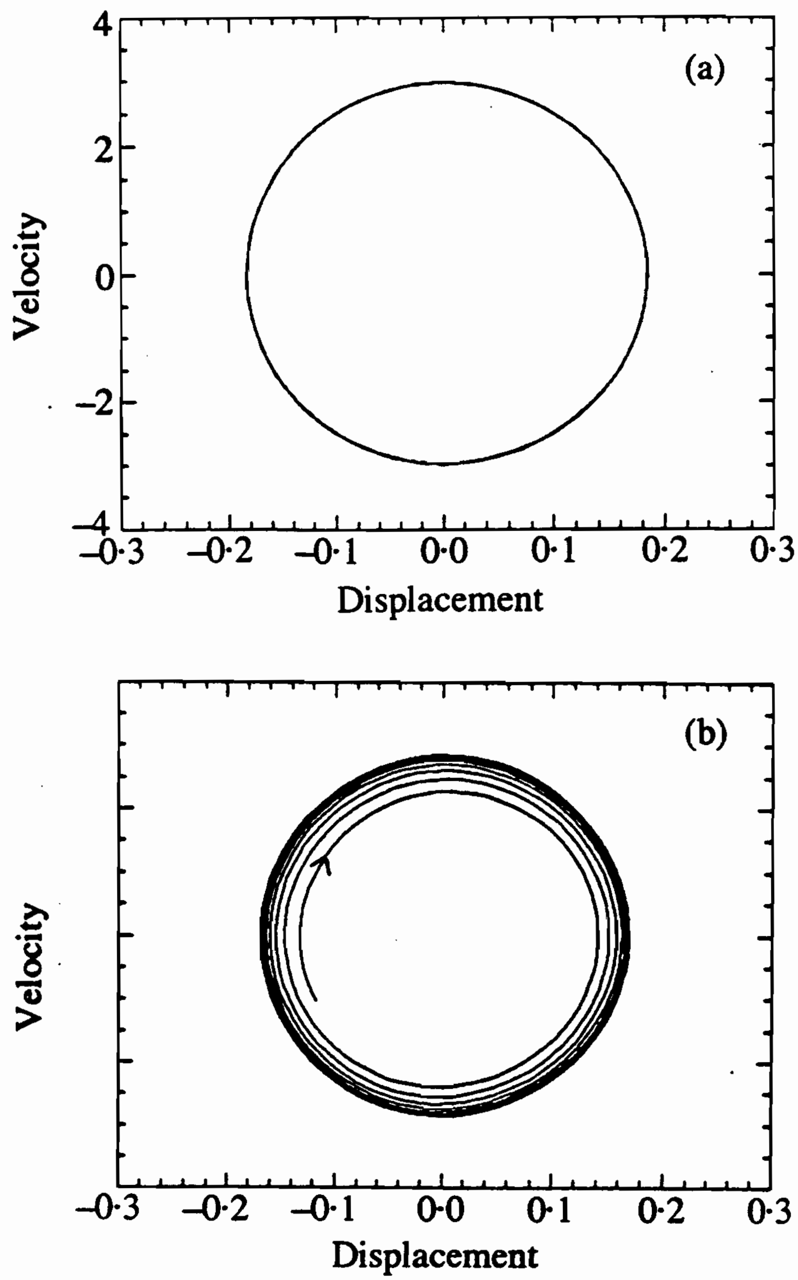

Figure 3.10: Supercritical Hopf bifurcation. Comparison between (a) centre manifold and (b) numerical integration for $\mu = 0.3$; $u_{cr} = 7.09$ for $\gamma = 25$, $\beta = 0.2$, $\kappa = 0$ and $\alpha = 5 \times 10^{-3}$. (c) Bifurcation diagram: —, centre manifold approximation; o, numerical integration.

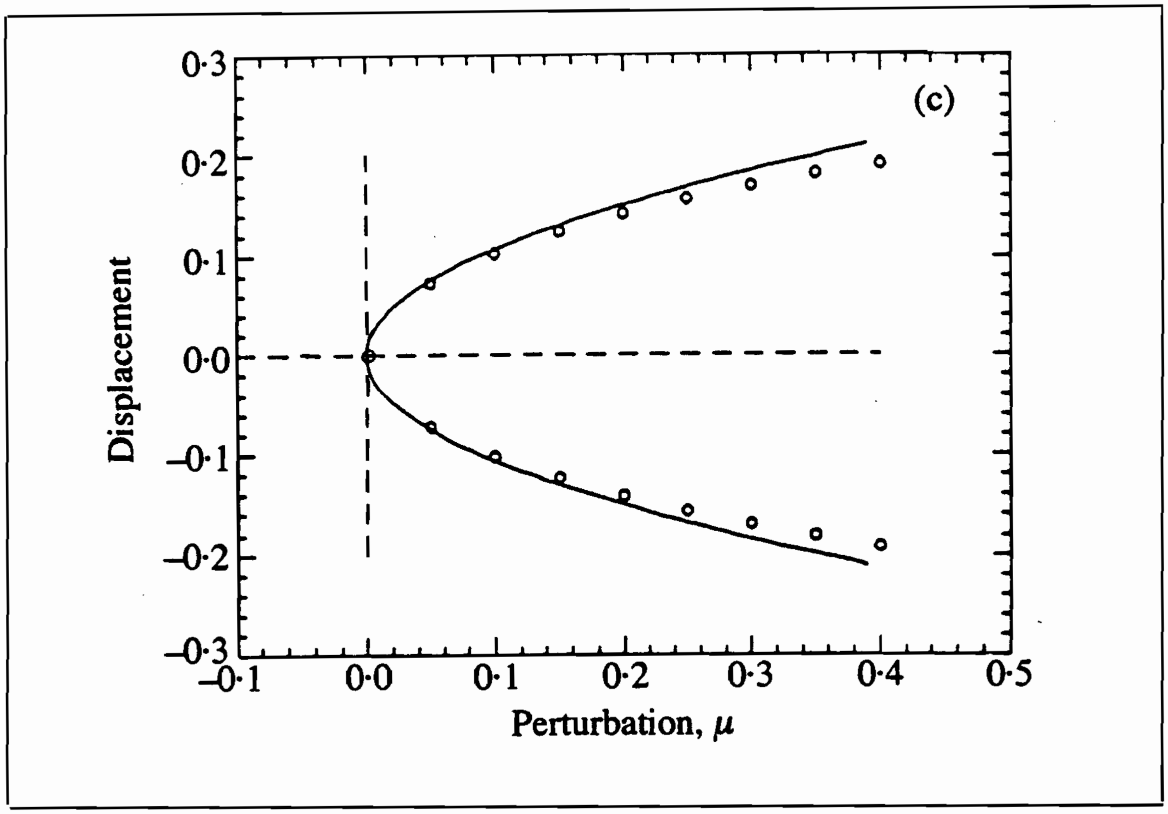

Figure 3.10: Continued.

3.5.4.3 Doubly degenerate case

A complete bifurcation analysis near the doubly degenerate fixed point was undertaken by Sethna & Shaw (1987). The strategy used in this section follows the one described in the case of the zero eigenvalue: after evaluating the flow on the centre manifold and neglecting the other components, the autonomous subsystem is brought to the form

$$\dot{x} = \begin{bmatrix} 0 & -\omega_0 & 0 \\ \omega_0 & 0 & 0 \\ 0 & 0 & 0 \end{bmatrix} x + \begin{bmatrix} \varepsilon\,\mu_1 & -\varepsilon\,\mu_3 & 0 \\ \varepsilon\,\mu_3 & \varepsilon\,\mu_1 & 0 \\ 0 & 0 & \varepsilon\,\mu_2 \end{bmatrix} x + \varepsilon\, f(x)\,. \qquad (3.47)$$

where f is a third-order polynomial in x.

In dynamics vocabulary, μ_1 and μ_2 are called unfolding parameters, and they represent the deviations of the real parameters from their critical values. These parameters are necessary to capture all the possible behavioural characteristics of the system. In the case of a double degeneracy, two parameters are necessary to unfold the dynamics of the problem (codimension-two bifurcation).

One follows the strategy of normal forms, in which all the non-essential nonlinear terms of f are eliminated ("non-essential" meaning that they do not affect the qualitative dynamics). First, one introduces the coordinate transformation

$$x = y + \varepsilon\, P(y)\,.$$

Differentiating with respect to time yields

$$\dot{x} = \dot{y}\,[I + \varepsilon\, D\, P(y)]\ ,$$

where DP is the Jacobian matrix of P. After substituting into (3.32) and simplifying, one obtains

$$\begin{aligned} \dot{y} \quad &= L(y) + \varepsilon\,(DL \cdot P(y) - DP \cdot L(y) + f(y)) + \mathcal{O}(\varepsilon^2) \\ &= L(y) + \varepsilon\, g(y) + \mathcal{O}(\varepsilon^2)\,, \end{aligned} \tag{3.48}$$

with

$$DL = \begin{bmatrix} 0 & -\omega_0 & 0 \\ \omega_0 & 0 & 0 \\ 0 & 0 & 0 \end{bmatrix},$$

and

$$g(y) = DL \cdot P(y) - DP \cdot L(y) + f(y)\,. \tag{3.49}$$

In the case of the double degeneracy with certain symmetry properties, the normal form is shown to be

$$\begin{aligned} \dot{r} &= \varepsilon\,[\mu_1\, r - (a_{11}\, r^2 + a_{12}\, z^2)]\, r + \mathcal{O}(\varepsilon^2)\,, \\ \dot{z} &= \varepsilon\,[\mu_2\, z + (a_{21}\, r^2 + a_{22}\, z^2)]\, z + \mathcal{O}(\varepsilon^2)\,, \\ \dot{\phi} &= \omega_0 + \mathcal{O}(\varepsilon)\,, \end{aligned} \tag{3.50}$$

where $r^2 = y_1^2 + y_2^2$ (Takens 1974; Guckenheimer & Holmes 1983). The problem now becomes the following: knowing $L(y)$, $f(y)$ and $g(y)$, what is the polynomial P which satisfies (3.49)? Recalling that f, g and P are third-order polynomials, they can be written as

$$\begin{aligned} f_i(y) &= f_{i,k_1,k_2,k_3}\, y_1^{k_1}\, y_2^{k_2}\, y_3^{k_3}\,, \quad g_i(y) = g_{i,k_1,k_2,k_3}\, y_1^{k_1}\, y_2^{k_2}\, y_3^{k_3}\,, \\ p_i(y) &= p_{i,k_1,k_2,k_3}\, y_1^{k_1}\, y_2^{k_2}\, y_3^{k_3}\,, \end{aligned}$$

with $i = 1, 2, 3$ and $k_1 + k_2 + k_3 = 3$.

Equating the different coefficients leads to 24 constraint conditions, with 30 unknown coefficients p_{i,k_1,k_2,k_3}. Finally, the coefficients a_{11}, a_{12}, a_{21}, a_{22} in (3.50) are obtained:

$$\begin{aligned} &a_{11} = -\tfrac{1}{8}\left(f_{2,210} + 3\, f_{2,030} + 3\, f_{1,300} + f_{1,120}\right)\,, \quad a_{12} = -\tfrac{1}{2}\left(f_{2,012} + f_{1,102}\right)\,, \\ &a_{21} = \tfrac{1}{2}\left(f_{3,201} + f_{3,021}\right)\,, \quad a_{22} = f_{3,003}\,. \end{aligned} \tag{3.51}$$

Up to $\mathcal{O}(\varepsilon)$ this result is the same as that obtained by the method of averaging (Sethna & Shaw 1987.)

In physical terms, r in equations (3.50) represents the amplitude of oscillatory motions of the pipe, z represents the buckled positions of the pipe and $\mathrm{d}\phi/\mathrm{d}t$ the frequency of oscillations. It is interesting to note that the first two equations of (3.50) and the third one are decoupled, providing immediately

$$\phi = \omega_0 t + \phi_0 + \mathcal{O}(\varepsilon)\,.$$

A rescaling procedure can transform the first two equations to their usual form (Guckenheimer & Holmes 1983; pp. 396-411),

$$\dot{r} = r\left(\mu_1 + r^2 + b\, z^2\right)\,, \quad \dot{z} = z\left(\mu_2 + cr^2 + d\, z^2\right)\,, \quad d = \pm 1\,. \tag{3.52}$$

This system has been studied by Takens (1974) who found nine topologically distinct equivalent classes. Results obtained from three different sets of parameters are presented now for comparison:

Case 1:	$u = 2.245$	$\gamma = -46.001$	$\beta = 0.20$	$\kappa = 0$,
Case 2:	$u = 12.598$	$\gamma = 71.941$	$\beta = 0.18$	$\kappa = 100$,
Case 3:	$u = 15.111$	$\gamma = 46.88$	$\beta = 0.25$	$\kappa = 100$.

The location of the linear spring is constant, $\xi_s = 0.8$. In all three cases, $d - bc \neq 0$. Table 3.1 shows the coefficients found and the corresponding equivalence class (last column) defined in Guckenheimer & Holmes (1983, p. 399).

	d	c	b	$d - bc$	Class
Case 1	$-1 < 0$	$-1.52 < 0$	$3.954 > 0$	$+$	VIa
Case 2	$-1 < 0$	$-0.07 < 0$	$-24.3 < 0$	$-$	VIII
Case 3	$-1 < 0$	$-3.39 < 0$	$1.656 > 0$	$+$	VIa

Table 3.1: Normal form coefficients and equivalence class

Starting from system (3.52) and referring to Figure 3.11, the classification of the different unfoldings can be undertaken. For example, one can easily show that pitchfork bifurcations occur from $\{0\}$ on the lines $\mu_1 = 0$ and $\mu_2 = 0$, and also that pitchfork bifurcations occur from $(r = \sqrt{-\mu_1},\ z = 0)$ on the line $\mu_2 = c\,\mu_1$, and from $\left(r = 0,\ z = \sqrt{\mu_2}\right)$ on the line $\mu_2 = -\mu_1/b$ (see Appendix F). The behaviour of the system remains simple, as long as Hopf bifurcations do not occur from the newly fixed point. This is the case when $d - bc < 0$. Hence, in Case 2, no Hopf bifurcation can occur, while it is possible in Cases 1 and 3. The bifurcation sets, and the associated phase portraits can be constructed for the different unfoldings; it is evident that in Case 2 [Figure 3.11(b)], no global bifurcations are involved, while in the other two cases, a heteroclinic loop (or saddle loop) emerges [Figure 3.11(a)].

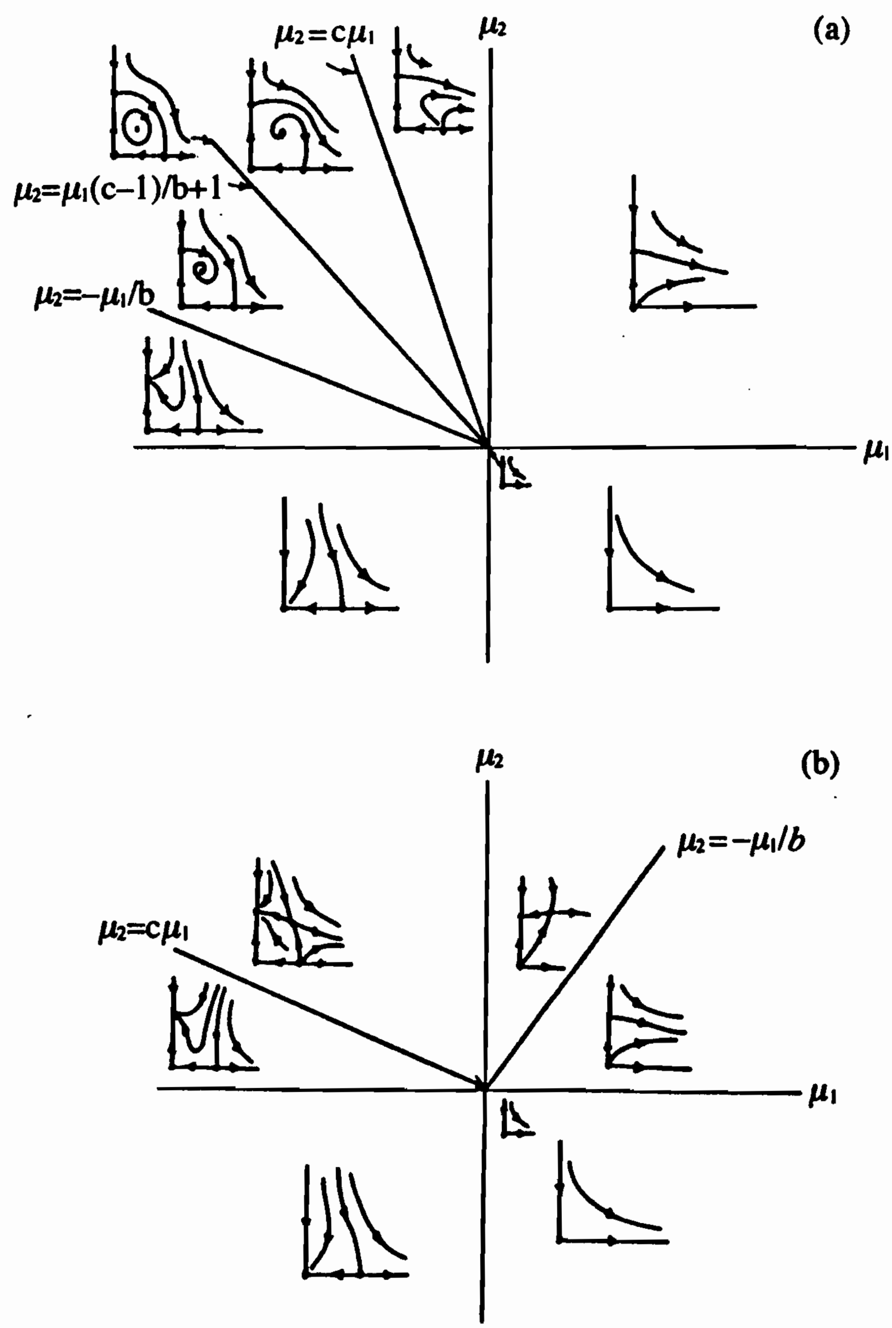

Figure 3.11: Codimension-2 bifurcation diagram for the doubly-degenerate fixed point. (a) Cases 1 and 3 (taken from Guckenheimer & Holmes 1983); (b) Case 2, calculated here.

To get a physical understanding of the motions of the tube from the phase portraits of Figure 3.11, it may be useful to recall that (a) a fixed point on the $r = 0$ axis represents a static equilibrium position and (b) a fixed point with $r \neq 0$ represents a periodic solution because of the angular variable ϕ. By integrating numerically the equations of motion, some of the results obtained by the normal forms were verified. For example, it was possible to find (i) the stable fixed point $\{0\}$; (ii) the stable fixed point $\{\pm 1\}$ corresponding to the buckled state; (iii) oscillatory motions around the origin $\{0\}$. However, attempts to obtain some of the more unusual features of the system shown in Figure 3.11(a), such as amplitude-modulated motions, have not been successful. In Figure 3.11 it is seen that most of the limit sets are unstable. On the other hand, by numerical integration of the equations it is possible to find only the stable hyperbolic sets.

3.5.4.4 Double zero eigenvalue problem

This case was also investigated and the normal form computed (Semler 1991). Although the analysis of the normal form brought out the emergence of global bifurcations involving the coalescence of closed orbits as well as saddle connections, it was not possible to verify the results, since among the four eigenvalues, one of them is strictly positive, making the fixed point $\{0\}$ unstable (thus, an unstable manifold exists here).

3.6 NUMERICAL INVESTIGATION NEAR DEGENERATE POINTS

The study of the normal forms for different sets of parameters has allowed the classification of degenerate fixed points through very rich bifurcation sets. It has proved that under certain conditions, heteroclinic bifurcations may occur, also demonstrating that global bifurcations can be detected by means of local analysis.

Moreover, it is well known that it is possible to find regions where chaotic oscillations exist in the vicinity of the doubly-degenerate point, when these heteroclinic orbits are perturbed. Here, the perturbations are associated with the variation of the flow velocity assumed to be equal to

$$u \to u + \nu \sin \omega t \,,$$

and Case 3, $u = 15.1$, $\gamma = 43.8$, $\kappa = 100$, $\xi_s = 0.8$ and $\beta = 0.25$ is considered. All the conditions for obtaining chaotic motions are satisfied, and chaotic motions are indeed found to exist. This is illustrated by a bifurcation diagram, the corresponding phase portraits, some theoretical FFT power spectra and the calculation of the Lyapunov exponents (see Figures 3.12 and 3.13).

Through the variation of the perturbation ν, different characteristics of the system may be observed: (i) oscillations around one of the fixed points [$\nu = 0.5$, Figure 3.12(a)]; (ii) quasiperiodic oscillations around the whole system, since the attracting limit cycles of the two fixed points are involved [$\nu = 2$, Figure 3.12(b)]; (iii) periodic oscillations around the two fixed points with considerable subharmonic content, [$\nu = 5$, Figure 3.12(c)]; (iv) periodic oscillations involving richer subharmonic (and superharmonic and combinational) content, [$\nu = 8$, Figure 3.12(d)]; (v) chaotic oscillations [$\nu = 11$, Figure 3.12(e)]. A proper analysis of parametric resonances would be required to identify all pertinent characteristics of the system for $\nu \neq 0$.

The magnitude of the values of ν necessary to display interesting dynamical behaviour in Figure 3.12 shows that the results obtained may not be tied to the analysis of Section 3.5.4.3. The chaos shown in Figure 3.12, and also in Figure 3.13, may be related to other dynamical features, such as moderate-amplitude geometrical structures, not captured at all by the analysis. In this sense, this part of the study is less intimately connected to the earlier parts of the chapter than might appear; nevertheless, the results are of sufficient interest to be presented.

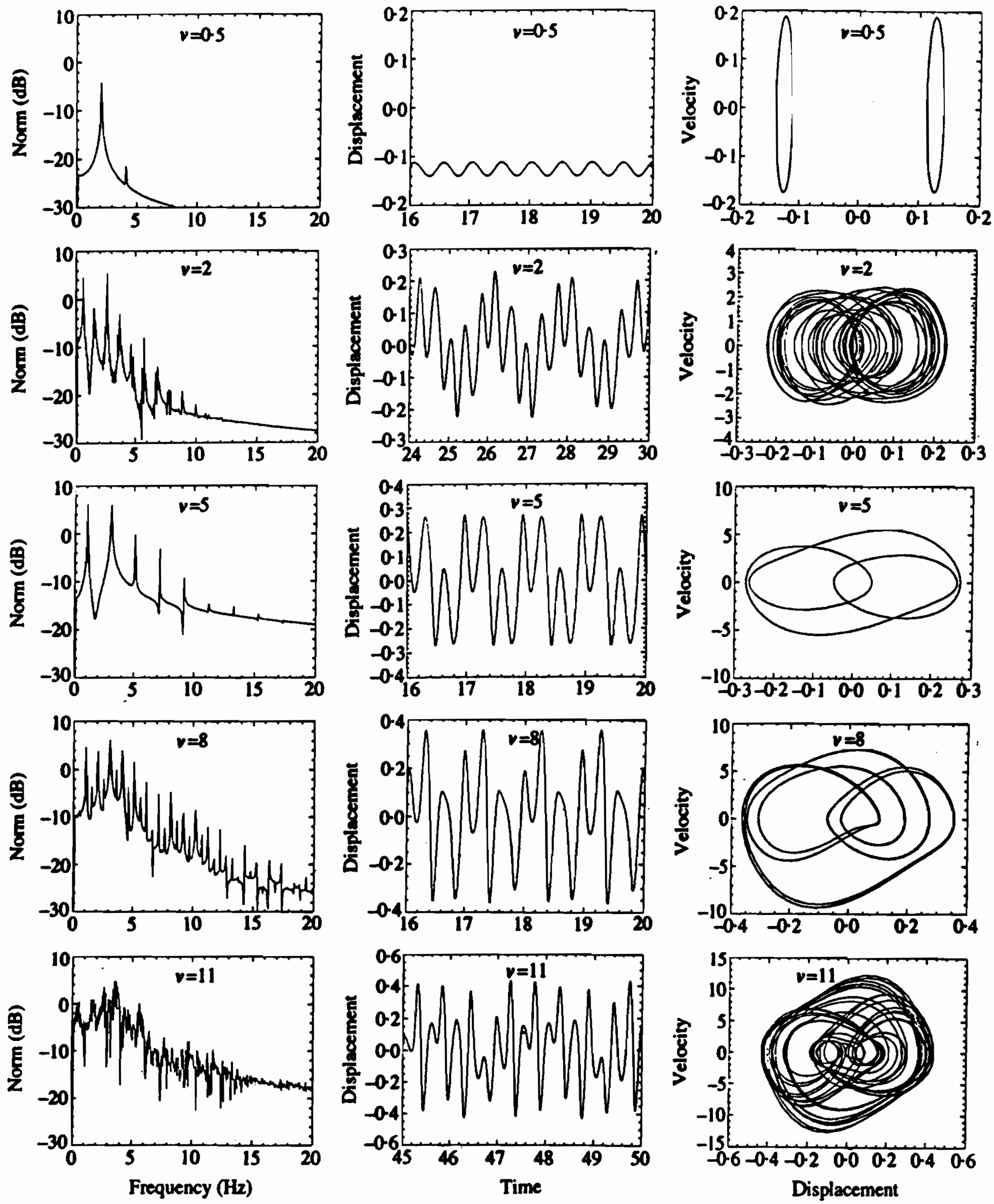

Figure 3.12: Power spectra, time traces and phase plots for various values of the amplitude of harmonic flow velocity perturbations, ν. Case 3 (see Section 3.5.4.3), $u = 15.1$, $\gamma = 43.8$, $\beta = 0.25$, $\kappa = 100$, $\alpha = 5 \times 10^{-3}$, $\xi_s = 0.8$

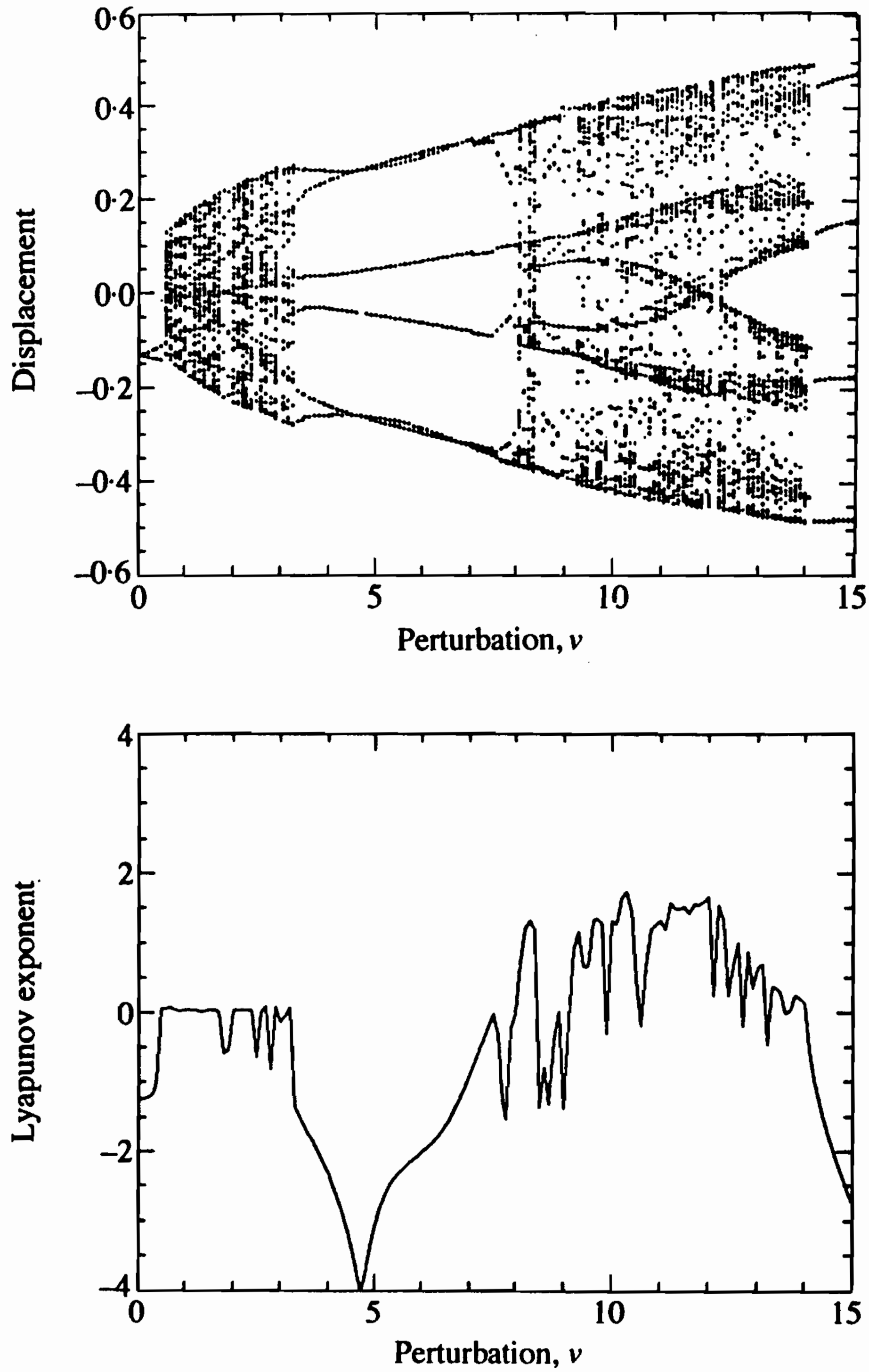

Figure 3.13: (a) Bifurcation diagram for tip displacement and (b) the corresponding Lyapunov exponents versus the perturbation velocity amplitude ν.

All results are summarized in two bifurcation diagrams. Figure 3.13(a) represents the maximum displacement of the tip (free end) as a function of the perturbation ν. Periodic regions are clearly defined. However, in order to distinguish between quasiperiodic and chaotic oscillations, the calculation of the Lyapunov exponents, shown in Figure 3.13(b), is necessary (Moon 1987).

The sign of the Lyapunov exponent provides the qualitative dynamics of the system: $\sigma > 0$ for chaotic motions, $\sigma = 0$ for periodic motions, and $\sigma < 0$ for a stable fixed point. However, for periodically-forced dynamical systems, the n-dimensional ordinary differential equation (ODE),

$$\dot{x} = f(x,t), \qquad x \in \mathcal{R}^n ,$$

can always be recast in an $(n+1)$-dimensional ODE,

$$\dot{x} = f(x,\theta)\,, \qquad \dot{\theta} = 1\,; \quad (x,\theta) \in \mathcal{R}^n \times \mathcal{R}\,.$$

The exponent corresponding to the time variable is always zero. Hence, since this zero exponent is always missing in the computation, for the non-autonomous system the case $\sigma < 0$ also corresponds to periodic motions (oscillations at the externally applied frequency). When $\sigma = 0$, both the forcing frequency and the system response frequency are present.

Finally, it should be mentioned that the forcing frequency is very important. It was chosen close to the natural frequency of the system ($\omega_0 = 12.79$) to "achieve" resonance. A numerical investigation has proved that for some values of the forcing frequency near the natural frequency, periodic oscillations may develop, instead of chaotic ones; while chaotic oscillations may arise for ω relatively far from ω_0. Hence, further study is required into the effect of the forcing frequency as done in previous analyses (Tousi & Bajaj 1985; Bajaj 1987; Tang & Dowell 1988; Namachchivaya & Tien 1989). This question will be adressed in Chapter 7.

3.7 CONCLUSION

Starting with the nonlinear equations of motion of the system, a discretized four-dimensional (two-degree-of-freedom) nonlinear analytical model was obtained, which is adequate (for $\beta < 0.3$ approximately) for the purposes of this study.

The stability of the system in the neighbourhood of the original equilibrium state was investigated first. This, for a given spring constant and location, allowed the determination of stable and unstable (by Hopf or pitchfork bifurcations) regions of the (β, γ, u) parameter space. This analysis also predicted post-instability behaviour (as u is increased, restabilization of the system or post-divergence flutter), as shown in Figure 3.6, but this should properly be done by considering the nonlinear equations and the other fixed points (other than the origin) that emerge as parameters are varied.

This was done next, in Section 3.4, where the stability of the whole set of fixed points, created and annihilated with increasing flow velocity, is examined by local eigenvalue analysis and supplemented by numerical simulations. A very rich set of bifurcations was found to exist, so that the dynamics for various system parameters could involve, for instance, coexisting stable, unstable equilibria and periodic limit sets, weakly or strongly attracting fixed points and/or limit cycles, as well as globally stable oscillations. One of the results obtained by this analysis was the 'complete' stability map of Figure 3.6, which includes the area of global oscillations.

The qualitative dynamics of the system was subsequently examined through lower-dimensional subsystems obtained by centre manifold and normal form techniques, in the neighbourhood of pitchfork, Hopf and double degeneracy bifurcations. It was shown that the reduced subsystems were capable of capturing faithfully the qualitative dynamics of the full system, as obtained through simulation, and of achieving remarkable quantitative agreement — see, for example, Figure 3.10.

The dynamical behaviour of the system in the vicinity of a double degeneracy was given special attention. It was possible to draw on previous work (Sethna & Shaw 1987; Takens 1974; Guckenheimer & Holmes 1983) to unfold this bifurcation, leading to the bifurcational sets shown in Figure 3.11, which display immensely variegated dynamical behaviour. Of particular interest is that heteroclinic orbits exist for certain combinations of the unfolding parameters, which are known to lead to chaotic oscillations under appropriate perturbation of the system. This was tested by harmonic perturbations of the flow velocity, whereby it was found that for certain ranges of frequency and amplitude of these perturbations, chaotic oscillations are indeed possible — as demonstrated by phase-plane plots, PSDs and by the calculation of the corresponding Lyapunov exponents. Unfortunately, the values of the perturbation for which chaos has been found are not satisfactorily small, throwing some doubt on the applicability of the local analysis to the results shown in Figures 3.12 and 3.13.

Chapter 4

THE PIPE CONSTRAINED BY MOTION-LIMITING RESTRAINTS[§]

4.1 INTRODUCTION

The linear and nonlinear dynamics of pipes conveying fluid has been studied quite extensively, both theoretically and experimentally, over the past thirty years. In a recent survey of the subject, over two hundred papers on various aspects of the problem were reviewed (Païdoussis 1991).

In recent years, increasing attention has been devoted to nonlinear aspects of the dynamical behaviour of the system; notable contributions were made by Holmes (1977), Lundgren *et al.* (1979), Bajaj *et al.* (1980) and Rousselet & Herrmann (1981). From these and several other studies, it is clear that the basic system of a pipe conveying fluid and variants thereof are capable of displaying an extremely rich and variegated dynamical behaviour. Thus, the pipe conveying fluid is fast becoming a premier paradigm in

[§]This corresponds to the article by Païdoussis & Semler 1993 Nonlinear and chaotic oscillations of a constrained cantilevered pipe conveying fluid: a full nonlinear analysis. *Nonlinear Dynamics* 4, 655-670. Reprinted by permission of Kluwer Academic Publishers.

dynamics, on a par with, but richer than, the classical problem of a column subjected to compressive loading (Païdoussis & Li 1993).

In the past years, some interest was shown to the question of whether this system is capable of displaying chaotic behaviour. Variants of the basic system were considered, modified to include strong nonlinear forces, known to be conducive to chaos. Thus, Tang & Dowell (1988) considered a cantilevered pipe with an inset steel strip and equispaced magnets on either side, buckling the pipe into one or the other potential well thus generated. Once the flow velocity is sufficiently above the threshold for flutter about the buckled state, chaotic motions were shown to be possible. Another variant of the basic system was studied by Païdoussis & Moon (1988), involving motion-limiting restraints on which the cantilevered pipe would impact, once the post-Hopf limit-cycle motion becomes sufficiently large as the flow velocity is increased. It was shown, both theoretically and experimentally, that chaotic oscillations occur at sufficiently high flow velocities. This, by the way, was the first closely-knit theoretical-experimental study of chaotic dynamics of an *autonomous* mechanical system.

In the experiments (Païdoussis & Moon 1988), motions were made to be planar by embedding a steel strip into the flexible pipe. The motion-limiting restraints were parallel bars on either side of the pipe, much stiffer than the pipe itself (Figure 4.1); hence, a good representation of the stiffness of these constraints was by a trilinear spring: zero stiffness in the gap, and a large stiffness once contact with the restraining bars was made. In the theoretical component of this study three principal idealizations were introduced: (i) because the constraining bars were not far apart and the amplitude of motion is therefore not large, the linearized equations of motion derived by Païdoussis & Issid (1974) were utilized, apart from the nonlinear impact force term; (ii) a two-mode Galerkin discretization of the equations of motion was used for analysis; (iii) the trilinear spring was idealized by a cubic one, which has the advantage of being represented by an analytic function, hence permitting the calculation of Lyapanov exponents — thereby being able to prove conclusively that the chaotic-looking oscillations obtained numerically, after a period-doubling cascade, were indeed chaotic.

Despite these idealizations, the correspondence between theoretical and experimental results was remarkably close qualitatively; but, quantitatively, there remained a fair margin for possible improvement. The problem was further studied theoretically with the same equations of motion by Païdoussis *et al.* (1989), and the route to chaos more clearly defined.

One of the practical limitations associated with the analytical model utilized by Païdoussis & Moon (1988) and Païdoussis *et al.* (1989) was the following: it was not possible to undertake numerical simulations with the correct (high) value of impact stiffness (and its equivalent cubic-stiffness counterpart) and the correct axial location of the impact constraint, for the solution would then diverge ("blow up" in common language). This was attributed to the inability of the two-degree-of-freedom approximation to represent the physical system. Nevertheless, parametric studies showed that, as these parameters were varied and were made to approach the experimental ones, short of blowing up, the qualitative dynamics remained the same; so, this aspect was not considered to be of undue concern.

Analysis of typical experimental signals yielded an estimate for the fractal dimension of 3.2 in the chaotic regime (Païdoussis *et al.* 1992), suggesting that, although two-degrees-of-freedom (d.o.f.) modelling may be reasonable, four or five d.o.f. models may be necessary to capture all essential features of the dynamics. This idea was pursued by Païdoussis *et al.* (1989), still utilizing the linearized basic equations of motion, but (i) with the number of degrees of freedom, N, in the discretization varied between two and seven, (ii) with a modified trilinear spring model for the impact restraints. It was found that for $N > 2$ it was possible to do simulations with the correct location of the restraint and value of the impact stiffness, without the solution blowing up. Furthermore, with $N = 4$ and 5, excellent agreement could be obtained between theoretical and experimental threshold flow velocities for the Hopf and period-doubling bifurcations, as well as for the onset of chaos: of the order of 10% or better.

Although better agreement between theory and experiment could hardly be expected, it was nevertheless decided to undertake the present study, which completes the circle of these studies by examining the effect of other than restraint-related nonlinearities in the equations of motion on the dynamics of the system — even when the overall amplitudes are not excessively large. Hence, the full nonlinear equations of motion will be utilized and the results compared to those in the foregoing studies. Some rather interesting and unexpected results have been obtained, as will be seen in what follows.

4.2 THE ANALYTICAL MODEL

4.2.1 The equation of motion

The system under consideration consists of a tubular beam of length L, internal cross-sectional area A, mass per unit length m, flexural rigidity EI and coefficient of Kelvin-Voigt damping a, conveying a fluid of mass M per unit length with an axial velocity U. The pipe is assumed to be initially along the x-axis (in the direction of gravity) and to oscillate in the (x, y) plane; free motions of the pipe are restrained by motion-limiting constraints as shown in Figure 4.1.

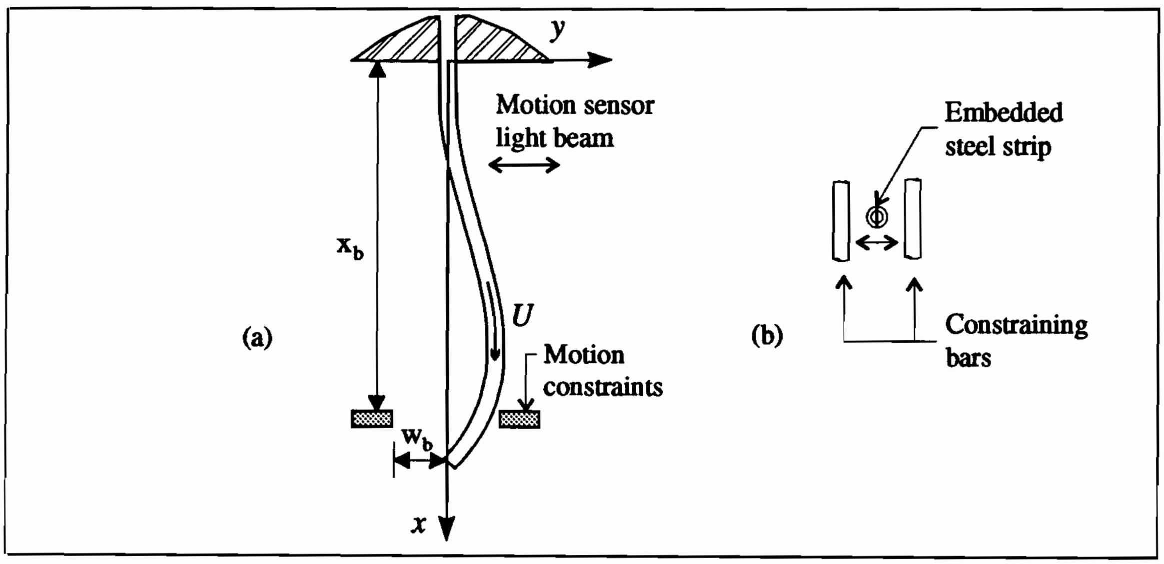

Figure 4.1: (a) Schematic of the system; (b) scheme for achieving planar motions with steel strip embedded in the pipe, also showing motion constraining bars.

The nonlinear equation of motion of a vertical cantilevered pipe derived in Chapter 2 is modified to take into account the presence of motion limiting restraints (Païdoussis *et al.* 1989); for U not varying with time, it can be written as

$$EI\,(y'''' + a\dot{y}'''') + 2MU\dot{y}' + MU^2 y'' - (m+M)\,g(L-s)\,y'' + (m+M)gy' + (m+M)\,\ddot{y} + N_1(y) + N_2(y) = 0\,, \tag{4.1}$$

where

$$\begin{aligned} N_1(y) &= F(y)\,\delta(s-s_b)\,, \\ N_2(y) &= 2MU\dot{y}'\,y'^2 + y''\,y'^2\left[MU^2 - \tfrac{3}{2}(m+M)\,g(L-s)\right] \\ &+ \tfrac{1}{2}\,g\,(m+M)\,y'y'^2 + EI\,(y''''y'^2 + 4y'y''y''' + y''^3) \\ &- y''\left[\int_s^L \int_0^s (m+M)\,(\dot{y}'^2 + y'\ddot{y}')\,\mathrm{d}s\,\mathrm{d}s + \int_s^L (2MUy'\dot{y}' + MU^2 y'y'')\,\mathrm{d}s\right] \\ &+ y' \int_0^s (m+M)\,(\dot{y}'^2 + y'\ddot{y}')\,\mathrm{d}s\,; \end{aligned}$$

$F(y)$ is the nonlinear force on the restraint due to impact, and the dot and the prime denote the derivative with respect to time, t, and the curvilinear coordinate along the centreline of the pipe, s, respectively. In equation (4.1), $y(s,t)$ is the lateral deflection of the pipe, δ is the Dirac delta function and g is the acceleration due to gravity. Thus, in this case, the nonlinearities in the equation of motion are not only associated with the motion constraints but also with flow-dependent, gravitational and flexural terms. Therefore, equation (4.1) is also valid for large amplitude motions.

Introducing next the same nondimensional quantities as in the linear case,

$$\begin{aligned} \xi &= \frac{s}{L}, \quad \eta = \frac{y}{L}, \quad \tau = \left(\frac{EI}{m+M}\right)^{1/2} \frac{t}{L^2}, \quad \alpha = \left(\frac{EI}{m+M}\right)^{1/2} \frac{a}{L^2}, \\ u &= \left(\frac{M}{EI}\right)^{\frac{1}{2}} U\,L, \quad \gamma = \frac{m+M}{EI} L^3 g\,, \quad \beta = \frac{M}{m+M}, \quad f(\eta) = \frac{F(y)L^3}{EI}, \end{aligned} \tag{4.2}$$

and removing the nonlinear inertial terms by a perturbation method (see Chapter 3 or Païdoussis & Semler 1993), equation (4.1) may be rewritten in dimensionless form as follows:

$$\alpha\dot{\eta}'''' + \eta'''' + 2u\sqrt{\beta}\dot{\eta}' + \eta''\left[u^2 - \gamma(1-\xi)\right] + \gamma\eta' + \ddot{\eta} + N_3(\eta) + N_4(\eta) = 0\,, \quad (4.3)$$

where the prime and the dot are now derivatives with respect to nondimensional ξ and τ, and

$$\begin{aligned} N_3(\eta) &= f(\eta)\,\delta(\xi-\xi_b)\,, \\ N_4(\eta) &= 2u\sqrt{\beta}\dot{\eta}'\eta'^2 + \eta''\left[u^2 - \tfrac{3}{2}\gamma(1-\xi)\right]\eta'^2 - \tfrac{1}{2}\gamma\eta'^3 + 3\eta'\eta''\eta''' + \eta''^3 \\ &+ \eta'\int_0^\xi \left\{\dot{\eta}'^2 - 2u\sqrt{\beta}\eta'\dot{\eta}'' - \eta'\eta'''\left[u^2 - \gamma(1-\xi)\right] + \eta''\eta''''\right\} \mathrm{d}\xi \\ &- \eta''\int_\xi^1\int_0^\xi \left\{\dot{\eta}'^2 - 2u\sqrt{\beta}\,\eta'\dot{\eta}'' - \eta'\eta'''\left[u^2 - \gamma(1-\xi)\right] + \eta''\eta''''\right\} \mathrm{d}\xi\mathrm{d}\xi \\ &- \eta''\int_\xi^1 \left\{-\gamma\eta'^2 + 2u\sqrt{\beta}\,\eta'\dot{\eta}' + u^2\eta'\eta'' + \eta''\eta'''\right\} \mathrm{d}\xi\,. \end{aligned}$$

4.2.2 Discretization

The infinite dimensional model is discretized by Galerkin's technique, with the cantilever beam eigenfunctions, $\phi_r(\xi)$, being used as a suitable set of base functions and $q_r(\tau)$ being the corresponding generalized coordinates; thus,

$$\eta\,(\xi,\tau) = \sum_{r=1}^{N} \phi_r(\xi)\, q_r(\tau)\,. \quad (4.4)$$

Substituting expression (4.4) into (4.3), multiplying by $\phi_i(\xi)$ and integrating from 0 to 1, leads to

$$\ddot{q}_i + c_{ij}\dot{q}_j + k_{ij}q_j + \alpha_{ijkl}\, q_jq_kq_l + \beta_{ijkl}\, q_jq_k\dot{q}_l + \gamma_{ijkl}\, q_j\dot{q}_k\dot{q}_l = 0, \quad (4.5)$$

where c_{ij}, k_{ij}, α_{ijkl}, β_{ijkl} and γ_{ijkl} are coefficients computed from the integrals of the eigenfunctions $\phi_i(\xi)$, analytically (Païdoussis & Issid 1974) or numerically (Appendix C); repeated indices implicitly follow the summation convention.

For purposes of numerical simulation, equation(4.5) is reduced to its first-order form,

$$\begin{Bmatrix} \dot{q} \\ \dot{p} \end{Bmatrix} = \begin{bmatrix} 0 & I \\ -K & -C \end{bmatrix} \begin{Bmatrix} q \\ p \end{Bmatrix} + \{g\,(q,p)\}\,, \quad (4.6)$$

i.e.

$$\dot{y} = [A]\, y + g(y) \,, \tag{4.7}$$

where $p_i = \dot{q}_i$, g is a third order polynomial function, and $[A] = [A(u, \gamma, \beta)]$ is a $2N \times 2N$ matrix. In equation(4.6), $\{q\}$ and $\{p\}$ are the generalized displacement and velocity vectors, so that the deflection of the pipe and its velocity at any point ξ may be expressed easily as

$$\eta(\xi, \tau) = \sum_{r=1}^{N} \phi_r(\xi) q_r(\tau), \quad \dot{\eta}(\xi, \tau) = \sum_{r=1}^{N} \phi_r(\xi)\, p_r(\tau) \,.$$

4.2.3 Modelling of the impact and damping forces

Various mathematical models may be used to represent properly the impact forces. The first approximation used by Païdoussis & Moon (1988) and Païdoussis *et al.* (1989) was to model the restraining forces by a cubic spring, i.e. $f(\eta) = \kappa\eta^3$. A more realistic representation was that utilized by Païdoussis *et al.* (1991) involving a "smoothened" trilinear spring model, $f(\eta) = \kappa_n\{\eta - 0.5(|\eta + \eta_{bn}| - |\eta - \eta_{bn}|)\}^n$. This enables to represent adequately the free gap (in which the constraints are zero) and to smoothen the sharp discontinuity at $|\eta| = |\eta_b|$. Here, the "cubic" ($n = 3$) trilinear model is chosen, $\kappa_3 = 5.6 \times 10^6$ and $\eta_{b3} = 0.044$, to represent the experimental constraints; the force-displacement curves of the real and the idealized constraints are shown in Figure 4.2(a,b). From Figure 4.2(a), the approximation of the cubic spring with $\kappa = 100$ seems appropriate. However, the impact forces are very small. Comparing with curves where κ is larger [Figure 4.2(b)] emphasizes the inadequacy of the cubic-spring model.

Païdoussis *et al.* (1989) took the value of $\kappa = 100$ to overcome some numerical problems, since with values closer to the experimental ones the numerical scheme diverged. The results obtained with such a "soft" spring were sometimes quantitatively unrealistic: e.g., the displacement of the pipe was in some cases greater than the length of the pipe itself. Nevertheless, calculations with $\kappa = 10^3$ showed that the amplitudes became more reasonable, while the critical flow velocities for the various bifurcations

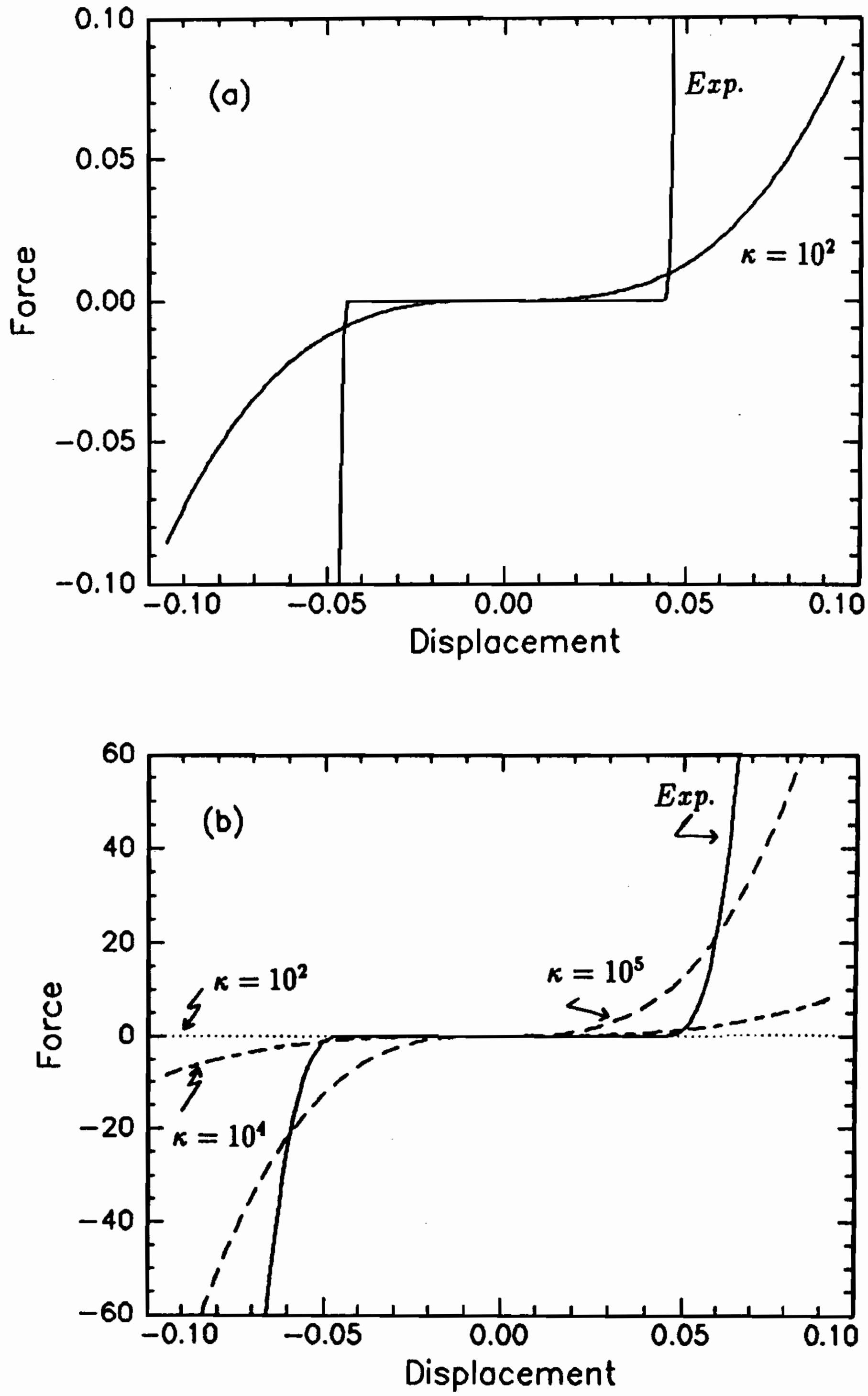

Figure 4.2: Force-displacement curves for different spring stiffness κ; *Exp.* represents the experimental curve.

did not change appreciably; hence $\kappa = 100$ was used for computational convenience. As mentioned in the Introduction, the non-convergence of the solution with the more physically realistic values of $\kappa = \mathcal{O}(10^5)$ was attributed to the two-degree-of-freedom model being insufficient to physically represent the real system.

In the present study, the nondimensional stiffness chosen for the cubic spring representation is $\kappa = 10^5$, and the idealized curve is very close to the experimental one (Figure 4.2), while for the trilinear model, $\kappa_3 = 5.6 \times 10^6$ and $\eta_{b3} = 0.044$.

As in previous work the dissipative forces will be modelled in two ways: either as a simple viscoelastic dissipation with $\alpha = 5 \times 10^{-3}$, or as a more realistic viscous damping representation with the individual modal logarithmic decrements, δ_j, corresponding to the experimentally measured values (Païdoussis & Moon 1988; Païdoussis *et al.* 1991): $\delta_1 = 0.028$, $\delta_2 = 0.081$, $\delta_3 = 0.144$, and $\delta_4 = 0.200$ linearly extrapolated.

4.3 RESULTS

4.3.1 Calculations to be performed and objectives

In what follows, results will be presented with $N = 2, 3$ and 4, with both the cubic and smoothened trilinear model for the constraints. Throughout, the results will be compared with those of the foregoing studies (Païdoussis & Moon 1988; Païdoussis *et al.* 1989; Païdoussis *et al.* 1991). In this respect it ought to be recalled that it was shown that the $N = 2$ model is reasonably good, in terms of linear dynamics, provided that $\beta < 0.3$ (Gregory & Païdoussis 1966).

The experimental parameters to which the theoretical results will ultimately be compared were selected to be $\gamma = 26.75$, $\beta = 0.213$, $\xi_b = 0.65$, $\eta_b = y_b/L = 0.055$ (Figure 4.1), $\kappa = 10^5$ for a true trilinear-spring representation and the experimental δ_j. For these parameters, the experimental nondimensional threshold flow velocities for the Hopf and first period-doubling bifurcations and for the onset of chaos were

$$u_H = 8.04, \quad u_{pd} = 8.43, \quad u_{ch} = 8.72 \;, \tag{4.8}$$

respectively, ±5%.

The main aim of the calculations is to explore the effect on the dynamics of the nonlinear terms in the unconstrained equation of motions. For that reason, calculations with the same parameters as those utilized, e.g., by Païdoussis *et al.* (1989) were also sometimes used — rather than the experimental values: i.e., $\beta = 0.2$, $\gamma = 10$, $\alpha = 5 \times 10^3$, $\kappa = 100$ and $\xi_b = 0.82$.

Throughout, solutions of equation 4.7 were obtained by using a fourth order Runge-Kutta integration algorithm, with a step size of 0.005 and different initial conditions (although in most cases they were $y_1(0) = 0.1$, $y_j(0) = 0$, $j > 1$). The results are presented in the form of bifurcation diagrams, phase portraits, power spectra and Lyapunov exponents.

4.3.2 Two-Degree-of-Freedom Model ($N = 2$)

4.3.1.1 $N = 2$ and cubic-spring restraints

To check the numerical scheme, the case $\kappa = 100$ with no other nonlinear terms was investigated first with the same parameters as Païdoussis *et al.* (1989): $\beta = 0.2$, $\gamma = 10$, $\xi = 0.82$ and $\alpha = 5 \times 10^{-3}$. Chaos was found to occur at $u = 8.03$ after the classical sequence of period-doubling bifurcations. However, when the intrinsic nonlinear terms [represented by $N_4(\eta)$ in equation 4.3] were added, no chaotic motion could be found, even for higher flow velocities; the nonlinearities of the pipe evidently "kill" the big amplitudes, reducing the motion of the pipe to simple oscillations! Hence, the system becomes much more stable, from a physical and from a numerical point of view.

Theoretical results were then obtained for parameter values as in the experiments, as given in Section 4.3.1, and with the full nonlinear equation of motion. It is of interest that computations *can* now be carried out with the correct κ without the solution blowing up. This shows that one of the problems (the value of κ) encountered previously and thought to be related to the $N = 2$ modelling is in fact seen to be related to the previous neglect of nonlinear terms; however, a second problem, related to ξ_b remains: it is only possible to find chaotic oscillations provided ξ_b is sufficiently large, as compared to the experimental $\xi_b = 0.65$.

Indeed, for $\xi_b = 0.75$, after the Hopf bifurcation, a pitchfork bifurcation, followed by a series of period-doubling bifurcations, arises, leading to chaotic motions. Sample results are shown in Figure 4.3 for various values of u. At $u = 7.35$, a Hopf bifurcation occurs, leading to periodic oscillations [Figure 4.3(a)]. A new periodic orbit is created through a pitchfork bifurcation, at $u = 9.22$, which breaks the "symmetry" of the system [Figure 4.3(b)]; mathematically, this comes from the crossing of a Floquet multiplier associated with the periodic trajectory, with the unit circle at $+1$ (Païdoussis *et al.* 1989; Tousi & Bajaj 1985). Physically, the system oscillates around a newly generated steady-state. Finally, the period-doubling bifurcation is clearly visible at $u = 10.2$ [Figure 4.3(c)] and at $u = 10.295$ [Figure 4.3(d)]. For $u > 10.35$, the motion becomes narrow-band chaotic, and wide-band chaotic at $u > 10.38$ [Figure 4.3(e,f)]. From a physical point of view, the mechanism leading to chaos is related to the interaction of limit-cycle motion and potential wells associated with divergence of the pipe at the constraints.

In all the results presented in Figure 4.3, it should be noted that the displacement amplitudes are now quite reasonable, the tip amplitude being of the same order of magnitude as the gap to the constraint, unlike the results obtained previously by Païdoussis & Moon (1988) and Païdoussis *et al.* (1989).

All these characteristics can be observed either in the phase-plane portraits or in the corresponding power spectra (chaotic oscillations being associated with a wide frequency band). Notice, however, that the main frequency is still discernible at $u = 10.4$ [Figure 4.3(i)].

The results are summarized in two bifurcation diagrams where the maximum tip displacement and the Lyapunov exponents σ are plotted as functions of the flow velocity u [Figure 4.4(a,b)]. For the autonomous system, $\sigma < 0$ represents stable

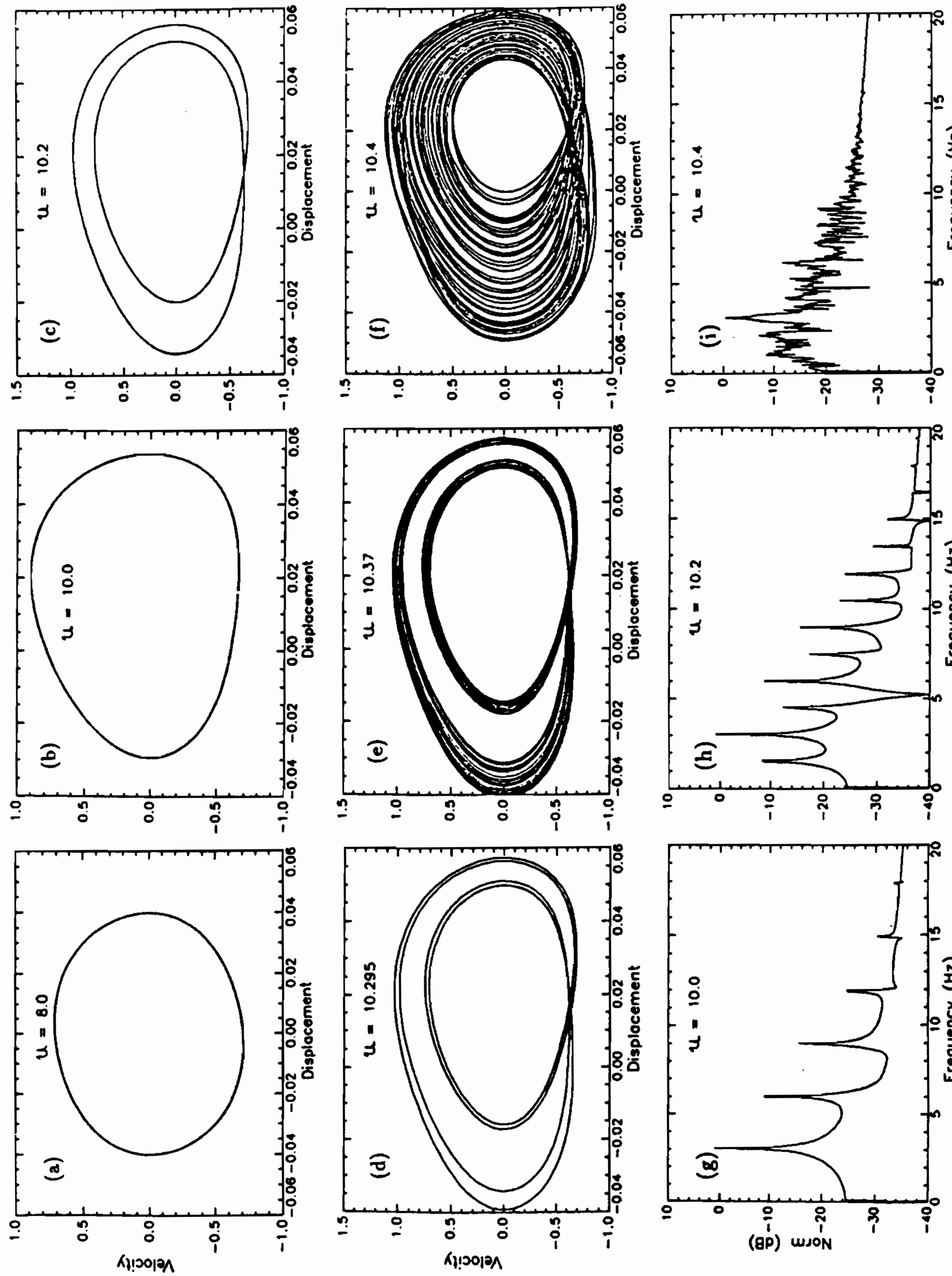

Figure 4.3: Phase portraits and power spectra for $N = 2$, $\kappa = 10^5$, $\xi_b = 0.75$, $\beta = 0.213$, $\gamma = 26.75$, $\alpha = 5 \times 10^{-3}$, and different values of u.

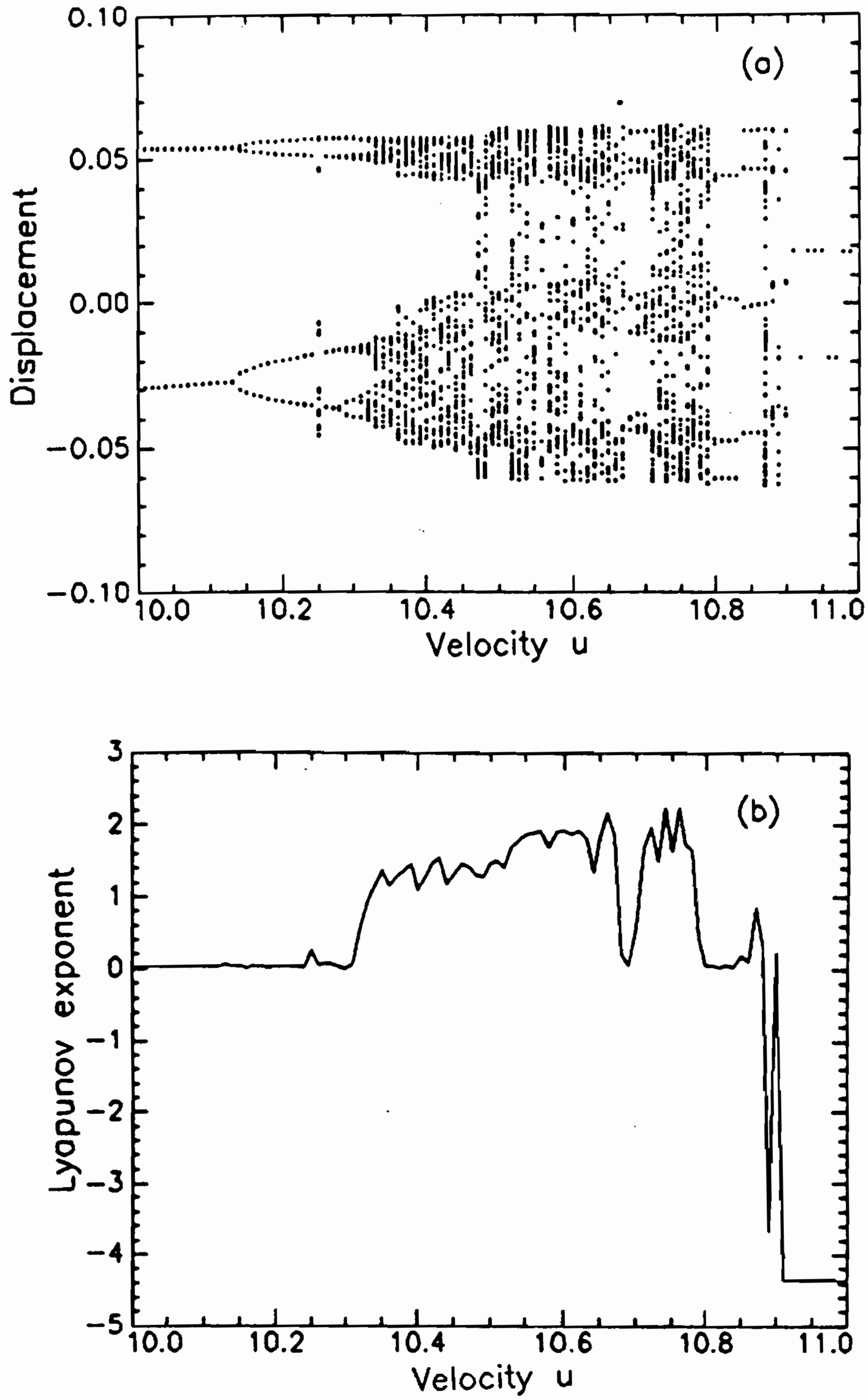

Figure 4.4: (a) Bifurcation diagram for the $N = 2$ model: the tip (end) displacement as a function of the flow velocity u; (b) Lyapunov exponents, also as a function of u; $\kappa = 10^5$, $\xi_b = 0.8$, $\beta = 0.18$, $\gamma = 26.75$, $\alpha = 5 \times 10^{-3}$.

equilibria, $\sigma = 0$ corresponds to periodic oscillations and $\sigma > 0$ to chaotic motions (Moon 1987).

It is observed that, after the region of chaos, the system "regains stability", the solutions being attracted to a new stable equilibrium point. This corresponds exactly to experimental observations: for higher flow velocities, beyond the chaotic regions, the system attaches itself permanently to one of the constraints; i.e., the system becomes unstable by divergence. This clearly appears in the bifurcation diagrams as well as in Figure 4.5. The oscillations are periodic for $u = 10.82$ and are overdamped for even higher flow velocities [Figure 4.5(a)]. An investigation of the existence of fixed points indicates that a subcritical saddle-node bifurcation occurs at $u = 9.85$; two fixed points exist beyond that value of u: one of them stable, and the other one unstable (Iooss & Joseph 1981). The computation of their respective eigenvalues leads to the conclusion that the stable fixed point becomes "more and more" stable when u increases [Figure 4.4 and 4.5(b)], until finally it becomes the strongest limit set in the system. By setting initial conditions close to the stable equilibrium, the detection of the fixed points is possible, even within the chaotic regions [Figure 4.5(c)]. Hence, different attractors coexist all along.

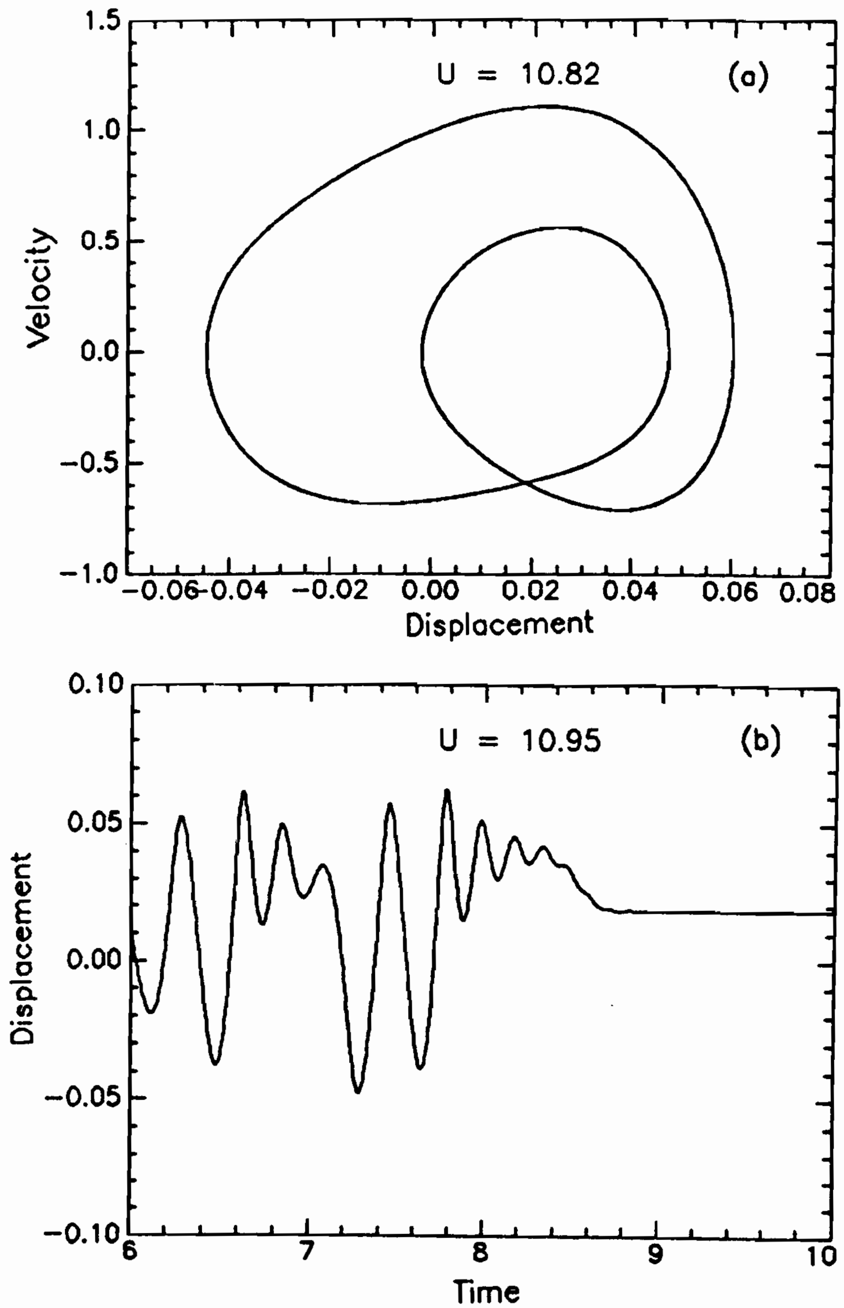

Figure 4.5: Corresponding phase portrait and time traces showing (a) periodic oscillations beyond the chaotic region at $u = 10.82$; (b) static instability beyond the chaotic and periodic regions at $u = 10.95$; (c) existence of a stable fixed point in the chaotic region for $u = 10.40$.

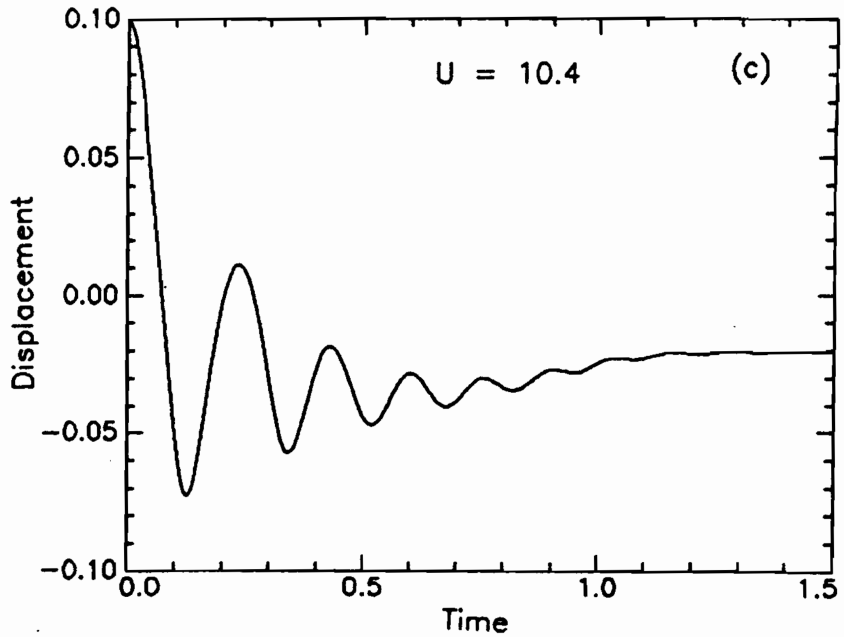

Figure 4.5: Continued.

4.3.2.2 $N = 2$ and smoothed trilinear restraints

Similar bifurcation diagrams and phase plots were constructed, but without giving more new insight of the problem. Therefore, the results will be discussed, without any additional figures being given.

First, it is interesting to note that for $\xi_b = 0.8$, a bifurcation diagram similar to the one shown in Figure 4.4 is found, but with lower nondimensional flow velocities u. Indeed, in this case, denoting by pf and pd the pitchfork and the period-doubling bifurcations, one finds $u_{pf} = 7.6$ and $u_{pd} = 7.75$, while chaotic oscillations occur at $u_{ch} = 8.0$. These values are lower than in the case of the cubic spring. Moreover, an inspection of the influence of the impact location ξ_b proves that for $u = 8.7$, chaotic motions occur only in the range $0.75 < \xi_b < 0.82$ (for $\xi_b < 0.75$ the system oscillates and for $\xi_b > 0.82$ it converges to one of the stable fixed points). Qualitatively, this has been observed in the experiments. However, for $\xi_b = 0.65$, which is the experimental value, chaos does not occur; this shows that, in the case $N = 2$, the better model of the impact forces does not improve very much the thresholds at which period-doubling or chaos may occur.

4.3.2.3 Concluding remarks for the $N = 2$ model

The principal findings of this series of calculations were three. First, the nonlinear terms in the equation of motion play a very important role, to the extent of invalidating some of the qualitatively attractive results obtained earlier with the linearized equation (always apart of the nonlinear constraint term). Second, it is now possible to conduct simulation with realistic values of the spring constraint ($\kappa = \mathcal{O}(10^5)$), and the limit-cycle amplitudes are now quite reasonable. Third, bifurcation diagrams with ξ_b as a variable were constructed (since experimentally the location of the constraints may be varied very easily), and the cascade of period-doubling bifurcations was observed, followed by a "static restabilization", confirming the qualitative agreement with the experiments of the nonlinear $N = 2$ model. However, it is not possible to find chaotic oscillations for the experimental $\xi_b = 0.65$. Finally, with the parameter values close to the experimental ones (except for ξ_b), the $N = 2$ model generates critical values for the various bifurcations which are fairly close to those observed experimentally.

4.3.3 Three- and Four-Dimensional Models ($N = 3$ or 4)

Based on the quite reasonable and promising results obtained with the $N = 2$ system with the experimental parameter values, it was fully expected that the results with $N = 3$ would be similar, and perhaps closer to the experimental values. However, the dynamical behaviour in this case was much more complex and less close to the experiments. A typical bifurcation diagram for the case of a cubic spring is shown in Figure 4.6(a), where it is seen that, beyond the pitchfork bifurcation (occurring at

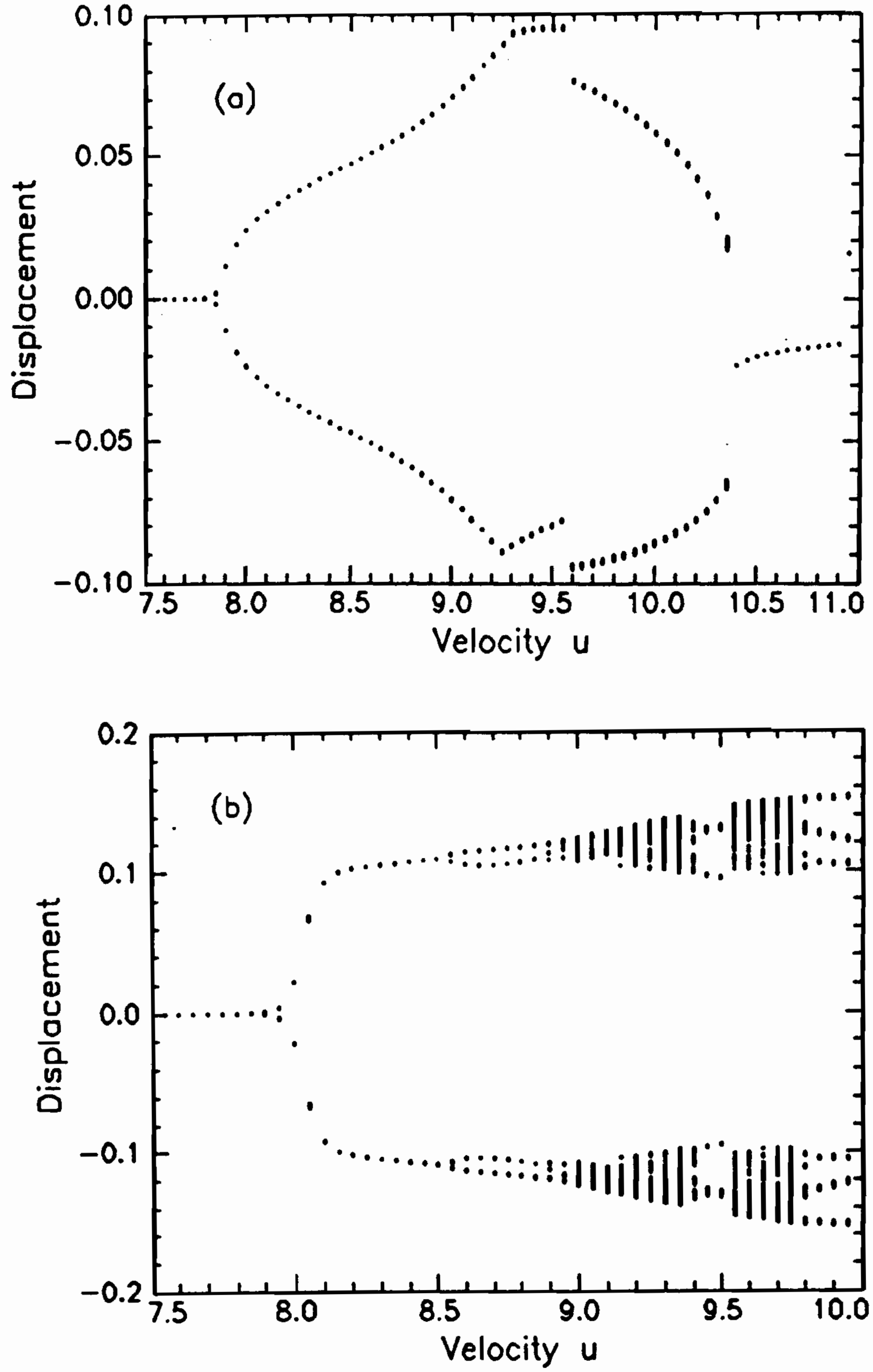

Figure 4.6: Bifurcation diagram for the $N = 3$ model with (a) the cubic spring and (b) the trilinear representation of the constraints. All other parameters are adjusted to the experimental ones (see Section 4.3.1).

$u = 9.25$), rather than obtaining the usual cascade of period-doubling bifurcations, the amplitude of the oscillations decreases until the oscillations finally die out for $u = 10.4$. Therefore, for $u > 10.4$, the system settles down to one of the stable equilibrium points. It should be mentioned that the asymmetry due to the pitchfork bifurcation has been kept in Figure 4.6(a), but if opposite initial conditions had been used, the other part of the curve could have been obtained very easily.

It ought to be remarked that similar atypical results had been obtained for $N = 3$ in the study by Païdoussis *et al.* (1991), utilizing the linearized equation of motion; they were in the original paper but were eventually left out because of space limitations.

However, the results for Figure 4.6(b), obtained with a smoothened trilinear spring, are less atypical and much more reasonable, both qualitatively and quantitatively. Period-doubling is obtained at $u = 8.8$ and chaos at $u = 9.2$. Nevertheless, a complete qualitative agreement with the experiments is not achieved since no restabilization can be found. Different configurations have been tried to obtain this static restabilization [using for example the Kelvin-Voigt representation or different constraint configurations as in Païdoussis *et al.* (1991)], but no better agreement was obtained.

The reason why $N = 3$ gives such atypical results is not understood. Perhaps it should be mentioned that physically discrete, articulated systems also display a discontinuous "convergence" in terms of increasing N for $N = 2$ and 3 (Païdoussis & Deksnis 1970); for $N > 3$, on the other hand, the convergence to the continuous system — cf. the results obtained here to the $N = \infty$ case — is smooth.

Calculations were performed also with $N = 4$ for the case of a trilinear representation of the restraint stiffness. As expected again, very good agreement, both qualitatively and quantitatively, is achieved. First period-doubling bifurcation and chaotic oscillations occur at $u_{pd} = 9.1$ and $u_{ch} = 9.2$, respectively [Figure 4.7(a)] — cf. values in (4.8). After a range of velocity for which periodic oscillations are observed ($9.35 < u < 9.55$), stronger chaotic motions appear again ($u = 9.6$) in Figure 4.7(b), and for $u > 9.7$, the system settles down onto one of the constraints. This is exactly what has been observed experimentally.

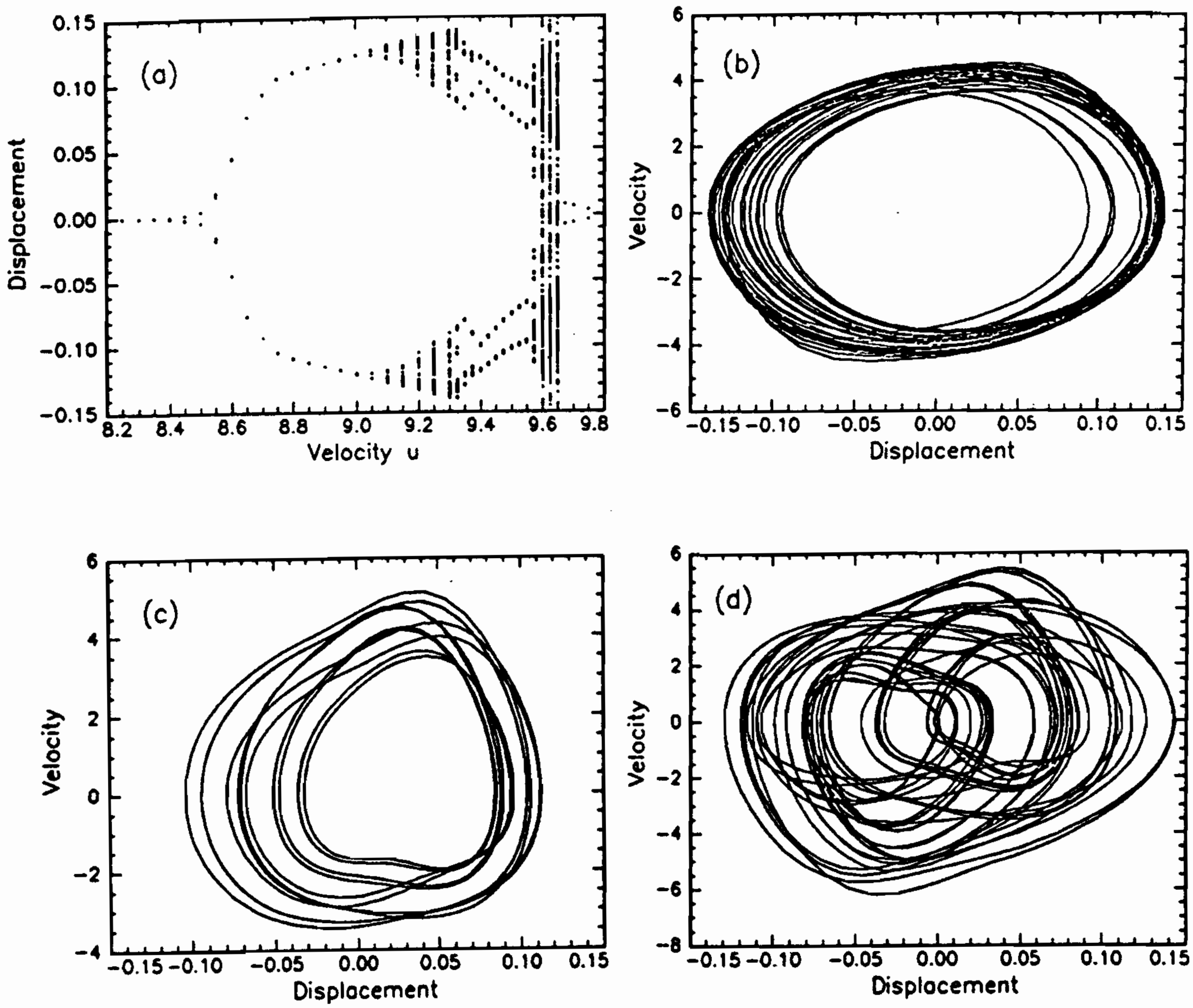

Figure 4.7: (a) Bifurcation diagram and (b-d) some corresponding phase portraits for the $N = 4$ model and the trilinear representation of the constraints. All other parameters are adjusted to the experimental ones (see Section 4.3.1). For (b) $u = 9.3$, (c) $u = 9.57$, (d) $u = 9.6$.

Again, many configurations have been tested for $N = 4$. For viscous damping ($\alpha = 0.005$) the same qualitative bifurcation diagram was obtained, with $u_{pd} = 8.6$, $u_{ch} = 9.0$ and static restabilization at $u_{re} = 9.7$, while for another impact model, $u_{pd} = 8.95$, $u_{ch} = 9.2$ and $u_{re} = 9.65$ were found. Therefore, the maximum difference with the experimental values is less than 8%.

It should be mentioned that in the case $N = 4$, almost no difference among the critical velocities u was found when the intrinsic nonlinear terms were removed. The static restabilization however was then not observed, which leads to the conclusion that the nonlinear terms still play an important role in the dynamics of the system.

As seen in Table 4.1, the results for $N = 4$ appear to be close to convergence. This compares well with the results obtained by Païdoussis *et al.* (1991), which is meaningful, in view of the observation made in the previous paragraph; in Païdoussis *et al.* (1991), convergence was found to have been achieved between $N = 4$ and $N = 5$. This conclusion of convergence *circa* $N = 4$ is further reinforced by noting that the Hopf bifurcation limit cycle has nondimensional amplitude of ~ 0.1 for $N = 3$ and ~ 0.12 for $N = 4$; the corresponding maximum amplitudes for chaos are 0.15 in both cases.

	$N = 3$	$N = 4$	*Experimental*
u_H	7.95	8.40	8.04
u_{pd}	8.90	9.05	8.43
u_{ch}	9.20	9.20	8.72
u_{re}	10.35	9.65	~ 9.0

Table 4.1: Convergence of nondimensional flow velocities, u, for the key bifurcations; subscripts *H, pd, ch* and *re* stand for *Hopf, period doubling, chaos* and *restabilization* (divergence), respectively.

4.4 CONCLUSION

In this chapter, the effect of the nonlinear terms in the equation of motions on the dynamics of a constrained cantilevered pipe conveying fluid was explored. However, more broadly, this is a multidimensional investigation of the effects of (i) the aforementioned nonlinearities (of the type associated with large motions), (ii) the number of degrees of freedom in the modelling of the system, and (iii) the impact model for the motion constraints.

Of course, this is a very specific problem, and this study can be justified only in terms of the more general conclusions that are reached concerning the analytical modelling of nonlinear systems when trying to match experimentally observed behaviour. Such questions as the effect of selective straining of parameters to give "good agreement" in some sense, how easy it is to misinterpret the reasons for "failure" of an analytical model, the fragility versus robustness of the theoretically predicted behaviour, etc., are some of the aspects of this study that *are* of generic interest. The problem at hand, may then be considered simply as a vehicle in the exploration of some of these questions, in the sense of the previous paragraph. Having said that, however, there is no question that the study of large-amplitude-related nonlinearities in the equation of motions of the specific problem under consideration had to be studied, in order to complete the circle of studies of Païdoussis & Moon (1988) and Païdoussis *et al.* (1989; 1991; 1992) — e.g., to remove any suspicion that the excellent agreement between theory (without these nonlinear terms) and experiment achieved by Païdoussis *et al.* (1991) may have been fortuitous.

It is shown that one can "force" the system to some extent, by straining (relaxing) some of the physical parameters, to yield dynamical behaviour which is qualitatively similar to that observed — and with reasonable quantitative prediction of some of this behaviour. This was achieved with the $N = 2$ models, with a cubic-spring representation of the constraints (Païdoussis & Moon 1988): if the values for constraint location (ξ_b) and spring stiffness (κ) were strained, critical flow velocities for the bifurcations (Hopf, period-doubling, onset of chaos) could be predicted remarkably well. Admittedly, some other aspects of the predicted behaviour are then unrealistic, e.g., the amplitudes of limit-cycle motion.

It is of interest that the straining in the values of ξ_b and κ ($N = 2$ model) was *forced* on Païdoussis & Moon (1988) and Païdoussis *et al.* (1989) by the fact that no convergent solutions could be obtained for the correct values. One of the findings of this study is that the reasons supposed to be responsible ($N = 2$, intead of higher N) were erroneous: once the nonlinear terms are included in the equations of motion, then convergent solutions with the correct κ *are* possible. Thus, one of the main conclusions is that the nonlinear terms in the equation of motions, despite "small motions" being modelled, can have an important effect on system dynamics — the extent of which cannot be gauged *a priori*. Moreover, as more realism is introduced (e.g. in the modelling of the constraint stiffness), the model can be tightened up to predict (i) realistic amplitudes of motion, (ii) the hitherto never predicted new equilibrium resulting (in the experiments) in the "sticking" of the pipe to one of the constraints at sufficiently high flow velocities, u, (iii) critical u for the important bifurcations reasonably close to the experimental ones.

One looks at the behaviour of the system in the multidimensional parameter space, and hence the "section" of the dynamics for $N = 2$, and at the changes occurring as nonlinear terms are included or κ is increased, and so on. Hence, the model $N = 2$ can be considered fragile. Therefore, it is essential to look at other "sections", notably for higher-dimensional models (corresponding to $N > 2$), to probe the robustness of the analytical model, since dimension calculations by Païdoussis *et al.* (1992) have shown that to be able to capture the essential behaviour of the system, $N = 4$ or 5 would be needed, as confirmed by the excellent agreement obtained even when the nonlinear terms in the equations of motion were absent (Païdoussis *et al.* 1991). It is shown here that the inclusion of the nonlinear terms, although it still has an effect on the dynamics, otherwise *improves* the agreement between theory and experiment, by (i) being able to predict the static restabilization (sticking) observed experimentally at high u, (ii) predicting more realistic amplitudes, while (iii) not having a detrimental effect on the excellent agreement between experimental and theoretical values of u for the key bifurcations (Hopf, period-doubling, *et seq.*). Equally interestingly, the number of parameters that need to be strained and the degree of straining are greatly diminished when the full nonlinear equation is used, even with $N = 2$. For $N = 4$, the degree of agreement with experiment becomes excellent, with *zero* straining of the parameters when the full nonlinear equation is used. More importantly, it is shown that the behaviour of the system is now very robust, and small excursions in this part of the parameter space have little effect on the predicted dynamics of the system.

The final conclusion is something that has been known for some time: one should be chary of "good agreement" between observed and modelled behaviour, unless all aspects of the analytical model and its robustness have been looked into. This study documents one such case where the initial model was in a fragile parameter sub-space, but the final, modified model is very robust and capable of predicting well almost all essential aspects of the observed dynamical behaviour.

Chapter 5

NUMERICAL SOLUTIONS OF SECOND-ORDER IMPLICIT NONLINEAR ODES[§]

5.1 INTRODUCTION

The genesis of this study is owed to difficulties in achieving convergent solutions in one specific problem: the nonlinear dynamics of cantilevered pipes conveying fluid, modified by the addition of a point-mass at the free end[†]. In this case, in addition to other nonlinearities (structural for instance), there are inertial nonlinearities which can be quite large; most of the aforementioned difficulties are related to these inertial nonlinearities. Some methods of solution were tried in turn and failed, even if they were shown to work well with large structural (displacement-dependent) nonlinearities, and for which it was tacitly said by their authors that they "should also work in the case of inertial nonlinearities", or words to that effect, without actually having tried them. It was then discovered that they failed also for other cases in which large inertial

[§]This corresponds to the article by Semler, Gentleman & Païdoussis 1996 Numerical solutions of second-order implicit ordinary differential equations. Accepted in *Journal of Sound and Vibration.*

[†]See Chapter 6.

nonlinearities existed, not just the pipe problem. As a result, a systematic search was made of existing methods to find some that do work, and to assess their applicability and success in solving such problems.

This study presents an abbreviated account of the fruits of this research. Most of the methods are described in detail by their authors in archival publications, and hence, in the interests of brevity, only an outline is given here. After a general classification of available methods, those showing promise will be identified at the end of this Introduction, and will be described and used in the rest of the chapter.

Bolotin (1964), in his work on parametric excitation, showed that the nonlinear equation of motion of a beam contains *nonlinear* inertia, damping and elasticity. Semler *et al.* (1994) proved that this was also the case for a cantilevered pipe conveying fluid. After discretization, the equation to be solved can be considered as a set of second-order *implicit* nonlinear differential equations, of the type

$$\mathbf{M}\ddot{\mathbf{x}} + \mathbf{C}\dot{\mathbf{x}} + \mathbf{K}\mathbf{x} = \mathbf{F}(\mathbf{x}, \dot{\mathbf{x}}, \ddot{\mathbf{x}}, t), \tag{5.1}$$

with appropriate initial conditions $\mathbf{x}(0)$ and $\dot{\mathbf{x}}(0)$. Equation (5.1) is said to be implicit because of the presence of the *nonlinear* inertial terms $\ddot{\mathbf{x}}$ in $\mathbf{F}$ that cannot be removed or transformed. $\mathbf{M}$, $\mathbf{C}$ and $\mathbf{K}$ are the mass, damping and stiffness matrices associated with the linear part of the system; if N is the number of degrees of freedom, these matrices will be of order $N \times N$. All nonlinearities are included in $\mathbf{F}$. This equation is so complicated that it precludes an exact analytical solution; hence, an approximate one must be sought.

In some situations, it is impossible, or undesirable, to express equation (5.1) as an explicit relation, i.e. in the form

$$\dot{\mathbf{y}} = \tilde{\mathbf{F}}(\mathbf{y}, t), \quad \mathbf{y}(0) = \mathbf{y}_0. \tag{5.2}$$

In these instances, methods of solution must be applied directly to the implicit relation, equation (5.1). "Depending on the area, equations of the form of (5.1) have been called: singular, implicit, differential-algebraic, descriptor, generalized state space, noncanonic, noncausal, degenerate, semi-state, constrained, reduced order model, and nonstandard" (Brenan *et al.* 1989, p. 2). It is for these types of equations that difficulties with the solution may arise. Different approaches may be adopted to tackle problems defined by (5.1) and (5.2); they may be analytical, numerical, or a combination of the two. Here we follow the classification proposed by Nayfeh (1985).

Irrational analytic methods are generally the easiest approach to solving a nonlinear ordinary differential equation. They entail simplifying the equation by neglecting and approximating various terms, sometimes to the extent that the resulting equation is no longer nonlinear. In mechanics for example, this is illustrated by using small-angle or small-deflection approximations. Usually, this type of solution is only valid over a small range of parameters or for small deviations from an equilibrium state.

Rational analytic methods, such as the method of averaging or the multiple time-scale method, represent the solution by an asymptotic expansion or perturbation. The expansions are usually in terms of a parameter ϵ ($\epsilon << 1$) that can be either present in the equation or artificially introduced. These approaches are also called "small parameter techniques", because they are based on the assumption that all nonlinear terms in the equations of motion are small and proportional to ϵ. The methods involve equating powers of the expansion and solving the resulting simplified equations successively (see Nayfeh & Mook (1979) and Nayfeh (1985) for details), while terms of order ϵ^{m+1} are disregarded while constructing the mth approximation.

Numerical time-difference methods (Gear 1971; Lambert 1973) are based on approximating the solution by its value at a sequence of discrete points or times. Most treatments of ordinary differential equations make the assumption that equation (5.1) can be rewritten in the explicit, or normal form (5.2), which explains why theorems and numerical techniques have mostly been developed to tackle this latter situation. For this case, methods of solution have been classified as single-step or multi-step, depending upon the number of previous steps used to provide information for the next value of the solution. Single-step methods like Runge-Kutta only require the value of $\mathbf{x}$ and $\dot{\mathbf{x}}$ at one point in order to compute the solution to the next; i.e., knowing the solution at time t_n, that at t_{n+1} is calculated by estimating higher derivatives in the interval $[t_n, t_{n+1}]$. Multi-step methods like Adams-Bashforth-Moulton accumulate the information from the values of $\mathbf{x}$ and $\dot{\mathbf{x}}$ at $t_n, t_{n-1}, t_{n-2}, ..., t_{n-k}$, in which case they are called k-step methods.

Finally, *combinations of analytical and numerical methods*, such as Rayleigh, Ritz, Galerkin or the harmonic balance method, require an initial assumption as to the form of the approximate solution as a function of time. In some cases, they are called series expansions since the solution is written in terms of independent functions or series, such as power series, Taylor series, orthogonal series (Chebyshev, Fourier or Legendre series), or functions which are the solution of a simpler problem. The assumed form includes coefficients that are to be determined by imposing certain conditions on the residuals of the equation of motion. These conditions involve minimizing requirements (Ritz method) or orthogonality (Galerkin, harmonic balance). This has the effect of converting the nonlinear differential equation into a set of linear algebraic equations in terms of the series coefficients that are then solved for iteratively. The strength of these techniques is that they are not based on the assumption that nonlinear terms are small (Meirovitch 1967), and hence are applicable to a wide variety of problems.

Analytical techniques have been applied to the problem of a cantilevered pipe conveying fluid subjected to lateral constraints by Païdoussis & Semler (1993) and to a beam-mass oscillator by Ekwaro-Osire & Ertas (1994). In both cases, the nonlinear inertial terms have been eliminated by carrying out small parameter expansions and neglecting higher order terms. Rational techniques have been used farther back by Atluri (1973) and more recently by Nayfeh *et al.* (1989).

Some time-difference methods such as Runge-Kutta cannot be used directly for equation (5.1), as they require the equation to be in the form of (5.2). It might be possible to use a modification of Runge-Kutta that does not require $\ddot{\mathbf{x}}$ to be written explicitly, but this formulation would need to be solved iteratively at each step (Gear 1971). This seems disadvantageous from the point of view of computational cost.

In the study of nonlinear systems, it is often of interest to find the time response for specific initial conditions. In the case of systems that can be represented as first-order systems, excellent codes are nowadays available from netlib, such as *LSODE* written by Hindmarsh (1983) or those by Hairer *et al.* (1993), obtainable by anonymous ftp at ftp.unige.ch. They enable the understanding of the dynamics of nonlinear systems and the classification of the types of response, e.g. periodic, quasiperiodic or chaotic. The analyst, however, does not have that much of a choice when implicit second-order ordinary differential equations are to be solved. This fact is hardly mentioned at all.

The numerical technique to be used must of course satisfy two major criteria: it must be stable and consistent (Lambert 1973), i.e. the accumulated numerical errors must damp out as the solution progresses in time, and truncation errors must tend to zero if the time step is refined (which means that the numerical solution must in fact tend to the "true" solution of the differential equation).

In this chapter, three different approaches are proposed and analysed to determine solutions of (5.1). Their strength and applicability are investigated, thus enabling the analyst to choose an appropriate method to solve his or her problem.

5.2 PICARD ITERATION WITH CHEBYSHEV SERIES

5.2.1 Method

This technique falls into the category of series expansions. The basic method for solving a nonlinear differential equation using Chebyshev series in connection with a Picard type iteration scheme has first been described by Clenshaw & Norton (1963). To illustrate how this method works, let us consider the simple equation*

$$\dot{x} = g(x,t), \quad x(a) = \xi, \tag{5.3}$$

*As shown by Clenshaw & Norton (1963), the method can be extended easily to the case of explicit second-order equations, simply by integrating twice and applying the initial conditions at each step.

where $x \in \mathcal{R}$, $a \le t \le b$, g is a nonlinear functional and ξ represents the initial condition. It is well known that if g is continuous in an interval $[a,b]$, and if there exists a function $G(t)$ such that $\dot{G}(t) = g(t)$, then

$$\int_a^b g(t)\,dt \;=\; G(b) - G(a). \tag{5.4}$$

Thus, provided g is a continuous function, it follows that

$$x(t) \;=\; \xi \;+\; \int_a^t g[x(\tau),\tau]\,d\tau. \tag{5.5}$$

One way of solving this integral equation is by using Picard's method of successive approximations (Clenshaw & Norton 1963),

$$x_{k+1}(t) \;=\; \xi + \int_a^t g[x_k(\tau),\tau]\,d\tau, \tag{5.6}$$

starting with $x_0 = \xi$ as the first iterate.

Chebyshev series are well-suited to this iteration procedure, especially when g is nonlinear (in practice, because Chebyshev polynomials are defined for $-1 \le t \le 1$, the time interval $[a,\ b]$ is mapped to $[-1,\ 1]$). Indeed, if the solution x and the functional g are expanded in a Chebyshev series, then, because of special properties of these series (see Fox & Parker (1968) or Sinha & Wu (1991) for details), equation (5.6) can be solved easily. The series coefficients of g can be determined from interpolation formulae if the value of g is known at $M+1$ specific points, $\tau_s = \cos(s\pi/M)$, $s = 0,1,2,...,M$. This is known as collocation. The Picard method begins by making an initial guess for the coefficients of the solution, based upon the initial conditions. Once the coefficients for x_k (the approximation of the solution at the kth iteration) are known, the set of values $x(\tau_s)$ can be found. Then, it is easy to evaluate $g[x_k(\tau_s),\tau_s]$ at the $M+1$ points, and thereafter to find the coefficients of g in the Chebyshev series. The series for g is then "integrated" by using a recurrence relation and the initial conditions. This yields the coefficients for x_{k+1}. The entire process is then repeated until a convergence criterion is met.

In a recent paper, Sinha *et al.* (1993) formalized this approach and applied the technique successfully to single and multi-degree of freedom nonlinear systems. They were able to predict periodic as well as chaotic responses, in agreement with other methods such as Runge-Kutta or Adams-Moulton. The "new" scheme was applied to equations of the type of (5.2) and directly to second-order differential equations that do *not* contain nonlinear inertial terms. Therefore, it was decided to use the same approach here to solve implicit second-order differential equations of the type of (5.1), containing nonlinear inertial terms.

The general idea is similar to what was presented previously: knowing the complete response at the iterate k, defined by $\mathbf{x}^{(k)}, \dot{\mathbf{x}}^{(k)}, \ddot{\mathbf{x}}^{(k)}$, one wants to obtain the response at the next iterate, $k+1$, by solving the following equation:

$$\mathbf{M}\,\ddot{\mathbf{x}}^{(k+1)} + \mathbf{C}\,\dot{\mathbf{x}}^{(k+1)} + \mathbf{K}\,\mathbf{x}^{(k+1)} = \mathbf{F}[\mathbf{x}^{(k)}, \dot{\mathbf{x}}^{(k)}, \ddot{\mathbf{x}}^{(k)}, t], \quad k = 0, 1, 2, \ldots \tag{5.7}$$

This equation is similar to equation (2) of Sinha's paper, except that the right-hand side (rhs) may also contain nonlinear inertial terms. Following their procedure leads to the same equation (5.3), except that

$$\mathrm{rhs} = \int_0^t \mathbf{F}[\mathbf{x}^{(k)}(\eta), \dot{\mathbf{x}}^{(k)}(\eta), \ddot{\mathbf{x}}^{(k)}(\eta), \eta]\, d\eta. \tag{5.8}$$

After the collocation procedure and a second integration (because the equation is of second-order), one finds finally a set of linear algebraic equations for the unknown vector $\alpha^{(k+1)}$:

$$\mathbf{W}\,\alpha^{(k+1)} = \mathbf{f}, \tag{5.9}$$

where $\mathbf{W}$ and $\mathbf{f}$ are complicated expressions defined by Sinha *et al.* (1993); $\alpha^{(k+1)}$ are the unknown Chebyshev coefficients representing the solution at the next iterate, $\mathbf{x}^{(k+1)}$. The only difference from Sinha's formulation lies in one component of $\mathbf{f}$ that also contains nonlinear inertial terms.[†] On the other hand, the discussion concerning the size of the interval of integration $[a,\ b]$, the use of analytic continuation and time-stepping, the number of terms in the series expansion M and the convergence criterion is the same.

[†]It corresponds to the last term $(I_n \oplus G^2)\,\mathrm{e}^{(k)}$ which is defined by Sinha *et al.* (1993).

5.2.2 Results

To verify its validity, the Picard method was tested on simple examples. In order to compare the results with standard numerical methods, examples were chosen in such a way that the equations could be formulated in an implicit or an explicit relation. Consider van der Pol's equation in which a nonlinear inertial term is added. It can be expressed in an *implicit* form

$$\ddot{x} + c\dot{x} + x = -x^2(\dot{x} + \ddot{x}), \tag{5.10}$$

or in an *explicit* one

$$\ddot{x} = (-c\dot{x} - x - x^2\dot{x})/(1 + x^2); \tag{5.11}$$

c represents the damping coefficient, negative in van der Pol's equation. As can be seen in Figure 5.1(a, b), the *explicit* Picard method produces solutions in agreement with those of Runge-Kutta. The *implicit* formulation with $c = -0.1$ yields a solution that also matches these two, but it can be seen in Figure 5.1(b) that convergence is not achieved for the case of $c = -0.3$. Although the implicit formulation initially yields the exact response, in the time interval[‡] $29 < t < 30$, the iteration scheme fails to converge. Since the code incorporates time-stepping using $b - a$ and M both set to be constant, the only factors that change between various time intervals (for example between $4 < t < 5$ and $16 < t < 17$) are the initial conditions. Thus, for $c = -0.3$, it is the initial conditions that make the difference between a convergent situation and one where the iteration method breaks down. Later tests revealed that non-convergence resulted from several other initial conditions with nothing notably similar about them. These same initial conditions, applied to both the explicit formulation with $c = -0.3$ and the implicit one with $c = -0.1$ *did* converge easily. The method was tried on other equations, with and without explicit time-dependence, and the same conclusions were reached.

[‡]This value might change if other initial conditions are used, or if the size of the time interval $b - a$ is varied.

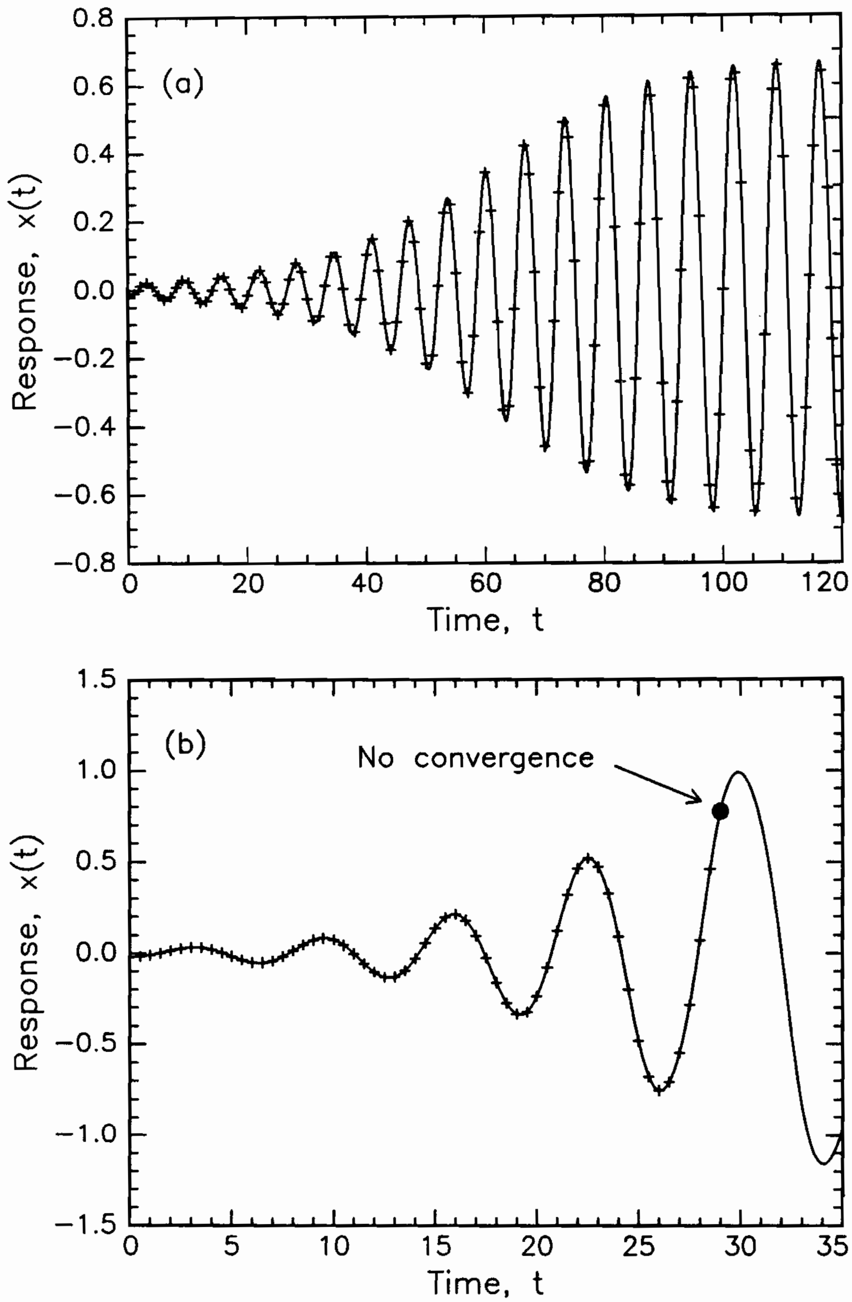

Figure 5.1: Solution of van der Pol's equation with initial conditions $x(0) = -0.02, \dot{x}(0) = 0$, using Picard iteration with Chebyshev series for (a) $c = -0.1$ and (b) $c = -0.3$: —, Runge-Kutta and explicit Picard method; +, implicit Picard method ($b - a = 2$ and $M = 18$).

Since the method works under some conditions and not others, a reasonable conclusion is that the expansion has encountered singularities for certain time intervals. This would be the result if, for a particular c and a set of initial conditions, the value of $b - a$ is larger than the radius of convergence. Such a situation is conceivable, since a large time interval (for example $b - a = 10$) leads to divergence even with the explicit formulation, probably for this reason. Hence, in an attempt to force convergence for the implicit case, various other intervals $b - a$ were tested, ranging between 1 and 10^{-4}. However, reducing the interval by four orders of magnitude does not aid in bringing about convergence for the divergent situations; further reduction is pointless because of the increasing effect of round-off error.

In Picard's method, the initial guess is derived from the initial conditions. Since the convergence of many iterative methods is dependent upon a good initial guess, this presents another plausible explanation of divergence for certain initial conditions. In fact, inspection of the initial and final value of the first coefficient in the Chebyshev series in convergent situations revealed that it had changed sometimes by orders of magnitude. It is therefore possible that certain initial conditions may have generated a poor initial guess, causing divergence. If this were the case, then it might be possible to rectify the problem by implementing a predictor-corrector method. This would help guide the scheme towards the true solution. Predictor-corrector methods have been used with some degree of success for the explicit equation by Wright (1963) and Norton (1964). But before actually incorporating predictor-corrector techniques, it is important to find out if convergence can be achieved with a better initial guess. The first 10 coefficients, determined from the explicit formulation, were each set to be correct to four significant digits. Despite such good initial accuracy, however, the Picard method still diverged for problematic initial conditions. This implies that the inclusion of predictor-corrector methods may not be useful, as the cause of divergence is not simply due to a poor initial guess.

The scheme was tested on different equations and for various parameters. This led us to the conclusion that convergence for the implicit scheme was influenced by:

(i) the size of $\partial f/\partial \dot{x}$ (i.e. the value of the damping coefficient, c, that "determines" the amplitude of the limit-cycle), (ii) the initial conditions, (iii) to a certain extent the size of the time interval $[a,\ b]$ (i.e. convergence only occurred for relatively small values of $b - a$), and (iv) of course, the size of the nonlinear inertial term (if the nonlinear inertial term is large, the generating solution $\mathbf{x}_k$ is no longer a reasonable solution and convergence is not guaranteed (Sinha 1994)). Even for situations that appeared convergent, there may still exist initial conditions for which divergence may occur.

For these reasons, it was decided to abandon the Picard method as a possible scheme for solving second-order implicit nonlinear differential equations and to explore other possibilities, to be discussed next.

5.3 FINITE DIFFERENCE METHOD

5.3.1 Method

From the literature, it has been known for some time that Houbolt's 4th-order finite difference method (Houbolt 1950) is a good candidate for computing the time response of initial value problems: Tillerson & Stricklin (1970) and Wu & Witmer (1973) investigated Houbolt's method, the trapezoidal method (also called Newmark average acceleration method) and the central difference method on nonlinear beam and shell structures, and concluded that Houbolt's method was probably the most efficient time integrator for elastic-plastic structural dynamical problems. Moreover, it is also known that Houbolt's method is unconditionally stable for linear systems (Johnson 1966). However, as shown by Park (1975), it introduces some numerical damping, as well as some frequency distortion. Nevertheless, this is also the case for other popular schemes. It should be mentioned finally that Nath & Sandeep (1994) showed that Houbolt's scheme became unstable for their problem if the time step Δt was *smaller* than a critical value that depended upon the physical parameters. Hence, care should be taken when reducing the time step. It is believed, however, that more investigation is necessary to confirm or invalidate this rather unusual feature.

Houbolt's finite difference method is based on two approximations,

$$\ddot{x}_{j,n+1} = [2x_{j,n+1} - 5x_{j,n} + 4x_{j,n-1} - x_{j,n-2}]/(\Delta t)^2, \tag{5.12}$$

$$\dot{x}_{j,n+1} = [11x_{j,n+1} - 18x_{j,n} + 9x_{j,n-1} - 2x_{j,n-2}]/(6\ \Delta t), \tag{5.13}$$

where $x_{j,n} = x_j(n\Delta t)$ and Δt is the time step. To see how the method works, consider van der Pol's equation, written in implicit form, at the step $n+1$,

$$(1 + x_{n+1}^2)\,\ddot{x}_{n+1} + (c + x_{n+1}^2)\,\dot{x}_{n+1} + x_{n+1} = 0, \tag{5.14}$$

where, for simplicity, the index j has been suppressed because the system has only one degree of freedom. Substituting (5.12) and (5.13) into equation (5.14), and multiplying throughout by $(\Delta t)^2$ leads to

$$\begin{aligned} &(1 + x_{n+1}^2)\,(2x_{n+1} - 5x_n - 4x_{n-1} - x_{n-2}) \\ &+ (c + x_{n+1}^2)(11x_{n+1} - 18x_n + 9x_{n-1} - 2x_{n-2})\Delta t/6 + x_{n+1}(\Delta t)^2 = 0. \end{aligned} \tag{5.15}$$

For an N-dimensional problem, this can be expressed symbolically as

$$\mathbf{f}(\mathbf{x}_{n+1}) = \mathbf{0}, \tag{5.16}$$

where $\mathbf{f}$ is an N-dimensional nonlinear function of $\mathbf{x}_{n+1}$ that has to be solved numerically; $\mathbf{x}_n, \mathbf{x}_{n-1}$ and $\mathbf{x}_{n-2}$ are known from the previous steps. The time step being small, it can be assumed that $\mathbf{x}_n$ and $\mathbf{x}_{n+1}$ are relatively close to each other, so that a good initial guess is available for the solution of (5.16). The Newton-Raphson method is designed to deal with such situations, and is known to converge very fast (quadratically). The only possible difficulty lies in the computation of the Jacobian of $\mathbf{f}$, $[\partial f_i/\partial x_{j,n+1}]$, which may generally be obtained either analytically or numerically. However, even in the case of piece-wise linear systems that arise in impact problems or when dry friction is present, it is possible to overcome this difficulty. In most of the vibration problems, and in the cases considered here, it is assumed that the Jacobian may be obtained analytically. For example, for equation (5.14), one obtains

$$(\Delta t)^2 \frac{\partial[\text{Eq.}(5.14)]}{\partial x_{n+1}} = 2[x_{n+1}\ddot{x}_{n+1} + (1 + x_{n+1}^2)] + [2x_{n+1}\dot{x}_{n+1} + 11(c + x_{n+1}^2)/6]\Delta t + (\Delta t)^2. \tag{5.17}$$

Finally, it should be mentioned that Jones & Lee (1985) also investigated higher order finite difference schemes. They concluded that the $\mathcal{O}(\Delta t^6)$ scheme was unconditionally unstable, while the $\mathcal{O}(\Delta t^8)$ was stable provided $\Delta t/T < 0.11$, i.e. when more than 10 steps per cycle are used, which is not restrictive from a practical point of view. Therefore, the 8th-order scheme will also be investigated here. It is defined by

$$\ddot{x}_{j,n+1} = \sum_{p=0}^{7} \alpha_{p+1}\, x_{j,n+1-p}/(\Delta\tau)^2; \quad \dot{x}_{j,n+1} = \sum_{p=0}^{7} \beta_{p+1}\, x_{j,n+1-p}/\Delta\tau, \tag{5.18}$$

where α_p and β_p are given in Table 5.1.

Velocity Coefficients	Acceleration coefficients
$\alpha_1 = 13068/5040$	$\beta_1 = 13132/2520$
$\alpha_2 = -35280/5040$	$\beta_2 = -56196/2520$
$\alpha_3 = 52920/5040$	$\beta_3 = 110754/2520$
$\alpha_4 = -58800/5040$	$\beta_4 = -132860/2520$
$\alpha_5 = 44100/5040$	$\beta_5 = 103320/2520$
$\alpha_6 = -21168/5040$	$\beta_6 = -50652/2520$
$\alpha_7 = 5880/5040$	$\beta_7 = 14266/2520$
$\alpha_8 = -\ 720/5040$	$\beta_8 = -1764/2520$

Table 5.1: Coefficients of the 8th-order finite difference scheme

A starting procedure at time $t = 0$ is necessary for both Houbolt's and the 8th-order scheme. The easiest approach is to use a Taylor series expansion. As a first approximation, one may assume that $x_{j,-p} = x_0 - (p\Delta t)\,\dot{x}_0,\ p = 1,..,3$ or $p = 1,..,7,$

since both $\mathbf{x}_0$ and $\dot{\mathbf{x}}_0$ are known at time $t = 0$. If a better approximation is needed, it is possible — though sometimes complicated — to evaluate $\ddot{\mathbf{x}}_0$ through (5.1) and then to approximate $x_{j,-p}$ using $x_{j,-p} = x_{j,0} - (p\Delta t)\,\dot{x}_{j,0} + \frac{1}{2}(p\Delta t)^2\,\ddot{x}_{j,0}$. To get even higher order approximations, it is necessary to differentiate (5.1) and obtain higher order derivatives of $\mathbf{x}_0$ or to use for the first iteration a single step method (indeed, if the accuracy on the initial conditions is not of the same order as the numerical scheme, the global error might be bigger than what is initially assumed). However, if the solution sought is periodic (e.g. a stable limit cycle), then a very accurate initial condition is not necessary; if the attractor is chaotic, again one is usually more interested in the long-term behaviour and not in the transients. It is only when basins of attraction are to be computed precisely that more accurate approximations on the initial conditions may be of importance.

5.3.2 Results

The finite difference method has been tested on numerous examples, both on single and multi-degree-of-freedom systems. In order to investigate the accuracy and the efficiency of the schemes, comparison with the code *DOP853* developed by Hairer *et al.* (1993) and based on an explicit Runge-Kutta method of order 8 was undertaken. Again, van der Pol's equation is used in implicit and explicit form. A typical comparison is presented in Figure 5.2. As can be seen in Figure 5.2(a), all three methods yield the same result for $c = -2$, $0 \leq t \leq 80$, and $\Delta t = 10^{-1}$. However, if one is interested in the long term behaviour, it can be observed that Houbolt's method induces a phase shift in the response. This shift is much smaller for the 8th-order scheme, as shown in Figure 5.2(b).

Different cases were investigated without any convergence problem, even for damping coefficients equal to $c = -10$ (i.e. 30 times bigger than the value for which the Picard approximation did not converge), even though the periodic response in this case looks more like an impulse.

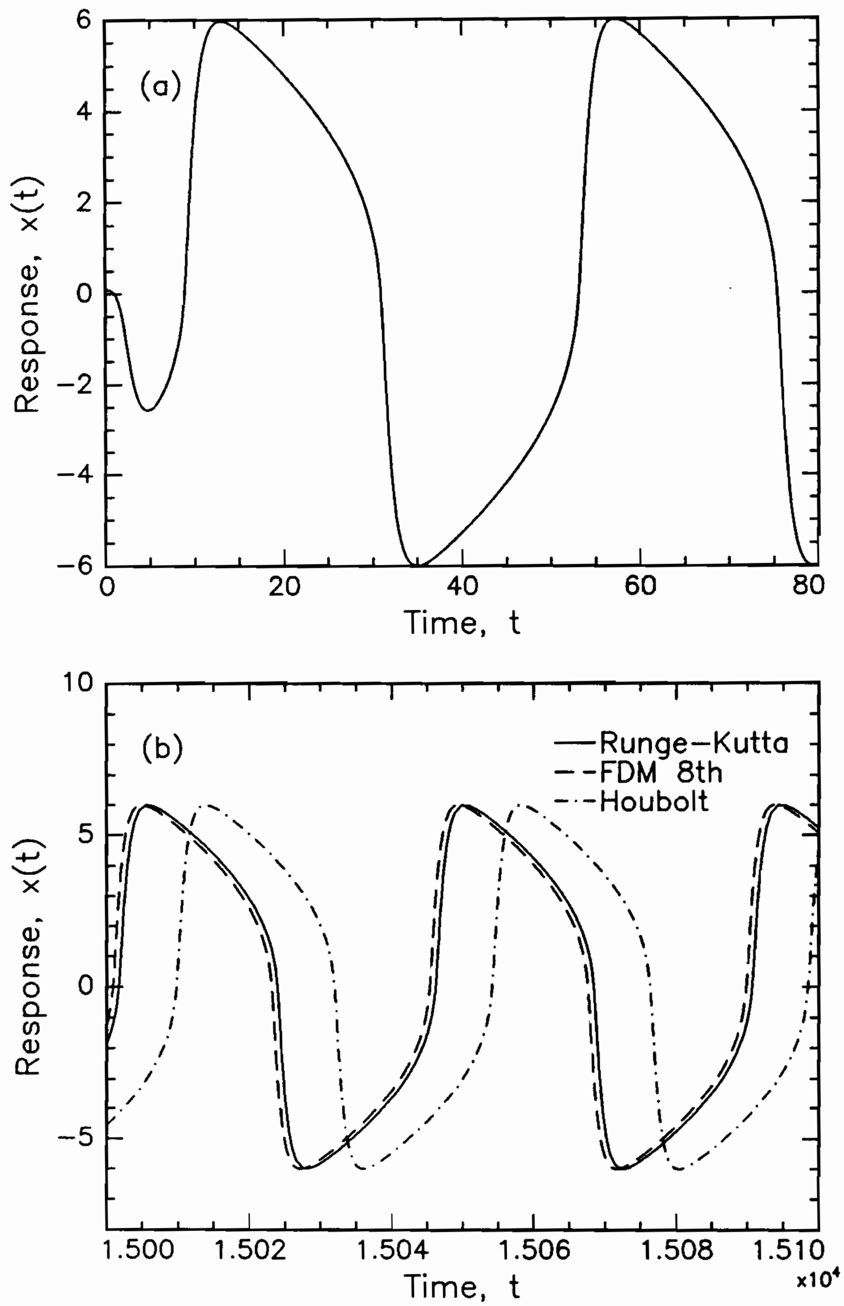

Figure 5.2: Solution of van der Pol's equation with $c = -2$ computed with Runge-Kutta and Finite Difference methods: (a) first transients; (b) after $t = 1.5 \times 10^4$. —, Runge-Kutta; – – –, 8th-order FDM; —·—, Houbolt scheme.

Except for the phase shift, observable in the time trace, the responses are very similar from a qualitative point of view. The amplitude is the same in all three cases, as well as the frequency, for any practical purposes. Therefore, the "geometrical" behaviour of the system, as defined in most of the books in nonlinear dynamics, is the same for the three methods, which enables the dynamicist to characterize the motion adequately. Nevertheless, to achieve excellent agreement, especially for Houbolt's scheme, the time step must be chosen to be rather small, sometimes up to 400 steps per cycle, though usually 250 is enough. In contrast, the number of steps for the 8th-order can be reduced considerably, to approximately 100 steps per period. Hence, the 8th-order scheme, despite being slower than Houbolt's by a factor of 1.2 and being a bit more difficult to implement, can be regarded as much more efficient, since for the same accuracy, a much larger step length Δt can be used.

	DOP853		FDM4		FDM8	
	Adapt. step	$\Delta t_{max} = 0.1$	$\Delta t = 0.45$	$\Delta t = 0.1$	$\Delta t = 0.45$	$\Delta t = 0.1$
Time	13 s	32 s	10 s	36 s	12 s	40 s
Acc.	S.P.S	Yes	S.D.A	S.P.S	S.P.S	Yes

Table 5.2: Comparison of the efficiency and the accuracy between the 8th-order Runge-Kutta method (DOP853), Houbolt's scheme (FDM4) and the 8th-order finite difference method (FDM8). S.P.S. stands for small phase shift, S.D.A. for small difference in amplitude; 'Yes' indicates good accuracy. For the adaptive step size, $\Delta t_{av} \simeq 0.45$.

Table 5.2 presents a brief comparison of the three methods, for $c = -0.3$. Some remarks may be added, as follows. (i) If the maximum time step for *DOP853* is equal to the time step used by the finite difference methods, then the speed is similar to that for both *FDM4* and *FDM8*. (ii) *DOP853* when used with an adaptive step size has an average time step of $\Delta t = 0.45$, which is 4 times larger than the permissible time step for *FDM4* and twice that of *FDM8*, for the same accuracy; therefore it can be considered more efficient. (iii) These differences in the time step depend upon the problem and the parameter values. Hence, in any vibration analysis using finite difference methods, particular attention should be paid to the choice of Δt. (iv) It might be possible to implement an adaptive step size controlled by a tolerance criterion on the finite difference schemes as well, in order to improve both efficiency, by allowing the biggest possible step size, and accuracy, by decreasing the time step when necessary.

A second example investigated is considered next: it corresponds to the nonlinear motion of a parametrically exited column hinged at its ends, represented by a two-term Galerkin expansion. The parameters here are the same as those used by Sinha *et al.* (1993). This example is particularly interesting since no damping is present in the equation of motion. If Houbolt's scheme is used with $\Delta t > 0.025$, then artificial damping is introduced and the response, instead of being quasi-periodic, becomes periodic with one frequency, $\omega = 1$, which means that the higher frequency is completely damped out. This value of Δt corresponds again to 250 steps per cycle. For the 8th-order scheme, this number is reduced to 80, which represents approximately a factor of 3 in terms of gain in efficiency. On the other hand, *DOP853* gives accurate results up to $\Delta t = 0.15$ and introduces some errors (though not drastic) with $\Delta t = 0.2$. Hence the time step is twice as big as the maximum value permissible with the 8th-order scheme.

The introduction of numerical damping may in fact have some positive effects: (i) it may stabilize the numerical scheme; indeed it is well known that artificial viscosity is sometimes added in fluid dynamics problems to ensure convergence of the numerical scheme (Press *et al.* 1992); (ii) the response of the system may be more realistic from a physical point of view, since some degree of damping is usually present in most of the vibration problems (the artificial damping is very small).

The last aspect to be considered concerns the computation of chaotic responses. Indeed, it is well known that the 4th-order Runge-Kutta method with a constant step size can induce artificially spurious chaos into non-chaotic problems (Cartwright &

Piro 1992). For that purpose, a last example is examined. It has been analysed by Szemplinska-Stupnicka *et al.* (1989) using standard numerical integration and by Sinha *et al.* (1993) with Chebyshev polynomials, and is defined by

$$(1+\alpha x^2)\ddot{x} + 0.2\dot{x} + (1+0.9\cos\Omega t)x + 1.5x^2 + 0.5x^3 = 0; \tag{5.19}$$

when $\alpha \neq 0$, this equation contains a nonlinear inertial term. The parameter to be varied is the forcing frequency Ω. Using Houbolt's and the 8th-order finite difference method, it was possible to obtain the same phase-plane plots as with *DOP853*, and period-two, -four and -eight motion were found, as well as chaotic responses. A bifurcation diagram computed with Houbolt's scheme is shown in Figure 5.3, together with the values of the first three bifurcation points as Ω is decreased. For clarity, the bifurcation diagram obtained using an 8th-order Runge-Kutta integration is not presented because it is very similar, both qualitatively and quantitatively. The difference in the value of the bifurcation points is less than 0.3%, i.e. it is negligible. After the sequence of period-doubling, both methods yield chaotic responses. The regions referred to as chaos II and III by Szemplinska-Stupnicka *et al.* (1989) were also detected by both *DOP853* and finite difference methods, for the same values of Ω. Therefore, it can be concluded that both finite difference methods are reliable in computing responses in the chaotic regime. The case $\alpha \neq 0$ was also considered, with no change in the conclusions.

Through the three examples presented above, it has been shown that finite difference methods may be used to compute accurate solutions of nonlinear implicit second-order differential equations. Except for a minor phase shift and some numerical damping when the time step is too large, both Houbolt's and the 8th-order scheme yield accurate responses and bifurcation points, when compared to an optimized 8th-order Runge-Kutta scheme.

The study of nonlinear dynamical systems often implies the understanding of the appearance or disappearance of new types of solution — referred to as bifurcations. Of particular interest is the computation of *periodic* solutions. This is the subject of the next section, when implicit equations are considered.

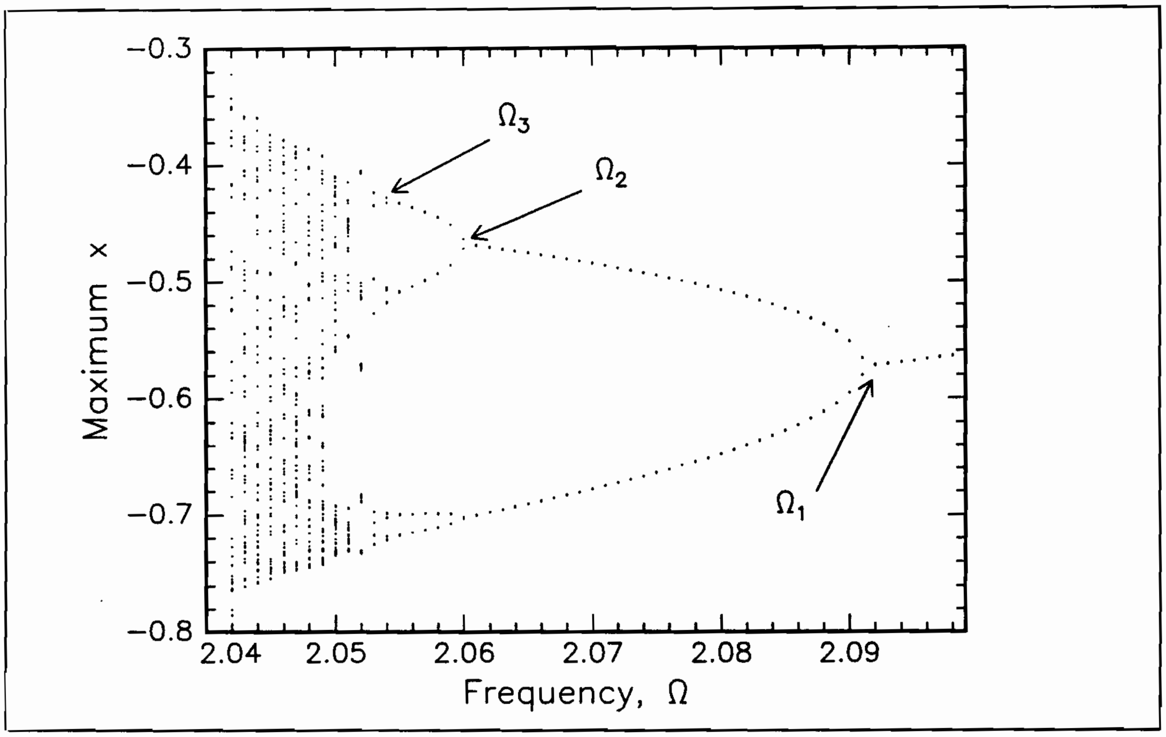

Figure 5.3: Bifurcation diagram obtained using Houbolt's scheme (FDM) and representing the solution of equation (5.19) with $\alpha = 0$; Ω_i are the bifurcation points. $\Omega_{1,FDM} = 2.091$ versus the value obtained by Runge-Kutta integration, $\Omega_{1,RK} = 2.095$; $\Omega_{2,FDM} = 2.060$ vs $\Omega_{2,RK} = 2.063$; $\Omega_{3,FDM} = 2.054$ vs $\Omega_{3,RK} = 2.056$.

5.4 INCREMENTAL HARMONIC BALANCE

5.4.1 Method

The purpose of this section is to describe a method that can be used for finding periodic solutions of nonlinear oscillators of the type of equation (5.1). One of the most popular methods for approximating the frequency response of nonlinear systems is known as the Harmonic Balance (HB) method in the vibration literature (e.g. Nayfeh & Mook 1979), and as the Describing Function (DF) approach in the control and aeroelasticity literature (e.g. Gelb & Vander Velde 1968). It is computationally very efficient for obtaining steady-state solutions of nonlinear dynamics problems, but it is usually too restrictive, mainly because (i) the solution is assumed to have one dominant frequency component — or at most two — and the nonlinearity has to be small, and (ii) one needs to know a great deal about the solution *a priori* or to carry enough terms in the solution and check the order of the coefficients of all the neglected harmonics, since otherwise one might obtain an inaccurate approximation, as shown by Nayfeh & Mook (1979).

Contrary to small parameter techniques that require the nonlinear terms to be small, it is preferable to have a scheme that is applicable in a more general case. Urabe (1965) was one of the first to introduce a multi-harmonic balancing procedure. He combined it with the Newton-Raphson iteration technique to treat strong nonlinearities and he referred to this as a Galerkin approximation with a characteristic function containing trigonometric functions. Similarly, the Incremental Harmonic Balance (IHB) method was developed by Lau *et al.* (1982) to take into account multiple harmonic components due to the nonlinear forces. Hence, in the usual terminology, the IHB can be referred to as a combined Incremental Ritz-Galerkin Harmonic Balance method or as a Harmonic Balance Newton-Raphson (HBNR) method. Indeed, Ferri (1986) showed that the IHB and the HBNR methods are equivalent. The IHB method was successfully applied to various types of nonlinear structural systems, ranging from systems with continuous cubic nonlinearities (Lau *et al.* 1982) to dry friction damper problems where the nonlinear force is discontinuous (Pierre *et al.* 1985).

For generality, we shall assume that there exist a free parameter λ and a periodic function $\mathbf{x}_*(t)$, of frequency Ω, which is a solution of (5.1). Introducing a new time $\tau = \Omega t$, equation (5.1) can easily be put in the general form

$$\mathbf{f}(\mathbf{x}, \dot{\mathbf{x}}, \ddot{\mathbf{x}}, \Omega, \lambda, \tau) = \Omega^2 \mathbf{M}\,\ddot{\mathbf{x}} + \Omega\,\mathbf{C}\,\dot{\mathbf{x}} + \mathbf{K}\,\mathbf{x} - \mathbf{F}(\mathbf{x}, \Omega\,\dot{\mathbf{x}}, \Omega^2\,\ddot{\mathbf{x}}, \lambda, \tau) = \mathbf{0}. \qquad (5.20)$$

Hence, $\mathbf{f}$ represents a set of second-order implicit nonlinear ordinary differential equations, in which all derivatives are now with respect to τ. The aim of the IHB method is to find the periodic function $\mathbf{x}_*(\tau)$, of period 2π, that is a solution of (5.20). Two steps are necessary to solve the problem: (i) a perturbation or an incrementation of the solution from some initial guess of the solution of (5.20) using a Taylor series and (ii) a Galerkin procedure, where the solution $\mathbf{x}$ and the increments $\Delta\mathbf{x}$ are expanded in a *finite* Fourier series and where the error arising from the assumption that the space is finite is minimized. As mentioned already, Ferri (1986) proved that the order to which these two steps are performed is not important because the resulting algebraic equations are the same in either case.

Urabe and Lau's original methods were subsequently improved from a computational point of view. Ling & Wu (1987) developed the Fast Galerkin (FG) method in which Urabe's approach was implemented in a computationally efficient way by making use of the Fast Fourier Transform (FFT), and Cameron & Griffin (1989) modified the FG method and proposed the alternating frequency/time (AFT) method in which the Fourier components of the nonlinear terms are obtained by FFT, while those of the linear terms are obtained by direct differentiation. In the FG method, the Galerkin approximation is followed by the incrementation process, while in the IHB it is the contrary. Globally, the FG, the AFT and the IHB methods are very similar (Ling 1990). However, none of them was ever applied to second order *implicit* nonlinear differential equations, in which case convergence may not be achieved, as was shown for the Picard iteration with Chebyshev polynomials.

In essence, solving the implicit nonlinear differential equation is not very different from solving an explicit one. The first step in applying the IHB method is similar to a Newton-Raphson procedure: starting from a known solution $(\mathbf{x}_0, \Omega_0, \lambda_0)$ of an equation $\mathbf{f}_0$, or from an initial guess of the solution of (5.20), a neighbouring solution is reached through an incrementation $(\Delta\mathbf{x}, \Delta\Omega, \Delta\lambda)$ using a Taylor series expansion. Neglecting the nonlinear terms in $\Delta\mathbf{x}$, $\Delta\Omega$ and $\Delta\lambda$, a linearized incrementation equation is obtained

$$\left.\frac{\partial \mathbf{f}}{\partial \ddot{\mathbf{x}}}\right|_0 \Delta\ddot{\mathbf{x}} + \left.\frac{\partial \mathbf{f}}{\partial \dot{\mathbf{x}}}\right|_0 \Delta\dot{\mathbf{x}} + \left.\frac{\partial \mathbf{f}}{\partial \mathbf{x}}\right|_0 \Delta\mathbf{x} = -\mathbf{f}_0 - \left.\frac{\partial \mathbf{f}}{\partial \lambda}\right|_0 \Delta\lambda - \left.\frac{\partial \mathbf{f}}{\partial \Omega}\right|_0 \Delta\Omega. \tag{5.21}$$

Equation (5.21) is an N-dimensional second-order linear ordinary differential equation with time-dependent coefficients. On the right-hand side of (5.21), $\mathbf{f}_0$ is a corrective term that goes to zero when the solution is reached. Hence, the perturbation step attempts to find an increment to the current approximation $\mathbf{x}_0$, which when added to that approximation, will produce the exact solution $\mathbf{x}_*$. The second step in the IHB method is the Galerkin procedure. The Galerkin method is used because although (5.21) is linear, it has variable coefficients, and is thus difficult to solve. It yields an approximate solution, assumed to be periodic.

Consequently, the perturbation step of the IHB method generates a new equation in terms of a different variable, while the Galerkin step provides a means of solving this equation by minimizing the error caused by approximating the solution. The general procedure of the IHB method is as follows.

(a) Starting from $(2M+1) \times N$ known or estimated coefficients a_{ki} and b_{ki}, the assumed or sought periodic solution is written as

$$x_{0,k} \;=\; b_{k0} \;+\; \sum_{i=1}^{M}(a_{ki}\sin i\tau + b_{ki}\cos i\tau), \tag{5.22}$$

where M represents the number of harmonics. For simplicity, the constant terms b_{k0} are neglected; it is not difficult to include them in a numerical scheme. By differentiation of (5.22), it is straightforward to obtain $\dot{\mathbf{x}}_0$ and $\ddot{\mathbf{x}}_0$ as well. Similarly, the increments are also expanded as a Fourier series. For example,

$$\Delta\ddot{x}_k = -\sum_{i=1}^{M}(i^2\,\Delta a_{ki}\sin i\tau + i^2\,\Delta b_{ki}\cos i\tau). \tag{5.23}$$

For later use, it is in fact necessary to have values of $\mathbf{x}_0$, $\dot{\mathbf{x}}_0$ and $\ddot{\mathbf{x}}_0$ at $2M$ points $\tau_s = \pi(s-1)/M$, $1 \le s \le 2M$, that are equally spaced between 0 and 2π. The reason for evaluating the various functions at twice the number of harmonics is related to the use of the Fourier series. Indeed, the Nyquist sampling theorem states that a minimum of $2M$ values of the function are needed to accurately determine the Fourier coefficients (Weaver 1989).

(b) Knowing $\mathbf{x}_0$, $\dot{\mathbf{x}}_0$, $\ddot{\mathbf{x}}_0$, λ_0 and Ω_0, it is then easy to evaluate the different terms in (5.21), such as $\partial\mathbf{f}/\partial\ddot{\mathbf{x}}|_0$, $\partial\mathbf{f}/\partial\dot{\mathbf{x}}|_0, \ldots, \partial\mathbf{f}/\partial\Omega|_0$, again at $2M$ points τ_s.

(c) Since (5.22) represents only an approximate solution, and because of the truncation error, the corrective term $\mathbf{f}_0$ is not zero in general, but some time-varying quantity $\varepsilon(\tau)$. The Galerkin method requires that the increments are chosen so as to minimize this error, by making $\varepsilon(\tau)$ orthogonal to each term in the expansion (5.22), via

$$\int_0^{2\pi} \varepsilon(\tau) \left\{ \begin{array}{c} \sin i\tau \\ \cos i\tau \end{array} \right\} d\tau = 0, \quad i = 1, \ldots, M. \tag{5.24}$$

Since $\varepsilon(\tau)$ is formed from summing the Fourier series terms of (5.21), $\varepsilon(\tau)$ will also be a Fourier series. Hence, here the Galerkin step reduces to a projection onto the basis vectors. This step is very important because of the strong theory that lies behind it, which guarantees that this approach to solving (5.21) will actually yield the *best* solution.

Equation (5.24) represents a set of $2N \times M$ algebraic linear equations, which may be written (Ferri 1986) as

$$\mathbf{R} = [\mathrm{C}]\,\Delta\mathbf{x} + \mathbf{P}\Delta\lambda + \mathbf{Q}\Delta\Omega. \tag{5.25}$$

$\Delta\mathbf{x} = \{\Delta a_{k1}, \ldots, \Delta a_{kM}, \Delta b_{k1}, \ldots, \Delta b_{kM}\}^{\mathrm{T}}$, $1 \le k \le N$, is a vector of dimension $2N \times M$. Equation (5.25) defines an iterative solution algorithm for solving equation (5.21). In practice, the coefficients of $[\mathrm{C}], \mathbf{P}, \mathbf{Q}$ and $\mathbf{R}$ are obtained using an FFT algorithm. Hence, instead of computing numerically the numerous integrals defined by Ferri (1986), the FFT is used. For example,

$$\mathbf{R} = \left\{ \begin{array}{c} R_{2k-1,i} \\ R_{2k,i} \end{array} \right\}, \tag{5.26}$$

with

$$\sum_{i=1}^{M} (R_{2k-1,i} \sin i\tau_s + R_{2k,i} \cos i\tau_s) = \mathrm{FT}[-f_k(\tau_s)]. \tag{5.27}$$

In (5.26) and (5.27), it is understood that $1 \le k \le N$, $1 \le s \le 2M$, and FT[ ] stands for the Fourier Transform.[§] The elements of $\mathbf{P}$ and $\mathbf{Q}$ may be defined similarly, simply by replacing $f_k(\tau_s)$ by $[\partial f_k/\partial\lambda](\tau_s)$ and $[\partial f_k/\partial\Omega](\tau_s)$, respectively. The evaluation of $[\mathbf{C}]$ is a bit more complicated. In this case one has to introduce an additional integer, $1 \le j \le M$, such that

$$[\mathbf{C}] = \begin{bmatrix} \mathbf{C}^1 & \mathbf{C}^3 \\ \mathbf{C}^2 & \mathbf{C}^4 \end{bmatrix} = \begin{bmatrix} C_{(2k-2)M+i,(2l-2)M+j} & C_{(2k-2)M+i,(2l-1)M+j} \\ C_{(2k-1)M+i,(2l-2)M+j} & C_{(2k-1)M+i,(2l-1)M+j} \end{bmatrix}, \qquad (5.28)$$

with

$$\begin{aligned} \textstyle\sum_{i=1}^{M}(\mathbf{C}^1 \sin i\tau_s + \mathbf{C}^2 \cos i\tau_s) = &\ \mathrm{FT}[\tfrac{\partial f_k}{\partial x_l} \sin j\tau_s + j\tfrac{\partial f_k}{\partial \dot{x}_l} \cos j\tau_s - j^2\tfrac{\partial f_k}{\partial \ddot{x}_l} \sin j\tau_s], \\ \textstyle\sum_{i=1}^{M}(\mathbf{C}^3 \sin i\tau_s + \mathbf{C}^4 \cos i\tau_s) = &\ \mathrm{FT}[\tfrac{\partial f_k}{\partial x_l} \cos j\tau_s - j\tfrac{\partial f_k}{\partial \dot{x}_l} \sin j\tau_s - j^2\tfrac{\partial f_k}{\partial \ddot{x}_l} \cos j\tau_s]. \end{aligned} \qquad (5.29)$$

(d) Obviously, $[\mathbf{C}]$ is of dimension $(2N \times M)^2$, which means that the number of unknowns exceeds the number of equations by 2, because $\Delta\lambda$ and $\Delta\Omega$ are not known. Hence, one needs to add two constraints. Recalling that the solution sought is for a given parameter, or of a predefined frequency, the first constraint is either $\Delta\lambda = 0$ or $\Delta\Omega = 0$. If $\Delta\lambda = 0$, λ is said to be the active increment and the solution for a different λ is obtained by incrementing λ from point to point. Similarly, if $\Delta\Omega = 0$, Ω is the active increment. In practice, the active increment is chosen as the one that varies faster (Pierre & Dowell 1985). Finding the second constraint is more subtle. Lau *et al.* (1982) simply set one of the coefficients equal to zero ($\Delta a_{11} = 0$ or $\Delta b_{11} = 0$). This is valid if the system is autonomous (it only causes a phase shift in the time response) or if it is linear (in this case one is more interested in the *existence* of the periodic solution that is independent of the amplitude). In general, as shown by Pierre & Dowell (1985), there is an interdependence between the frequency and the amplitude of the response and the nonlinear terms. Therefore, the state of vibration has to be characterized by the norm of the response $||\mathbf{x}||$ which may or may not be incremented. This incrementation (or lack thereof) constitutes the second constraint. The norm $||\,.\,||$ may be the infinite or the Euclidian norm. Once the two constraints are included, the

[§]The Fourier Transform as defined here follows the convention and notation of Press *et al.* (1992).

linear system of equations can be solved using standard algebra routines.

(e) Once the incremental coefficients $(\Delta a_{ki}, \Delta b_{ki})$ are found, the assumed solution can be updated and the process is repeated until a convergence criterion is met. This criterion may be defined as the infinite norm of the incremental vector having to be smaller than a certain value ϵ_0.

(f) Once the solution of the differential equation is found, nothing can be said about its stability. Indeed, the IHB method finds ***equilibrium*** solutions (in fact, the Galerkin and harmonic balance methods as well), regardless of their stability. This is a major advantage compared to direct numerical solution such as Runge-Kutta or the Finite Difference methods where only ***dynamically stable*** solutions can be computed. In practice, the stability of the solution is determined by Floquet theory. Consider a small perturbation of the steady-state solution $(\mathbf{x}_*, \Omega, \lambda)$,

$$\mathbf{x} = \mathbf{x}_* + \mathbf{u}, \tag{5.30}$$

at Ω and λ. Substituting (5.30) into (5.20) and taking into consideration the fact that $\mathbf{x}_*$ satisfies (5.20), one obtains the linearized equation for $\mathbf{u}$

$$\left.\frac{\partial \mathbf{f}}{\partial \ddot{\mathbf{x}}}\right|_* \ddot{\mathbf{u}} + \left.\frac{\partial \mathbf{f}}{\partial \dot{\mathbf{x}}}\right|_* \dot{\mathbf{u}} + \left.\frac{\partial \mathbf{f}}{\partial \mathbf{x}}\right|_* \mathbf{u} = 0. \tag{5.31}$$

This is an N-dimensional linear second-order differential equation the time-dependent periodic coefficients of which are known for all $0 \leq \tau \leq 2\pi$. For example, $\partial \mathbf{f}/\partial \ddot{\mathbf{x}}|_*$ is an $N \times N$ matrix with elements $\partial f_k/\partial \ddot{x}_l$, evaluated at $\mathbf{x}_*(\tau)$. Hence, equation (5.31) may be integrated numerically very easily (using a Runge-Kutta or Finite Difference method) for any initial conditions. Because the IHB method yields a periodic solution the period of which is known (it is 2π in nondimensional time), it is obvious that it is very powerful in investigating the dynamical stability of the system. Indeed, it is well known that the stability of the periodic solution is related to the eigenvalues of the transition matrix at the end of one period. The eigenvalues of the transition matrix are complex in general, and the solution is stable if all the moduli of the eigenvalues are less than unity, and unstable otherwise. One of the eigenvalues is equal to 1 (it corresponds to the periodicity of the solution), which may be used to check the accuracy of the multipliers. Usually, the Floquet multipliers are obtained after rewriting the variational equation (5.31) in state variable form, but this step is not necessary. Let us define the vector $\mathbf{v}(\tau) = \{\mathbf{u}(\tau), \dot{\mathbf{u}}(\tau)\}^{\mathrm{T}}$, of length $2N$, and the corresponding unit vectors $e_j = \{0, ..., 0, 1, ..., 0\}^{\mathrm{T}}$, null everywhere except at the jth column $(1 \leq j \leq 2N)$. Each unit vector corresponds to an initial condition for $\mathbf{u}$ and $\dot{\mathbf{u}}$. Equation (5.31) may be integrated $2N$ times for each initial condition and $0 \leq \tau \leq 2\pi$, and the transition matrix is formed by the resulting $2N$ vectors $\mathbf{v}(2\pi)$.

Some additional remarks may be necessary. (i) In practice, some turning points may be encountered when incrementing one parameter or another, and hence the program must have the capability of automatically changing the incrementation parameter. (ii) In some cases, it may be difficult to converge to a solution. Ideally, it is best to start the process from a known solution and then to increment from there. This is often possible, and in this sense, the IHB method can be regarded as a continuation or *homotopy* method. (iii) From a conceptual point of view, it can be seen that neither the order of the differential equation, nor the nonlinear inertial terms introduce additional difficulty, which renders the IHB very attractive. (iv) As shown by Sekar & Narayanan (1994) it is also possible to find subharmonic solutions of order n, simply by introducing $\tau = n\Omega t$. Therefore, together with the stability analysis, the IHB method may be used to show the existence of period-doubling bifurcations. (v) It was shown by Lau *et al.* (1983) that the IHB method could be modified to treat almost-periodic steady-state vibrations such as combination resonances that contain more than one frequency, by employing multiple time variables (see also Lau *et al.* 1989). (vi) In a computer program, the number of harmonics may be changed very easily to obtain a desired accuracy. Usually, $M = 8$ or 16 gives a good approximation.

5.4.2 Results

As for the Finite Difference methods, the Incremental Harmonic Balance method has been tested on numerous examples. The strategy used here is the same as before, namely to choose a second-order differential equations that can be cast in both implicit and explicit form. However, instead of just looking at the time response, bifurcation diagrams are also constructed to show the evolution of the response when one parameter is varied. In this case, AUTO is used for comparison, because it is known to be very effective in bifurcation analyses (Doedel & Kernéves 1986). Figure 5.4(a,b) shows how the frequency of the response and the two Floquet multipliers vary with $\lambda = -c$ for van der Pol's equation (5.10) or (5.11). It can be concluded that the IHB yields accurate frequencies for $0 \leq \lambda \leq 1.5$, but the discrepancy increases if $\lambda > 1.5$, even for $M = 32$. Moreover, the first Floquet multiplier is only accurate for $\lambda < 1$, which indicates that the computation of the transition matrix should be refined. On the other hand, the *second* multiplier in this example as well as in others, was found to be more accurate. One reason that might explain this discrepancy is that the response, although periodic, is closer to an impulse-type motion, with an abrupt change at $\tau = \pi$, as shown in Figure 5.5, for $c = -2.7$ and $c = -6.0$. When the response has a more "regular" shape, i.e., when the number of harmonics needed to represent it accurately is less than 16, the IHB method is a very powerful tool, e.g. the case of $c = -0.2$ in Figure 5.5.

The IHB method was also applied successfully to two coupled van der Pol oscillators, with and without nonlinear inertial terms, and the two branches emanating from the Hopf bifurcation could be detected (Lau & Yuen 1993).

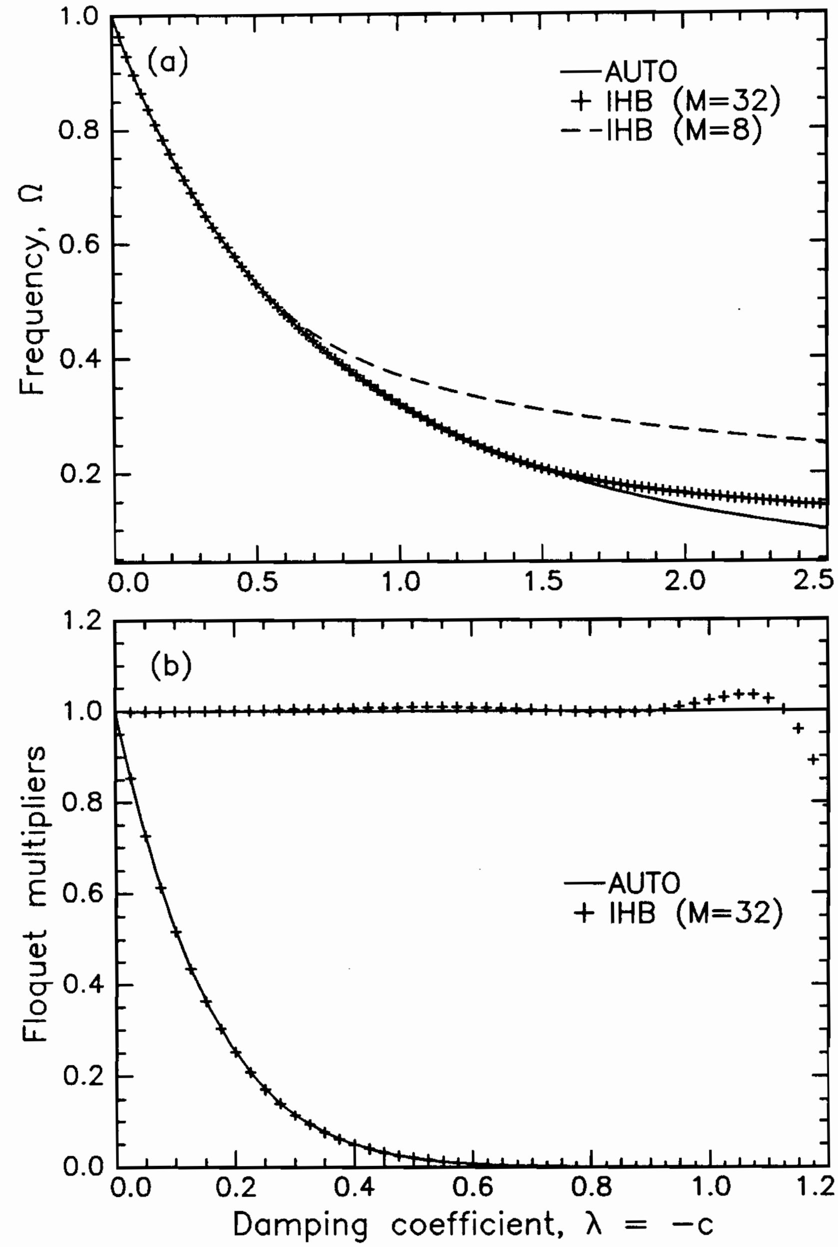

Figure 5.4: Bifurcation diagrams of van der Pol's equation representing (a) the frequency of the response and (b) the two Floquet multipliers as functions of the damping coefficient, computed with AUTO and the Incremental Harmonic Balance (IHB) method: —, AUTO; +, IHB ($M = 32$); − − −, IHB ($M = 8$).

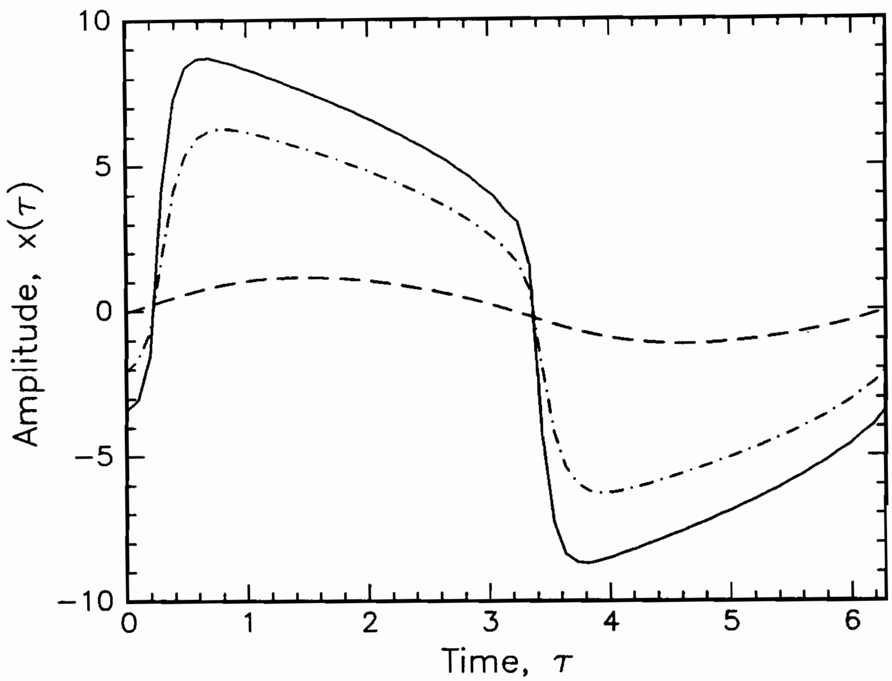

Figure 5.5: Time response of van der Pol's equation using the IHB method for three values of the damping coefficient: —, $c = -6.0$; —·—, $c = -2.7$; – – –, $c = -0.2$.

As will be seen, this method was also applied to the problem of parametric resonances of pipes conveying fluid (see Semler & Païdoussis 1995 or Chapter 7) and to the pipe with a point-mass fitted at the free end. The equation of motion in this case is given by (Semler & Païdoussis 1994)

$$[\delta_{ij} + \Gamma\phi_i(1)\phi_j(1) + \gamma_{ilkj}q_k q_l]\ddot{q}_j + c_{ij}\dot{q}_j + k_{ij}q_j + \ \alpha_{ijkl}\ q_j q_k q_l + \beta_{ijkl}\ q_j q_k \dot{q}_l + \gamma_{ijkl}\ q_j \dot{q}_k \dot{q}_l = 0. \tag{5.32}$$

The different coefficients in (5.32) are computed analytically and numerically, and it can be shown that the nonlinear inertial terms $\gamma_{ilkj}q_k q_l$ after the Hopf bifurcation are not small compared to the linear ones. The dynamics of this system depends mainly on two nondimensional parameters, u, the flow velocity, and Γ, which is proportional to the mass added at the free end. For comparison, bifurcation diagrams obtained by the IHB and Houbolt's methods have been constructed for $\Gamma = 0.1$, and are presented in Figure 5.6 (here AUTO or Runge-Kutta methods do not apply). As can be seen, remarkable agreement is achieved, at least when the solution sought is stable. The two bifurcation diagrams illustrate perfectly the advantages and disadvantages of the two methods: Houbolt's method is only able to find *stable* solutions, that may be equilibria, limit-cycles, quasiperiodic or even chaotic oscillations (here the response for $u = 8.1$ is quasiperiodic). On the other hand, the IHB method yields only *periodic* solutions that can be either stable or unstable. It is also able to follow any periodic solution, which helps to explain where and how new dynamical behaviour arises. In this example, it is shown how the high-frequency periodic solution (the low-amplitude stable motion in Figure 5.6(a) or the upper region in Figure 5.6(b)) appears, which proves that this solution does not come from a second Hopf bifurcation (and hence that it might only be detected through a nonlinear analysis). This illustrates how the combination of the IHB and Houbolt's methods is a powerful tool for the analysis of systems represented by second-order implicit nonlinear differential equations.

5.5 CONCLUSION

In this chapter, numerical solutions of second-order implicit nonlinear ordinary differential equations were proposed. The literature review undertaken showed that most textbooks on ordinary differential equations (ODEs) assume that second-order differential equations can be cast into a set of first-order equations, thereby elaborating numerical schemes only for this "general" case. In the last decade, some authors derived new methods of solution (other than the well-known Runge-Kutta or Adams-Bashforth methods) and claimed that they were applicable also to implicit differential equations, i.e. equations where nonlinear inertial terms are present. These methods were presented here and adapted for the implicit equations, and applied to various problems.

It was shown that Picard iteration using Chebyshev series is not valid in the case of implicit differential equations, and the cause for divergence in certain situations was

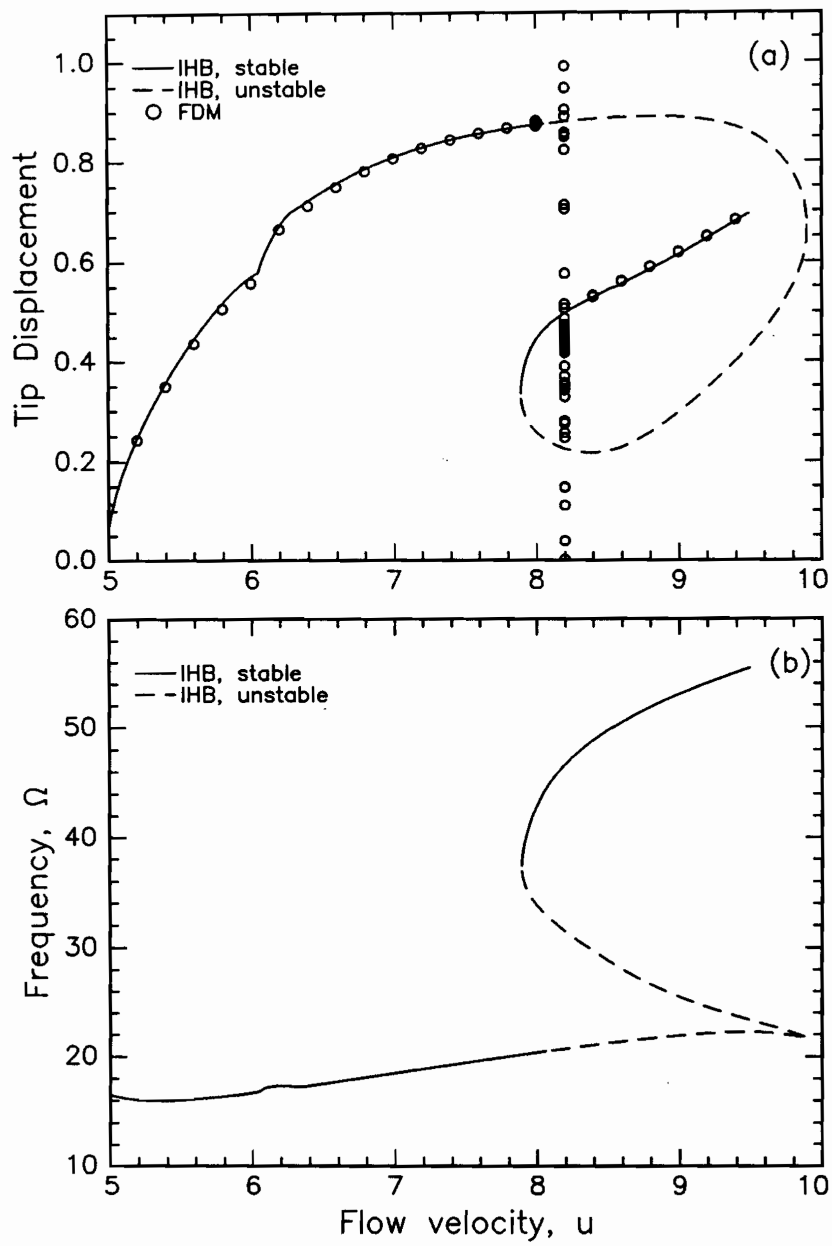

Figure 5.6: Bifurcation diagrams of the cantilevered pipe conveying fluid and fitted with an end-mass $\Gamma = 0.1$, representing (a) the tip displacement of the pipe and (b) the frequency of the response as functions of the nondimensional flow velocity u, computed with the Incremental Harmonic Balance (IHB) and Houbolt's methods: —, IHB, stable solution; – – –, IHB, unstable solution; o, solution by Houbolt's method.

elucidated to some extent. The divergence was not simply a result of encountering singularities during the analytic continuation procedure, as convergence could not be achieved even for very small interval sizes. It was also verified that predictor-corrector processes would not help, since a significant improvement in the accuracy of the initial guess did not aid in convergence. Consequently, even if it might be very efficient to treat explicit ODEs, this numerical scheme should not be used to solve implicit ones.

Then, two existing finite difference methods (Houbolt's 4th-order and an 8th-order scheme) were proposed to compute time histories of systems defined by second-order implicit differential equations, and comparison was made with an existing and reliable software package. It was shown that when the time step is sufficiently small, e.g. 250 time steps per cycle, both methods yield accurate results. The 8th-order scheme, despite being a bit slower than Houbolt's method, is more efficient since the number of time steps to be used can be much smaller, approximately 100 steps per cycle. Nevertheless, in most cases, the only deficiency in Houbolt's scheme is that it introduces some very small numerical damping together with a phase shift, which might be negligible when dealing with dissipative systems. It is of importance to note that the FDM yields only *stable* orbits that may be periodic, quasiperiodic or chaotic.

Finally, the Incremental Harmonic Balance method was proposed to predict the existence of *periodic* solutions. As suggested (but not previously demonstrated) in the literature, it is capable of solving problems defined by implicit equations. Being a continuation method, it is particularly useful for bifurcation analyses since it is very easy to "follow" a solution and to assess its stability. Together with Floquet theory, it can be used to detect qualitative changes in the dynamics, as well as the appearance or disappearance of new solutions, which is of major importance in nonlinear problems. It has hence been proved that the combination of the two methods, FDM and IHB, represents a powerful tool for the analysis of systems containing nonlinear inertial terms.

Chapter 6

THE PIPE WITH A SMALL MASS AT THE FREE END

6.1 INTRODUCTION

Ever since the early work on the dynamics of pipes conveying fluid, e.g. by Housner (1952) and Benjamin (1961), well over 200 papers have been published on the subject. Indeed, as recently discussed in an extensive review of the topic (Païdoussis & Li 1993), this system has now become a new paradigm in dynamics, on a par with the classical problems of a column subjected to axial loading and a rotating shaft. This is especially so for the inherently nonconservative system of a cantilevered pipe conveying fluid (Benjamin 1961; Gregory & Païdoussis 1966; Herrmann & Nemat–Nasser 1967).

More recently, increased effort has been devoted to the study of the nonlinear dynamics of the cantilevered system (e.g., Bajaj *et al.* 1980; Rousselet & Herrmann 1981; Bajaj & Sethna 1991; Li & Païdoussis 1994), as well as on chaotic dynamics in variants of the basic system (Tang & Dowell 1988; Païdoussis & Moon 1988; Païdoussis *et al.* 1991, 1992). Païdoussis & Moon (1988) studied theoretically and experimentally the planar dynamics of a cantilevered pipe conveying fluid and interacting with motion–limiting restraints. They showed that, after the Hopf bifurcation, which arises in all cantilevered pipes at sufficiently high flow velocity, the resulting limit cycle undergoes a cascade of period–doubling bifurcations, leading to chaos. Fractal dimension calculations (Païdoussis *et al.* 1992) showed definitively that the essential dynamics may indeed be captured by a two–degree–of–freedom ($N = 2$) discrete model (as heuristically done in the earlier study), but that $N = 4$ or 5 may be necessary for adequate quantitative prediction. This was found to be the case, and agreement with experiment to within $5 - 10\%$ was obtained for the Hopf and first period–doubling bifurcations and the onset of chaos (Païdoussis *et al.* 1991). This was later confirmed by Païdoussis & Semler (1993), in which, in contrast to previous studies, the full nonlinear form of the equation of motion was utilized, and through which one can also predict the experimentally observed "sticking" of the pipe to the restraints at very high flow velocities.

Chaos was never found in the case of planar motions of the *plain* autonomous cantilevered system, i.e., without lateral restraints (Païdoussis and co–workers) or magnets (Tang & Dowell 1988). The same was concluded by Copeland & Moon (1992) for *three–dimensional* motions of the system, who nevertheless found that chaotic motions are indeed possible, provided that a mass is attached to the free end of the cantilevered pipe.

The present study was initiated to investigate the *planar* version of Copeland and Moon's system. In Section 6.2, the nonlinear equation of motion of the system is first modified to account for the presence of a lumped end–mass. In Section 6.3, the dynamics of the system is then studied for the case of a mass–defect at the free end, which is the same as the addition of a negative end–mass. There is no particular engineering application for the system, although it is obvious that a pipe with a reduction in the outer diameter over a segment near the free end is easily physically possible (as much as an addition of a lumped mass would be); nevertheless the justification for the study —as in the case for most if not all of what has already been done on the dynamics of pipes conveying fluid (Païdoussis & Li 1993; Païdoussis 1993) — owes more to fundamental interest in its dynamical behaviour than to practical applications. In the subsequent sections, the more realistic case of a positive end–mass is considered, both experimentally (Section 6.4.1) and numerically (Section 6.4.2), and some final conclusions are drawn.

6.2 THE ANALYTICAL MODEL

The system under consideration (Figure 6.1) is the same as that considered by Copeland & Moon (1992). The equations of motion without the end–mass have been derived in Chapter 2, and are similar to those derived earlier by Lundgren *et al.* (1979); they are here modified to take into account the presence of the end–mass, modelled as a lumped point–mass, $\mathcal{M}$, at $x = L$.

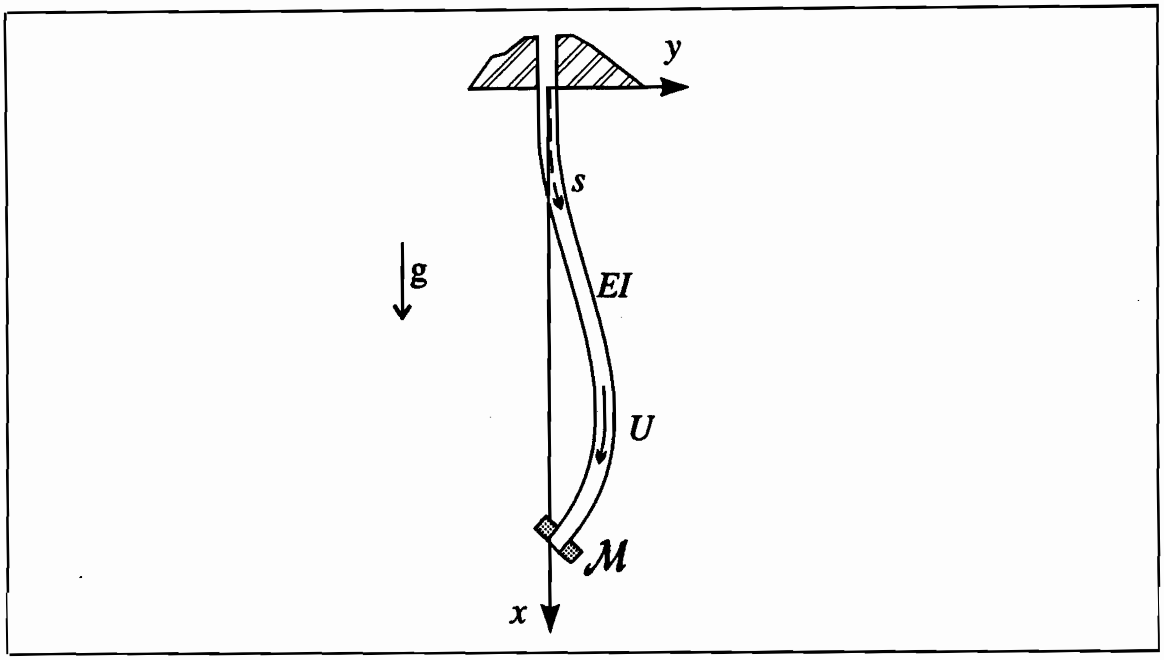

Figure 6.1: Schematic of the system (from Semler & Païdoussis 1995; permission granted by the American Society of Mechanical Engineers).

The addition of a lumped end–mass to an otherwise uniform vertical pipe conveying fluid makes inertial and gravitational contributions to the equation of motion. In the context of a Lagrangian derivation of the equations, these contributions will be derived here as additional components in the kinetic and potential energies of the system.

The variation of the kinetic energy component associated with the lumped end–mass is

$$\delta \int_{t_1}^{t_2} T_{\mathcal{M}}\, \mathrm{d}t = \delta \int_{t_1}^{t_2} \tfrac{1}{2}\mathcal{M} v_L^2\, \mathrm{d}t = -\int_{t_1}^{t_2} \mathcal{M}(\ddot{x}_L \delta x_L \;+\; \ddot{y}_L \delta y_L)\, \mathrm{d}t \;=\; A + B, \tag{6.1}$$

in which the dot stands for $\partial(\;)/\partial t$. Introducing the Dirac delta function (of dimension L^{-1}), the B term may be written as

$$B \;=\; -\int_{t_1}^{t_2} \int_0^L \mathcal{M}\ddot{y}\delta(s-L)\, \delta y\, \mathrm{d}s\, \mathrm{d}t. \tag{6.2}$$

To compute the A term in (6.1), the inextensibility condition (2.3) and its variational form (2.21) are used, namely,

$$\begin{gathered} x'^2 + y'^2 = 1\,, \\ \delta x = -\left(y' + \tfrac{1}{2}\, y'^3\right)\delta y + \int_0^s \left(y'' + \tfrac{3}{2}\, y'^2\, y''\right)\delta y\, \mathrm{d}s\,, \end{gathered} \tag{6.3}$$

where $(\;)' = \partial(\;)/\partial s$, with the aid of which,

$$A = -\int_{t_1}^{t_2} \mathcal{M}\ddot{x}_L\, \delta x_L\, \mathrm{d}t = \int_{t_1}^{t_2} \mathcal{M} \int_0^L (\dot{y}'^2 + y'\ddot{y}')\, \mathrm{d}u \left\{ -y_L' \delta y_L + \int_0^L y''\delta y\, \mathrm{d}u \right\} \mathrm{d}t. \tag{6.4}$$

Using again the delta function, A becomes

$$A = \mathcal{M} \int_{t_1}^{t_2} \int_0^L \left[-y'\delta(s-L) \int_0^s (\dot{y}'^2 + y'\ddot{y}')\, \mathrm{d}u + y'' \int_0^L (\dot{y}'^2 + y'\ddot{y}')\, \mathrm{d}u \right] \delta y\, \mathrm{d}s\, \mathrm{d}t. \tag{6.5}$$

This can be transformed into

$$\int_0^L \left[-y'\mathcal{M}\delta(s-L) \int_0^s (\dot{y}'^2 + y'\ddot{y}')\, \mathrm{d}u + y'' \int_s^L \mathcal{M}\delta(u-L) \int_0^u (\dot{y}'^2 + y'\ddot{y}')\, \mathrm{d}v\mathrm{d}u \right] \delta y\, \mathrm{d}s \tag{6.6}$$

which depends on the fact that $y''(L) = 0$. This equation is now of similar form to the equation for the inertial terms in the equation of motion, and hence may directly be incorporated in it.

For the gravitational term, one needs to compute

$$\delta \int_{t_1}^{t_2} \mathcal{G} \mathrm{d}t = \delta \int_{t_1}^{t_2} \mathcal{M} g x_L \mathrm{d}t = \int_{t_1}^{t_2} \mathcal{M} g \delta x_L \mathrm{d}t, \tag{6.7}$$

which, after use of (6.3), becomes equal to

$$\int_{t_1}^{t_2} \mathcal{M}g \int_0^L \left[-(y' + \tfrac{1}{2}y'^3)\delta y\ \delta(s-L)\right] \mathrm{d}s\mathrm{d}t + \int_{t_1}^{t_2} \mathcal{M}g \int_0^L (y'' + \tfrac{3}{2}y'^2 y'')\delta y\ \mathrm{d}s\mathrm{d}t. \quad (6.8)$$

Consequently, incorporating equations (6.6) and (6.8), the complete equation of motion for the cantilevered pipe with an end–mass, containing steady flow ($\dot{U} = 0$), becomes

$$\begin{aligned}
&[m+M + \mathcal{M}\delta(s-L)]\, \ddot{y} + 2MU\, \dot{y}' \left(1 + y'^2\right) + [m + M + \mathcal{M}\delta(s-L)]\, g\, y' \left(1 + \tfrac{1}{2}\, y'^2\right) \\
&+\ y'' \left[MU^2 \left(1 + y'^2\right) - \left(1 + \tfrac{3}{2}\, y'^2\right) \int_s^L (m + M + \mathcal{M}\delta(u-L))\, g\ \mathrm{d}u\right] \\
&+\ EI \left[y'''' \left(1 + y'^2\right) + 4\, y'\, y''\, y''' + y''^3\right] \\
&-\ y'' \left[\int_s^L \left([m + M + \mathcal{M}\delta(u-L)] \int_0^u \left(\dot{y}'^2 + y'\, \ddot{y}'\right)\ \mathrm{d}v\right) \mathrm{d}u \right. \\
&\qquad\qquad \left. + \int_s^L \left(2\, MU\, y'\, \dot{y}' + MU^2\, y'\, y''\right) \mathrm{d}u\right] \\
&+\ y' \left[m + M + \mathcal{M}\delta(s-L)\right] \int_0^s \left(\dot{y}'^2 + y'\, \ddot{y}'\right) \mathrm{d}u = 0, \qquad (6.9)
\end{aligned}$$

correct to $\mathcal{O}(\epsilon^3)$ for lateral displacements of the pipe, y, of $\mathcal{O}(\epsilon)$. In this equation, m is the mass of the pipe per unit length, EI its flexural rigidity, and L its length; M is the mass of the fluid per unit length, flowing in the pipe with mean velocity U. The contribution of the terms due to the end–mass was also determined independently by using the Newtonian approach (force balance method), confirming that (6.9) is indeed correct. This equation of motion is essentially very similar to that derived by Copeland (1992), with some differences: (i) the inextensibility condition has been used to obtain a single equation, instead of one each for the axial and the lateral components of motion; (ii) only one equation is needed since *planar* motion is considered; (iii) the effect of the lumped mass $\mathcal{M}$ is incorporated in the equation itself, rather than in the boundary conditions (Hill & Swanson 1970).

Comparing equation (6.9) to that without the end–mass, it is seen that by the judicious utilization of the Dirac delta function, $m + M$, representing the mass per unit length of the pipe and the contained flow, is replaced by

$$m + M \rightarrow m + M + \mathcal{M}\delta(s-L). \qquad (6.10)$$

Equation (6.9) contains nonlinear inertial terms that cannot be removed from the partial differential equation, because of the presence of the delta function $\delta(s-L)$. Therefore, they will be removed from the discretized ordinary differential equation (o.d.e.), obtained by Galerkin's technique.

To simplify the analysis, the equation of motion is first put in nondimensional form. The same nondimensional quantities as before (Païdoussis 1970) are used, plus a nondimensional end-mass parameter Γ, namely

$$\begin{aligned} \xi = \frac{s}{L}, \quad \eta = \frac{y}{L}, \quad \tau &= \left(\frac{EI}{m+M}\right)^{\frac{1}{2}} \frac{t}{L^2}, \quad \Gamma = \frac{\mathcal{M}}{(m+M)L}, \\ u = \left(\frac{M}{EI}\right)^{\frac{1}{2}} U\, L, \quad \gamma &= \frac{m+M}{EI} L^3 g, \quad \beta = \frac{M}{m+M}. \end{aligned} \tag{6.11}$$

In physical terms, u is the nondimensional fluid velocity, γ represents the relative measure of gravity to flexural forces, and β is the ratio of the fluid mass to the total mass per unit length. The resulting nondimensional equation of motion may be written in the compact form

$$\begin{aligned} \ddot{\eta}\,[1+\Gamma\delta(\xi-1)] + \eta''\left[u^2 - \gamma\int_\xi^1 (1+\Gamma\delta(\xi-1))d\xi\right] + \gamma\,[1+\Gamma\delta(\xi-1)]\eta' \\ + 2\,u\sqrt{\beta}\,\dot{\eta}'\eta'''' + N(\eta) = 0\,, \end{aligned} \tag{6.12}$$

where

$$\begin{aligned} N(\eta) \;=\; & 2\,u\sqrt{\beta}\dot{\eta}'\,\eta'^2 + \eta''\left[u^2 - \tfrac{3}{2}\int_\xi^1 \gamma[1+\Gamma\delta(\xi-1)d\xi]\right]\eta'^2 + \tfrac{1}{2}\gamma[1+\Gamma\delta(\xi-1)]\eta'^3 \\ & + \eta''''\,\eta'^2 + 4\,\eta'\,\eta''\,\eta''' + \eta''^3 + \eta'[1+\Gamma\delta(\xi-1)]\int_0^\xi (\dot{\eta}'^2 + \eta'\,\ddot{\eta}')d\xi \\ & - \eta''\left[\int_\xi^1 [1+\Gamma\delta(\xi-1)]\int_0^\xi (\dot{\eta}'^2 + \eta'\,\ddot{\eta}')d\xi\,d\xi \right. \\ & \left. + \int_\xi^1 \left(2\,u\sqrt{\beta}\,\eta'\,\dot{\eta}' + u^2\,\eta'\,\eta''\right)d\xi\right]. \end{aligned} \tag{6.13}$$

The system is discretized by expressing $\eta(\xi,\tau) = \sum_{r=1}^{N}\phi_r(\xi)q_r(\tau)$, in which the cantilever beam eigenfunctions $\phi_r(\xi)$ are used as a suitable set of base functions, and $q_r(\tau)$ represent the corresponding generalized coordinates. This leads to

$$[\delta_{ij} + \Gamma\phi_i(1)\phi_j(1) + \gamma_{ilkj}q_kq_l]\ddot{q}_j + c_{ij}\dot{q}_j + k_{ij}q_j + \alpha_{ijkl}\,q_jq_kq_l + \beta_{ijkl}\,q_jq_k\dot{q}_l + \gamma_{ijkl}\,q_j\dot{q}_k\dot{q}_l = 0; \tag{6.14}$$

δ_{ij} is the Kronecker delta, c_{ij} and k_{ij} are elements of the damping and stiffness matrices, and α_{ijkl}, β_{ijkl} and γ_{ijkl} are coefficients, computed numerically, involving the integrals of the eigenfunctions $\phi_i(\xi)$ — see Appendix G; note the inversion of the indices (j,l) for the nonlinear inertial term and the fact that the indices implicitly follow the summation convention.

6.3 INTERMITTENCY ROUTE TO CHAOS OF THE PIPE WITH A MASS DEFECT§

In this section, the case of a negative end-mass is considered. Before presenting the results, the method of solution and the physical parameters are presented, together with the assumptions made on Γ and the equation of motion.

6.3.1 Method of solution

The inertia matrix can be inverted by assuming q_r small — as will be explained in Section 6.3.3— so that equation (6.14) may be converted into a second–order o.d.e. of more standard form, and then put into first–order form,

$$\dot{y} = [A]\, y + f(y)\,, \tag{6.15}$$

where f is a third–order polynomial function, $[A]$ is a $2N \times 2N$ matrix, and $\{y\} = \{q, \dot{q}\}^{\mathrm{T}}$. Solutions of equation (6.15) are obtained principally by a fourth–order Runge Kutta integration algorithm, with a time step size of 0.001, and different initial conditions representing a pipe with no initial velocity, $y_{i+N}(0) = 0$. From the numerical integration of (6.15), time traces and the corresponding power spectra, phase plane plots and bifurcation diagrams can easily be constructed and Lyapunov exponents calculated. However, in order to find also unstable limit cycles, AUTO (Doedel 1981) was

§It corresponds to the article by Semler & Païdoussis 1995 Intermittency route to chaos of a cantilevered pipe conveying fluid with a mass defect at the free end. *Journal of Applied Mechanics* **62**, 903-908.

used. Indeed, AUTO can deal with o.d.e.s of the type of (6.15) and with computing both stable and unstable limit cycles, as well as determining how they lose or gain stability; see also Seydel (1988), for a good introduction on the subject. The results obtained may be presented in the form of bifurcation diagrams, where the maximum values of any generalized coordinate, or the period of oscillation, can be displayed as functions of one parameter (usually the flow velocity u). In this section, $N = 4$ is used as an appropriate approximation.

6.3.2 Physical parameters

In order to simplify the analysis, most of the parameters are kept constant, with values equal to those in the experiments of Païdoussis & Moon (1988): $\gamma = 26.75$ and $\beta = 0.216$. Also, the dissipative forces are modelled via a viscous damping idealization with the individual modal logarithmic decrements, δ_j, corresponding to the experimentally measured values (Païdoussis *et al.* 1991): $\delta_1 = 0.028, \delta_2 = 0.081, \delta_3 = 0.144$; with $\delta_4 = 0.200$ linearly extrapolated. The nondimensional flow velocity u and end–mass Γ are the main parameters to be varied. Physically, a negative Γ represents a small mass defect over a small segment of the free end of the pipe to be modelled as a negative mass. Denoting the external and internal radii of the pipe by r_0 and $r_i = \alpha' r_0$, and considering the external radius of the pipe reduced to αr_0 over a segment of length L', then the end-mass defect is given by $\mathcal{M} = mL'(1-\alpha^2)/(1-\alpha'^2)$. For example, for $\beta = 0.15$, $\alpha' = 0.5, \alpha = 0.55$, and $L'/L = 0.12$, one obtains $|\Gamma| = 0.093$.

6.3.3 Analysis

Assuming Γ to be sufficiently small (of the same order as $q_k q_l$), the inversion of the inertia matrix is simply

$$[\delta_{ij} + \Gamma\phi_i(1)\phi_j(1) + \gamma_{ilkj}q_k q_l]^{-1} \sim \delta_{ij} - \Gamma\phi_i(1)\phi_j(1) - \gamma_{ilkj}q_k q_l, \qquad (6.16)$$

so that (6.14) can easily be recast in its first–order form. Moreover, as $\Gamma \sim \mathcal{O}(q_k q_l)$, the nonlinear inertial terms due to Γ may be neglected in the analysis. Approximation

(6.16) suggests that $\Gamma << 1$. For computational convenience, the results shown in the sequel correspond to the case $\Gamma = -0.3$, but qualitatively similar results were obtained for more physically realistic values of Γ (e.g., $\Gamma = -0.085$).

The equations of motion in their first–order form are integrated numerically with the fourth–order Runge Kutta scheme. For $\Gamma = 0$, after the Hopf bifurcation at $u = u_H = 8.7$, the system performs limit–cycle motion. For $\Gamma = -0.3$, however, the situation is more complex and interesting, as seen in Figure 6.2; in this case, $u_H = 7.07$.

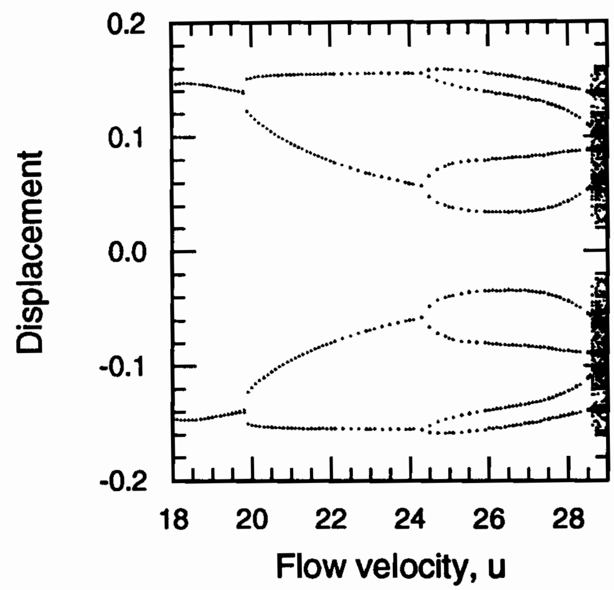

Figure 6.2: Bifurcation diagram for the free–end displacement versus dimensionless flow velocity after the Hopf bifurcation, $\Gamma = -0.3$ (from Semler & Païdoussis 1995; permission granted by the American Society of Mechanical Engineers).

At $u = 19.82$, the limit cycle becomes unstable: a new periodic orbit is created through a pitchfork bifurcation, which breaks the symmetry of the system. At $u = 24.37$, the system undergoes a period–doubling bifurcation. However, instead of developing the usual period–doubling cascade, an interesting phenomenon occurs: at $u = 28.56$, this newly generated steady state undergoes another bifurcation which leads the system to chaos.

In order to understand what kind of bifurcation takes place, it is of interest to compute the Floquet multipliers (Hartman 1964) in the neighbourhood of the different points of instability. Indeed, the multipliers are a mathematical representation of the type of instability that occurs for a periodic orbit, while the trajectory on the phase plane is a more geometrical picture of the dynamics (Figure 6.3). As expected (Guckenheimer & Holmes 1983), $\lambda = +1$ for $u = 19.82$, and $\lambda = -1$ at $u = 24.37$. The major finding is that one of the multipliers crosses the unit circle at $\lambda = +1$ for $u = 28.56$, which is characteristic of a ***"type I" intermittency*** route to chaos (Bergé *et al.* 1984). This route to chaos is also evident in the bifurcation diagram of Figure 6.2, since no transition is found between the period–2 orbit at $u = 28.56$ of Figure 6.3(c) and the chaotic–looking trajectory at $u = 28.60$ of Figure 6.3(d), even when the step size in u is greatly refined. A Poincaré map (not shown), representing the displacement versus velocity of the pipe end when the velocity of the pipe at $x = 0.2$ is zero, gives additional proof that the signal never repeats itself, even over a very long period of time.

Finally, the transition to intermittency is definitely established by Figure 6.4, which is a different type of map: for each cycle, the first–mode component $q_1(\tau)$ is tracked, and it is saved when it reaches its maximum (i.e., when $q_5 = 0$ in our eight–dimensional system). It is then possible to compute the map $q_1(n+1) = f(q_1(n))$, for a very long period of time ($\sim$ 8 200 cycles). On the map obtained — also called a Lorenz map or a return map — four curves, almost tangent to the 45° "identity line" are obviously present, showing the presence of four "channels". The resulting behaviour is nearly of period–2; thus, the system visits two steady states, but the dynamics is interspersed with bursts of aperiodic behaviour. As u is increased, the nearly periodic intervals become shorter on the average, while aperiodic motion becomes predominant. This is characteristic of intermittency (Bergé *et al.* 1984). The structure of the map itself is also of importance, demonstrating, once again, the existence of order in chaos.

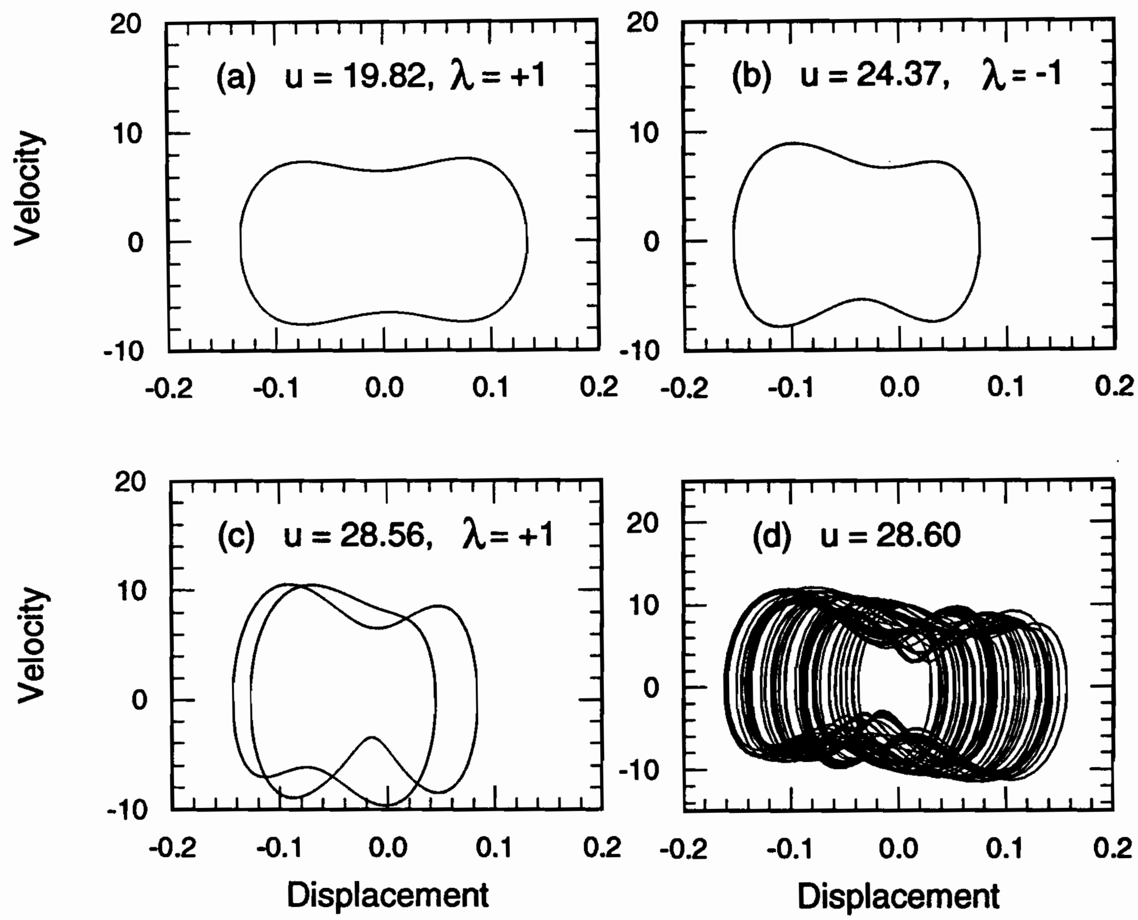

Figure 6.3: Phase portraits representing (a) the symmetric limit cycle before the pitchfork instability ($\lambda = +1$), (b) the asymmetric limit cycle before period–doubling ($\lambda = -1$), (c) the period–two motion before intermittency ($\lambda = +1$), (d) chaotic oscillations; $\Gamma = -0.3$ (from Semler & Païdoussis 1995; permission granted by the American Society of Mechanical Engineers).

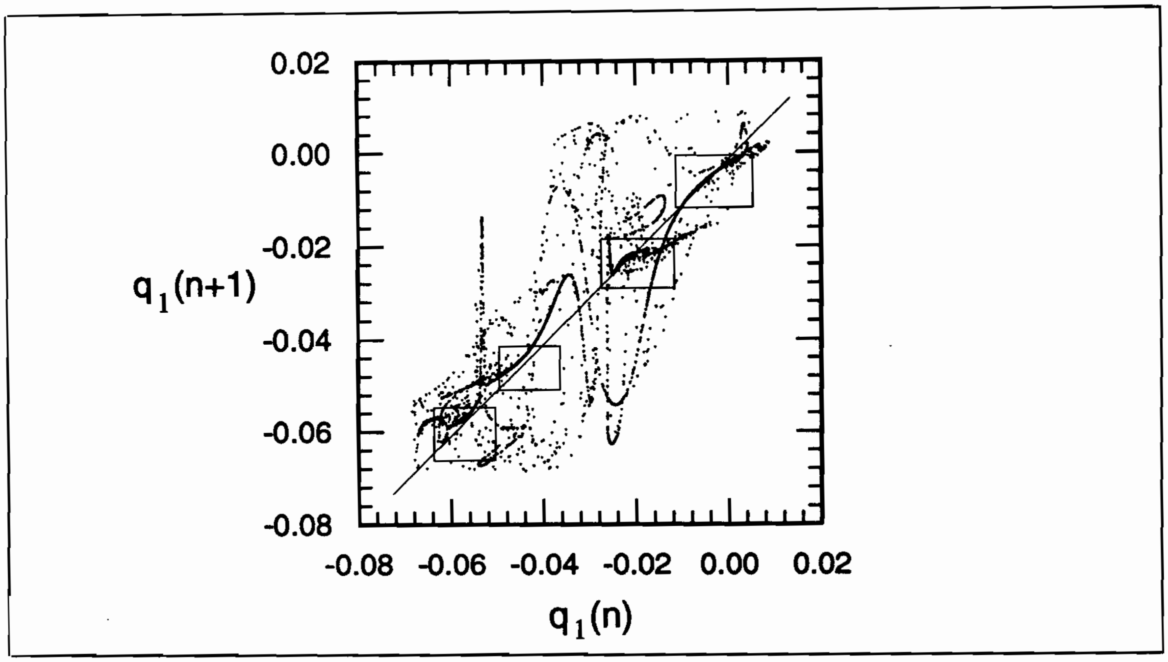

Figure 6.4: One–dimensional return map of successive maxima of the q_1 coordinate, demonstrating the existence of four channels in the neighbourhood of the identity line $y = x$; $u = 28.6$, $\Gamma = -0.3$, $20 \leq \tau \leq 1\,000$ (from Semler & Païdoussis 1995; permission granted by the American Society of Mechanical Engineers).

Bergé *et al.* (1984) have studied type I intermittency in detail, by constructing a "generic form" representing a function f on a Poincaré map, which describes the dynamics of the problem

$$y_{n+1} = f(y_n) = y_n + \mu + \alpha y_n^2. \tag{6.17}$$

If $\mu \equiv u - u_{int} < 0$ (u_{int} represents the flow velocity at which intermittency occurs), equation (6.17) has two fixed points: one stable, the other unstable. When $\mu > 0$, these fixed points disappear: the system defined by (6.17) undergoes a saddle–node bifurcation at $\mu = 0$.

The bifurcation diagram shown in Figure 6.5 has been obtained by using AUTO; it is a plot of the period of oscillation T as a function of u. The pitchfork bifurcation is indicated by P and the period–doubling bifurcation, clearly detected by the jump in the period of oscillation, by PD. Of more interest is what happens in the neighbourhood of the limit point — or turning point — LP; the same qualitative behaviour as that given by (6.17) is observed: for $u < u_{int} = 28.56$, one stable and one unstable limit cycles coexist, and for $u > u_{int}$, they have both disappeared, indicating the occurrence of a saddle–node bifurcation at $u = u_{int}$.

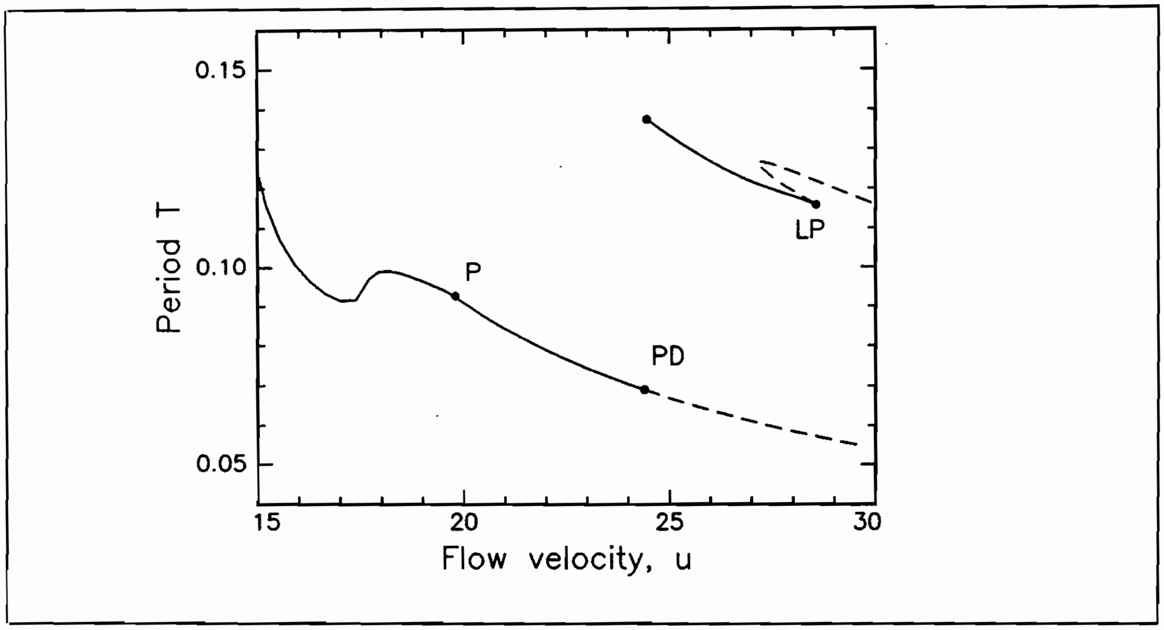

Figure 6.5: Bifurcation diagram obtained by AUTO showing the period of oscillation as a function of the dimensionless flow velocity, u. Dotted lines represent unstable limit cycles and full lines stable ones. The letters P and PD refer to pitchfork and period–doubling bifurcations, and LP to limit point (from Semler & Païdoussis 1995; permission granted by the American Society of Mechanical Engineers).

Therefore, the dynamics given by (6.17) is the same as in the eight-dimensional system. Moreover, the difference equation can be approximated by a differential equation, and it can be shown that the Lyapunov exponent varies like $\mu^{\frac{1}{2}} = \sqrt{u - u_{int}}$, while the period between bursts is given by $T \sim 1/\sqrt{u - u_{int}}$ (Manneville & Pomeau 1980). This is nicely demonstrated in Figure 6.6, obtained by numerically integrating the equation of motion: the maximum Lyapunov exponent has been computed [the procedure for calculating this exponent may be found in Moon (1992), for example], and the period between two bursts can also be found, for several values of u. Qualitative agreement between the generic form and the complete equations is excellent.

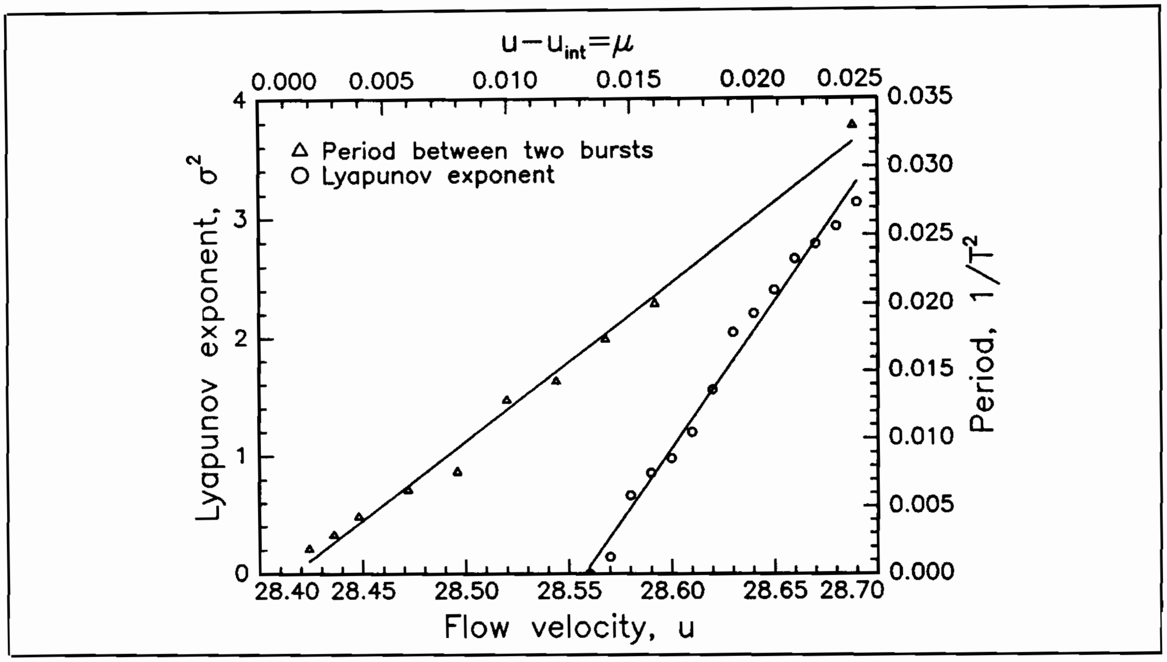

Figure 6.6: Lyapunov exponent σ, squared, as a function of the flow velocity u, and the period between two bursts as a function of $\mu = u - u_{int}$ (from Semler & Païdoussis 1995; permission granted by the American Society of Mechanical Engineers).

It was also attempted to obtain *quantitative* agreement between the period obtained for the normal form (6.17) and the period computed numerically, without success. Three reasons for this may be put forward: (i) the period found from (6.17) represents the longest duration between two bursts due to the randomness in the reinjection process (Manneville & Pomeau 1980), while only a few periods were tracked from the direct numerical integration, (ii) the normal form predicts a distribution of periods between bursts, and not a unique period (Bergé *et al.* 1984); the normal form describes only the local dynamics; whereas one also needs global information about how the orbits are reinjected into the channels to obtain a quantitative agreement; and (iii) it is believed that equation (6.17) is only a "trace" of the normal form. Indeed, as can be seen from Figure 6.4, the coefficient α (introduced in (6.17) and representing the curvature of the parabola) for the four curves is not the same. This is due to the fact that the q_1 direction used to compute the return map is not the centre manifold before the onset of intermittency. Therefore, the Poincaré section used is not perpendicular to the centre manifold, so that the trace obtained on Figure 6.4 represents a projection of the normal form rather than the normal form itself. Finding this centre manifold is not an obvious task — especially for an eight–dimensional system — and it would be a challenging task to solve the problem of a more simple "analytical" set of equations.

6.3.4 Conclusion for the case $\Gamma < 0$

The results presented confirm, for planar motions also, Copeland and Moon's (1992) finding for three–dimensional motions that for $\Gamma = 0$ no chaotic motion occurs — indeed, no major qualitative change in the dynamics beyond the Hopf bifurcation. If $\Gamma < 0$ (end–mass defect), however, it is the principal finding of this study that chaotic oscillations do become possible, even for planar motions. Furthermore, it is shown that the route to chaos is via type I intermittency (Bergé *et al.* 1984). This route to chaos was illustrated for $\Gamma = -0.3$, but the same results were also obtained for $\beta = 0.15$ and $\Gamma = -0.085$ that can be achieved easily in experiments. Nevertheless, the velocities for which chaotic oscillations are then found are much higher, $u \sim 60$.

In order to examine the robustness of the dynamics obtained, all *nonlinear* terms associated with Γ were neglected, as it has been assumed that $\Gamma = \mathcal{O}(q_k q_l)$; these terms are due to gravity, and hence may easily be put to zero by taking $\gamma = 0$. No qualitative change in the dynamics was observed, namely the route to chaos via intermittency was still the same. It is believed that post–Hopf–bifurcation dynamics is mostly influenced by the nonlinear inertial term γ_{ilkj}, which appears directly in the transformation of α_{ijkl} and β_{ijkl} in equation (6.14).

6.4 THE CASE OF A POSITIVE END-MASS§

In this section, the more realistic case of a positive end-mass is examined theoretically and experimentally. The description of the apparatus is given first, followed by the most interesting and representative results, which are then compared with those obtained numerically.

6.4.1 Experimental investigation

6.4.1.1 Apparatus and procedure

Various experiments are conducted with five silicone rubber pipes of different characteristics, and with eight masses, their geometrical and physical characteristics being summarized in the Tables 6.1 and 6.2. The masses are made of plastic, aluminum or brass to vary the end-weight while keeping uniform dimensions. The pipes are cast from liquid silicone rubber and catalyzed to elastic solid in specially prepared moulds to insure uniformity and straightness. The detailed procedure and the instructions for the construction of the pipes can be found in Appendix H. In all experiments, the pipes are hung vertically downwards.

End-mass	#1	#2	#3	#4	#5	#6	#7	#8
Mass (g)	2.4	2.7	3.9	9.2	19.3	22.9	33.9	37.8
Material	plastic	plastic	plastic	aluminum	brass	brass	brass	brass

Table 6.1: Physical properties of the end-masses

The experimental apparatus is similar to that used previously by Païdoussis & Issid (1976) with some modifications: (i) the flow is supplied from recirculating pumped

§It is based on the main parts of the article by Païdoussis & Semler 1996 Nonlinear dynamics of a fluid-conveying cantilevered pipe with a small mass attached at the free end. Submitted to the *International Journal of Non-Linear Mechanics.*

Pipe number	1	3	4	5	6
Particularity	-	-	Thin rubber at the free end	Rubber ring at the free end (1.17 g)	Thin metal ring inside the pipe (1 g)
Length L (cm)	46.1	44.7	46.7	47	45.5
Total mass (g)	87.3	85	88.1	90.1	82.7
Rigidity EI (10^{-3} Nm^2)	8.7	8.24	10.54	10.30	8.65
Int. diameter (mm)	5.8	6.4	6.5	6.3	6.5
Ext. diameter (mm)	15.6	15.9	15.6	15.7	15.8
Mass m (kg/m)	0.189	0.190	0.188	0.191	0.192
Mass M (kg/m)	0.027	0.033	0.034	0.032	0.034
Mass parameter β	0.125	0.143	0.152	0.142	0.150
Gravity parameter γ	20.8	20.2	17.8	18.9	20.5
Frequency f_1 (Hz)	1.07	1.05	1.01	1.03	1.06
Second mode f_2	4.04	3.91	3.90	3.75	4.02
Third mode f_3	10.25	9.95	9.58	9.45	10.21
Log. decrement δ_1	0.04	0.035	0.039	0.037	0.04
In second mode δ_2	0.12	0.13	0.12	0.11	0.12
In third mode δ_3	0.16	0.19	0.20	0.16	0.20

Table 6.2: Physical properties of the pipes

water passing through an accumulator tank with an air cushion to attenuate pulsations from the pump and with piping geometry chosen to achieve straight and uniform flow at the pipe inlet; (ii) the mass-flow rate is measured with an Omega FMG-700 magnetic flowmeter connected to an Omega DPF60 ratemeter, enabling fast and accurate readings. The calibration is made by measuring the time necessary to collect a certain amount of water in the collecting tank resting on weighing scales (in general, the flow was found to be very steady); (iii) the displacement of a point along the length of the pipe is measured with an optical tracking system (Optron 806a), and the signal analysed by a FFT analyzer or stored on disk via a Nicolet 310 digital oscilloscope. The tracking system allows measurements of the horizontal displacement of the pipe without contacting it, thereby not loading or changing its dynamics in any way.

In a given test, a single end-weight is selected and the flow rate is slowly (quasi-statically) increased from zero, through flutter and post-flutter bifurcations, until (i) the motion is no longer planar, or (ii) the amplitudes become so large that the pipe impacts on the collecting tank. More specifically, the procedure is as follows:

(a) fix a mass at the free end and start the pump at low flow-rate;

(b) check that there are no air bubbles in the piping, and, if there are, to vent them;

(c) increase the flow-rate until the onset of the Hopf bifurcation where the pipe begins to oscillate; both critical flow-rate Q_c and frequency of oscillation f_c are recorded;

(d) increase the flow-rate further and note, if it occurs, the second bifurcation value Q_s for which the qualitative behaviour of the pipe changes;

(e) repeat steps 1 to 4 with an other mass.

In the course of the experiment, it appeared necessary to make two further modifications to improve the apparatus. The first became necessary when it was noticed that the motion of the pipes was fairly planar when the masses used were light, even without the moulded strip, but not so in some cases, especially for high flow-rates and the heaviest end-masses. In such cases, the pipe had to be laterally restrained between two parallel flat plates to ensure perfectly planar motion; the clearance was typically 1 mm. The plates did not affect the dynamics since the results obtained with and without them were consistent. Futhermore, it was found that the end-masses had the tendency to deform the end section of the pipe, affecting strongly the fluid velocity at the outlet; consequently, the critical flow velocity Q_c tended to decrease when the masses were tightened more firmly. To solve this problem, a second modification was introduced, namely to alter slightly the end of the pipe so that it does not deform, either (a) by moulding a small rubber ring at the free end, on which the masses were set and tightened only to an interference fit, as for pipes 4 and 5, or (b) by inserting a thin metallic ring at the end of the pipe, having a diameter equal to the internal diameter of the pipe, so that the masses could be tightened without deforming the end-section (pipe 6). The two configurations are depicted schematically in Figure 6.7 and in both cases, the additional mass is taken into account.

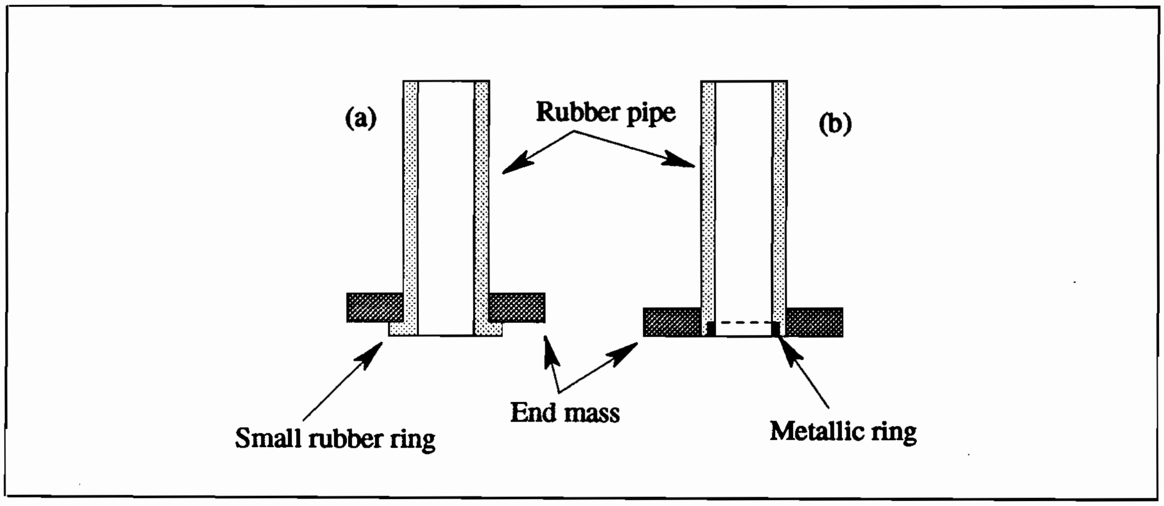

Figure 6.7: Modification of the pipe at the outlet: (a) by moulding of a small external rubber ring (pipes 4 and 5); (b) by inserting a thin metallic ring (pipe 6).

6.4.1.2 General observations

Globally, because the pipes have similar characteristics, the behaviour of the system is similar for most of the pipes and end-masses. Two distinct bifurcations are generally observed: first, a Hopf bifurcation leading to single degree-of-freedom flutter (or oscillations in the second mode), followed, at higher flow rates, by a second bifurcation for which a change in the dynamics is detected. These two bifurcations can be described in more detail as follows.

(i) Hopf bifurcation

Increasing the flow from zero, the effective damping of the system first increases gradually, as ascertained by perturbing the system with a small push. Continuing to increase the flow-rate further, the effective damping begins to decrease precipitously, to the point where it becomes negative, leading therefore to a Hopf bifurcation. For this critical value of the flow-rate Q_c, the pipe begins to oscillate in a plane in its second mode at the critical frequency, denoted by f_c. This phenomenon is well-known and has been observed previously by many researchers, e.g. Benjamin (1961) and Gregory & Païdoussis (1966).

(ii) Second bifurcation and chaotic motion

As the flow-rate is increased further, the fundamental frequency of the response increases slightly, to a point where a change in behaviour is observed. Depending on the mass at the free end, two distinct phenomena occur, as follows.

(a) With the heaviest masses (#4 to #8 in Table 6.1) and for a certain flow-rate, denoted by Q_s, the frequency of oscillation suddenly increases. From an initial frequency approximately equal to 2.5 Hz, the frequency jumps to a value around 4.5 Hz. The change is sudden and appears for Q_s approximately equal to 0.27 kg/s. As the flow-rate is increased further, this frequency increases gradually, until the pipe leaves its plane of oscillation and the motion becomes chaotic, with the pipe hitting the collecting tank.

(b) With the lighter masses (#1 to #3), the change is not so easy to pin-point but for approximately the same values of Q_s, the motion of the upper part of the pipe, of length estimated as $L/4$, becomes very different from that of the lower end: the upper part oscillates with a small amplitude and a lower frequency than the lower part, and there exists a point between the two regions that seems more or less immobile. This is assessed on the analyzer by the presence of a small peak of frequency approximately equal to half the main frequency. With increasing flow-rate, this second frequency decreases slightly while the main frequency increases; the ratio of the two, therefore, is not constant. Again, for higher flow-rates ($Q > 0.35$ kg/s), the pipe leaves the plane of oscillation, impacts on the collecting tank, and the motion becomes chaotic.

The following additional observations were made.

1. Even with the metal strip inside the pipe, for high enough flow-rates, the pipe left its plane of oscillation and the response became chaotic, provided that an end-mass was used. Because of the violence of the motion, the pipe was damaged after a very short period of time, which explains why it was preferred to consider only small masses or to add the two lateral plates in some cases.

2. In one case (pipe 1 and end-mass #3), a series of period doubling bifurcations leading to chaos was observed, instead of the motion becoming chaotic after hitting the tank or becoming non-planar. For $Q = 0.354$ kg/s, the pipe frequency was equal to 5.18 Hz and the response slightly modulated. Then, for $Q = 0.355$ kg/s, the period of the motion doubled. Increasing the flow-rate further, another period doubling bifurcation appeared but was too brief to be recorded, the motion then becoming chaotic.

3. The behaviour of the pipe without any mass (but with the small rubber ring as in Figure 6.7(a) installed) was slightly different: after the second bifurcation, the frequency of the motion increased with increasing the flow-rate up to the maximum value allowed by the pump, but the motion did not become chaotic. It is however possible that the motion *might* have become chaotic if higher flow-rates had been possible.

For all these reasons, it was not possible to analyse properly how and why chaotic oscillations suddenly emerged, and it was equally difficult to study the dynamics after the second instability, again because of the violence of the motion.

6.4.1.3 Quantitative results

In this section, the two bifurcations described previously are examined from a quantitative point of view.

(i) Critical flow velocity (Hopf bifurcation)

As shown in Figure 6.8, the added mass has a strong effect on critical flow-rate, Q_c. For the range of masses tested, Q_c is always smaller than the value without any mass. For $0 < \Gamma < 0.4$, where Γ is the nondimensional end weight, Q_c decreases when Γ increases, which is consistent with the results obtained by Hill & Swanson (1970).

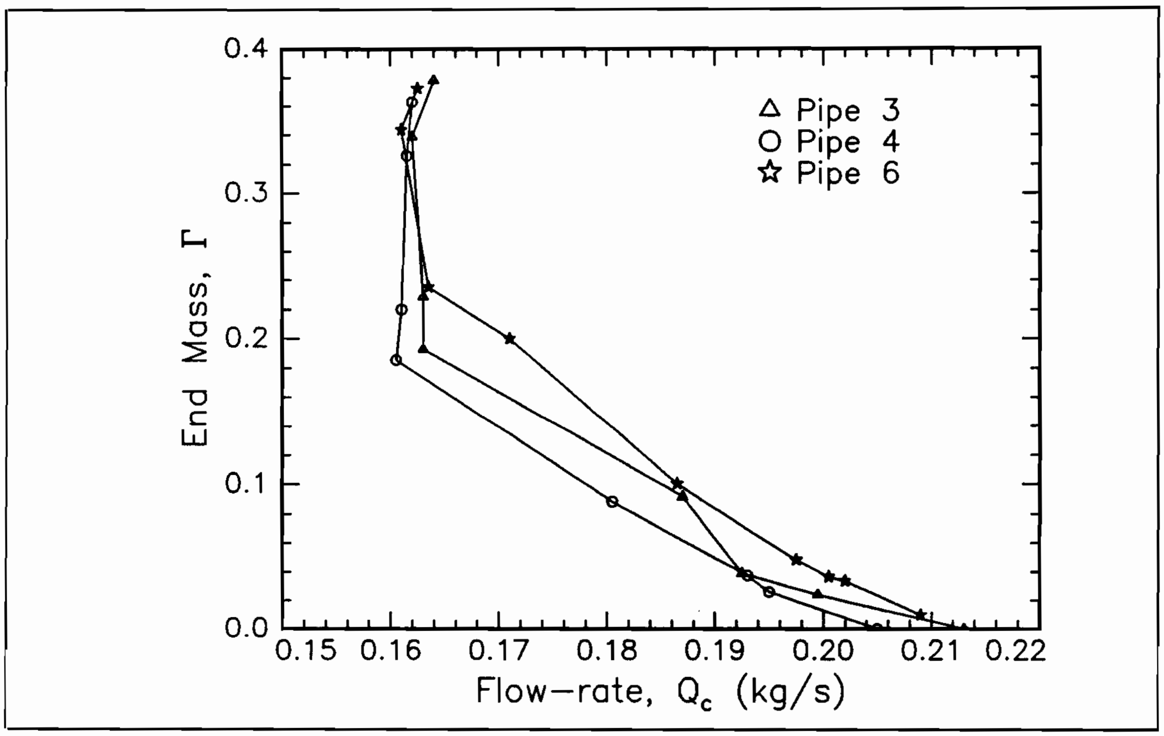

Figure 6.8: Experimental critical flow-rate Q_c for different pipes and end-masses.

These results are also consistent with the results by Copeland & Moon (1992), even though the values of Γ used here are much smaller. In fact, they correspond to the lower portion of the curve found by Copeland & Moon (1992), where, indeed, the end-mass has a *destabilizing* effect. In a sense, however, the results presented here contradict one of Copeland & Moon remarks, namely that "there is apparently not a smooth transition to the cantilever case"; as shown in Figure 6.8, this transition could have been observed by choosing smaller increments in the values of Γ.

The uncertainties in Q_c are due to two factors: (i) a fluctuation of the reading displayed by the ratemeter, estimated to be ± 0.0005 kg/s, and, (ii) the difficulty to determine *objectively* the flow-rate at which the pipe begins to oscillate. This uncertainty is approximately equal to 0.0010 kg/s. Figure 6.9 shows the critical flow-rate in nondimensional form for pipe 5, together with the error bars, when the flow is increased. As can be seen, the difference is of the order of 10%, which means that good agreement is achieved between experiments and theory predicted by a linear model. The discrepancy is mainly due to the difficulty in representing accurately the damping in the system. Figure 6.9 also shows the critical value when the flow is decreased, i.e. corresponding to the *restabilization* of the pipe. The value of Q_c is not exactly the same as when the flow is increased, and the differences increase with the end-mass Γ. However, for the lightest end-masses, this difference is of the same order as the uncertainties. It is difficult to say if this is due to a hysteresis phenomenon (itself due to a *subcritical Hopf bifurcation*); however, these observations are consistent with (i) the observations made by Copeland & Moon (1992), and (ii) with the fact that immediately after the Hopf bifurcation, the amplitudes of the oscillations were never small when increasing the flow-rate.

For the range of the masses considered, the critical frequency of the pipes f_c does not vary regularly with Γ, and is approximately constant for most of the pipes ($f_c \simeq 2.4$ Hz), which explains why it is not shown here.

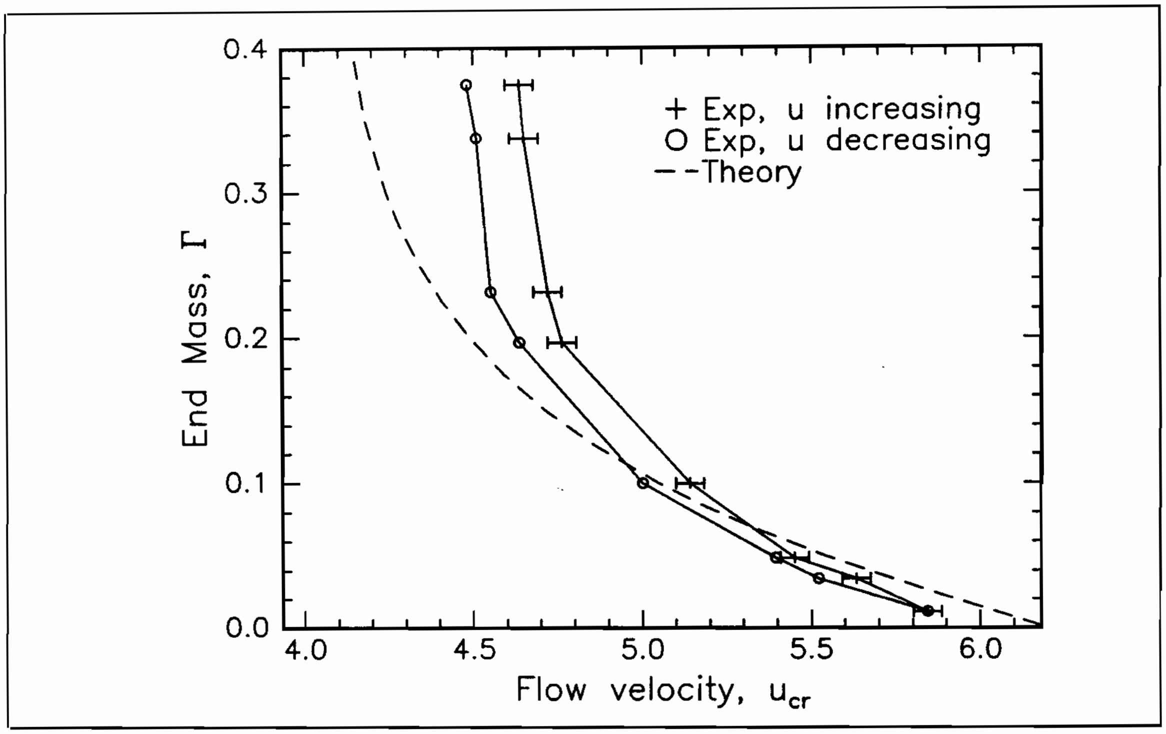

Figure 6.9: Theoretical and experimental nondimensional critical flow velocity, u_{cr}, for different masses: – –, linear theory; +, experiments, for increasing u; o experiments, for decreasing u. Horizontal bars correspond to the maximum error.

(ii) Post-critical behaviour

As mentioned in Section 6.4.1.2, a second bifurcation is observed when increasing the flow-rate beyond the first instability. The frequency of oscillation is recorded before and immediately after this second bifurcation, as well as the corresponding flow-rate Q_s. The results for pipe 5 are shown in Figure 6.10(a) for the nondimensional flow velocities, while the frequencies are presented in Figure 6.10(b). The experimental results for both the first instability (first Hopf bifurcation) and to the second bifurcation are shown. Theoretical results based on linear stability analysis are also given, to determine where this second bifurcation may come from. It is found that, after the first Hopf bifurcation, *two* additional Hopf bifurcations are detected, for $\Gamma \geq 0.087$, one corresponding to an

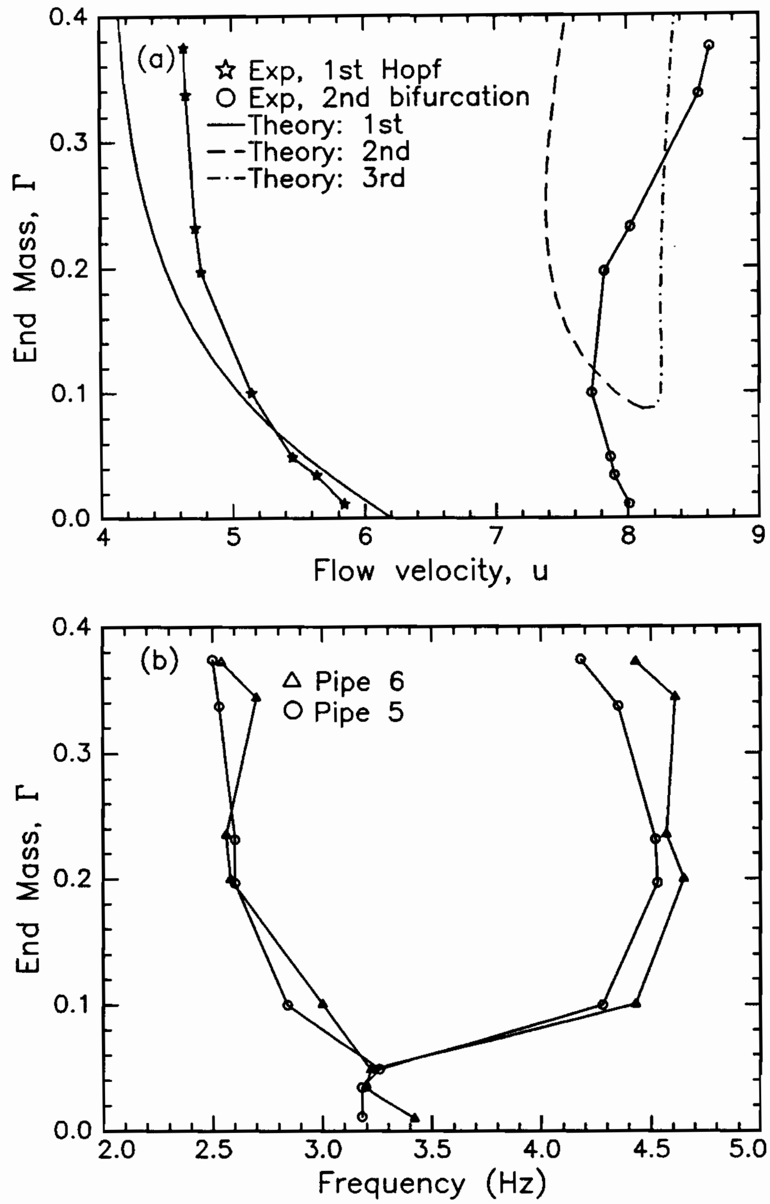

Figure 6.10: (a) Experimental flow velocities corresponding to the two bifurcations and theoretical Hopf bifurcation points for pipe 5; (b) dominant experimental frequencies before and after the second bifurcation.

instability in the third mode and the other to a *restabilization* in the same mode. The values of u for these two bifurcations are shown on the right-side of Figure 6.10(a) and lead to following remarks: (a) these values are indeed relatively close to the values found experimentally, but (b) they do not explain the change of dynamical behaviour observed for values of Γ smaller than 0.087; moreover, (c) caution must be exercised, because the predictions of the linear theory are only valid up to the first instability.

Figure 6.10(b) shows the experimental frequencies for the pipes 5 and 6; the left branch corresponds to the frequency of the pipe before the second bifurcation while the right one to the frequency immediately after. For small values of Γ, only one frequency is given because no jump is observed. As can be seen, there is a similarity in behaviour between the two pipes, and this was also the case for the other ones. The values for the *theoretical* linear frequencies are not shown here because they strongly depend on the nonlinearities and will be discussed in detail in the next section. However, to give an order of magnitude, the linear frequencies before and after the second bifurcation for $\Gamma = 0.3$ are found equal to 2.2 Hz and 5.7 Hz at $u = 7.46$, which are, respectively, 12% below and 26% above the experimental (nonlinear) frequencies.

It is interesting to note that, together the two Figures 6.10(a) and (b) may give an explanation for the difference in behaviour for the cases of Γ below or above 0.08. Indeed, from Figure 6.10(b), the jump in frequency is observed only for $\Gamma > 0.06$, which is close to the theoretical value for which a second Hopf bifurcation is found. It will be seen in the nonlinear analysis that this is not the case.

6.4.2 Theoretical investigation

The dynamics of the system is now investigated from a numerical point of view to gain a better understanding of the dynamical behaviour and to see if the experimental observations can be predicted with our model. Methods of solutions are described very briefly here, and more emphasis is put on the results.

6.4.2.1 Methods of solution

In order to compare the theoretical results with the experiments, equation (6.14) is solved directly, without assuming that the end-mass or the nonlinear inertial terms are small. Consequently, the numerical schemes developed in Chapter 5, the Finite Difference Method (FDM) and the Incremental Harmonic Balance method (IHB), are employed here without further justification since the appropriateness for the task has been discussed previously in detail (see Chapter 5 or Semler *et al.* 1996). What should be mentioned is that the FDM is an "initial-value problem solver", which means that the system of equations is integrated numerically for one initial condition at a time, and is able to reproduce the state of the system thereafter at any time τ. The final steady-state represents a ***stable attractor***, i.e. a physically possible state. On the other hand, the IHB is a "periodic solution continuation-solver", which means that it finds *periodic solutions* of the equation close to a previously known or computed solution. The advantage of the IHB is that both stable or unstable solutions can be computed, and the easy evaluation of the Floquet multipliers helps to explain how new solutions emerge. Unfortunately, it is "blind" to non-periodic solutions, e.g. quasiperiodic or chaotic, so that it is the combination of the two methods that is particularly powerful, as adopted here.

6.4.2.2 Physical parameters

In the results presented here, only two major parameters are varied, namely the flow velocity, u, and the end-mass parameter, Γ, because the physical properties of a given pipe are assumed constant. It will be seen that these two parameters enable us to clarify many questions and that the system exhibits a very diverse bifurcational behaviour. The other parameters correspond to pipe 5 (see Table 6.2), i.e. $\gamma = 18.9, \beta = 0.142$; dissipation is represented by the measured modal damping in the different modes: $\delta_1 = 0.037, \delta_2 = 0.108, \delta_3 = 0.161$; because it could not be obtained experimentally, $\delta_4 = 0.220$ was linearly extrapolated.

6.4.2.3 Results

To simplify the discussion and draw a parallel with the experiments, the distinction is made between the cases Γ smaller or larger than 0.1 (cf. Figure 6.10(a)).

(i) Small values of the end mass, $\Gamma \leq 0.1$

The dynamics of the system is first investigated for small values of Γ using FDM. For a constant end-mass, the flow velocity u is varied and the equation of motion (6.14) integrated for one specific initial condition, yielding bifurcation diagrams of the form of the maximum tip displacement as a function of u (for clarity, the transients representing at least the first 50 cycles are not shown). As in Chapter 4, the number of modes N may be of importance, so that results are presented for both $N = 3$ and 4.

From Figure 6.11(a), it can be seen that in the absence of an end-mass ($\Gamma = 0$), the system performs only limit cycle oscillations, while the dynamics is much richer for $\Gamma = 0.06$, as in Figure 6.11(b). Furthermore, the results are the same from a *qualitative* point of view for both $N = 3$ and 4 and the differences are quantitatively minor.

For $\Gamma = 0$, only two distinct regions may be identified: $u < u_{cr} = 6.15$, where the system is stable, and $u > u_{cr}$, where stable periodic solutions exist. The Hopf bifurcation occurs in the second mode and is supercritical, as ascertained by the facts that (a) no non-zero solutions are found for $u < u_{cr}$ and (b) the amplitude of oscillation after the bifurcation increases as $\sqrt{u - u_{cr}}$. This parabolic increase is observed only up to a flow velocity $u \simeq 9$, and the amplitudes decrease thereafter. As will be seen, this is due to the fact that the frequency of oscillation steadily increases, so that the second mode becomes more and more similar to a "third-mode". The results of Figure 6.11(a) are the same as in the experiments: for $\Gamma = 0$, the pipe performs limit cycle oscillations only, with a frequency increasing with u.

For $\Gamma = 0.06$, four distinct regions may be identified for both $N = 3$ and 4 (critical values are given for $N = 3$ only): the system is stable for $u < u_{cr} = 5.35$, bifurcates into periodic oscillations for $5.35 \leq u \leq 8.2$, performs quasiperiodic motions

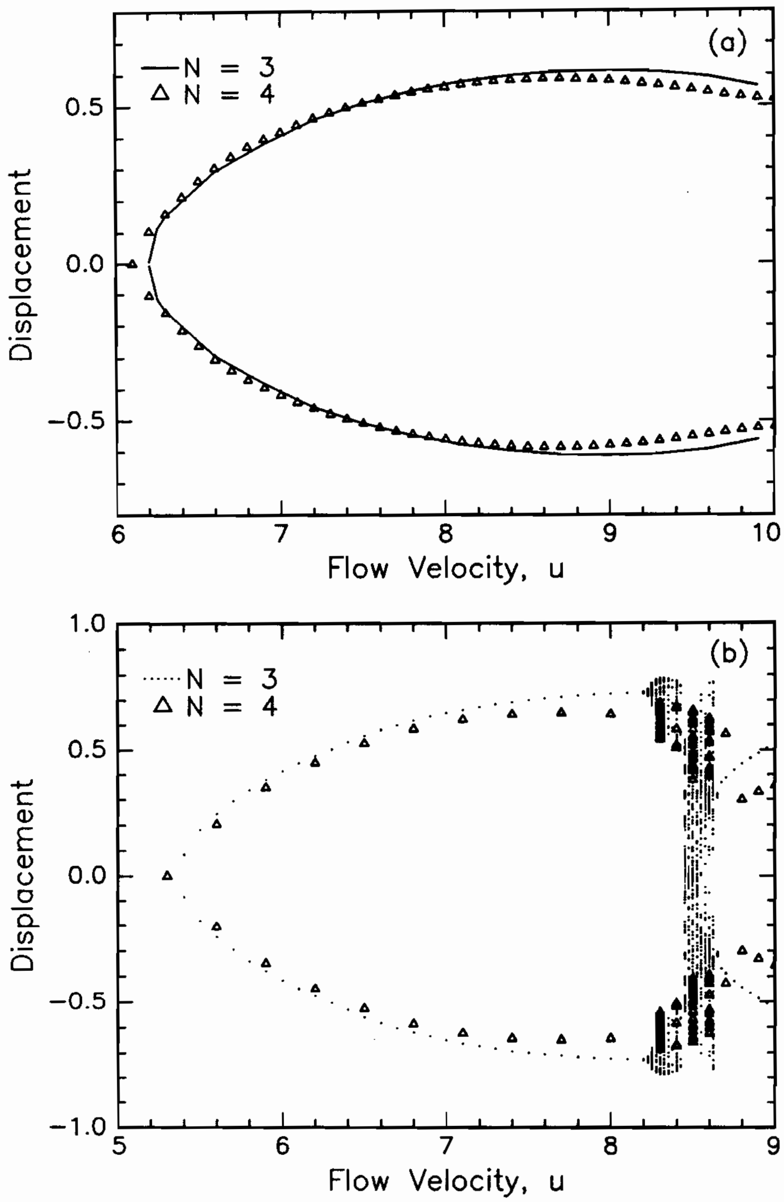

Figure 6.11: Bifurcation diagram for (a) $\Gamma = 0$, and (b) $\Gamma = 0.06$, for $N = 3$ and 4.

for $8.2 < u \leq 8.625$, and then periodic oscillations again, but of smaller amplitude, for $u \geq 8.65$. This evolution bears some resemblance with the behaviour observed experimentally, but there are some obvious discrepancies as well. Comparing the results of Figure 6.10 for $\Gamma = 0.06$ with those of Figure 6.11(b), it can be seen that there is agreement between theory and experiment in the following aspects: (a) the values of u_{cr} for the first Hopf bifurcation are similar ($u_{cr} \simeq 5.3$ in the experiments); (b) the nonlinear model and the experiments both predict a qualitative change in the behaviour of the pipe at a higher flow; and (c) the values of u for the second bifurcation are relatively close ($u_{theory} \simeq 8.2$ versus $u_{exp} \simeq 7.8$). On the other hand, only periodic solutions are predicted in the experiment (before the onset of chaos), while the motion is also found to be quasiperiodic in theory, prior to becoming periodic again. To visualize the type of motion predicted numerically, relevant time traces and power spectra are presented in Figure 6.12 for $\Gamma = 0.06$ and different values of u. It can be seen from Figure 6.12(c) and (d) that the amplitude is much smaller for $u \geq 8.65$ than for $u < 8.2$, mainly because the frequency of oscillation is low for $u = 8.0$ ($f = 3.1$), while it is higher for $u = 8.8$ ($f = 6.5$).

The same pattern, i.e. periodicity $\rightarrow$ quasiperiodicity $\rightarrow$ small amplitude periodicity, is observed for $0.03 \leq \Gamma \leq 0.1$, the upper limit ($\Gamma = 0.1$) being again close to the value found in the experiments, as in Figure 6.10(b). To explain this evolution and the changes in the dynamics, it is instructive to investigate how bifurcations take place in the nonlinear system. Indeed, from the linear point of view, only one Hopf bifurcation is detected, so that new solutions can be found only through a nonlinear analysis. The IHB method is the ideal tool for that: it computes periodic solutions, "follows" them, and determines their stability. The results for different values of Γ are shown in Figure 6.13(a), in terms of the amplitude, and in Figure 6.13(b), in terms of the nondimensional frequency. From the two figures, the following remarks can be made:

(a) for $\Gamma = 0$, the frequency increases dramatically after $u = 9.5$, while the maximum amplitude decreases;

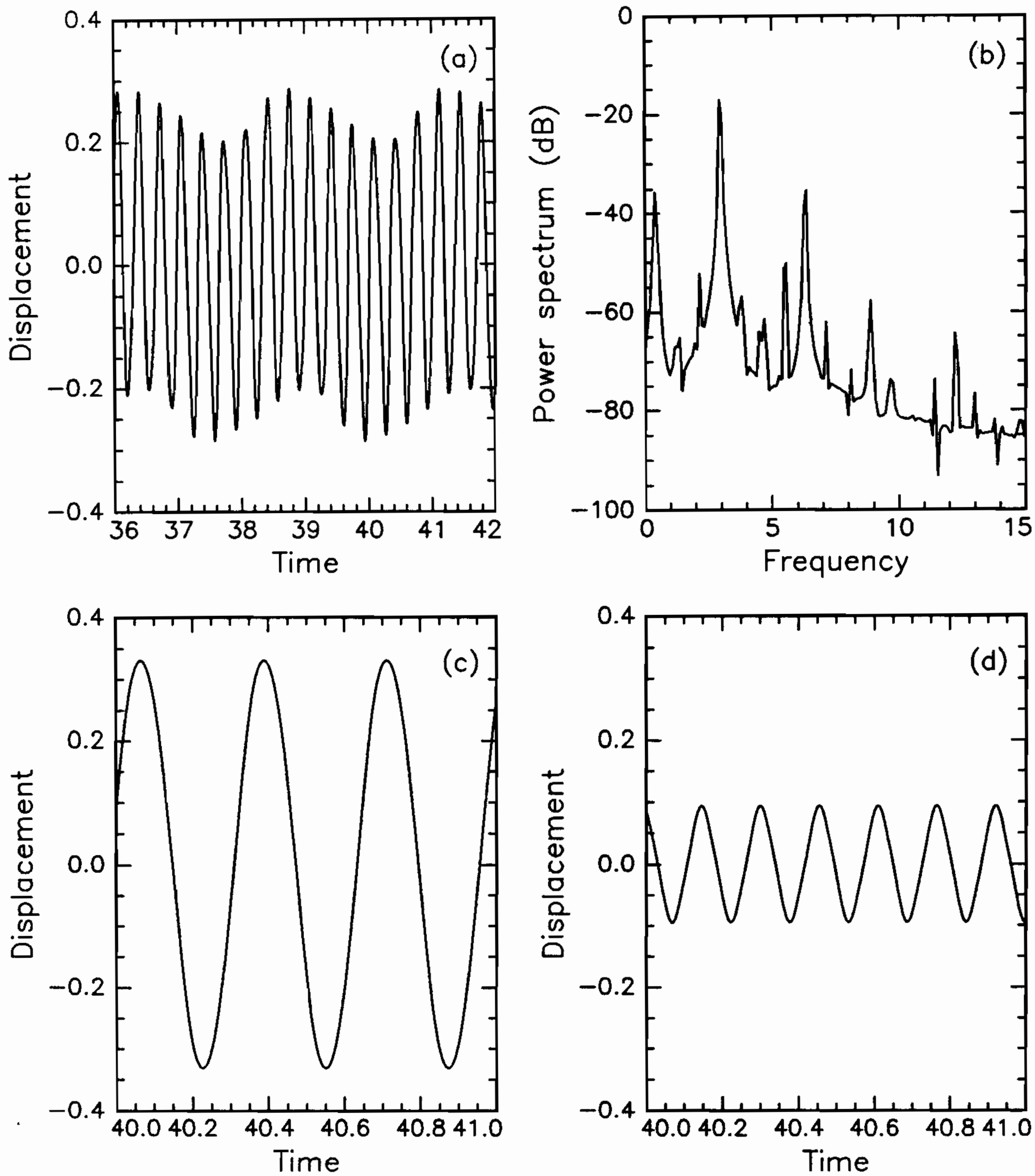

Figure 6.12: Time traces and power spectrum for $\Gamma = 0.06$, $N = 3$ and different values of u: (a) time trace for $u = 8.5$, and (b) the corresponding power spectrum; (c) time trace for $u = 8$, and (d) for $u = 8.8$.

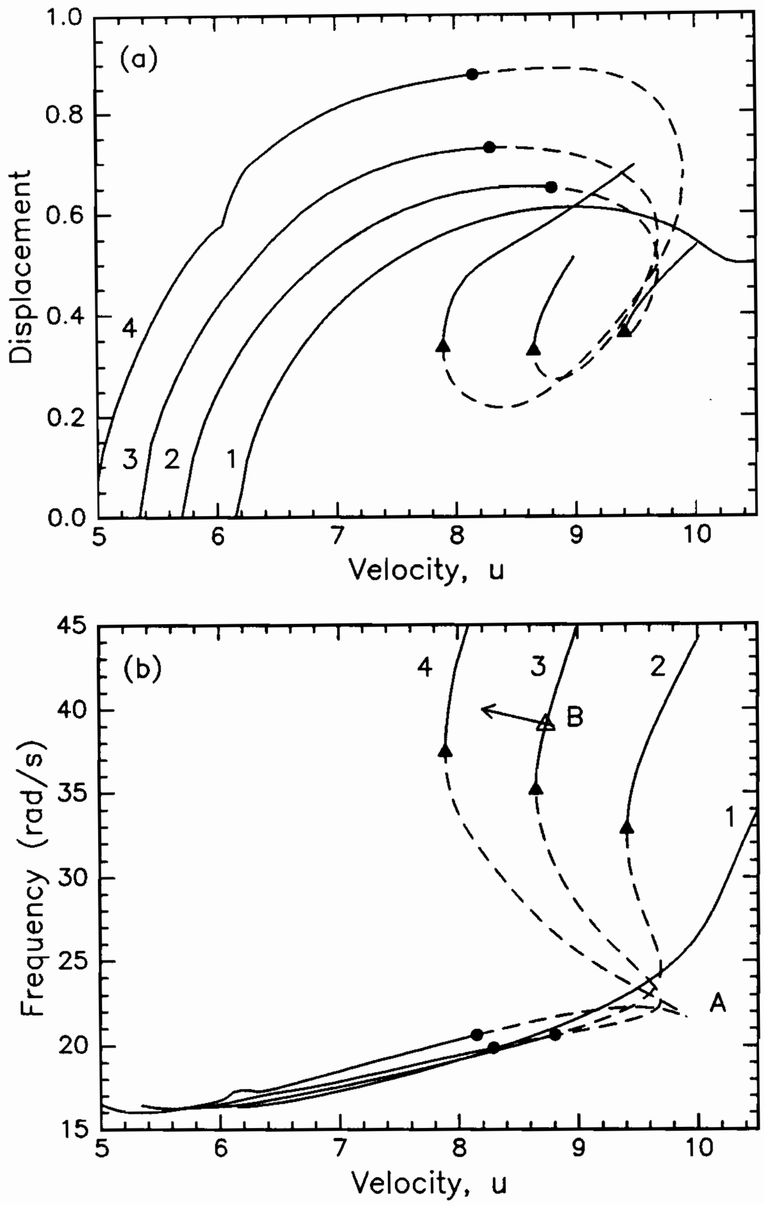

Figure 6.13: Bifurcation diagrams obtained using the IHB method showing (a) the maximum tip displacement, and (b) the circular nondimensional frequency, as a function of u, for different values of Γ and $N = 3$; curve "1" is for $\Gamma = 0$, curve 2 for $\Gamma = 0.03$, curve 3 for $\Gamma = 0.06$ and curve 4 for $\Gamma = 0.1$. The bullet • represents the point of loss of stability, the filled triangle the point of restabilization; point A corresponds to the cusp, and B is an arbitrary point on the stable high frequency solution.

(b) for $\Gamma > 0$, the original stable limit cycle loses stability at the points with a bullet ($\bullet$), a pair of complex conjugate Floquet multipliers crossing the unit circle (the modulus becomes greater than 1), which means that quasiperiodic solutions are possible after the bifurcation point (Bergé *et al.* 1984), in agreement with FDM;

(c) following the unstable solutions, two additional saddle-node bifurcations are detected: the first one corresponding to a limit or turning point, and the second one, represented by the filled triangles at lower values of u, corresponding at the same time to a turning point *and* a restabilization, for which stable periodic oscillations of small amplitude and high frequency appear;

(d) the appearance of the second stable periodic solution explains clearly where the fourth region detected by FDM comes from, and it is obvious that this solution can only be found through a nonlinear analysis;

(e) the value of u of the bifurcation point corresponding to the appearance of stable periodic solutions decreases dramatically with Γ, which means that the range where quasiperiodic oscillations can be detected decreases with Γ, to a point where they no longer exist. This was confirmed using FDM, and for $\Gamma = 0.1$, there exist only a very narrow range of quasiperiodic solutions (see also Figure 5.6 on page 161 or Semler *et al.* 1996);

(f) the case of $\Gamma = 0.1$ can be considered as a limiting case for two distinct reasons: the first one is related to the previous remark, while the second is related to the "jump" observed in Figure 6.13(a) for $u \simeq 6.1$ or the small "hump" in Figure 6.13(b): the evolution of the stable periodic solutions emerging from the Hopf bifurcation is no longer smooth for $\Gamma \geq 0.1$, and new phenomena start to occur;

(g) the case of $\Gamma = 0.1$ is also interesting from a numerical viewpoint: if the IHB method has only the capability to have the frequency incrementation and one parameter incrementation (in this case u), it is not possible to find a new solution at the extreme right limit-point A depicted in Figure 6.13(b), because that saddle-node bifurcation is a cusp if seen in the $(u,\ \Omega)$-plane. However, it can be found by an amplitude incrementation, as in Figure 6.13(a), or by starting at the point B shown in

Figure 6.13(b) and incrementing a second parameter (Γ in this case, and the solution evolves in the direction of the arrow);

(h) it should be mentioned that the results obtained with the IHB method were always confirmed using the FDM, both in terms of amplitude and frequency. Of course, only stable solutions can be found with FDM.

(ii) Higher values of the end mass, $\Gamma > 0.1$

The case where the end mass is greater than $\Gamma = 0.1$ is investigated now. To illustrate remark (h) above, Figure 6.14 shows a comparison between the FDM and the IHB method for $\Gamma = 0.15$. As can be seen, there is an excellent agreement between the two methods. Again, the IHB method helps to explain the jump in amplitude occurring around $u \simeq 6$ and the appearance of small amplitude periodic oscillations at $u = 7.6$ (which exist in fact for $u \geq 7.26$).

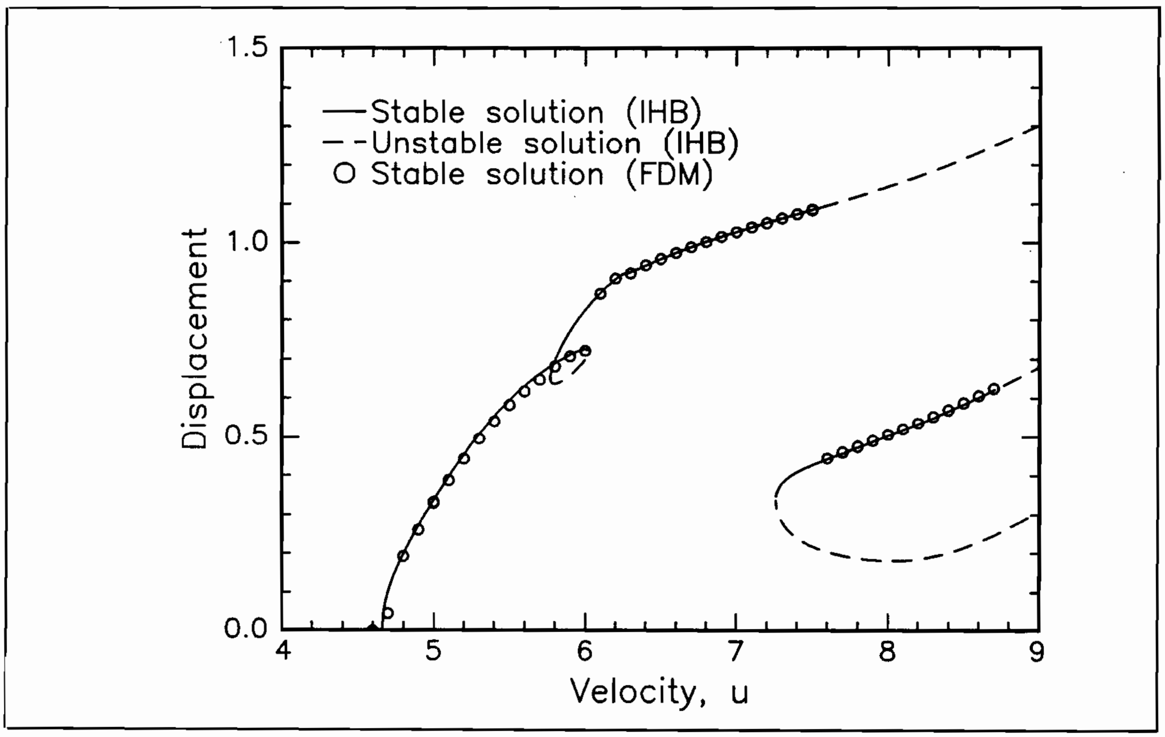

Figure 6.14: Bifurcation diagram obtained using the IHB method (—, stable periodic solution; – –, unstable periodic solution) and using FDM (o); $\Gamma = 0.15$ and $N = 3$.

Unstable solutions emerging at $u = 7.54$ exist up to a value of $u = 11.69$ which is out of the scale of the figure. Furthermore, although the system is always unstable in this big loop, the number of Floquet multipliers inside the unit circle varies several times ($4 \to 5 \to 3 \to 5 \to 6$). These bifurcations are not of great importance because the system is unstable in any case. Of more interest is the bifurcation occurring at the small-amplitude stable periodic solution at $u = 8.76$: increasing the flow velocity further, the stable solution becomes unstable, again because two complex conjugate multipliers cross the unit circle, but the solution thereafter is not quasiperiodic but chaotic, as shown in Figure 6.15.

Consequently, from a physical viewpoint, four distinct types of solutions may be observed: (i) solutions converging to the stable equilibrium for $u \leq 4.66$; (ii) periodic solutions whose frequency increases with u for $4.66 < u < 7.54$; (iii) periodic solutions of higher frequency and smaller amplitudes for $7.26 < u < 8.76$ (implying a jump in the response); and (iv) chaotic oscillations for $u > 8.76$. This is exactly what is observed in the experiment. As shown in Table 6.3, the quantitative comparison between theory and experiment is relatively good in terms of flow velocity and frequency before the "jump", but not in terms of the frequency after the jump. Nevertheless, there are enough similarities to have confidence in the results.

	Values of u		Values of f	
	Exp't	Theory	Exp't	Theory
Hopf bifurcation	4.8	4.66	2.3	2.6
Second bifurcation	7.6	7.26	$2.8 \to 4.5$	$3.0 \to 6.3$
Chaos	$\simeq 8$	8.76	—	—

Table 6.3: Comparison between theory and experiment of the flow velocity and the frequency of the pipe corresponding to the three bifurcations; the arrow represents the jump in frequency.

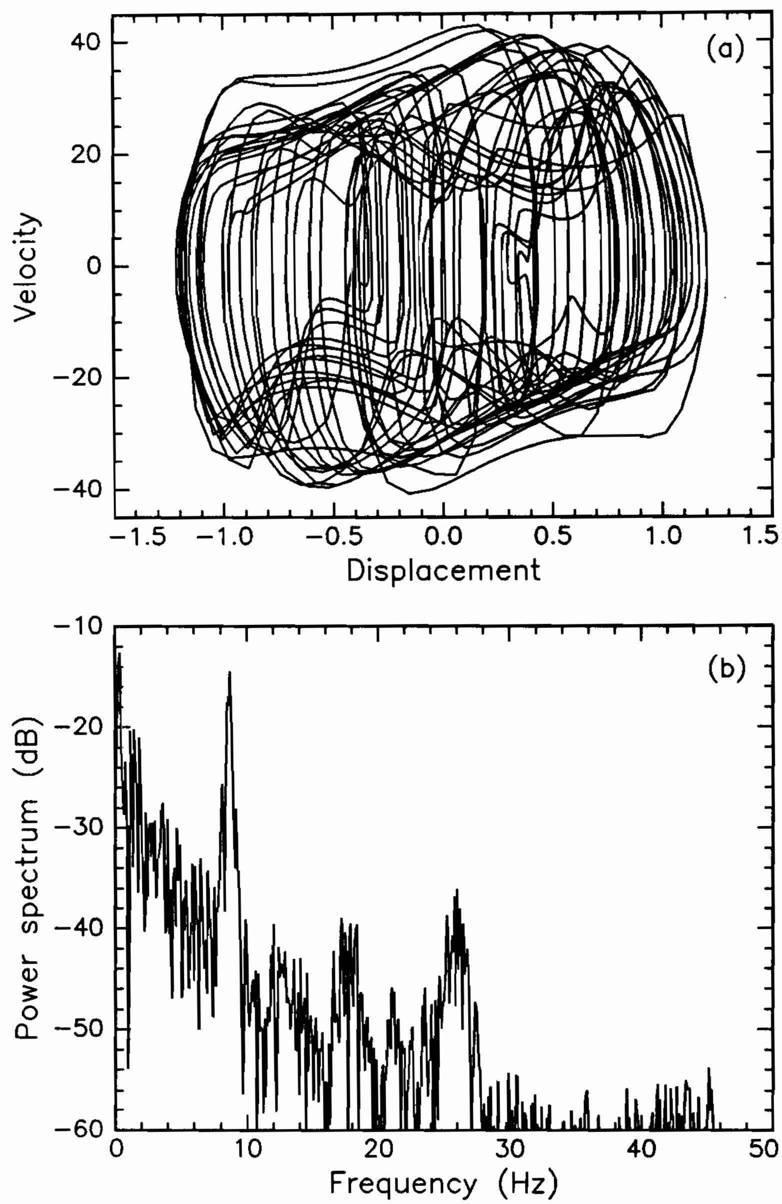

Figure 6.15: Phase-plane plot and corresponding power spectrum illustrating chaotic oscillations for $u = 8.8$, $\Gamma = 0.15$ and $N = 3$.

If the value of the end-mass Γ is increased further, the results obtained numerically are qualitatively similar to those for $\Gamma = 0.15$, except that the number of "humps" increases, which means that the number of bifurcations in the system increases as well. Alas, from a quantitative point of view, the agreement between theory and experiment becomes worse, since the values of u for the second bifurcation (followed almost immediately by chaotic oscillations) increase in the experiment (Figure 6.10), while they decrease in theory (see Table 6.4). Before giving reasons for that, the effects of the nonlinear inertial terms on the dynamics are first investigated; these terms have been included in the analysis so far.

	u_{exp}	u_{theory}	
		$N = 3$	$N = 4$
$\Gamma = 0.2$	8.0	6.9	6.5
$\Gamma = 0.3$	8.2	6.0	5.9
$\Gamma = 0.4$	8.6	6.0	5.9

Table 6.4: Flow velocity corresponding to the appearance of chaotic oscillation: comparison between theory and experiment.

For that purpose, the equation of motion (6.14) is integrated numerically for $\Gamma = 0.2$ with FDM, assuming $\gamma_{ijkl} = 0$. To validate the results and to explain the emergence of chaotic oscillations, AUTO is used in parallel to construct bifurcation diagrams, since it becomes applicable if these assumptions are made. The full results obtained by AUTO are shown in Figure 6.16(a), while the results obtained by FDM, together with the "main" branch computed by AUTO are presented in Figure 6.16(b). From the first figure, it can be seen that the original periodic solution loses stability through a subcritical pitchfork bifurcation at $u = 8.6$ (marked by the bullet $\bullet$) prior

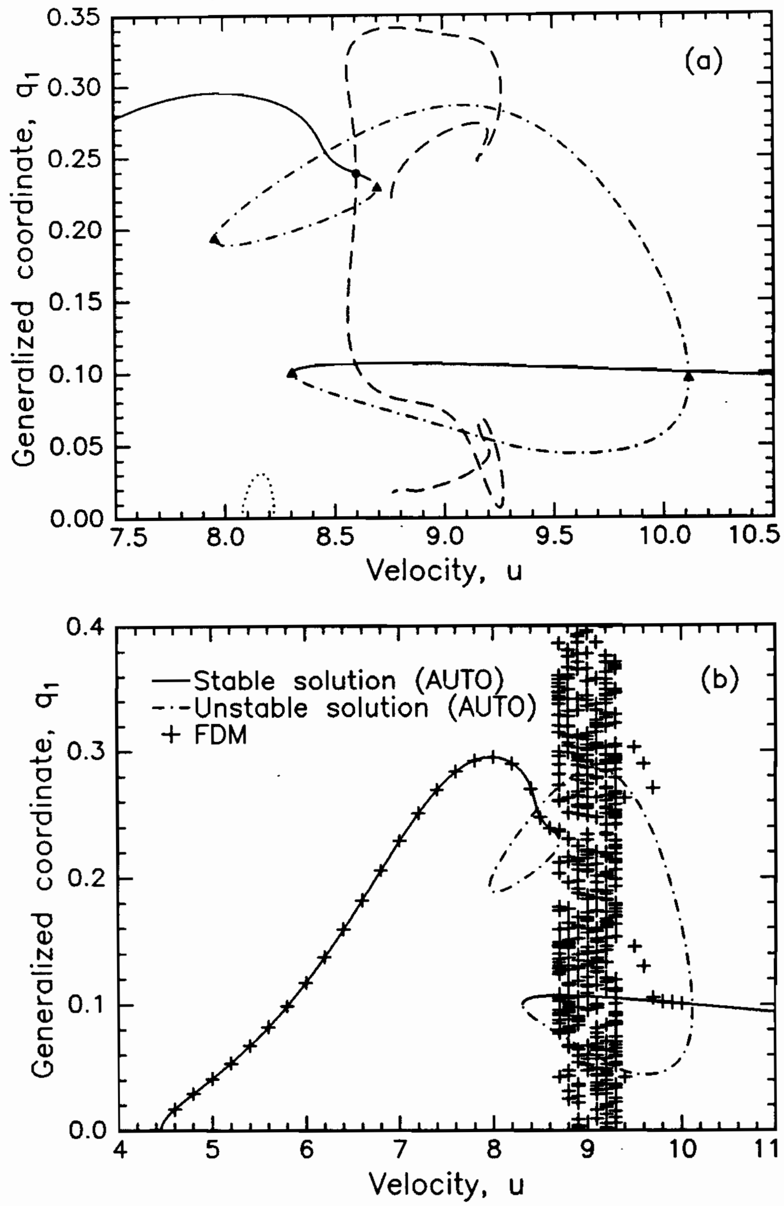

Figure 6.16: Bifurcation diagrams for $\Gamma = 0.2$ and $N = 3$ showing the maximum generalized coordinate q_1 as a function of u: (a) stable (—) and unstable periodic solutions found using AUTO (—·— represents the main branch; – – the branch emerging from the bifurcation point •, and ··· the branch connecting the two Hopf bifurcation points, amplified by a factor 20); (b) only the main branch computed using AUTO is shown, together with the results obtained with FDM (+). The filled triangles represent the limit points on the main branch.

to the saddle-node bifurcation occurring at $u = 8.7$ (filled triangle). This means that the solution after $u = 8.6$ becomes unstable and that two unstable periodic solutions emerge at the bifurcation point. Following the original solution after the saddle-node bifurcation, three additional limit points are encountered (represented again by filled triangles), the first one at $u = 7.96$, the second at $u = 10.11$ and the third at $u = 8.3$. This last bifurcation point, as in previous cases, corresponds to a restabilization of the periodic solution and the appearance of stable limit cycles of small amplitude and high frequency. This means that the same qualitative results are obtained when the nonlinear inertial terms are neglected or ignored.

On the other hand, the results obtained by FDM indicate that not only periodic solutions exist, but also chaotic ones, in the flow range $8.6 \leq u \leq 9.3$. Consequently, although stable periodic solutions exist for all flow velocities, as demonstrated in Figure 6.16(a), there is a large range of velocity for which these stable periodic solutions are not able to attract the trajectory. This is due to the fact that in the same range, many *unstable* or *repelling* periodic solutions are present, on which the trajectory may "bounce". Some of those unstable attractors emerging from the subcritical pitchfork bifurcation have been computed with AUTO (dashed-dotted line in Figure 6.16(a)), but there may in fact exist an infinite number of them (indeed, more branch points and period-doubling bifurcation points were detected in this range, but no attempt was made to "switch" to other solutions). To give additional proof that the presumed chaotic solutions computed by FDM are really chaotic, the numerical scheme developed by Hairer *et al.* (1993) is used, since it is known to be particularly accurate in chaotic regimes, in the sense that it does not induce artificial chaos numerically. The phase-plane plot for $u = 9$ is shown in Figure 6.17, proving once again that the motion is indeed chaotic (the same conclusion as drawn from the power spectrum, not shown).

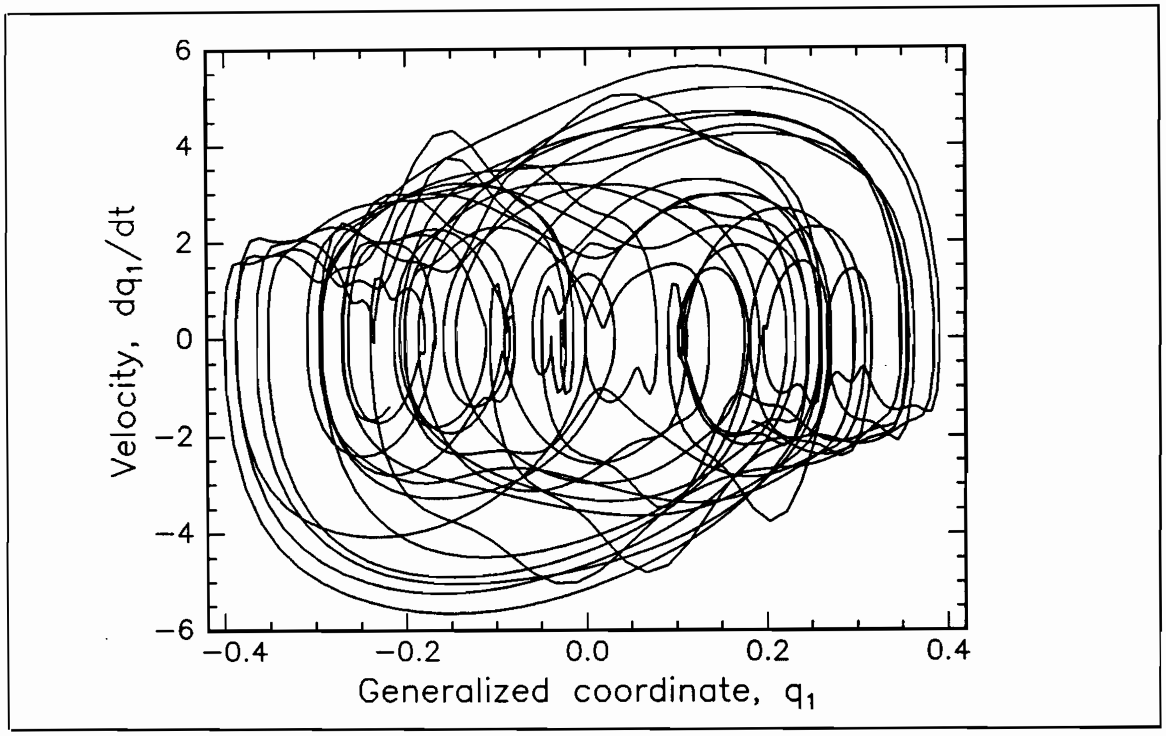

Figure 6.17: Phase-plane plot illustrating chaotic oscillations for $u = 9$, $\Gamma = 0.2$ and $N = 3$ computed using DOP853 (Hairer *et al.* 1993).

The results obtained by AUTO and FDM in the previous case help to explain why the discrepancies between theoretical predictions and experimental observations increase with Γ: when the end-mass Γ becomes large ($\Gamma > 0.2$), the number of humps, i.e. of corresponding unstable solutions, increases, even though there might still exist one or two stable ones. The solution obtained by numerical integration rapidly becomes chaotic, though in reality a stable periodic solution exists. Similarly, in the experiments, it was noticed that stable periodic solutions could be destroyed by small perturbations (or a small manual push), showing that these stable periodic oscillations were only weakly stable. An additional point may help explain the discrepancy: the nondimensional amplitudes of the end of the pipe, based on the third-order nonlinear model, are larger than unity for $\Gamma \geq 0.15$ (see for instance Figure 6.14), while in reality they must necessarily be considerably smaller (it is recalled that the nondimensional amplitude is defined as the ratio of the amplitude over the total length of the pipe, $\eta = y/L$). Consequently, to increase the accuracy of the model, a fifth-order approximation should be used, which represents an enormous task. It should be mentioned that the model without the nonlinear inertial terms predicts lower maximum amplitudes (this is also the case in Chapter 7), and therefore higher values of u for chaotic solutions, closer to the experiments. Nevertheless, it is difficult to say which one should be regarded as the most accurate. The question is not of major importance in this context, because in the experiments, large amplitudes tend to induce three-dimensional motions, so that it would be more appropriate to develop a three-dimensional model. This, however, is beyond the scope of the Thesis.

The investigation of the dynamics based on the model without the nonlinear inertial terms clarifies another point: the second and third Hopf bifurcations detected by linear theory are neither responsible for the appearance of the new periodic solutions nor for the emergence of chaotic solutions. Indeed, the results found by FDM on the equations of motion (6.14) with the coefficients $\gamma_{ijkl} = 0$ show the existence of the jump in the response even if there is no second (and third) Hopf bifurcation. Moreover, the two Hopf bifurcation points are connected by an unstable limit cycle of small amplitude — see the closed curve close to the x-axis in Figure 6.16(a). The amplitudes of these unstable solutions are so small (they have been amplified by a factor 20 in the figure), that they probably do not play an important role, any more than the unstable (static) equilibrium point does.

6.4.3 Conclusion for the case $\Gamma \geq 0$

In general, the agreement between theory and experiment for the system with an end-mass is very good, and the major features observed in the experiments are predicted numerically. Moreover, the theoretical model provides explanations for the changes in behaviour and reveals a very rich dynamical system. From the experimental investigation, the following conclusions may be drawn:

(i) two successive bifurcations are detected in the presence of an end-mass (even if it is small), and the second bifurcation is qualitatively different for values of Γ smaller or larger than 0.1;

(ii) in general, after the second bifurcation, three-dimensional chaotic oscillations are observed, emerging usually very suddenly, which means that it probably arises after a loss of stability of the second periodic solution;

(iii) as mentioned already by Copeland & Moon (1992), the case with *no* end-mass is singular, in the sense that only the first bifurcation is observed, at least with the apparatus and pipes used.

On the other hand, from the theoretical model, one might conclude the following.

(a) The linear stability analysis gives a possible explanation of the jump observed in the experiment, but the nonlinear analysis, necessary once the system has become unstable, contradicts this explanation to a certain extend.

(b) Again, the dynamics is different depending on the values of Γ: for $\Gamma = 0$, the response is trivial since only stable limit cycles exist after the Hopf bifurcation. For $0 < \Gamma \leq 0.1$, several bifurcations are predicted, and two periodic solutions of different frequency are found, together with a range of velocity for which quasiperiodic motions take place. The change in behaviour, as well as the values of u corresponding to these changes agree in general with those found in the experiments, but there are some discrepancies as well; for $\Gamma > 0.1$, the dynamics is much more complicated, and chaotic oscillations are shown to exist, in agreement with the experiments.

(c) For large values of Γ, the amplitudes of the pipe are very large so that a three-dimensional model should be considered, in agreement again with the experiment.

6.5 CONCLUSION OF THE CHAPTER

As mentioned in the Introduction of the chapter, this study was initiated to investigate the *planar* version of Copeland & Moon's system, to see if chaotic oscillations can be found in this case also. For $\Gamma < 0$, a type I intermittency route to chaos was discovered numerically while for $\Gamma > 0$, the dynamical behaviour is even richer, from both theoretical and experimental points of view. In fact, it may be said that the addition, or the removal, of small masses at the end of the fluid-conveying pipe enriches the dynamics considerably, in fact revealing the existence of a completely new dynamical system. Indeed, not only were different types of periodic solutions detected, but also jump phenomena, quasiperiodic and chaotic oscillations. Only a few parameters were varied here; so, it is reasonable to expect that, by changing the physical properties of the pipe, even richer dynamics might be discovered.

Chapter 7

PARAMETRIC RESONANCES OF THE PIPE WITH A PULSATING FLOW§

7.1 INTRODUCTION

In a recent extensive review (Païdoussis & Li 1993), it has been suggested that the system of a pipe conveying fluid is a model dynamical problem and a new paradigm in dynamics. It has been known for some time that the cantilevered pipe with steady flow, which is a nonconservative system, loses stability at sufficiently high flow velocity by flutter through a Hopf bifurcation (Païdoussis & Issid 1974). If the flow has a time-dependent harmonic component superposed on the steady flow [such that $U = U_0(1 + \nu \sin \omega t)$, where ν is generally small], then parametric instabilities (in the linear sense) can occur. These parametric resonances are akin to those experienced by a column subjected to a pulsating end load $F = F_0(1 + \nu \sin \omega t)$.

§This corresponds to the article by Semler & Païdoussis 1996 Nonlinear analysis of the parametric resonances of a planar fluid-conveying cantilevered pipe. Submitted to the *Journal of Fluids and Structures*.

Païdoussis & Issid (1974) obtained solutions for subharmonic resonances by means of Bolotin's (1964) method, and the analysis was extended to deal with both parametric and combination resonances via a Floquet analysis by Païdoussis & Sundararajan (1975). The results were confirmed experimentally by Païdoussis & Issid (1976). The parametric and, to a certain extent, the combination resonance regions predicted theoretically were found to correspond reasonably closely to those found in the experiments. Furthermore, it was shown that a pipe which would be unstable by the mean (steady) flow could be restabilized by parametric excitation at certain frequencies and amplitudes (ω, ν), again as predicted by theory. Further work has been undertaken for the linear dynamics of both cantilevered and supported pipes (i.e. with both ends fixed), as discussed by Païdoussis & Li (1993).

In contrast, only a few studies have been devoted to the nonlinear aspects of the dynamics of pipes conveying flow with a pulsatile component. Yoshizawa *et al.* (1986), Namachchivaya (1989) and Namachchivaya & Tien (1989) considered the problem of *supported pipes* by taking into account nonlinear terms. The problem is somewhat simplified by the fact that the system is conservative, albeit gyroscopic: in this case, one or two modes in the Galerkin expansion are usually sufficient, and the equations of motion can be written easily in a standard form as those of one or two nonlinear oscillators. Consequently, the method of averaging or of multiple scales can easily be applied. Things are considerably more complex in the case of *cantilevered pipes.* Bajaj (1984, 1987) was the only one to consider the nonlinear cantilevered pipe subjected to pulsating fluid, but only when the forcing frequency ω is close to $2\omega_n$ — the principal primary region (Bolotin 1964). He showed, for example, that when $\eta = U_0 - U_{0c} < 0$, there exist non-trivial periodic solutions, while for $\eta > 0$, the zero solution is always unstable, and that the pipe may perform small or large modulated motions, and/or large periodic motions, depending on some "unfolding" parameters.

The nonlinear equations of motion of the cantilevered pipe contain *nonlinear inertial* terms, so that it is difficult to recast them in the form of a set of first-order nonlinear ODEs for numerical integration. To circumvent this difficulty, several approaches may be adopted. In this study, four of them are used, some being analytical, others numerical, or a combination of the two, as outlined in items (a)-(d) in the following.

(a) In order to analyse nonlinear systems, quantitative techniques, such as perturbation methods and averaging methods, can yield reliable results provided the nonlinearities are small (Nayfeh & Mook 1979). But this condition is not necessarily satisfied for the system under consideration. Nevertheless, perturbation methods may simplify the analysis of the problem and yield interesting results. For the purpose of describing *qualitatively* the dynamics, the normal form method (NFM) can be used equally well (Guckenheimer & Holmes 1983). The problem here is somewhat more complicated by the fact that (i) the dimension of the system is high, and (ii) the equations are *non-autonomous.* To reduce the dimension of the system, the centre manifold theory can be applied by projecting the original flow on the centre manifold, even if the equations are non-autonomous (Carr 1981). This can be done for example by replacing the explicit time-dependence by coupling a simple oscillator to the original equations. Other methods are also available to reduce the dimension of the system, e.g. the method of Alternate Problems (Hale 1969) or the Lyapunov-Schmidt reduction (Wiggins 1988). Once the dimension of the system becomes low, normal form theory can thereafter by applied easily, following for example the methodology described in very simple terms by Nayfeh (1993). The resulting set of equations becomes that of a periodically perturbed Hopf bifurcation, which was tackled almost simultaneously by Bajaj (1986) and Namachchivaya & Ariaratnam (1987), and where, for the case of *parametric* perturbation, principal or primary resonances exist at the first order (when $\omega \simeq 2\omega_0$, ω_0 being the natural frequency of the system) and fundamental or secondary resonances may arise at the second order when $\omega \simeq \omega_0$ (Nayfeh 1986).

(b) Païdoussis & Semler (1993) and Li & Païdoussis (1994) used a perturbation method and, with the aid of the linear equation, transformed the nonlinear inertial term into equivalent stiffness and velocity-dependent terms (see Chapter 3). The resulting equations becoming of first-order, well-known numerical methods such as Runge-Kutta were thereafter being used. However, a certain degree of approximation is involved in the use of the perturbation method, and hence other ways of getting around this problem continued to be sought, especially from a numerical point of view.

(c) For time integration, Sinha and his co-workers (Sinha & Wu 1991; Sinha *et al.* 1993) developed some interesting and efficient methods to solve ODEs, but convergence is not achieved when strong nonlinear inertial terms are present, as is the case in the problem at hand (Chapter 5). In their book, Brenan *et al.* (1989) show how algebraic differential equations are solved using the finite difference method. The software they developed (DASSL) treats only index-one algebraic differential equations; equations with nonlinear inertial terms do not belong to that category (index ≥ 2). Moreover, the higher the index of the equation, the more difficult it is to solve it. Therefore, it was decided to use a robust backward finite difference method, based on Houbolt's scheme (Houbolt's 1950; Nath & Sandeep 1994). In this case, the approximation made via the perturbation method is no longer required.

(d) As mentioned already, the condition of small nonlinearities is not necessarily satisfied, and therefore, the response may contain higher-order harmonics. To overcome this difficulty, Lau and his co-workers developed the incremental harmonic balance (IHB) method (Lau *et al.* 1982). Ling & Wu (1987) and Cameron & Griffin (1989) further developed the IHB idea and proposed a computationally more efficient approach, by using the Fast Fourier Transform (FFT). This idea is extended here in the case where nonlinear inertial terms are present.

In this chapter, after a brief description of the model, the centre manifold theory is applied on the set of non-autonomous equations, followed by the derivation of the normal forms in the most general case, to determine all possible resonances as well as their general characteristics. The different numerical methods of solution are then discussed and many interesting results presented. Finally, comparison is made with data obtained experimentally.

7.2 MODELING OF THE SYSTEM

The system under consideration consists of a tubular beam of length L, internal cross–sectional area A, mass per unit length m, flexural rigidity EI, and coefficient of Kelvin–Voigt damping a, conveying fluid of mass M per unit length, flowing in the pipe with an axial velocity U. The pipe is assumed to lie initially along the x–axis (in the direction of gravity) and to oscillate in the (x, y) plane (Figure 7.1), with motion $y(s, t)$, s being the curvilinear coordinate and t the time.

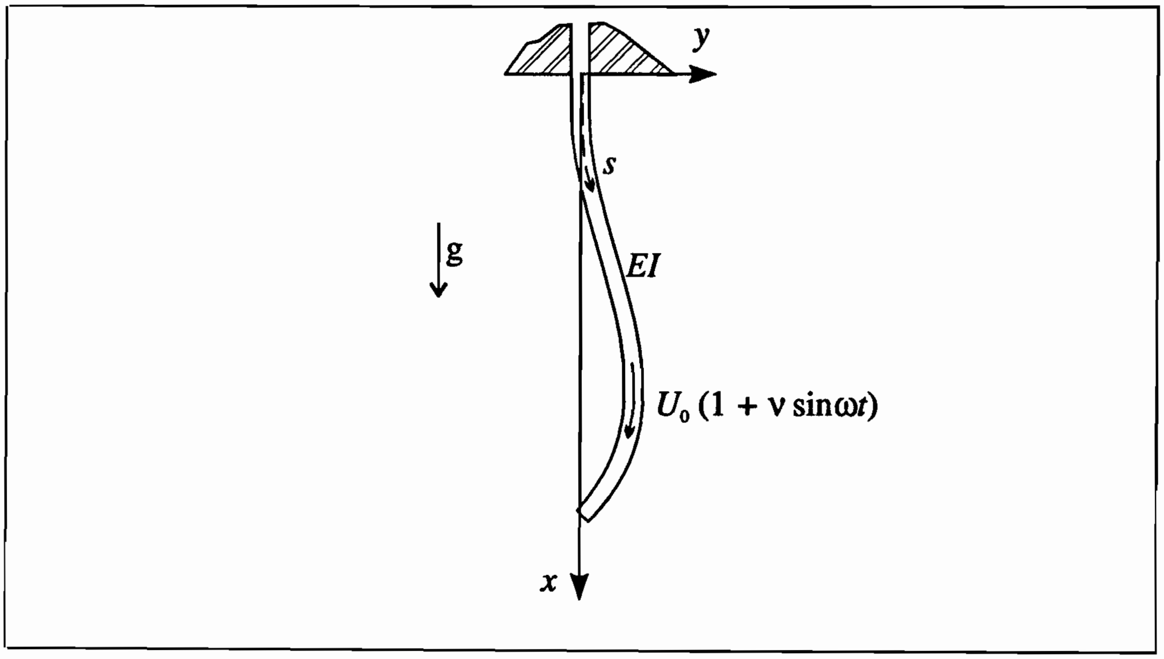

Figure 7.1: Schematic of the system.

The equation of motion was derived via both the Hamiltonian method and the Newtonian method by Semler *et al.* (1994) and may be written, in nondimensional form as follows:

$$
\begin{aligned}
& \alpha \;\; \dot{\eta}'''' + \eta'''' + \ddot{\eta} + 2\,u\,\sqrt{\beta}\,\dot{\eta}'(1+\eta'^2) + \eta''''\,\eta'^2 + 4\,\eta'\,\eta''\,\eta''' + \eta''^3 \\
+ \;& \eta'' \left[u^2(1+\eta'^2) + \left(\dot{u}\,\sqrt{\beta} - \gamma\right)(1-\xi)\left(1+\tfrac{3}{2}\,\eta'^2\right)\right] + \gamma\,\eta'\left(1+\tfrac{1}{2}\,\eta'^2\right) \\
- \;& \eta'' \left[\int_\xi^1 \int_0^\xi (\dot{\eta}'^2 + \eta'\,\ddot{\eta}')\,\mathrm{d}\xi\,\mathrm{d}\xi + \int_\xi^1 \left(\tfrac{1}{2}\dot{u}\sqrt{\beta}\,\eta'^2 + 2\,u\,\sqrt{\beta}\,\eta'\,\dot{\eta}' + u^2\,\eta'\,\eta''\right)\mathrm{d}\xi\right] \\
+ \;& \eta' \int_0^\xi (\dot{\eta}'^2 + \eta'\,\ddot{\eta}')\,\mathrm{d}\xi = 0\,; \qquad (7.1)
\end{aligned}
$$

the dot denotes the derivative with respect to nondimensional time τ, and the prime the derivative with respect to the nondimensional curvilinear coordinate along the centreline of the pipe, ξ; $\eta(\xi,\tau)$ represents the lateral deflection of the pipe, u the nondimensional flow velocity, γ a gravity parameter, β a mass parameter and α the visco-elastic dissipation, all nondimensional and related to the dimensional parameters via

$$\begin{aligned} \xi &= \frac{s}{L}, \quad \eta = \frac{y}{L}, \quad \tau = \left(\frac{EI}{m+M}\right)^{\frac{1}{2}} \frac{t}{L^2}, \quad \alpha = \left(\frac{EI}{m+M}\right)^{\frac{1}{2}} \frac{a}{L^2}, \\ u &= \left(\frac{M}{EI}\right)^{\frac{1}{2}} U\,L, \quad \gamma = \frac{m+M}{EI} L^3 g, \quad \beta = \frac{M}{m+M}. \end{aligned} \tag{7.2}$$

Moreover, it is assumed that the fluid flow is subjected to small sinusoidal fluctuations,

$$u = u_0(1 + \nu\, \sin\omega\tau), \tag{7.3}$$

where $\nu << 1$ and ω is the forcing frequency.* The infinite–dimensional model is discretized by Galerkin's technique, with the cantilever beam eigenfunctions, $\phi_r(\xi)$, being used as a suitable set of base functions, and $q_r(\tau)$ being the corresponding generalized coordinates; thus,

$$\eta(\xi,\tau) = \sum_{r=1}^{N} \phi_r(\xi)\, q_r(\tau)\,. \tag{7.4}$$

Considering for a moment the case when $u = u_0$, substitution of expression (7.4) into (7.1), multiplication by $\phi_i(\xi)$ and integration from 0 to 1 leads to

$$\ddot{q}_i + C_{ij}\,\dot{q}_j + K_{ij}\,q_j + \alpha_{ijkl}\,q_j\,q_k\,q_l + \beta_{ijkl}\,q_j\,q_k\,\dot{q}_l + \gamma_{ijkl}\,(\,q_j\,\dot{q}_k\,\dot{q}_l + q_j\,q_k\,\ddot{q}_l) = 0\,; \tag{7.5}$$

C_{ij} and K_{ij} represent the elements of the stationary (time-independent) damping and stiffness matrices. These, as well as α_{ijkl}, β_{ijkl} and γ_{ijkl}, are defined in Appendix G. The repeated indices in equation (7.5) implicitly follow the summation convention.

In the case of a fluctuating flow velocity, as in equation (7.3), additional terms have to be incorporated in the damping and stiffness matrices, which now become

$$\begin{aligned} C'_{ij}(\tau) &= C_{ij} + \left(2\sqrt{\beta}\,\nu\,u_0 \sin\omega\tau\right) b_{ij}, \\ K'_{ij}(\tau) &= K_{ij} + u_0^2\,(2\nu\sin\omega\tau + \nu^2\sin^2\omega\tau)\,c_{ij} + \left(\sqrt{\beta}\,\nu u_0\omega\,\cos\omega\tau\right)(d_{ij} - c_{ij}), \end{aligned} \tag{7.6}$$

*In Chapter 3, the definition of ν is slightly different — see equation (3.12).

where the coefficients b_{ij}, c_{ij} and d_{ij} are also defined in Appendix G. Introducing the generalized coordinates $p_i = \dot{q}_i$, equation (7.5) together with (7.6) can be put in first-order form,

$$\dot{y} = [A]\, y + \nu(\omega \cos \omega\tau [B_1] + \sin \omega\tau [B_2]) y \; + \nu^2 \sin^2 \omega\tau [B_3] y + \; f(y, \dot{y}), \tag{7.7}$$

where $\{y\} = \{q, p\}^{\mathrm{T}}$ is a vector of dimension $2N$ and

$$[A] = \begin{bmatrix} 0 & I \\ -K_{ij} & -C_{ij} \end{bmatrix}, [B_1] = \begin{bmatrix} 0 & 0 \\ -u_0\sqrt{\beta}(d_{ij} - c_{ij}) & 0 \end{bmatrix},$$

$$[B_2] = \begin{bmatrix} 0 & 0 \\ -2u_0^2 c_{ij} & -2\sqrt{\beta} u_0 b_{ij} \end{bmatrix}, [B_3] = \begin{bmatrix} 0 & 0 \\ -u_0^2 c_{ij} & 0 \end{bmatrix}, \tag{7.8}$$

$$f = \begin{Bmatrix} 0 \\ -\alpha_{ijkl} q_j q_k q_l - \beta_{ijkl} q_j q_k p_l - \gamma_{ijkl} \left(q_j p_k p_l + \; q_j q_k \dot{p}_l \right) \end{Bmatrix}.$$

7.3 ANALYTICAL METHODS: CENTRE MANIFOLD AND NORMAL FORM THEORY

In this section, the modern tools of nonlinear dynamics are used to describe the dynamical behaviour of the *non-autonomous* system. This is a difficult task because the dimension of the system is high. Consequently, it would be desirable to undertake some simplification. The idea is to reduce the dimension of the system by projecting the flow defined by the original equations (7.7) on the centre manifold and then to put it in a simplified or *normal form.* The procedure is similar to what was done earlier in Chapter 3, except that now the time-varying terms are also taken into account in the analysis.

Consequently, after putting the system into standard form, the centre manifold theorem is applied, followed by application of normal form theory. For the sake of completeness, the normal form theory is applied directly to the equation containing nonlinear inertial terms, to yield the simplest form of the vector field in the most general case. It is straightforward to deduce the case where these terms have been removed, as in Section 7.4.1.

7.3.1 Standard form

For cantilevered pipes hanging downwards, the gravity parameter $\gamma > 0$, and it is well-known (Païdoussis 1970) that in this case the only possible bifurcation of the linearized *autonomous* system is a Hopf bifurcation. If it is assumed that all the physical parameters are constant except the flow velocity u_0 which is the parameter varied, then the critical value is $u_0 = u_{cr}$. By a simple change of coordinate $\{y\} = [P]\{x\}$, where $[P]$ represents a modified modal matrix evaluated at u_{cr}, system (7.7) can be put into the standard form defined by

$$\dot{x} = [A'] \, x \; + \nu(\omega[B^1] \cos \omega\tau + [B^2] \sin \omega\tau) \, x + \; \nu^2 \sin^2 \omega\tau [B^3] x \; + F(x, \dot{x}), \qquad (7.9)$$

where

$$[A'] = [P]^{-1}[A][P] = \begin{bmatrix} [J] & 0 \\ 0 & [M] \end{bmatrix}, \qquad (7.10)$$

and

$$[J] = \begin{bmatrix} 0 & -\omega_0 \\ \omega_0 & 0 \end{bmatrix}. \qquad (7.11)$$

In general, $[M]$ is a square matrix of dimension $2N - 2$, of which all eigenvalues have negative real parts, the matrices $[B^k] = [P]^{-1}[B_k][P]$, for $k = 1, 2, 3$, are of dimension $2N$, and the vector F contains only cubic nonlinear terms. For the cantilevered pipe conveying fluid, it can be assumed without lack of generality that all $2N - 2$ eigenvalues of $[M]$ appear in *distinct* complex conjugate pairs with non-zero real parts, $\lambda_{2p-1,2p} = \sigma_p \pm \mathrm{i}\omega_p, p \; = 1, \; ..., \; N - 1$, and $\sigma_p \neq 0$, so that $[M]$ can be put in Jordan form,

$$[M] = \begin{bmatrix} R_1 & \cdots & 0 & \cdots & 0 \\ \vdots & \ddots & \vdots & & \vdots \\ 0 & \cdots & R_p & \cdots & 0 \\ \vdots & & \vdots & \ddots & \vdots \\ 0 & \cdots & 0 & \cdots & R_{N-1} \end{bmatrix}, \tag{7.12}$$

with

$$[R_p] = \begin{bmatrix} \sigma_p & -\omega_p \\ \omega_p & \sigma_p \end{bmatrix}. \tag{7.13}$$

In the following, we shall deal only with the standard form (7.9), assuming that this change of coordinate has already been performed.

7.3.2 Centre manifold

In the case of a non-autonomous system, special care must be taken for the centre manifold reduction. To obtain an approximation valid to a specific order, two stages are necessary: (i) first, the system is put into a set of *autonomous* equations, so that the standard centre manifold theory becomes applicable, and then, (ii) because it is not possible to find an exact solution of the non-unique centre manifold, a Taylor series expansion must be applied (Carr 1981).

To put the system in autonomous form, $\nu \cos \omega\tau$ and $\nu \sin \omega\tau$ are replaced by two new variables, v_1 and v_2, which are solutions of the following system of equations:

$$\begin{matrix} \dot{v}_1 = \\ \dot{v}_2 = \end{matrix} \begin{bmatrix} \nu^2 & -\omega \\ \omega & \nu^2 \end{bmatrix} \begin{Bmatrix} v_1 \\ v_2 \end{Bmatrix} \begin{matrix} - v_1(v_1^2 + v_2^2), \\ - v_2(v_1^2 + v_2^2). \end{matrix} \tag{7.14}$$

Indeed, it can be proved easily that the stable solution of (7.14) is a limit cycle of amplitude ν and of frequency ω. Consequently, this oscillator, represented in vector form by $v = \{v_1, v_2\}^{\mathrm{T}}$, can be coupled directly to equation (7.9), simply by replacing $\nu \cos \omega\tau$ and $\nu \sin \omega\tau$ by v_1 and v_2, respectively. It is important to mention that the system defined by (7.14) undergoes a Hopf bifurcation at $\nu = 0$, at which point the origin $v = (0, 0)$ is *nonhyperbolic*. It is therefore convenient to include ν in the system of equations as a trivial dependent variable ($\dot{\nu} = 0$) [see Guckenheimer & Holmes (1983), p.126] so that the global *autonomous* set of equations to be considered now becomes

$$\begin{aligned} \dot{z} &= [A_0]z + f(y, z), \\ \dot{y} &= [M]y + g(y, z), \end{aligned} \tag{7.15}$$

where $y = \{x_3, ..., x_{2N}\}^{\mathrm{T}}$, $z = \{\nu, v_1, v_2, x_1, x_2\}^{\mathrm{T}}$, and the five-dimensional matrix $[A_0]$ is

$$[A_0] = \begin{bmatrix} 0 & 0 & 0 & 0 & 0 \\ 0 & \nu^2 & -\omega & 0 & 0 \\ 0 & \omega & \nu^2 & 0 & 0 \\ 0 & 0 & 0 & 0 & -\omega_0 \\ 0 & 0 & 0 & \omega_0 & 0 \end{bmatrix}. \tag{7.16}$$

To be more specific, $f_1 = 0, f_2$ and f_3 represent the nonlinear terms of (7.14), and f_4 and f_5 represent the sum of the time-varying components (that can be regarded now as "quadratic" terms, because the cosine and the sine [see equation (7.9)], that are multiplied by x, are now replaced by the state variables v_1 and v_2) plus the cubic nonlinear terms of (7.9), i.e.

$$\begin{aligned} f_4 = &\ (v_1\omega B^1_{1,j} + v_2 B^2_{1,j} + v_2^2 B^3_{1,j})x_j + F_1(x, \dot{x}), \\ f_5 = &\ (v_1\omega B^1_{2,j} + v_2 B^2_{2,j} + v_2^2 B^3_{2,j})x_j + F_2(x, \dot{x}). \end{aligned} \tag{7.17}$$

In (7.17), it is understood that there is a summation on j, for $j = 1, ..., 2N$. Finally, finding the nonlinear term g is easy because $g_i = F_i$, $i = 3, ..., 2N$, the same F_i as in (7.9).

The equations of motion (7.15) have been partitioned into two: the system linearized around $z = 0$, represented by $[A_0]$, has either zero or purely imaginary eigenvalues, while the system linearized around $y = 0$ has only eigenvalues with negative real parts, because of the assumptions made. Therefore, for the linear system, the y-axes span the stable eigenspace, and the z-axes represent the centre eigenspace.

Consequently, in the neighbourhood of the origin, the centre manifold is five-dimensional. Because the eigenvalues of $[M]$ appear in complex conjugate pairs, the components of y must be sought in pairs, so that the centre manifold $y = h(z)$ may be written as

$$\begin{aligned} x_{2p+1} = \quad h_p^1(z) &= h_p^1(\nu, v_1, v_2, x_1, x_2), \\ x_{2p+2} = \quad h_p^2(z) &= h_p^2(\nu, v_1, v_2, x_1, x_2), \qquad p = 1, \ldots, N-1. \end{aligned} \tag{7.18}$$

Since the centre manifold is tangent to the centre space, the following boundary conditions must be satisfied:

$$h_p^i\Big|_0 = \left.\frac{\partial h_p^i}{\partial x_1}\right|_0 = \left.\frac{\partial h_p^i}{\partial x_2}\right|_0 = \left.\frac{\partial h_p^i}{\partial v_1}\right|_0 = \left.\frac{\partial h_p^i}{\partial v_2}\right|_0 = \left.\frac{\partial h_p^i}{\partial \nu}\right|_0 = 0, \qquad i = 1, 2 \text{ and } p = 1, \ldots, N-1, \tag{7.19}$$

with the different functions evaluated at $z = 0$. The centre manifold W^c is thus defined by the functions h^1 and h^2 satisfying the boundary conditions (7.19), such that W^c is invariant under the flow defined by (7.15). It is not unique but can be approximated using Taylor series (Guckenheimer & Holmes 1983).

To do this, in agreement with the assumptions made to derive the equation of motion, we assume x_1 and x_2 "small", $(x_1, x_2) = \mathcal{O}(\epsilon)$, as well as $\nu = \mathcal{O}(\epsilon)$ and $(v_1, v_2) = \mathcal{O}(\epsilon)$. Substituting y by $h^i(z)$ and using the chain rule, we obtain

$$\dot{y} = Dh^i(z)\dot{z} = Dh^i(z)\{[A_0]z + f(h^i(z), z)\} = [M]h^i(z) + g(h^i(z), z), \tag{7.20}$$

or

$$Dh^i(z)\{[A_0]z + f(h^i(z), z)\} - [M]h^i(z) - g(h^i(z), z) = 0, \tag{7.21}$$

where D represents the total derivative with respect to time. Because of the coupling between h_p^1 and h_p^2 arising from the fact that the eigenvalues of $[M]$ appear in complex conjugate pairs — see equation (7.13) — solving (7.21) is similar to solving $N-1$ equations of the type

$$\begin{aligned} Dh_p^1 &= \sigma_p h_p^1 - \omega_p h_p^2 + (v_1 \omega B_{2p+1,j}^1 + v_2 B_{2p+1,j}^2 + v_2^2 B_{2p+1,j}^3) x_j + g_{2p+1}(x, \dot{x}), \\ Dh_p^2 &= \omega_p h_p^1 + \sigma_p h_p^2 + (v_1 \omega B_{2p+2,j}^1 + v_2 B_{2p+2,j}^2 + v_2^2 B_{2p+2,j}^3) x_j + g_{2p+2}(x, \dot{x}), \end{aligned} \tag{7.22}$$

where

$$Dh_p^i = \frac{\partial h_p^i}{\partial x_1}\dot{x}_1 + \frac{\partial h_p^i}{\partial x_2}\dot{x}_2 + \frac{\partial h_p^i}{\partial v_1}\dot{v}_1 + \frac{\partial h_p^i}{\partial v_2}\dot{v}_2,$$

in which $\dot{x}_i$ are replaced using the first of equations (7.15) — see also equation (7.17) — and the $\dot{v}_i$ are replaced using (7.14). In equation (7.22), it is understood again that there is a summation on j ($j = 1, ..., 2N$), and that (x_{2p+1}, x_{2p+2}) must be replaced by (h_p^1, h_p^2).

Equation (7.22) represents a partial differential equation for h that cannot be solved exactly, but whose solution can be approximated as a Taylor series around the origin $z = 0$. Because of boundary conditions (7.19), h_p^i must be at least quadratic, i.e.

$$\begin{aligned} h_p^i(z) = \; & \alpha_{p,1}^i x_1^2 + \alpha_{p,2}^i x_2^2 + \alpha_{p,3}^i v_1^2 + \alpha_{p,4}^i v_2^2 + \alpha_{p,5}^i \nu^2 + \alpha_{p,6}^i v_1 x_1 + \alpha_{p,7}^i v_1 x_2 + \alpha_{p,8}^i v_2 x_1 \\ & + \alpha_{p,9}^i v_2 x_2 + \alpha_{p,10}^i v_1 \nu + \alpha_{p,11}^i v_2 \nu + \alpha_{p,12}^i \nu x_1 + \alpha_{p,13}^i \nu x_2 + \alpha_{p,14}^i x_1 x_2 + \alpha_{p,15}^i v_1 v_2. \end{aligned} \tag{7.23}$$

After some long but straightforward algebra, it can be proved that (i) the nonlinear terms do not play any role in the analysis because they are cubic and (ii) all the coefficients $\alpha_{p,k}^i$ are zero, except $\alpha_{p,6}^i$ to $\alpha_{p,9}^i$. For notation purposes, it is convenient to introduce the vector $\{b\} = \{B_{2p+1,1}^1; B_{2p+1,2}^1; B_{2p+1,1}^2; B_{2p+1,2}^2, B_{2p+2,1}^1; B_{2p+2,2}^1; B_{2p+2,1}^2; B_{2p+2,2}^2\}$. Recalling that $[I]$ is the identity matrix and introducing the matrix $[J_p]$ defined by

$$[J_p] = \begin{bmatrix} -\sigma_p & \omega_0 & \omega & 0 \\ -\omega_0 & -\sigma_p & 0 & \omega \\ -\omega & 0 & -\sigma_p & \omega_0 \\ 0 & -\omega & -\omega_0 & -\sigma_p \end{bmatrix}, \tag{7.24}$$

it can be proved that the remaining coefficients are given by

$$\begin{bmatrix} [J_p] & \omega_p[I] \\ -\omega_p[I] & [J_p] \end{bmatrix} \left\{\alpha_{p,6}^1; \alpha_{p,7,}^1; \alpha_{p,8}^1; \alpha_{p,9}^1; \alpha_{p,6}^2; \alpha_{p,7}^2; \alpha_{p,8}^2; \alpha_{p,9}^2\right\}^{\mathrm{T}} = \{b\}^{\mathrm{T}} \tag{7.25}$$

which has a unique solution, provided $\sigma_p \neq 0$, as per one of the assumptions made. The centre manifold then becomes

$$h_p^i(z) = h_p^i(\nu, v_1, v_2, x_1, x_2) = \alpha_{p,6}^i v_1 x_1 + \alpha_{p,7}^i v_1 x_2 + \alpha_{p,8}^i v_2 x_1 + \alpha_{p,9}^i v_2 x_2. \tag{7.26}$$

This result is general. If $\nu = 0$, which means that there is no perturbation in the flow velocity, then $h_p^i(z) = 0$. This is the same result as found by Sethna & Shaw (1987) and

Li & Païdoussis (1994): near the origin, the flow field restricted to the centre eigenspace provides the correct qualitative picture of the dynamics of the whole system. If $\nu \neq 0$, however, and remembering that $v_1 = \nu \cos \omega\tau$ and $v_2 = \nu \sin \omega\tau$, it can be seen that second-order terms due to the perturbation of the flow velocity do arise in the centre manifold reduction and, hence, should be included in the analysis.

7.3.3 Normal form theory

The goals of this section are twofold. First, one would like to find all possible parametric resonances that might occur in the system defined by (7.9), to order ϵ but also to order ϵ^2. Second, one wants to use the normal form theory to find the simplest set of equations that defines these parametric resonances. Assuming $x' = \epsilon x, \nu' = \epsilon\nu$ and $u_0 - u_{cr} = \epsilon\mu$ and then dropping the primes for simplicity of writing, the following two-dimensional system of equations, defined on the centre manifold, is thus considered:

$$\begin{aligned} \dot{x} &= [J]x + \epsilon\, (\mu[A^1] + \omega\nu \cos\omega\tau[A^2] + \nu \sin\omega\tau[A^3])x + \epsilon^2\, f(x, \dot{x}) \\ &+ \epsilon^2\nu^2(\cos^2\omega\tau[A^4] + \cos\omega\tau \sin\omega\tau[A^5] + \sin^2\omega\tau[A^6])x \\ &+ \epsilon^2\mu\nu(\cos\omega\tau[A^7] + \sin\omega\tau[A^8])x + \epsilon^2\mu^2[A^9]x. \end{aligned} \tag{7.27}$$

In (7.27), the first term on the right-hand side represents the harmonic solution, of frequency ω_0, that exists at the Hopf bifurcation point when $\epsilon = 0$ and $u = u_{cr}$, and f contains all "cubic" nonlinear terms that may or may not be inertial. Finally, the nine matrices $[A^i]$ are constant and known. The second-order terms are due to the harmonic perturbation of the flow velocity, to the deviation of the flow velocity with respect to the critical flow u_{cr} and to the nonlinear terms. The reason for representing the nonlinearities as "second-order" will become self-evident later.

As shown by Nayfeh (1993), it is more convenient to deal with complex quantities to compute the normal form. Following his notation, it can be seen that when $\epsilon = 0$, the solution of (7.27) can be written as

$$x_1 = \frac{\mathrm{i}}{\omega_0}\,(Be^{\mathrm{i}\omega_0\tau} - \overline{B}e^{-\mathrm{i}\omega_0\tau}), \quad x_2 = \frac{1}{\omega_0}\,(Be^{\mathrm{i}\omega_0\tau} + \overline{B}e^{-\mathrm{i}\omega_0\tau}), \tag{7.28a}$$

where B is a constant, $\overline{B}$ is the complex conjugate of B, and $\mathrm{i} = \sqrt{-1}$. When $\epsilon \neq 0$, the solution of (7.27) is still of the form of (7.28a), but with time-varying rather than constant B. Therefore, the following change of coordinates is made:

$$x_1 = \frac{\mathrm{i}}{\omega_0}\,(\zeta - \overline{\zeta}), \;\; x_2 = \frac{1}{\omega_0}\,(\zeta + \overline{\zeta}), \tag{7.28b}$$

where ζ is time-varying and $\overline{\zeta}$ is the complex conjugate of ζ. Similarly, it is convenient to introduce the complex variable $z = e^{\mathrm{i}\omega\tau}$, so that

$$\cos\omega\tau = \frac{1}{2}(z + \overline{z}), \quad \sin\omega\tau = \frac{1}{2\mathrm{i}}(z - \overline{z}) \tag{7.29a}$$

and

$$\dot{z} = \mathrm{i}\omega z. \tag{7.29b}$$

Using (7.28b) and (7.29a), equation (7.27) may be transformed into one complex equation defined, in general, by

$$\begin{aligned} \dot{\zeta} \;&=\; \mathrm{i}\omega_0\zeta + \epsilon\mu(\alpha_1\zeta + \alpha_2\overline{\zeta}) + \epsilon\nu\omega(z+\overline{z})(\alpha_3\zeta + \alpha_4\overline{\zeta}) + \epsilon\nu(z-\overline{z})(\alpha_5\zeta + \alpha_6\overline{\zeta}) \\ &+\; \epsilon^2\,[\beta_1\zeta^3 + \beta_2\zeta^2\overline{\zeta} + \beta_3\zeta\overline{\zeta}^2 + \beta_4\overline{\zeta}^3 + \beta_5\zeta^2\dot{\overline{\zeta}} + \beta_6\dot{\zeta}\overline{\zeta}^2] \\ &+\; \epsilon^2\,\nu^2\,[\gamma_1\zeta + \gamma_2\overline{\zeta} + (z^2+\overline{z}^2)(\gamma_3\zeta + \gamma_4\overline{\zeta}) + (z^2-\overline{z}^2)(\gamma_5\zeta + \gamma_6\overline{\zeta})] \\ &+\; \epsilon^2\,\mu\nu\,[(z^2+\overline{z}^2)(\delta_1\zeta + \delta_2\overline{\zeta}) + (z^2-\overline{z}^2)(\delta_3\zeta + \delta_4\overline{\zeta})] + \epsilon^2\mu^2(\delta_5\zeta + \delta_6\overline{\zeta}), \end{aligned} \tag{7.30}$$

where, as explained in Appendix I, α, β, γ and δ are complex constants that can be related to the coefficients of $[A^i]$, $i = 1, \ldots, 9$. As will be shown, the nonlinear inertial terms, represented by β_5 and β_6, can simply be included as "usual" cubic nonlinearities. From now on, we shall consider that (7.30) is the equation to be put in normal form. This means that by a simple change of coordinates,

$$\zeta = \eta + \epsilon h_1(\eta, \overline{\eta}, z, \overline{z}) + \epsilon^2 h_2(\eta, \overline{\eta}, z, \overline{z}), \tag{7.31}$$

equation (7.30) can be transformed into

$$\dot{\eta} = \mathrm{i}\omega_0\eta + \epsilon g_1(\eta, \overline{\eta}, z, \overline{z}) + \epsilon^2 g_2(\eta, \overline{\eta}, z, \overline{z}), \tag{7.32}$$

where g_1 and g_2 are "as simple as possible" (Guckenheimer & Holmes 1983). For that purpose, h_1 and h_2 have to be determined. Several steps are necessary. The first one is to differentiate (7.31), which leads to

$$\dot{\zeta} = \dot{\eta} + \epsilon \frac{Dh_1}{Dt} + \epsilon^2 \frac{Dh_2}{Dt}, \tag{7.33}$$

where D/Dt is the total derivative, defined by

$$\frac{D}{Dt} = \dot{\eta}\frac{\partial}{\partial \eta} + \dot{\overline{\eta}}\frac{\partial}{\partial \overline{\eta}} + \dot{z}\frac{\partial}{\partial z} + \dot{\overline{z}}\frac{\partial}{\partial \overline{z}}. \tag{7.34}$$

The second step is to equate the right-hand side of (7.33) with the right-hand side of (7.30), in which ζ and $\overline{\zeta}$ have been replaced by using (7.31). The final step is to collect terms of same order, which yields the following.

(a) Order ϵ^0

$$\dot{\eta} = \mathrm{i}\omega_0 \eta; \tag{7.35}$$

this means that the response is harmonic if $\epsilon = 0$, with ω_0 as the corresponding frequency.

(b) Order ϵ^1

$$g_1 + \mathcal{L}(h_1) = \mu(\alpha_1\eta + \alpha_2\overline{\eta}) + \nu\omega(z+\overline{z})(\alpha_3\eta + \alpha_4\overline{\eta}) + \nu(z-\overline{z})(\alpha_5\eta + \alpha_6\overline{\eta}), \tag{7.36}$$

where the operator $\mathcal{L}$, known as the Lie or Poisson bracket (Arnold 1983), is defined by

$$\mathcal{L} = \mathrm{i}\omega_0(\eta\frac{\partial}{\partial\eta} - \overline{\eta}\frac{\partial}{\partial\overline{\eta}} - 1) + \mathrm{i}\omega(z\frac{\partial}{\partial z} - \overline{z}\frac{\partial}{\partial \overline{z}}); \tag{7.37}$$

to obtain (7.36) and (7.37), equations (7.29b) and (7.35) were utilized, the latter being valid only to order ϵ^0.

(c) Order ϵ^2

$$\begin{aligned} g_2 + \mathcal{L}(h_2) \;&= -(\frac{\partial h_1}{\partial \eta} g_1 + \frac{\partial h_1}{\partial \overline{\eta}}\overline{g}_1) + \mu(\alpha_1 h_1 + \alpha_2 \overline{h}_1) \\ &+ \nu\omega(z+\overline{z})(\alpha_3 h_1 + \alpha_4\overline{h}_1) + \nu(z-\overline{z})(\alpha_5 h_1 + \alpha_6 \overline{h}_1) \\ &+ \beta_1\eta^3 + (\beta_2 - \mathrm{i}\omega_0\beta_5)\eta^2\overline{\eta} + (\beta_3 + \mathrm{i}\omega_0\beta_6)\eta\overline{\eta}^2 + \beta_4\overline{\eta}^3 \\ &+ \nu^2\,[\gamma_1\eta + \gamma_2\overline{\eta} + (z^2+\overline{z}^2)(\gamma_3\eta + \gamma_4\overline{\eta}) + (z^2-\overline{z}^2)(\gamma_5\eta+\gamma_6\overline{\eta})] \\ &+ \mu\nu\,[(z+\overline{z})(\delta_1\eta + \delta_2\overline{\eta}) + (z-\overline{z})(\delta_3\eta+\delta_4\overline{\eta})] + \mu^2(\delta_5\eta + \delta_6\overline{\eta}). \end{aligned} \tag{7.38}$$

It is interesting to mention that the nonlinear inertial terms in (7.38) are not "fundamentally different" from other nonlinear terms, such as nonlinear damping or stiffness; this is usually so when using perturbation or normal form methods. Nevertheless, they may modify the effects of the two coefficients β_2 and β_3.

The third step is to find h_1 and g_1. The right-hand side of (7.36) suggests seeking h_1 in the form

$$h_1 = \Gamma_1 \eta + \Gamma_2 \overline{\eta} + \Gamma_3 \eta z + \Gamma_4 \overline{\eta}\, \overline{z} + \Gamma_5 \eta \overline{z} + \Gamma_6 \overline{\eta} z. \tag{7.39}$$

Substituting (7.39) into (7.36), one can prove after some algebra, that can be automated using symbolic software such as Mathematica, that

$$\begin{aligned} g_1 &= \mu\alpha_1 \eta + (\mu\alpha_2 + 2\mathrm{i}\omega_0\Gamma_2)\, \overline{\eta} \\ &+ (\nu\omega\alpha_3 + \nu\alpha_5 - \mathrm{i}\omega\Gamma_3)\, \eta z + [\nu\omega\alpha_4 - \nu\alpha_6 + \mathrm{i}\Gamma_4(2\omega_0 + \omega)]\, \overline{\eta}\, \overline{z} \\ &+ (\nu\omega\alpha_3 - \nu\alpha_5 + \mathrm{i}\omega\Gamma_5)\, \eta\overline{z} + [\nu\omega\alpha_4 + \nu\alpha_6 + \mathrm{i}\Gamma_6(2\omega_0 - \omega)]\, \overline{\eta} z. \end{aligned} \tag{7.40}$$

It can be seen that applying $\mathcal{L}$ to h_1, Γ_1 "disappears", and hence is arbitrary. This means that the term η is a resonance term that *cannot* be removed: it is due to the fact that the solution of the unperturbed problem is proportional to $\exp(\mathrm{i}\omega_0\tau)$ which has the same frequency as η at order ϵ^0. Moreover, it follows from (7.40) that $\overline{\eta}z$ is a near-resonance term when $\omega \simeq 2\omega_0$. Two equivalent reasons may be put forward to explain this: (i) recalling that $\eta \sim \exp(\mathrm{i}\omega_0\tau)$ and $z = \exp(\mathrm{i}\omega\tau)$, the term $\overline{\eta}z$ has a frequency of $-\omega_0 + \omega$, which is equal to ω_0 when ω is near $2\omega_0$; (ii) the coefficient before Γ_6 vanishes if $\omega = 2\omega_0$ and may therefore produce small-divisor terms. Here, we follow Nayfeh's terminology: the resonance terms correspond to terms that produce secular terms, whereas the near-resonance terms correspond to terms that would produce small-divisor terms in the application of the method of multiple scales (Nayfeh 1981, 1993).

Because it appears at the first order, this resonance is usually referred to as the *principal parametric* resonance. Consequently, two distinct cases must be considered: the case of ω away from $2\omega_0$, treated first, and the case ω near $2\omega_0$, investigated next.

7.3.3.1 The case of ω away from $2\omega_0$

If $\omega \neq 0$ and $\omega \neq 2\omega_0$, all the coefficients Γ_m except Γ_1 are chosen to eliminate all the nonresonance terms, i.e.

$$\begin{aligned} &\Gamma_2 = \frac{i\mu\alpha_2}{2\omega_0}, \quad \Gamma_3 = \frac{-i\nu}{\omega}(\omega\alpha_3 + \alpha_5), \quad \Gamma_4 = \frac{i\nu}{2\omega_0 + \omega}(\omega\alpha_4 - \alpha_6), \\ &\Gamma_5 = \frac{i\nu}{\omega}(\omega\alpha_3 - \alpha_5), \quad \Gamma_6 = \frac{i\nu}{2\omega_0 - \omega}(\omega\alpha_4 + \alpha_6), \end{aligned} \tag{7.41}$$

which yields a very simple form for g_1,

$$g_1 = \mu\alpha_1\eta. \tag{7.42}$$

It is now possible to compute the right-hand side of (7.38). To simplify the calculations as much as possible, it is important to first find and classify all possible resonances that might occur when $\omega \neq 2\omega_0$. In this case again, $\eta, \eta z\bar{z}$ and $\eta^2\bar{\eta}$ are resonance terms (because they have a frequency equal to ω_0, independently of the forcing frequency), and if $\omega \simeq \omega_0$, for the reasons given previously, $\bar{\eta}z^2, \eta\bar{\eta}z$ and $\eta^2\bar{z}$ are near-resonance terms. Consequently, $\omega = \omega_0$ is the only possible near-resonance at this order, and it is called the *fundamental parametric* resonance (Nayfeh 1986, 1993).

Before finding the right-hand side of (7.38), some additional discussion might be useful. It is obvious that, depending on the approximation made when considering the nonlinear terms, the form for h_1 will be different: assuming the nonlinear terms proportional to ϵ instead of ϵ^2, h_1 will also have to contain "cubic" terms (e.g. $\eta^3, \eta^2\bar{\eta}$...), and therefore the right-hand side of (7.38) will include new terms, namely "quartics" (e.g. of the type $\bar{\eta}^3 z$) and "quintics" (e.g. of the type $\eta^4\bar{\eta}$). In such a case, a new resonance term appears, $\eta^3\bar{\eta}^2$, as well as near-resonance terms, at the fundamental frequency, $\omega \simeq \omega_0$, and also at the subharmonic resonance of order one-third ($\omega \simeq 3\omega_0$) and one-fourth ($\omega \simeq 4\omega_0$), due, respectively, to $\bar{\eta}^2 z$ and $\bar{\eta}^3 z$. Thus, in principle, they should also be included in the analysis. However, an approximation to this order would contradict the assumptions made for the derivation of the equation of motion, where only cubic terms were retained. This justifies, *a posteriori*, why the cubic nonlinearities must be regarded as "second-order" approximations. Nevertheless, if only a first-order approximation is sought and if one wants to keep the nonlinear terms in the analysis, they must appear as first-order. In the end, because ϵ is only a book-keeping device, it is set equal to one, and the same result will be obtained.

The usual procedure employed in determining the normal form is to choose h_2 so as to eliminate as many terms as possible from (7.38). This is the same as equating g_2 to the sum of the resonance and near-resonance terms, knowing that the nonresonance terms can be eliminated by a proper choice of h_2. Because the analysis is carried out to $\mathcal{O}(\epsilon^2)$, it is not necessary to determine h_2 explicitly. After some algebra, one obtains

$$\begin{aligned} g_2 + \mathcal{L}(h_2) &= (\mu\alpha_2\overline{\Gamma}_2 + \mu^2\delta_5 + \nu^2\gamma_1)\eta + (\beta_2 - \mathrm{i}\omega_0\beta_5)\eta^2\overline{\eta} \\ &+ \nu[(\Gamma_5 + \Gamma_3)\omega\alpha_3 + (\overline{\Gamma}_6 + \overline{\Gamma}_4)\omega\alpha_4 + (\Gamma_5 - \Gamma_3)\alpha_5 + (\overline{\Gamma}_6 - \overline{\Gamma}_4)\alpha_6]\,\eta z\overline{z} \\ &+ [\nu^2(\gamma_4 + \gamma_6) + \nu(\Gamma_6(\omega\alpha_3 + \alpha_5) + (\omega\alpha_4 + \alpha_6)\overline{\Gamma}_5)]\,\overline{\eta}z^2 + \mathrm{nrt}, \end{aligned} \tag{7.43}$$

where nrt stands for *nonresonance terms*. Two distinct cases must be considered now: for ω close to the fundamental frequency, or away from it.

The case of ω away from ω_0

Choosing g_2 to eliminate the resonance and near resonance terms in (7.43) yields

$$g_2 = (\mu\alpha_2\overline{\Gamma}_2 + \mu^2\delta_5 + \nu^2\gamma_1)\eta + (\beta_2 - \mathrm{i}\omega_0\beta_5)\eta^2\overline{\eta}. \tag{7.44}$$

Substituting (7.42) and (7.44) into (7.32), using the value of Γ_2 defined by (7.41) and assuming $\epsilon = 1$, the following normal form is obtained:

$$\dot{\eta} = \mathrm{i}\omega_0\eta + \mu\alpha_1\eta + \mu^2(\delta_5 - \frac{\mathrm{i}|\alpha_2|^2}{2\omega_0})\eta + \nu^2\gamma_1\eta + (\beta_2 - \mathrm{i}\omega_0\beta_5)\eta^2\overline{\eta}; \tag{7.45}$$

it is recalled that $\mu = u_0 - u_{cr}$ and α_i, β_i and γ_i are complex constants related to the coefficients of the original equations. Equation (7.45) indicates that the dynamics of the system is captured by a very simple equation: the first term represents the periodic solution due to the Hopf bifurcation, the second and third the effect of the unfolding parameter μ, at the first and second order, the fourth one takes into account the change of the constant flow velocity due to the perturbation, and finally, the last one represents the effects of the nonlinear terms. The normal form (7.45) to the first-order and with $\beta_5 = 0$ is in fact the same as already obtained in Chapter 3 — see equation (3.43). New terms arise at the second order.

<u>The case of ω near ω_0</u>

When $\omega \to \omega_0$, choosing h_2 to eliminate the nonresonance terms and approximating ω by ω_0, one obtains

$$\begin{aligned} g_2 &= (\mu\alpha_2\overline{\Gamma}_2 + \mu^2\delta_5 + \nu^2\gamma_1)\eta + (\beta_2 - \mathrm{i}\omega_0\beta_5)\eta^2\overline{\eta} \\ &+ \nu[(\Gamma_5+\Gamma_3)\omega_0\alpha_3 + (\overline{\Gamma}_6+\overline{\Gamma}_4)\omega_0\alpha_4 + (\Gamma_5-\Gamma_3)\alpha_5 + (\overline{\Gamma}_6-\overline{\Gamma}_4)\alpha_6]\ \eta z\overline{z} \\ &+ [\nu^2(\gamma_4+\gamma_6) + \nu(\Gamma_6(\omega_0\alpha_3+\alpha_5) + (\omega_0\alpha_4+\alpha_6)\overline{\Gamma}_5)]\ \overline{\eta}z^2, \end{aligned} \tag{7.46}$$

and hence, using (7.32), (7.41) and (7.42), the normal form

$$\begin{aligned} \dot{\eta} &= \mathrm{i}\omega_0\eta + \mu\alpha_1\eta + \mu^2(\delta_5 - \frac{\mathrm{i}|\alpha_2|^2}{2\omega_0})\eta + \nu^2\gamma_1\eta + (\beta_2 - \mathrm{i}\omega_0\beta_5)\eta^2\overline{\eta} \\ &- \frac{2\mathrm{i}\nu^2}{3\omega_0}\left[2\omega_0^2\alpha_4\overline{\alpha}_4 + \omega_0\alpha_4\overline{\alpha}_6 + \omega_0\alpha_6\overline{\alpha}_4 + 2\alpha_6\overline{\alpha}_6\right]\ \eta z\overline{z} \\ &+ \frac{\mathrm{i}\nu^2}{\omega_0}\ [-\mathrm{i}\omega_0(\gamma_4+\gamma_6) + (\omega_0\alpha_4+\alpha_6)(\omega_0(\alpha_3-\overline{\alpha}_3) + \alpha_5+\overline{\alpha}_5)]\ \overline{\eta}z^2 \end{aligned} \tag{7.47}$$

is obtained. It can be seen that in this case again, the effect of the sinusoidal perturbation of the flow velocity appears only at the second order, ν^2.

7.3.3.2 The case of ω near $2\omega_0$

If $\omega \to 2\omega_0$, it is not possible to eliminate $\overline{\eta}z$ because Γ_6 has a small divisor. It is thus included in g_1, now given by

$$g_1 = \mu\alpha_1\eta + [\nu(\alpha_6 + \omega\alpha_4) + \mathrm{i}\Gamma_6(2\omega_0 - \omega)]\overline{\eta}z. \tag{7.48}$$

To obtain g_1, the coefficients Γ_m, except Γ_6, have been chosen according to (7.41) so as to eliminate all nonresonance terms. Note that in (7.48), the constant Γ_6 is still arbitrary. Some additional clarifications are necessary on how it will be found. It should be recalled first that when $\epsilon = 0$, system (7.27) represents an oscillator with one degree of freedom. By introducing the change of coordinates $u = x_1$ and $v = \dot{u} = \omega_0 x_2$, it can be proved easily that the matrix $[J]$ in (7.11) and (7.27) can be transformed into the matrix $[J_0]$ defined by

$$[J_0] = \begin{bmatrix} 0 & 1 \\ -\omega_0^2 & 0 \end{bmatrix}. \tag{7.49}$$

This new matrix is the representation of the one degree-of-freedom oscillator $\{u, \dot{u}\}^{\mathrm{T}}$ satisfying the well-known equation $\ddot{u} + \omega_0^2 u = 0$. Consequently, because $x_1 = u$, it is equivalent to the displacement of the oscillator, while x_2 represents the velocity.

Having said that, the "displacement" x_1 may be evaluated. Substituting (7.31) into (7.28b) and using (7.39), one obtains, to the first order,

$$\begin{aligned} -\mathrm{i}\omega_0 x_1 &= \eta - \overline{\eta} + \epsilon[(\Gamma_1 - \overline{\Gamma}_2)\,\eta + (\Gamma_2 - \overline{\Gamma}_1)\overline{\eta} + (\Gamma_3 - \overline{\Gamma}_4)\eta z + \\ &\qquad (\Gamma_4 - \overline{\Gamma}_3)\overline{\eta}\,\overline{z} + (\Gamma_5 - \overline{\Gamma}_6)\eta\overline{z} + (\Gamma_6 - \overline{\Gamma}_5)\overline{\eta} z]. \end{aligned} \tag{7.50}$$

To uniquely define the amplitude of the fundamental frequency term, specified by $\eta - \overline{\eta}$ at $\mathcal{O}(\epsilon^0)$, the following relationships must therefore be satisfied:

$$\Gamma_1 = \overline{\Gamma}_2 \text{ and } \Gamma_6 = \overline{\Gamma}_5, \tag{7.51a}$$

which, with the aid of (7.41), yields

$$\Gamma_1 = \frac{-\mathrm{i}\mu\overline{\alpha}_2}{2\omega_0} \text{ and } \Gamma_6 = -\frac{\mathrm{i}\nu}{\omega}(\omega\overline{\alpha}_3 - \overline{\alpha}_5). \tag{7.51b}$$

Note that if one assumes, as is usually the case, that $\omega - 2\omega_0 = \mathcal{O}(\epsilon)$, then the last term in (7.48) can be neglected. However, if a second-order approximation is sought, it must be included, and the same procedure as for the fundamental frequency may then be employed to find g_2. When $\omega/\omega_0 = 2 + \epsilon\sigma$, where σ represents the detuning parameter (i.e. the perturbation from the resonant frequency), by choosing h_2 to eliminate the nonresonance terms and approximating ω with $2\omega_0$, one obtains

$$\begin{aligned} g_2 &= [\mu\alpha_2\overline{\Gamma}_2 + \mu^2\delta_5 + \nu^2\gamma_1]\eta + (\beta_2 - \mathrm{i}\omega_0\beta_5)\eta^2\overline{\eta} - \nu\Gamma_6(2\omega_0\alpha_4 + \alpha_6)\,\eta z\overline{z} \\ &+ \nu\,[2\omega_0(\Gamma_5 + \Gamma_3)\alpha_3 + 2\omega_0(\overline{\Gamma}_6 + \overline{\Gamma}_4)\alpha_4 + (\Gamma_5 - \Gamma_3)\alpha_5 + (\overline{\Gamma}_6 - \overline{\Gamma}_4)\alpha_6]\,\eta z\overline{z} \\ &+ [\mu(\Gamma_6\alpha_1 + \overline{\Gamma}_5\alpha_2 - \Gamma_6\overline{\alpha}_1) - \nu\Gamma_1(2\omega_0\alpha_4 + \alpha_6)]\overline{\eta} z, \end{aligned} \tag{7.52}$$

and hence the normal form

$$\begin{aligned}
\dot{\eta} &= \mathrm{i}\omega_0\eta + \mu\alpha_1\eta + \nu(\alpha_6 + \omega\alpha_4)\overline{\eta}z + (\beta_2 - \mathrm{i}\omega_0\beta_5)\eta^2\overline{\eta} \\
&+ \mu^2(\delta_5 - \frac{\mathrm{i}|\alpha_2|^2}{2\omega_0})\eta + \nu^2\gamma_1\eta + \frac{\mathrm{i}\nu^2}{4\omega_0}C_1\ \eta z\overline{z} \\
&+ \left[\mu\nu(\delta_2 + \delta_4) - \frac{\nu\sigma}{2}(2\omega_0\overline{\alpha}_3 - \overline{\alpha}_5) + \frac{\mathrm{i}\mu\nu}{\omega_0}C_2\right]\ \overline{\eta}z,
\end{aligned} \tag{7.53}$$

where C_1 and C_2 are complex constants, functions of ω_0 and the coefficients α_j. The first line in (7.53) represents the first-order approximation of the normal form of the problem at hand; it shows that only $\alpha_1, \alpha_4, \alpha_6, \beta_2$ and β_6 need to be "known" or computed to find the first-order approximation normal form. The last two lines take into account all second-order terms which are necessary if the parameters are far from the critical ones, or if the perturbation of the flow velocity is large. For the principal resonance, we shall assume that this is not the case, and only the first-order approximation will be studied in detail.

7.3.4 The principal parametric resonance

In this section, the principal parametric resonance is investigated when ω is close to $2\omega_0$. It will be seen that, starting with the first-order approximation of the normal form, a great deal of information can be obtained in closed form. Recalling that the purpose of this study is to get an overall picture of the dynamics rather than finding phenomena that exist in specific cases, only the most significant aspects will be considered, while the degenerate cases, such as values of the parameters for which two bifurcations occur simultaneously, will be ignored; these special points have been studied in detail by Guckenheimer & Holmes (1983) and by Namachchivaya & Ariaratnam (1987) for example. Only the key points of the analysis are presented here while the results are given in Section 7.6.

Introducing two real variables, r and ϕ, it is easy to put the first-order approximation represented by the first line of (7.53) into real form. Furthermore, to render the equation as general as possible, a new nondimensional time is introduced, $\tau' = \omega_0\tau$, so that the solution now has a periodicity of 2π. With $z = \exp(\mathrm{i}\omega\tau)$, η may be assumed to be of the form

$$\eta = r \exp\left[\mathrm{i}(\frac{\omega}{2}\tau + \phi)\right], \tag{7.54}$$

which leads to

$$\begin{aligned} \omega_0 \dot{r} = \; & \mu\mathcal{R}(\alpha_1)r + \mathcal{R}(\beta_2 - \mathrm{i}\omega_0\beta_5)r^3 \\ & \qquad + \nu r[\mathcal{I}(\alpha_6 + \omega\alpha_4)\sin 2\phi + \mathcal{R}(\alpha_6 + \omega\alpha_4)\cos 2\phi], \\ \frac{\omega}{2} + \omega_0\dot{\phi} = \; & \omega_0 + \mu\mathcal{I}(\alpha_1) + \mathcal{I}(\beta_2 - \mathrm{i}\omega_0\beta_5)r^2 \\ & \qquad + \nu[\mathcal{I}(\alpha_6 + \omega\alpha_4)\cos 2\phi - \mathcal{R}(\alpha_6 + \omega\alpha_4)\sin 2\phi], \end{aligned} \tag{7.55}$$

where differentiation is now with respect to nondimensional time τ' and where $\mathcal{R}(\;)$ and $\mathcal{I}(\;)$ represent, respectively, the real and the imaginary part of the quantity in parentheses. Introducing the constants $V_r = \mathcal{R}(\alpha_6 + \omega\alpha_4)/\omega_0, V_i = \mathcal{I}(\alpha_6 + \omega\alpha_4)/\omega_0$, $a = \mathcal{R}(\beta_2 - \mathrm{i}\omega_0\beta_5)/\omega_0, b = \mathcal{I}(\beta_2 - \mathrm{i}\omega_0\beta_5)/\omega_0, c = \mathcal{I}(\alpha_1)/\omega_0$, $d = \mathcal{R}(\alpha_1)/\omega_0$ and the detuning parameter $\sigma = (\omega - 2\omega_0)/\omega_0$, equations (7.55) become

$$\begin{aligned} \dot{r} = \; & d\mu r + ar^3 + \nu r(V_i \sin 2\phi + V_r \cos 2\phi), \\ \dot{\phi} = \; & -\frac{\sigma}{2} + c\mu + br^2 + \nu(V_i \cos 2\phi - V_r \sin 2\phi); \end{aligned} \tag{7.56}$$

they represent the parametric perturbation of the Hopf bifurcation. To simplify the algebra as much as possible, two new parameters are introduced, θ and η, as well as the Cartesian coordinates v_1 and v_2: with $\tan 2\theta = V_i/V_r$, $\eta = \sqrt{V_r^2 + V_i^2}$, $v_1 = r\cos(\phi + \theta)$ and $v_2 = r\sin(\phi + \theta)$, the equations to be studied become

$$\begin{aligned} \dot{r} = \; & d\mu r + ar^3 + \nu r\eta \sin 2(\phi + \theta), \\ \dot{\phi} = \; & -\frac{\sigma}{2} + c\mu + br^2 + \nu\eta\cos 2(\phi + \theta), \end{aligned} \tag{7.57a}$$

or, in Cartesian form,

$$\begin{Bmatrix} \dot{v}_1 \\ \dot{v}_2 \end{Bmatrix} = \begin{bmatrix} d\mu & \eta\nu - (c\mu - \frac{\sigma}{2}) \\ \eta\,\nu + (c\mu - \frac{\sigma}{2}) & d\mu \end{bmatrix} \begin{Bmatrix} v_1 \\ v_2 \end{Bmatrix} + \begin{Bmatrix} (av_1 - bv_2)(v_1^2 + v_2^2) \\ (bv_1 + av_2)(v_1^2 + v_2^2) \end{Bmatrix} \tag{7.57b}$$

Because these equations have been analysed in detail by Bajaj (1984, 1986) and Namachchivaya & Ariaratnam (1987), it is not necessary to repeat this work here. The procedure is straighforward: first, the stability of the origin is investigated using the linearized part of (7.57b) around the origin; then, non-zero solutions or fixed points are sought using (7.57a), and their stability examined. It can be proved that the origin of the reduced system loses stability either by a Hopf or by a pitchfork bifurcation depending on the parameters, except at one point where a double zero eigenvalue occurs, and that there exist *at most* two non-zero solutions, referred to as r_0^+ and r_0^-, with the smallest one r_0^- being always unstable (Namachchivaya & Ariaratnam 1987). Moreover, depending on the parameters, the stable fixed point r_0^+ may lose stability through a Hopf bifurcation. From a physical point of view, a stable (resp. unstable) non-zero fixed point in the reduced system represents a stable (resp. unstable) periodic solution of frequency $\omega/2 \simeq \omega_0$ in the original system, and the loss of stability of a fixed point through a Hopf bifurcation may lead to quasiperiodic motions. Finally, Bajaj (1984, 1986) showed also that in addition to "usual" jump responses, the system also exhibits stable and unstable isolated solution branches. This will also be discussed here, but only major results are given, with the emphasis put on the comparison between the results obtained using the normal form theory (i.e. on the reduced two-dimensional system) and the original equations, because this has apparently never been undertaken before.

7.3.5 The fundamental parametric resonance

The same procedure as for the principal resonance can be employed here, except that one needs to consider the normal form correct to the second-order. In polar coordinates, η may now be expressed as

$$\eta = r\exp[\mathrm{i}(\omega\tau + \phi)]. \tag{7.58}$$

Separating the real and imaginary parts, equation (7.47) becomes

$$\begin{aligned} \dot{r} = &\ (d\mu + C_r^1\mu^2 + C_r^2\nu^2)r + ar^3 + \nu^2 r(V_i\sin 2\phi + V_r\cos 2\phi), \\ \dot{\phi} = &\ (-\sigma + c\mu + C_i^1\mu^2 + C_i^2\nu^2) + br^2 + \nu^2(V_i\cos 2\phi - V_r\sin 2\phi), \end{aligned} \tag{7.59}$$

where a, b, c and d have the same definition as before, the detuning parameter is now defined by $1+\sigma = \omega/\omega_0$, and the subscripts r and i refer to the real and the imaginary part, respectively; the other coefficients are defined by $C^1 = \delta_5/\omega_0 - |\mathrm{i}\alpha_2|^2/2\omega_0^2$, $C^2 = \gamma_1/\omega_0 - 2\mathrm{i}\left[2\omega_0^2\alpha_4\overline{\alpha}_4 + \omega_0\alpha_4\overline{\alpha}_6 + \omega_0\alpha_6\overline{\alpha}_4 + 2\alpha_6\overline{\alpha}_6\right]/(3\omega_0^2)$, and $V = (\gamma_4+\gamma_6)/\omega_0 + \mathrm{i}/\omega_0^2(\omega_0\alpha_4+\alpha_6)(\omega_0(\alpha_3-\overline{\alpha}_3)+\alpha_5+\overline{\alpha}_5)$. These equations have the same structure as in the case of the principal resonance, except that ν appears at the second-order and that the linear matrix is slightly modified. Consequently, the methodology to be used is the same. Results will be given in Section 7.6.

7.4 NUMERICAL METHODS

In this section, the different numerical methods employed are described briefly. A detailed presentation can be found in Chapter 5. The purpose is to obtain accurate numerical solutions of the full system of equations, against which the results of the reduced system on the centre manifold may be compared.

7.4.1 The Perturbation Method

This method combines an order analysis and a standard numerical method and has been discussed previously in Chapter 3. The main idea is to assume that the lateral displacement η is small compared to unity, i.e. $\eta = \mathcal{O}(\epsilon)$, and to find an equivalent term for the nonlinear inertial terms. In other words, differentiating the linear equation with respect to ξ, multiplying by η' and integrating the result between 0 and ξ, one can find an equivalent term to $\int_0^\xi \eta'\,\ddot{\eta}'\,d\xi$. Replacing this term in (7.1) leads to a set of second-order differential equations that does *not* contain nonlinear inertial terms; the inertial nonlinearities are converted into equivalent stiffness and damping nonlinear terms. This set of equations can thereafter be put into first-order form, and the resulting equations integrated numerically using well-known methods such as the Runge-Kutta one. In order to find (dynamically) stable and unstable solutions, it may be useful to use other methods as well. AUTO (Doedel & Kernéves 1986), which is based on a collocation method, is the ideal tool for that. In order to introduce the forcing frequency into the scheme (because AUTO assumes the system to be in *autonomous* form), it is possible to couple a nonlinear oscillator of the type

$$\begin{aligned}\dot{u} &= u + \omega v - u(u^2 + v^2), \\ \dot{v} &= -\omega u + v - v(u^2 + v^2)\end{aligned} \tag{7.60}$$

to the original equation; again, ω is the forcing frequency [note the analogy with the oscillator (7.14)]. Of course, the system of equations to be solved then becomes of dimension $2N + 2$.

7.4.2 The Finite Difference Method (FDM)

To solve the original set of equations (7.5) directly, together with the time-dependent matrices (7.6), Houbolt's finite difference method may be used (Houbolt 1950). This method has been shown to be more effective than higher-order finite difference schemes (Jones & Lee 1985), yet to still have good accuracy. The derivatives at time $\tau + \Delta\tau$ are replaced by backward difference formulae using values at three previous time steps $\Delta\tau$. Hence,

$$\begin{aligned}\ddot{q}_j(\tau + \Delta\tau) &= [2q_j(\tau + \Delta\tau) - 5q_j(\tau) + 4\,q_j(\tau - \Delta\tau) - q_j(\tau - 2\Delta\tau)]/(\Delta\tau)^2, \\ \dot{q}_j(\tau + \Delta\tau) &= [11q_j(\tau + \Delta\tau) - 18q_j(\tau) + 9\,q_j(\tau - \Delta\tau) - 2q_j(\tau - 2\Delta\tau)]/(6\,\Delta\tau).\end{aligned} \tag{7.61}$$

Substituting (7.61) into (7.5) leads to a set of nonlinear algebraic equations of the type

$$F_i[q_j(\tau + \Delta\tau),\ q_j(\tau),\ q_j(\tau - \Delta\tau),\ q_j(\tau - 2\Delta\tau)] = 0, \quad 1 \le i, j \le N, \tag{7.62}$$

in which $q_j(\tau + \Delta\tau)$ are the unknowns. To solve equation (7.62), a Newton-Raphson technique is employed, where the initial guess for $q_j(\tau + \Delta\tau)$ is taken equal to its predecessor, $q_j(\tau)$. Note that the Newton-Raphson method requires the computation of the Jacobian of F, $DF_i/Dq_j(\tau + \Delta\tau)$. This can be obtained easily from (7.5) and (7.6). The validity of the FDM method was confirmed by comparing the results to those obtained with (i) a fifth-order adaptive step-size Runge-Kutta scheme in cases where the system of equations could be recast into a set of first-order ODEs and (ii) with the Incremental Harmonic Balance method, presented in the next section. Excellent agreement was found in all cases and it was shown that a time step $\Delta\tau = T/250$, where T is the period of oscillation, was an optimal value in terms of both numerical accuracy and efficiency. The advantage of the FDM over the Runge-Kutta scheme is that no approximation needs to be made to the original equation since the N second-order ODEs can be integrated directly.

7.4.3 The Incremental Harmonic Balance method

The Incremental Harmonic Balance method (IHB) has been developed by Lau to treat strong nonlinearities (Lau *et al.* 1982) and to take into account multiple harmonic components in the system response. It was successfully applied to various types of nonlinear structural systems and dry-friction damper problems (Pierre *et al.* 1985). The method finds periodic solutions $\mathbf{x}^*$ of equations of the type

$$\mathbf{f}(\mathbf{x}, \Omega\,\dot{\mathbf{x}}, \Omega^2\,\ddot{\mathbf{x}}, \lambda, \tau) = \mathbf{0}, \tag{7.63}$$

where Ω is the frequency of the periodic solution, λ is a free parameter to be varied, and $\mathbf{f}$ represents a set of implicit second-order nonlinear ODEs (this includes the case of first-order systems that may be treated equally well). The nondimensional time τ has been chosen in such a way that the solution of (7.63) has a period of 2π. Two steps are necessary to solve the problem: (i) a perturbation or an incrementation of the solution from some initial guess of the solution of (7.63) using a Taylor series; (ii) a Galerkin procedure, where the solution $\mathbf{x}$ and the increments $\Delta\mathbf{x}$ are expanded in a *finite* Fourier series and where the error arising from the assumption that the space is finite is minimized. Ferri (1986) showed that the order to which these two steps are performed is not important: the resulting algebraic equations are the same in either case.

Consequently, a Newton-Raphson procedure is first carried out, using a Taylor series expansion. Starting from a known solution $(\mathbf{x}_0, \Omega_0, \lambda_0)$ of an equation $\mathbf{f}_0$, a neighbouring solution is reached through a parameter incrementation:

$$\mathbf{x} = \mathbf{x}_0 + \Delta\mathbf{x}, \quad \Omega = \Omega_0 + \Delta\Omega, \quad \lambda = \lambda_0 + \Delta\lambda. \tag{7.64}$$

Substituting relations (7.64) into (7.63) and neglecting the nonlinear terms in $\Delta\mathbf{x}, \Delta\Omega, \Delta\lambda$, a linearized incremental equation is obtained

$$\mathbf{f}_0 + \left.\frac{\partial \mathbf{f}}{\partial \mathbf{x}}\right|_0 \Delta\mathbf{x} + \left.\frac{\partial \mathbf{f}}{\partial \dot{\mathbf{x}}}\right|_0 \Delta\dot{\mathbf{x}} + \left.\frac{\partial \mathbf{f}}{\partial \ddot{\mathbf{x}}}\right|_0 \Delta\ddot{\mathbf{x}} + \left.\frac{\partial \mathbf{f}}{\partial \Omega}\right|_0 \Delta\Omega + \left.\frac{\partial \mathbf{f}}{\partial \lambda}\right|_0 \Delta\lambda = \mathbf{0}. \tag{7.65}$$

This equation is an N-dimensional second-order linear ODE with time-dependent coefficients. A periodic solution is then sought of the form

$$x_{0,k} = b_{k0} + \sum_{j=1}^{\mathrm{NH}} (a_{kj} \sin j\tau + b_{kj} \cos j\tau), \tag{7.66}$$

where NH represents the number of harmonics. By differentiation, it is easy to obtain $\dot{\mathbf{x}}_0$ and $\ddot{\mathbf{x}}_0$ as well, and similarly the increments can also be expanded as a Fourier series. Using Galerkin's method, the error occurring from the projection of the solution on a *finite* dimensional space is then minimized, which leads to a set of algebraic equations that can be solved easily [see Chapter 5 for the complete derivation]. In practice, to decrease the computational time, the Fourier coefficients are obtained via a Fast Fourier Transform (FFT) algorithm, as shown by Ling & Wu (1987) and Cameron & Griffin (1989).

7.5 EXPERIMENTAL INVESTIGATION

The apparatus used for the experiments is similar to the one used previously by Païdoussis & Issid (1976) and involves the addition of a harmonic component to the flow with the aid of a plunger pump at a T-junction, through the main leg of which the mean flow is supplied. The water flow, properly straightened, is then supplied to the vertical test pipe, which is cast in our laboratory with Silastic RTV (which ensures nearly perfect straightness). However, some modifications were introduced *vis-à-vis* the apparatus described in Païdoussis & Issid (1976): (i) the flow is supplied from recirculating pumped water, passing through an accumulator tank with an air cushion to attenuate pulsations from the pump; (ii) the mass-flow rate is measured with an Omega FMG-700 magnetic flowmeter connected to an Omega DPF60 ratemeter, enabling faster and more accurate readings of flow-rate; (iii) the motion of the pipe is sensed by an Optron 860 and 806a optical tracking system, and the signal is analysed by a FFT analyzer or stored on disk via a Nicolet 310 digital oscilloscope; (iv) the periodic perturbation amplitude and frequency are no longer determined via a hot film anemometer but by a PX26-030GV pressure transducer: using the pressure reading and the magnetic flow meter, it is easier to obtain a reliable parabolic calibration curve of pressure as a function of flow velocity; the value of ν is thence simply obtained by measuring the amplitude of the oscillating pressure and by converting it through solving a second order equation; (v) the damping (logarithmic decrement δ) in the first three modes is measured by impact tests which involve plotting the time response of each mode on a log-scale. A schematic of the setup is shown in Figure 7.2.

Two experimental procedures are followed to determine the dynamics of the system. The first is the same as that followed by Païdoussis & Issid (1976): after calibration of the pressure transducer, the steady flow rate is kept constant, and with the stroke of the plunger pump fixed, the frequency of the pulsation is gradually increased until a change in the dynamic behaviour of the pipe is observed, in which case traces of the flow pressure are recorded, yielding the values of ν and ω. The stroke is subsequently changed and the procedure repeated. The main problem encountered is that at a fixed stroke, the parameter ν is not constant: depending on the frequency, the value of ν can either increase or decrease, repeatably but with no *a priori* predictable manner. In the second procedure, the forcing frequency ω is kept constant while either the mean flow velocity u_0 or the stroke is varied. This second method is slower, but yields more accurate results.

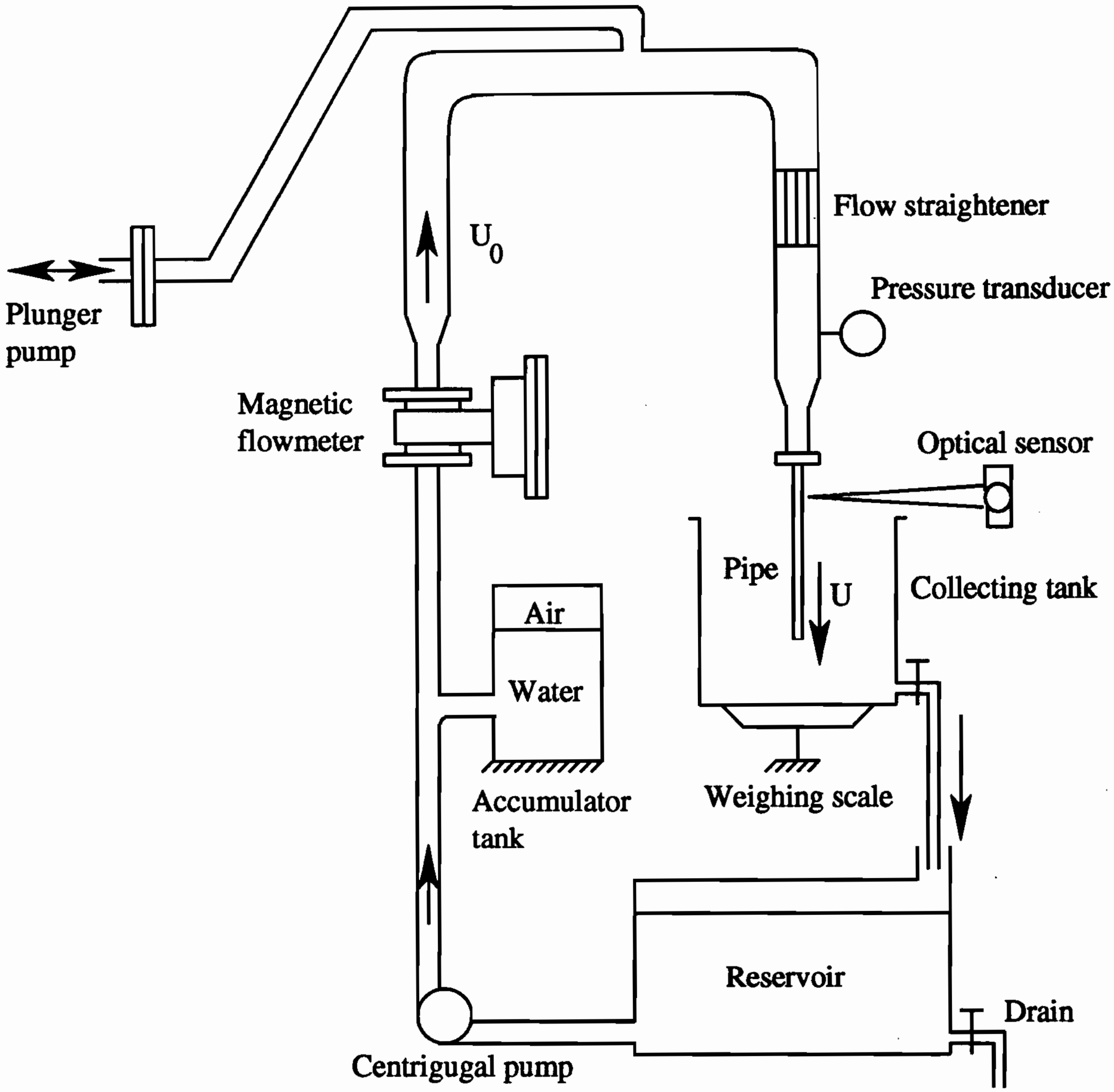

Figure 7.2: Schematic of the experimental system used; the main recirculating system provides a steady mean flow, perturbed by the oscillating flow component generated by a plunger pump.

Different types of motion are observed, as follows:

(a) the pipe is stationary and the system stable;

(b) the pipe performs limit cycle oscillations of large amplitude, with a pulsation frequency equal to twice the oscillation frequency; this corresponds to the principal or primary resonance in the second mode and is very easy to pin-point;

(c) the motion is quasiperiodic, with two frequencies in the power spectrum, typically only for flow velocities higher than the critical, u_{cr};

(d) the pipe is almost stationary, performing very small oscillations around the equilibrium (amplitude less than a diameter), with a frequency equal to the forcing frequency; this motion probably corresponds to the fundamental parametric resonance, but it is very difficult to decide when its onset occurs;

(e) in some isolated cases, the pipe oscillates about a quasi-stationary deflected shape; this occurs only for high values of ν ($\nu > 0.6$);

(f) when the value of the flow perturbation is high (again $\nu > 0.6$), the oscillation is not planar anymore and becomes chaotic, with the pipe hitting the edges of the collecting tank.

As already discussed by Païdoussis & Issid (1976), the experiments have certain limitations: (i) at low and at high strokes of the plunger pump, the accuracy in determining the oscillating pressure decreases; (ii) at high strokes, motions of the pipe are not planar anymore, and the pressure, though periodic, is no longer sinusoidal; (iii) because of the limitations of the pump, the mean flow velocity is not constant in the presence of the pulsation, but decreases slightly (approximately 3% when $\nu = 0.3$); (iv) the pipe dimension may change due to the pressurization associated with the pulsating flow, especially when the wall thickness is small, which explains why for the pipes used in these experiments, the mass parameter β is small ($\beta < 0.2$). For these reasons, and because the nonlinear terms play an important role in the dynamics only for large amplitudes, the experimental results to be presented are associated with the principal resonance only.

7.6 RESULTS

The system under consideration depends on many parameters. For this reason, and because of space limitations, only the most significant results will be presented to illustrate the behaviour of the system.

7.6.1 Theoretical results for $u < u_{cr}$

The principal primary region associated with the second mode represents by far the largest region of the parametric resonance for the cantilevered pipe (Païdoussis & Issid 1974). Therefore, this case will be considered first. The regions of parametric instabilities (in the linear sense) can be found easily, by using either the IHB method or AUTO and the results compared to those obtained through the normal form theory.

In the first case, a periodic solution is sought for a certain parameter μ (i.e. assuming a constant flow velocity, u_0) by seeking a corresponding solution $(q_j^* + \Delta q_j, \Omega^* + \Delta \Omega)$. Once this solution is found, an incrementation sequence in ν is started, by looking for a neighbouring solution $\nu + \Delta\nu$, $q_j^* + \Delta q_j$, $\Omega^* + \Delta\Omega$. The procedure is repeated until (i) a pre-determined value of ν is reached, or (ii) no convergence is achieved (this arising in the case of a turning point in the (ν, Ω) plane, in which case the Ω-incrementation is started).

In the second case, AUTO can vary any of the system parameters to compute bifurcation diagrams. Therefore, the forcing frequency ω is introduced as a parameter in the equation of motion, through equation (7.60). Starting the procedure, zero is the solution of the first $2N$ first-order equations, while $u = \sin\omega\tau$ and $v = \cos\omega\tau$ are the solutions of the last two. To detect bifurcations, AUTO then computes the Floquet multipliers λ of the system of $2N + 2$ ODEs as the forcing frequency ω is varied. If λ crosses the unit circle at -1, a period-doubling bifurcation occurs: it corresponds to finding a new periodic solution of frequency $\Omega = \frac{1}{2}\omega$, or to the principal resonance. If λ crosses the unit circle at $+1$, the bifurcation point is a branch point: it corresponds to the existence of another periodic solution having the same frequency as the forcing frequency ω, or to the fundamental resonance.

The full line in Figure 7.3 shows such a curve, for the system parameters $\beta = 0.2, \gamma = 10, \alpha = 0, u_0 = 6$, the same as used previously by Païdoussis & Sundararajan (1975). This represents the case where the steady flow velocity u_0 is below but close to the critical velocity, u_{cr}, for flutter: $u_{cr} = 6.35$ for $N = 3$, and $u_{cr} = 6.31$ for $N = 4$.

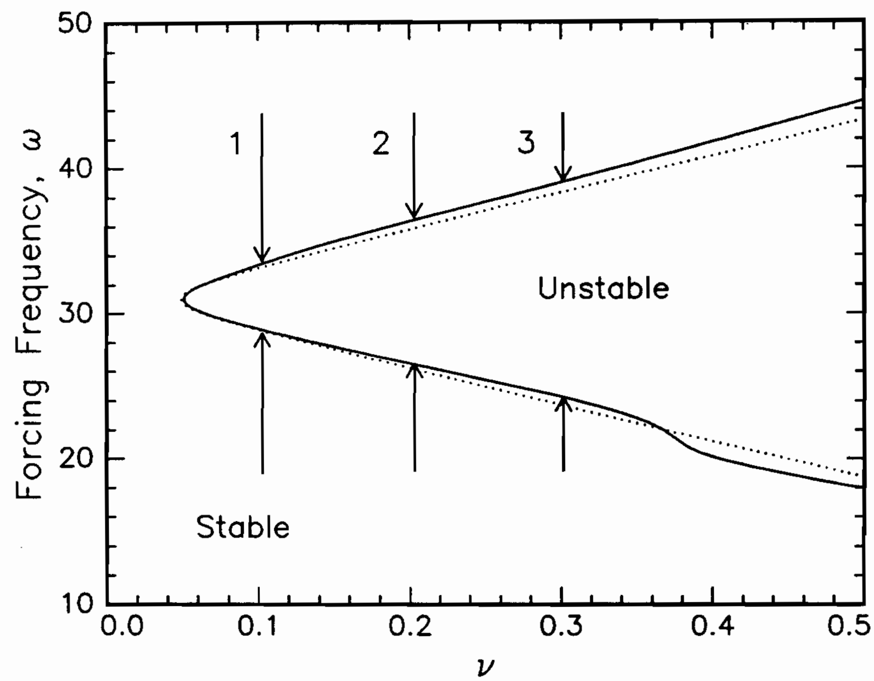

Figure 7.3: Boundaries of the principal parametric resonance in the second mode, for $u_0 = 6$, $\beta = 0.2$, $\gamma = 10$ and $\alpha = 0$: —, IHB and AUTO; $\cdots\cdot$, normal form theory.

In the outer region denoted by 'stable', all orbits starting in the neighbourhood of the origin converge to the zero solution: the zero-solution is *locally* stable. On the contrary, in the inner region, orbits diverge exponentially from the origin. Finally, on the boundary, there exists a periodic solution of frequency $\Omega = \frac{1}{2}\omega$, its amplitude being determined by the initial conditions. This is the well-known linear theory, as developed by Bolotin (1964).

The same results can be obtained using the normal form theory developed in Section 7.3. For the same parameters, the normal form corresponding to the principal resonance is given by (7.57a) or (7.57b). The values of the different coefficients can be found in Table 7.1, for $N = 2, 3$ and 4.

	$10^4 \times a$		$10^5 \times b$		$10^3 \times c$	d	η	θ
	NLI	Tr	NLI	Tr				
N=2	-1.039	-2.032	3.691	27.70	-44.9	0.0783	0.486	0.118
N=3	-1.290	-1.834	3.147	12.28	6.25	0.0651	0.400	0.114
N=4	-1.461	-1.832	3.408	10.58	1.33	0.0610	0.427	0.738

Table 7.1: Comparison of the coefficients of the normal form defined by (7.57a) for different number of modes, N. For the nonlinear coefficients a and b, two cases are considered: when the nonlinear inertial terms are kept in their original form (NLI), or when they are transformed (Tr)

From Table 7.1, the following may be noted.

(i) The values of η, which represents the effects of the amplitude of the pulsation in the normal form, are very close to each other for $N = 2, 3$ and 4, which means that the effects of the pulsation on the normal form, defined on the centre manifold, is not very sensitive to the number of modes used. This is very important because it means that in practice only a few modes are necessary to extract the essence of the dynamics.

(ii) There are some obvious discrepancies between the coefficients representing the nonlinear terms (a and b) for the two cases considered (NLI and Tr). This will be discussed later when the effects of the nonlinear terms will be analysed.

(iii) There are also some discrepancies in the value of c, but this coefficient does not have a large influence because $c\mu$ is usually much smaller than σ [see equation (7.57b)].

(iv) The coefficients a and b seem rather small: this arises from the normalization process that takes place through equation (7.28b) and, therefore, these coefficients should not be taken as "absolute" values. What is important is the relative value of one with respect to the other.

(v) Finally, it should be mentioned that the same results were obtained with the method of averaging, which gives additional confidence in the method. However, the computational time is smaller for the normal form method as compared to the method of averaging, because there is no need to perform any integration. This justifies the preliminary work undertaken in Section 7.3.3.

From equation (7.57b), the linear instability curves are simply given by two equations:

$$d\mu = 0 \tag{7.67a}$$

corresponds to the loss of stability of the origin through a Hopf bifurcation, and

$$(d\mu)^2 + (c\mu - \sigma/2)^2 - (\nu\eta)^2 = 0 \tag{7.67b}$$

to the loss of stability through a pitchfork bifurcation. The first condition is straightforward and since $d > 0$ in all cases, the stability is simply determined by μ: if $\mu < 0$ (or > 0) the origin is stable (respectively unstable). The second condition, (7.67b), belongs to a family of conic sections that may be drawn easily by keeping one of the parameters constant. Remembering that equations (7.57a) and (7.57b) have the same structure when computed by the normal form theory or the method of averaging, it is clear that the loss of stability in the "averaged" equations is related to the loss of stability in the original equation: the appearance of a non-zero fixed point through a pitchfork bifurcation corresponds to the appearance of a periodic solution of frequency $\frac{1}{2}\omega = \omega_0$ in the original system, while the solution after a Hopf bifurcation in the averaged equations will be on a two-dimensional torus and can therefore be quasiperiodic. The solution of (7.67b) has been computed for the same parameters and is shown in Figure 7.3 (dotted line) for $N = 3$. Because $\mu < 0$, equation (7.67a) is of no interest, except to say that, for values of the parameters (σ, ν) out of the parabola, the system is stable. As can be seen, the analytical results agree very well with the numerical ones, except for the lower part of the curve at high ν, where higher order harmonics may play an important role. The discrepancy in such a case is expected, because in the normal form theory the solution sought has only one harmonic component, as suggested by (7.54). Nevertheless, for small detuning parameters (μ, ν and σ), the normal form method is a remarkably effective tool because stability diagrams in two or even three dimensions can be constructed very easily. This will be seen in greater detail later.

It is now interesting to investigate what happens to the instability from a ***non-linear*** point of view. For that purpose, the existence of a periodic solution with a non-zero amplitude is first sought *numerically* for different values of ν. Three cases are investigated in detail (cases 1, 2 and 3 corresponding to $\nu = 0.1$, 0.2 and 0.3, as marked in Figure 7.3), each for three different approximations: (i) with the nonlinear inertial terms ignored completely and the solution computed both with AUTO and the IHB method; (ii) with the nonlinear inertial terms eliminated using the perturbation method, and the solution found again using both AUTO and IHB; (iii) with the non-linear inertial terms kept in their original form, and the solution obtained using the IHB method.

The results are presented in Figure 7.4 which shows a cross-section of the (ν, ω) plane for the three different values of ν. Dashed lines represent unstable solutions. Several observations can be made.

(i) As expected, the amplitude of the limit cycle increases with ν, as observed experimentally. Therefore, the nonlinear terms will have a more profound influence for larger ν (e.g. for $\nu = 0.3$, curve 3).

(ii) Having said that, it is obvious that the discrepancies between the three approaches will also increase with ν; e.g., for $\nu = 0.1$, the amplitudes are fairly close, while for $\nu = 0.3$, the nonlinear inertial terms have a much larger effect, increasing the amplitude by as much as 50%.

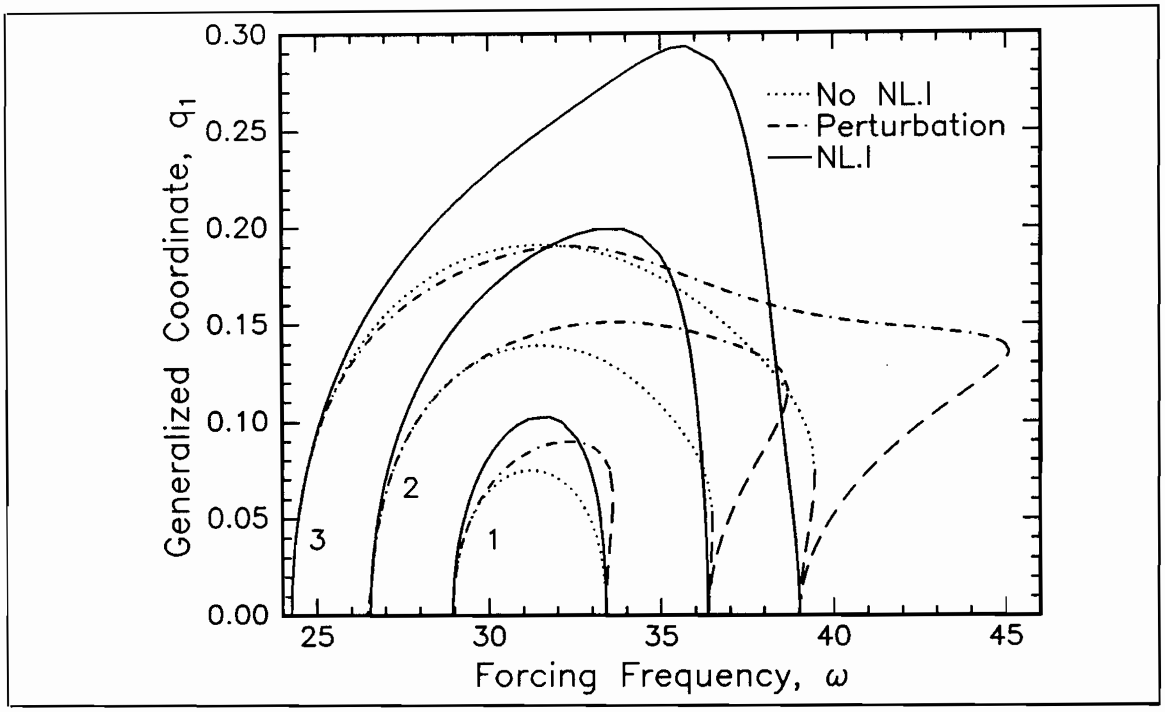

Figure 7.4: Amplitude of the periodic solutions for $\nu = 0.1, 0.2, 0.3$ (marked as curves 1, 2 and 3) using three different approximations, for the same parameters as in Figure 7.3: —, with all nonlinear inertial terms intact, as obtained by the IHB method; – —·— –, with inertial nonlinearities transformed, as obtained by the perturbation method and AUTO; · · · ·, with all nonlinear inertial terms eliminated, as obtained by AUTO and the IHB method. The dashed line (– – –) represents unstable solutions.

(iii) In all three cases, a portion of the solution obtained by the perturbation method is unstable, to an extent increasing with ν, while the other two methods do not predict this type of behaviour — except when ν becomes large and the nonlinear inertial terms are neglected. The existence of such an unstable solution implies hysteresis in an experiment, which means that the stability boundary is in fact *larger* than the boundary found from the linear theory. The conclusion that can be drawn is that the use of the perturbation method in this case may lead to qualitatively different (erroneous) results.

(iv) The curves are not symmetric and the asymmetry increases with ν (hence with the amplitude), which is another characteristic of nonlinear systems.

(v) Finally, the nonlinear inertial terms tend to increase the amplitude of oscillation.

To validate the results obtained numerically, it was decided to compute also the solutions for $\nu = 0.3$ by direct integration using the FDM. Moreover, these results are compared to those obtained with the normal form theory for two different cases: when the nonlinear inertial terms are completely ignored (no NLI) and when they are kept in their original form (NLI).

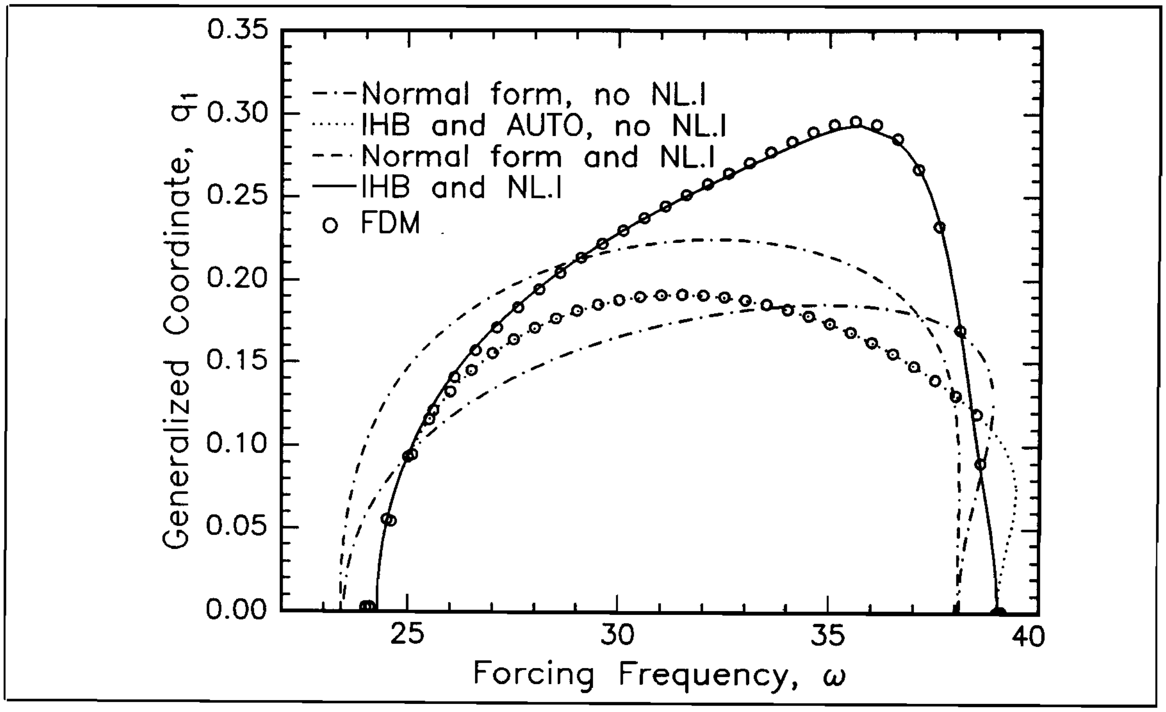

Figure 7.5: Comparison between IHB, FDM and the normal form theory for $\nu = 0.3$, with and without nonlinear inertial terms, for the system of Figures 7.3 and 7.4: —, with all nonlinear inertial terms intact, as obtained by the IHB method; $\cdot\cdot\cdot\cdot$, with all nonlinear inertial terms eliminated, as obtained by AUTO and the IHB method; — — · — —, with all nonlinear inertial terms intact, as obtained by the normal form method; —·—, with all nonlinear inertial terms eliminated, as obtained by the normal form method; o, solution by FDM.

From Figure 7.5, some important points may be raised, as follows.

(a) For the results obtained *numerically*, i.e. with IHB, AUTO and FDM, excellent agreement is obtained both with and without nonlinear inertial terms. Furthermore, it must be mentioned that the FDM (and also Runge-Kutta schemes) can only yield *stable* solutions. Hence, for periodic solutions, both the IHB method and AUTO are superior to direct numerical integration, since *unstable* solutions can be computed as well. Moreover, the Floquet multipliers give some insight into the change in dynamics, i.e. bifurcations can also be detected.

(b) The results obtained with the normal form method agree *qualitatively* well with those obtained numerically: stable and unstable solutions are found in the case where the nonlinear inertial terms are ignored, while only a unique solution is found when they are taken into account. Moreover, normal form theory predicts that the maximum value for q_1 is greater when the nonlinear inertial terms are present, which again is in agreement with the numerical analysis results.

(c) The onset of instability and restabilization on the ω-axis is predicted to be lower by the normal form than by the numerical methods. This is consistent with the results obtained by the linear theory in Figure 7.3.

In conclusion, for flow velocities below u_{cr}, the normal form theory predicts well, both qualitatively and quantitatively, the dynamics of the system.

7.6.2 Theoretical results for $u > u_{cr}$

The case where the flow velocity is above the critical is investigated next. Again, the system parameters are the same as those used by Païdoussis & Sundararajan (1975), with $u_0 = 6.5$ (figure 4 of their paper), i.e. $u_0 > u_{cr} = 6.34$. The two regions of *parametric* resonance were obtained easily, and hence are not reproduced here. Of more interest is what happens with the regions of *combination* resonance. For $\nu = 0.3$, the equations of motion (7.5) were integrated using the FDM, with the nonlinear inertial terms included. The results are plotted in Figure 7.6.

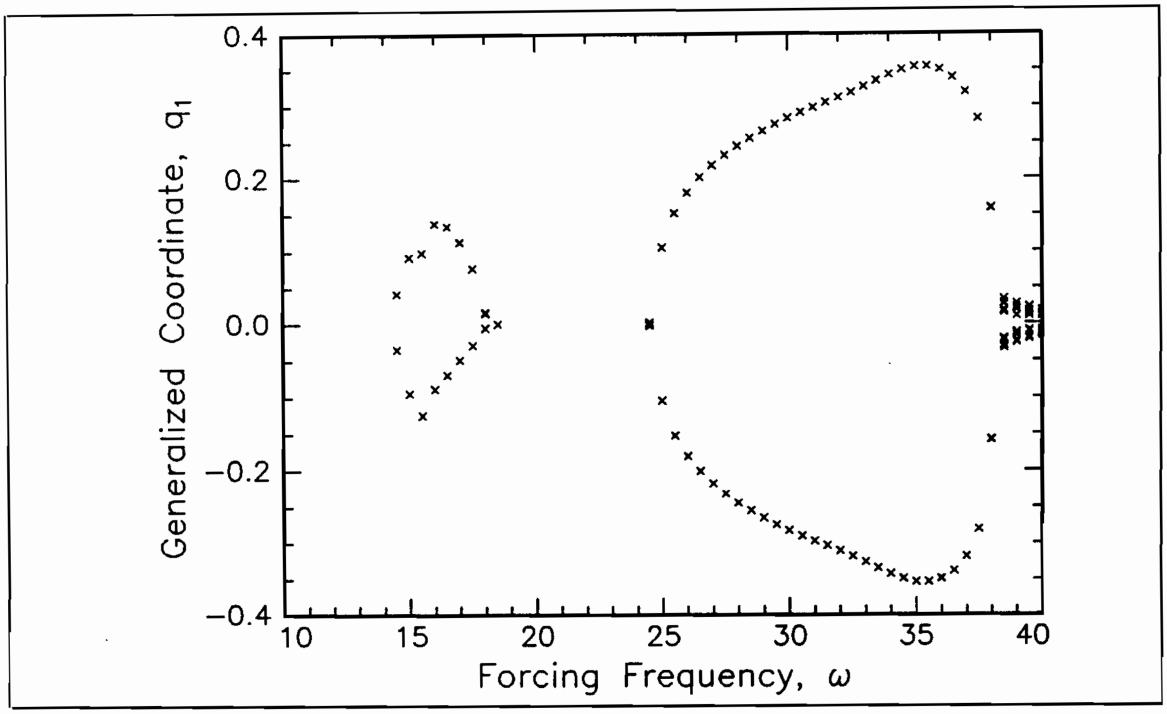

Figure 7.6: Bifurcation diagram illustrating the principal and secondary parametric resonances, for the same system, with $\nu = 0.3$ and $u_0 = 6.5$, obtained using the FDM.

It can be seen that the primary and secondary parametric resonances are obtained, occurring at $24.5 < \omega < 38$ and $14.5 < \omega < 18$, respectively. Looking at the bifurcation diagram, it can be seen that the maximum amplitude for the primary resonance is symmetric under the transformation $q_1 \rightarrow -q_1$, while this is not the case for the secondary resonance. This is also shown in Figure 7.7(a, b). For the principal resonance, the solution can be expressed as a Fourier series with only *odd* terms, while for the secondary resonance, *even* terms have to be included, hence containing a non-zero constant term.

Moreover, looking at the bifurcation diagram, it can be seen that for $\omega < 14.5$ and $18 < \omega < 24.5$, the system is stable, i.e. it converges to the zero-equilibrium. This was also observed by Païdoussis & Sundararajan (1975), except that they also found combination resonances for $\omega < 6$. This is not the case here. The time response for

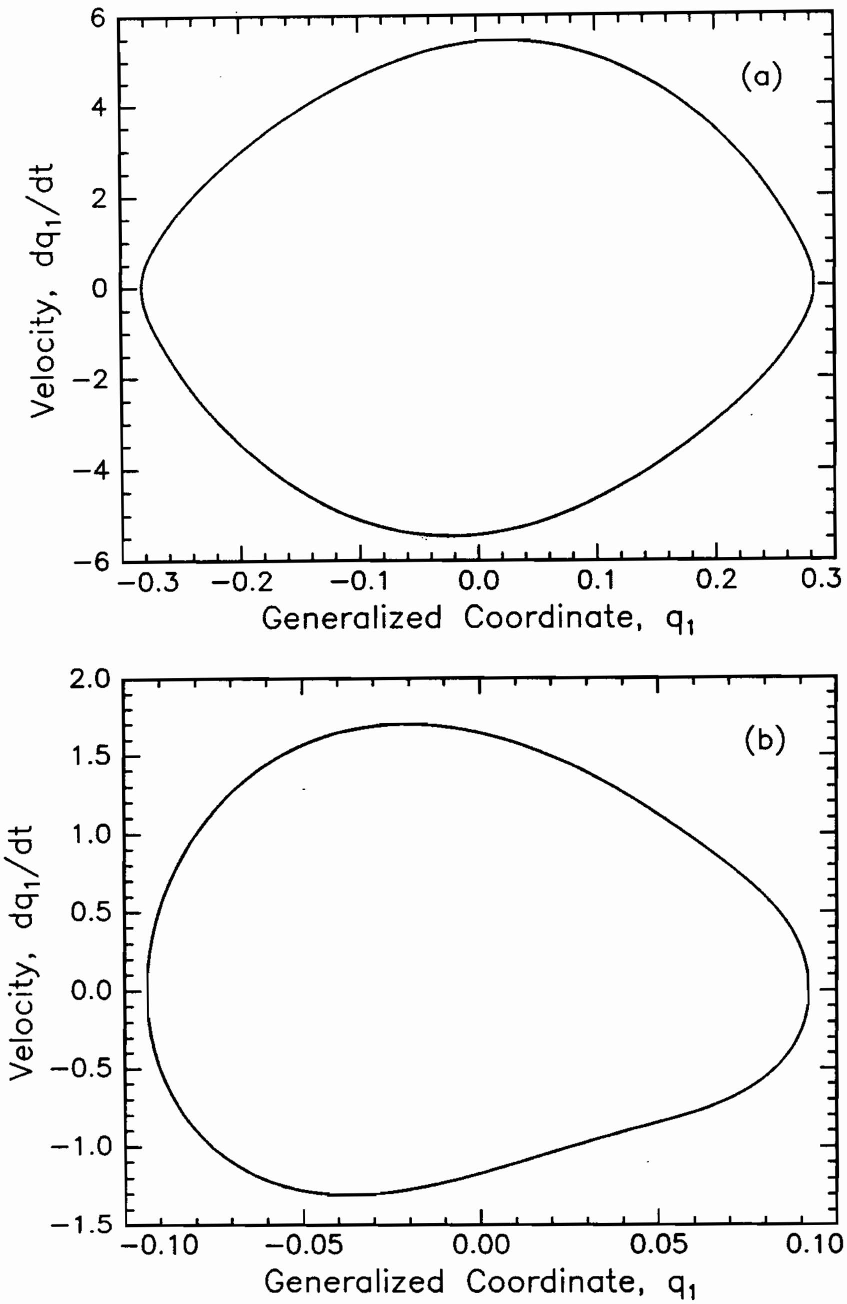

Figure 7.7: Phase-plane plots or time response for the same system, with $\nu = 0.3$: (a) $u_0 = 6.5$ and $\omega = 5$; (b) $u_0 = 6.5$ and $\omega = 15$; (c) $u_0 = 6.5$ and $\omega = 30$, (d) $u_0 = 7.5$ and $\omega = 40$.

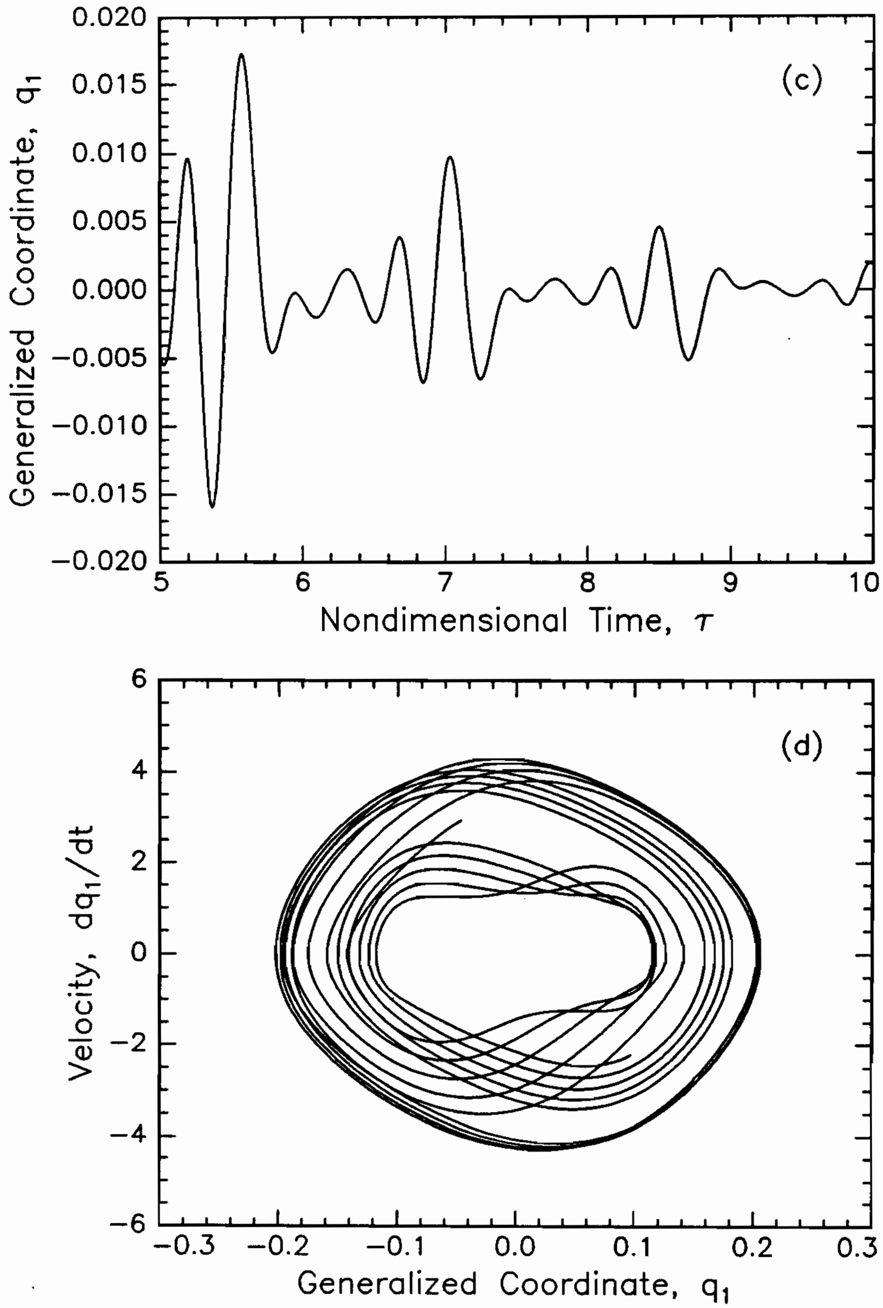

Figure 7.7: continued.

such a case is shown in Figure 7.7(c), for $\omega = 5$. As can be seen, there are indeed two frequencies, but the response converges to zero. The same phenomenon is observed for high values of ω ($\omega > 38$), even though it seems that quasiperiodic oscillations exist for that range of ω. The points appearing on the bifurcation diagram for $\omega > 38.8$ (Figure 7.6) represent only *transient* terms: by considering longer times, the response in this case also goes to zero. This contradicts Païdoussis & Sundararajan's (1975) results. One reason may be put forward: the flow velocity $u_0 (= 6.50)$ is too close to the critical one (6.34). It was decided to increase it to $u_0 = 6.8$. In this case, for $\omega = 2$ and for $\omega = 40$ for example, quasiperiodic oscillations are indeed found, as shown in Figure 7.7(d), a behaviour which agrees with Païdoussis & Sundararajan's combination resonance predictions.

The normal form theory was applied in this case as well, with good agreement with the results obtained numerically, and periodic and quasiperiodic oscillations were predicted. Before presenting this analysis, together with some experiments, another interesting set of parameters is investigated: it corresponds to figure 4 of Païdoussis & Issid (1976), with a larger value of β ($\beta = 0.307$). This case has been chosen because the theoretical boundaries are quite complicated. It was therefore attempted to reproduce them with the numerical methods developed here. The results are shown in Figure 7.8(a). The primary and secondary parametric resonances found are similar to Païdoussis and Issid's, except for the (lower) second branch of the secondary resonance. It is possible to get that also, but only when the structural damping α is put to zero. In fact, as will be seen later, the dynamics is then even more complicated. Again, the primary resonance is investigated in detail for $\nu = 0.3$ using the same three approximations as before in Figure 7.4. As can be seen from Figure 7.8(b), all three methods yield the same maximum amplitude, with similar shapes.

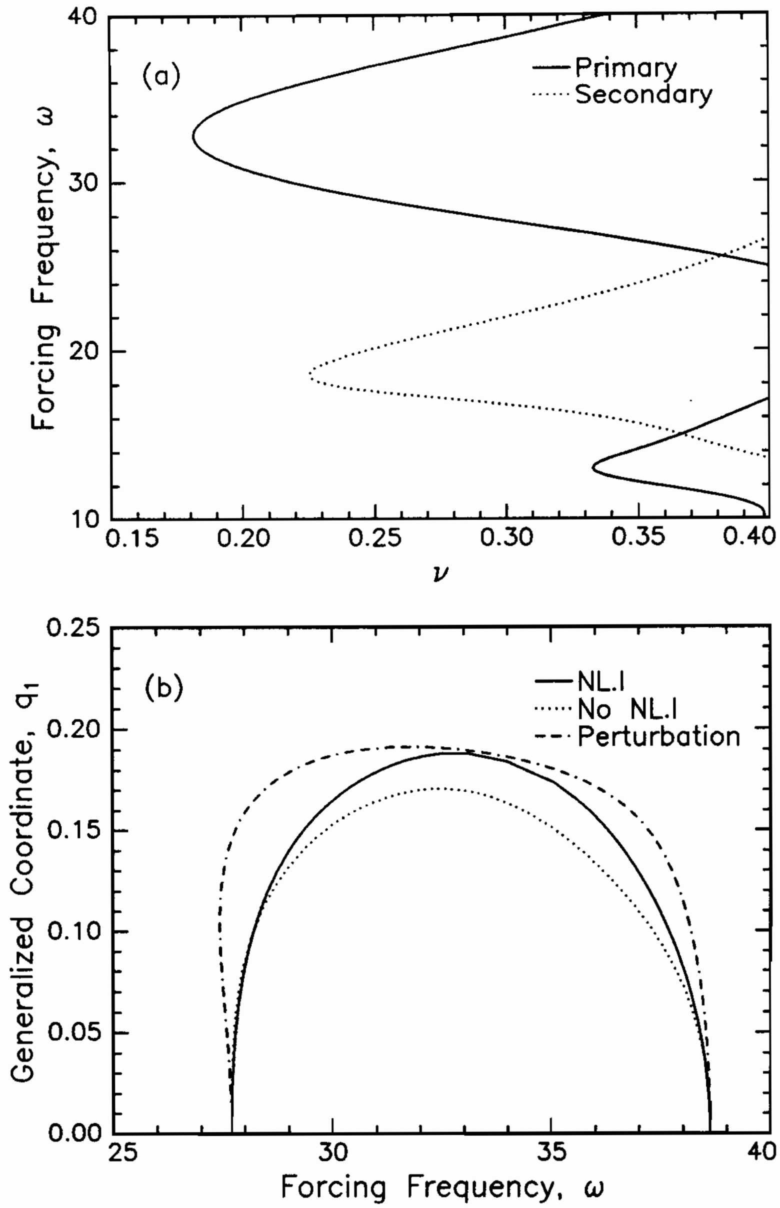

Figure 7.8: Linear and nonlinear behaviour for system parameters $u_0 = 7.68$, $\beta = 0.307$, $\gamma = 16.1$, and $\alpha = 3.65 \times 10^{-3}$: (a) linear stability boundaries; (b) amplitude of the principal parametric resonance, using three approximations and $\nu = 0.3$: —, with all nonlinear inertial terms intact, as obtained by the IHB method; $\cdots\cdot$, with all nonlinear inertial terms eliminated, as obtained by AUTO and the IHB method; $- \; - \cdot - \; -$, with inertial nonlinearities transformed, as obtained by the perturbation method and AUTO.

It was hence decided to look at the case of $\nu = 0.37$, both with $\alpha = 0$ and $\alpha = 3.65 \times 10^{-3}$ for a complete cross-section, i.e. for both primary and secondary resonances, ignoring the nonlinear inertial terms. The results are shown in Figure 7.9(a, b). If there is structural damping, three curves are obtained, as expected from the cross-section of Figure 7.8(a) for $\nu = 0.37$. The amplitude of oscillation for the primary region is twice as large as that for the secondary one, but the width of the region of instability is almost the same ($\Delta\omega \simeq 12$). The primary resonance associated with the third mode (the left curve) is approximately four times smaller, and the region of instability is not very wide. Moreover, some part of the curve is unstable (dashed portion) and even when the limit cycle is stable, it is only weakly stable, the (second) largest Floquet multiplier being close to one. This explains why in experiments this solution may not be found. When damping is ignored ($\alpha = 0$), more solutions are found to exist, as shown in Figure 7.9(b). This was also verified by integrating the equation of motion with the FDM. Hence, the dynamics may indeed be more complicated. As one can see, damping has a large effect: for the primary resonance associated with the second mode, the amplitude of oscillation is not much influenced, but the extent of the region where resonance can occur is. This is even more obvious for the secondary resonance. This leads to the conclusion that special care has to be taken when modelling or measuring damping in experiments.

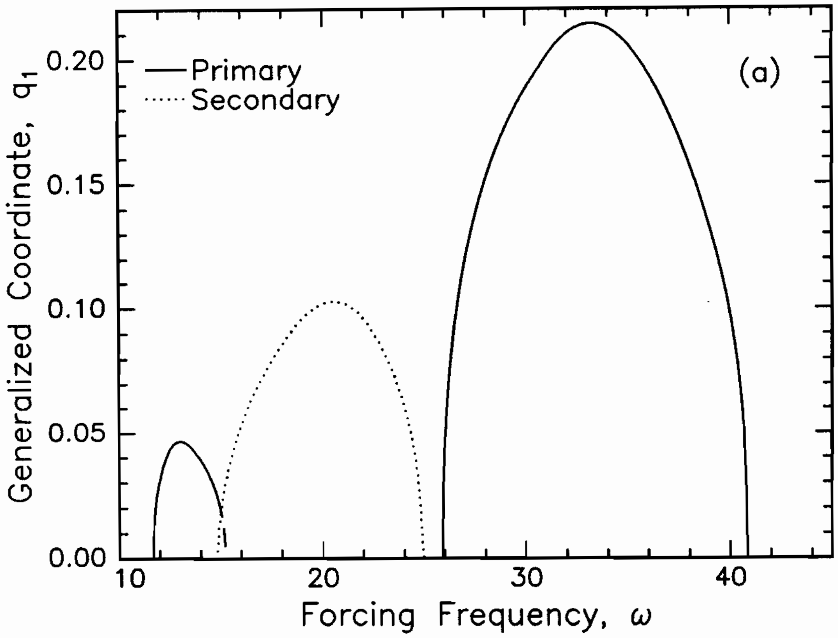

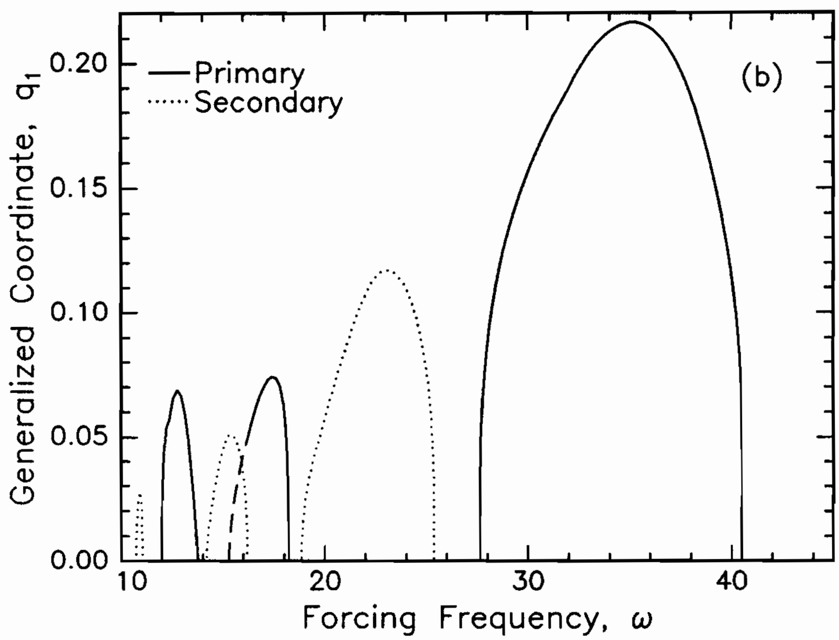

Figure 7.9: Complete nonlinear analysis for $\nu = 0.37$ for the system of Figure 7.8 with all nonlinear inertial terms removed for two values of the damping coefficient: (a) $\alpha = 3.65 \times 10^{-3}$; (b) $\alpha = 0$. —, Primary resonance; $\cdot\cdot\cdot\cdot$, secondary resonance; $---$ unstable solutions.

7.6.3 Results by the normal form method for the principal resonance

One case corresponding to experiments undertaken recently will now be considered. In this section, the dynamics is examined from the the normal form viewpoint. To get a complete picture of the nonlinear dynamics, it is necessary to take into account all three major parameters at the same time, μ, σ and ν. To simplify the analysis, the three-dimensional parameter space is divided into two-dimensional planes, keeping one parameter fixed while the other two are free. Figure 7.10 is a good example of a stability map for the principal parametric resonance in the (μ, ν)-plane, keeping $\sigma = -0.05$ constant.

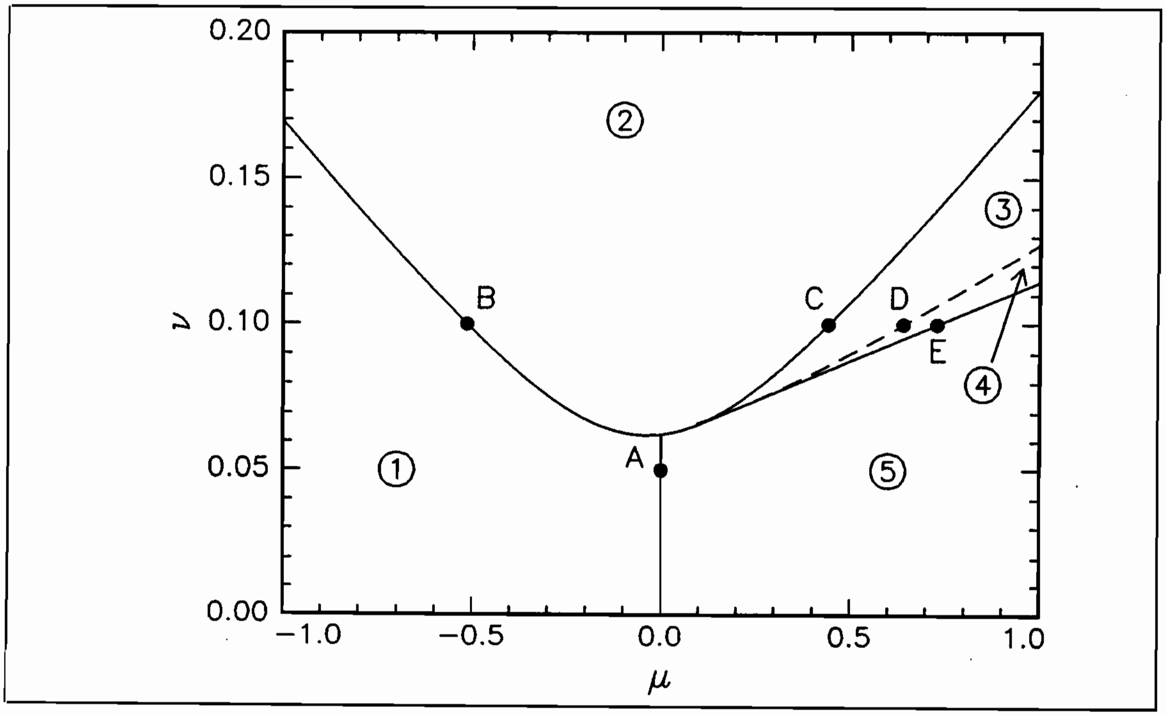

Figure 7.10: Instability regions in the (μ, ν) parametric space obtained by the normal form theory; $N = 3$, $\beta = 0.2$, $\gamma = 10$, $\alpha = 0$ and $\sigma = -0.05$.

Distinct zones separated by five segments of curves can be identified. The line segments separating 1 from 2 and 2 from 3, obtained by linear theory, correspond to (7.67b) or to the appearance of a non-zero fixed point in the normal form through a pitchfork bifurcation (periodic solution in the original equations). The dashed line between 3 and 4 can be obtained only by nonlinear theory and corresponds to the loss of stability of the periodic solution through a Hopf bifurcation. The line between 4 and 5 corresponds to the coalescence of the two fixed points, i.e. to a set of limit points. Finally, the straight line between 1 and 5 is predicted by linear theory: it corresponds to equation (7.67a) or to the loss of stability of the zero solution through a Hopf bifurcation. To simplify the analysis further, let us see how the dynamics changes when a second parameter (μ or ν) is set to a constant value; when μ is constant, one moves on a vertical line in Figure 7.10, starting from $\nu = 0$, and when ν is constant, one proceeds along a horizontal line, from left to right as μ is increased. Different cases may be considered, from "easiest" to most difficult.

Case 1: ν "small" and constant (e.g. $\nu = 0.05$). Increasing μ from a negative to a positive value, the system loses stability at $\mu = 0$ through a Hopf bifurcation (point A), i.e. it is stable when $\mu < 0$ (region 1) and exhibits quasiperiodic motion when $\mu > 0$ (region 5). This solution, shown in Figure 7.11(a), represents a stable limit-cycle in the normal form, i.e. the possibility of solutions on a two-dimensional torus in the full set of equations.

Case 2: $\mu < 0$ and constant (e.g. $\mu = -0.5$). When ν is gradually increased, the system is first stable and when ν crosses the boundary at point B, a stable fixed point appears in the normal form (region 2), or a stable limit cycle in the original equations. This boundary is predicted by the linear theory and corresponds to the principal or primary resonance. This shows, once again, that periodic solutions exist, even for flow velocities below the critical. This is depicted schematically in the bifurcation diagram obtained by the normal form in Figure 7.11(b).

Case 3: ν "large" and constant (e.g. $\nu = 0.1$). The situation here is a bit more complicated. In region 1, the origin is stable while a stable periodic solution exists in region 2. "Nothing happens" physically when crossing the line separating 2 and 3 because this linear boundary does not correspond to restabilization of the origin (through

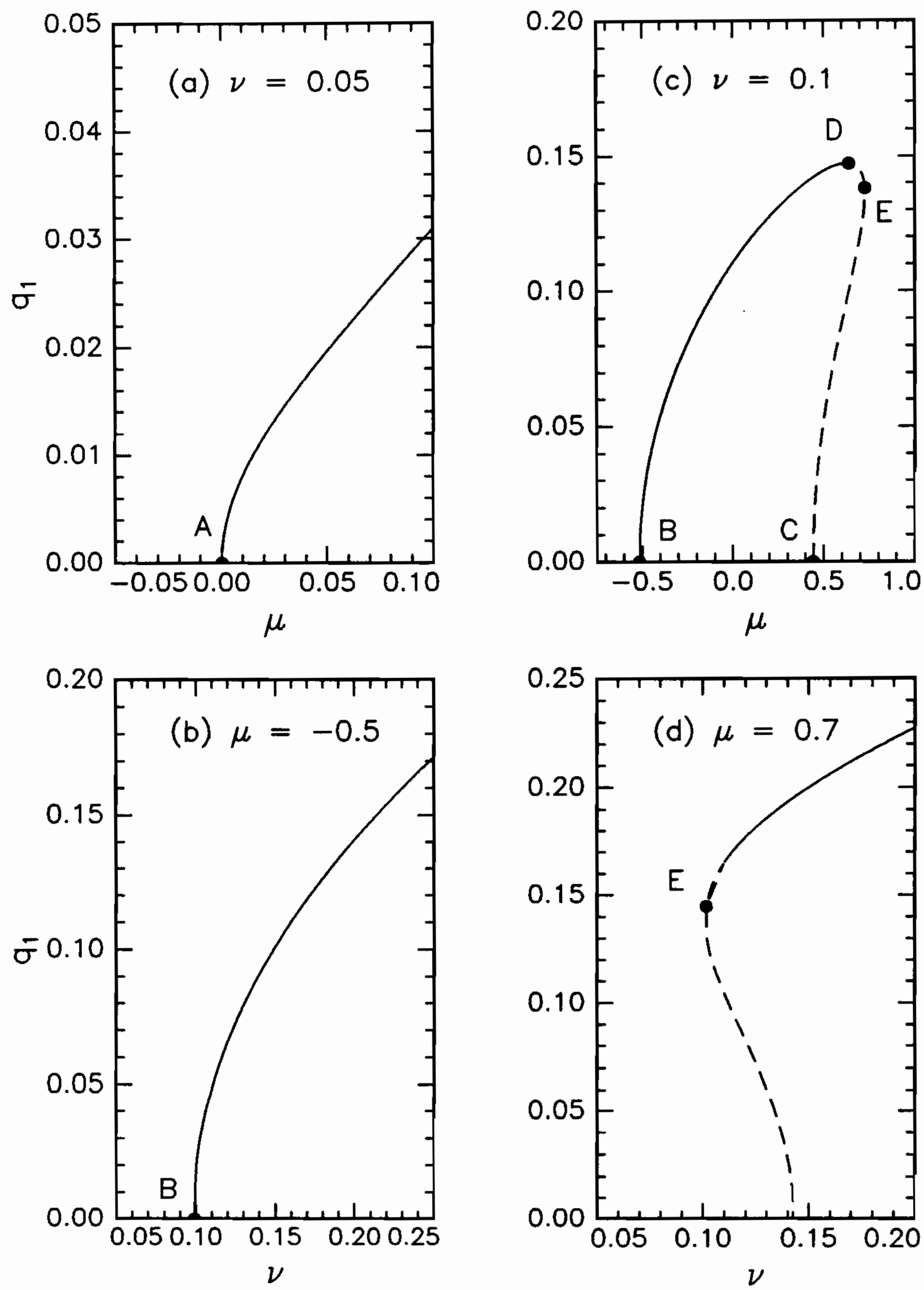

Figure 7.11: Corresponding bifurcation diagrams for 4 cases: (a) $\nu = 0.05$, (b) $\mu = -0.5$, (c) $\nu = 0.1$ and (d) $\mu = 0.7$. The full line in (a) represents the amplitude of the limit cycle in the *averaged* equation, while it represents stable limit cycles in the *original* (full) equations in cases (b,c,d). The dashed line represents unstable limit cycles.

disappearance of the fixed point) but to the *appearance* of a second periodic solution (point C). As already mentioned, this second solution is always unstable and implies the coexistence of two non-zero solutions as well as the possibility of hysteresis. When crossing the boundary between 3 and 4 the periodic solution loses stability through a Hopf bifurcation (point D), which may again lead the system to quasiperiodicity. It can be shown numerically that this Hopf bifurcation is supercritical and that the solution arising from this bifurcation is unstable, being therefore of little interest. Finally, the two non-zero fixed points coalesce at point E, in both bifurcation diagrams, 7.11(c) and 7.11(d).

Case 4: $\mu > 0$ and constant: In the light of what was discussed previously, the original system undergoes quasiperiodic motion in areas 4 and 5, periodic motion in 2, and one or the other in region 3 depending on whether ν is increased or decreased — see bifurcation diagram 7.11(d).

The same analysis was undertaken in the (σ, ν)-plane while keeping μ constant, and very similar stability maps were obtained. It can therefore be concluded that, depending on the three parameters, the normal form theory predicts either stable equilibria, periodic solutions or quasiperiodic oscillations. When $\mu < 0$, only the first two are possible.

7.6.4 Experimental results

In this section, results obtained experimentally for the principal parametric resonance are presented and compared with theory. First, the case corresponding to $\mu < 0$ is investigated, as in Figure 7.12, which shows regions of principal parametric resonance for $u_0 = 0.90u_{cr}$ and for $0.95u_{cr}$, both theoretical and experimental (for clarity, the results obtained by the normal form theory are not shown because they are very close to the numerical ones, as in Figure 7.3). As can be seen, the agreement between theory and experiment is reasonably good, except for the lower part of the boundary, where experimental points are consistently lower than the theoretical ones. This was already observed in previous studies (Païdoussis & Issid 1976): the extent of the region of the parametric resonance is larger in the experiments than in the theory, *even* if structural damping is completely ignored. Alas, the nonlinear analysis does not reveal any subcritical bifurcation that would explain the existence of periodic solutions before the linear boundary.

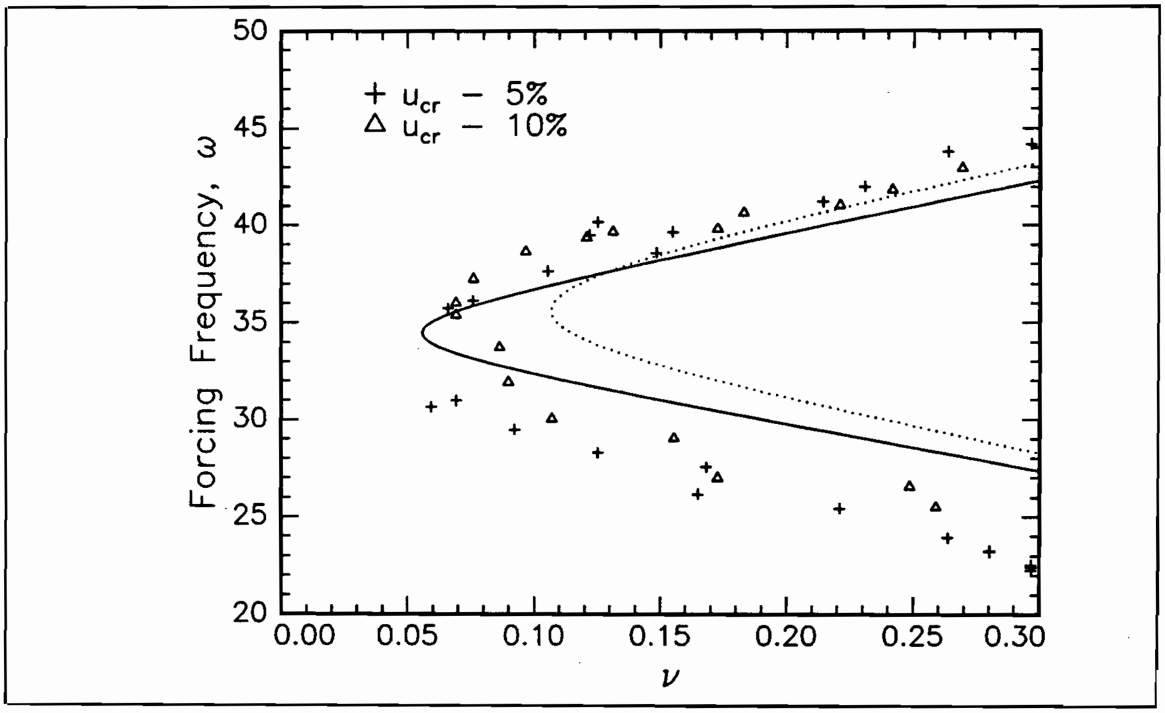

Figure 7.12: Comparison between theory and experiments of the principal parametric resonance. —, Theoretical linear stability boundary obtained for $u_0 = 6.18$; ...., for $u_0 = 5.85$; both sets obtained by IHB, for system parameters $\beta = 0.137$, $\gamma = 26.1$, and modal damping log-decrements $\delta_1 = 0.028, \delta_2 = 0.080, \delta_3 = 0.131$ and $\delta_4 = 0.180$. +, Experimental points for $u_0 = 6.18$ $(0.95u_{cr})$; Δ, for $u_0 = 5.85$ $(0.90u_{cr})$; $u_{cr} = 6.5$.

A second set of experiments was also undertaken by varying μ while keeping σ (or the forcing frequency ω) constant. The results of one such experiment, corresponding to $\sigma = -0.1$, are shown in Figure 7.13. The physical dimensional and nondimensional characteristics of the pipe are given in Table 7.2, together with a comparison of the critical flow velocity u_{cr} obtained numerically and experimentally; the difference is less than 10%. Again, three different regions can easily be distinguished: the lower-left one, where the system is stable; the upper one, in which limit cycles are found with a frequency of oscillation equal to half the forcing frequency; and the lower-right one, where quasiperiodic motions are observed. As can be seen, the predictions by the normal form theory are very close to the experiments. The same procedure can be repeated for different values of σ and the corresponding boundaries constructed and plotted. These are shown in Figure 7.14 by lines with markers on them, and compared with the boundaries found using the normal form theory. It should be mentioned that the theoretical results represent only boundaries of physical interest, i.e. for which *stable* periodic solutions exist, which explains why they are simpler than in Figure 7.10.

Natural frequencies: $f_1 = 1.1$ Hz, $f_2 = 4.04$ Hz, $f_3 = 10.25$ Hz
Logarithmic decrement: $\delta_1 = 0.04, \delta_2 = 0.123, \delta_3 = 0.157$
Stiffness: $EI = 8.7 \times 10^{-3}$ Nm^2
Mass per unit length: $m = 0.189$ kg/m
Length: $L = 0.46$ m
Inner and outer diameters: $d_i = 6.1$ mm, $d_o = 15.6$ mm
Mass and gravity parameters: $\beta = 0.131$, $\gamma = 26.1$
Experimental critical flow-rate: $Q_{cr} = 0.213$ kg/s ($u_{cr} = 5.9$)
Theoretical nondimensional critical flow velocity: $u_{cr} = 6.42 (N = 3)$

Table 7.2: Physical properties of the pipe used in the experiments

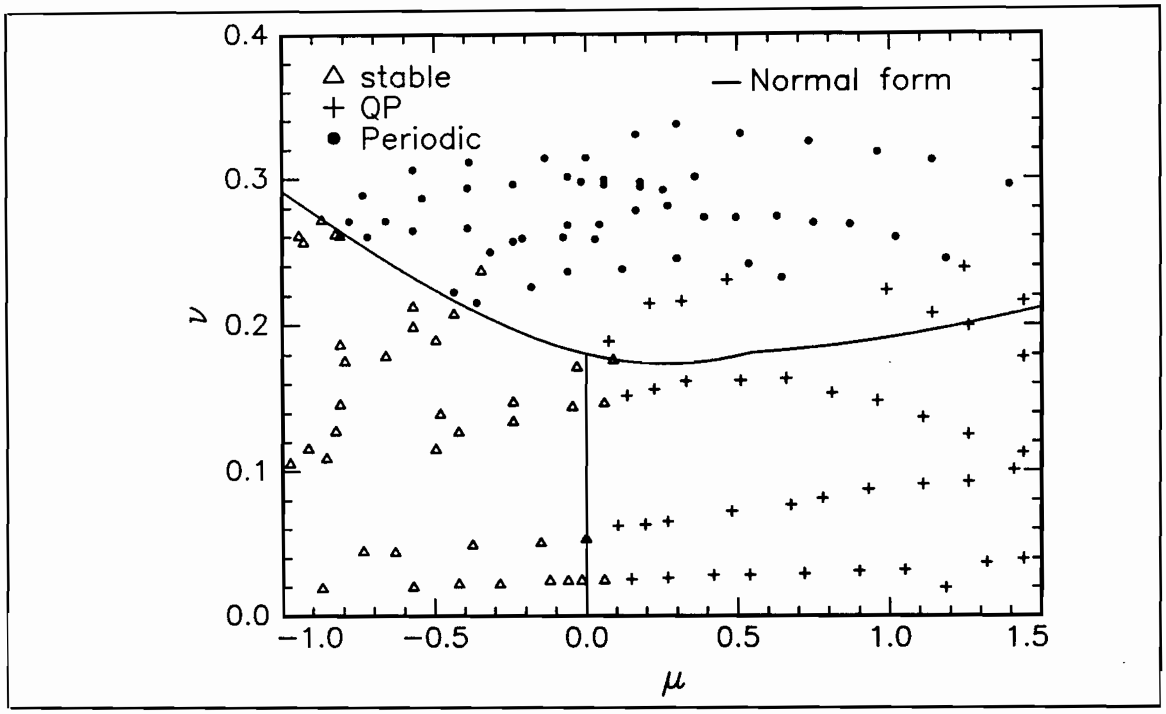

Figure 7.13: Comparison between theory and experiments for the principal parametric resonance in the (μ, ν) parameter space for $\sigma = -0.14$, $\beta = 0.131$ and $\gamma = 26.1$: Δ, experimental data points where the system is stable, $\bullet$, experimental data points where the response is periodic; $+$, experimental data points where the response is quasiperiodic; —, theoretical boundaries obtained by the normal form theory with $N = 3$ separating these three types of dynamical behaviour.

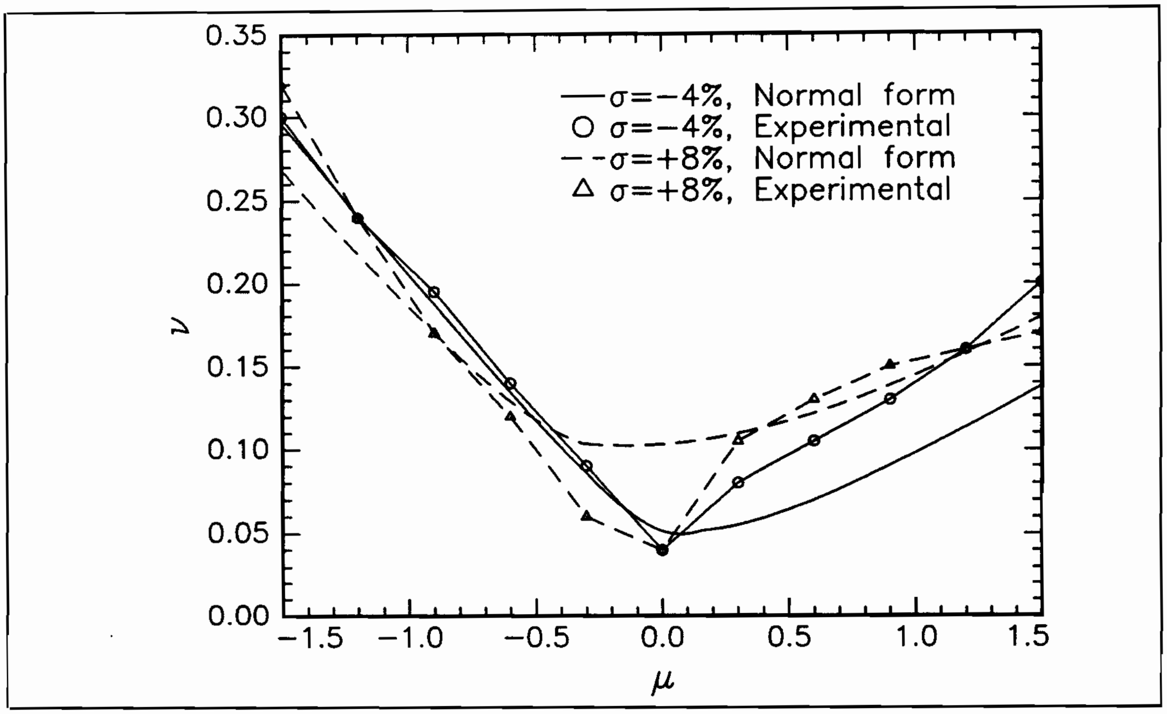

Figure 7.14: Comparison between theory and experiments of the principal parametric resonance in the (μ, ν) parametric space for the same parameters as in Figure 7.13: —, obtained by the normal form theory and $\sigma = -0.04$; – – –, normal form and $\sigma = 0.08$; o, experimental data points for $\sigma = -0.04$; Δ, experimental data points for $\sigma = 0.08$.

It can be seen in Figure 7.14 that (i) the agreement between theory and experiment is good for $\mu < 0$ in the three cases considered; (ii) the correspondence is best if, additionally, σ is small, i.e. when the forcing frequency is close to twice the natural frequency; however (iii) the discrepancies increase for positive μ and larger values of σ. Two reasons may be put forward for this last observation: (a) in the experiment, it is sometimes difficult to distinguish between quasiperiodic and periodic oscillations since the content of the second frequency may be small, and (b) the normal form solution proves that the periodic solution loses stability with two complex conjugate Floquet multipliers crossing the unit circle, but there may still exist a relationship between the frequency created and the existing one, so that the bifurcating solution may still be periodic. In fact, points (a) and (b) are interrelated. More experiments were undertaken with different values of σ, yielding similar conclusions, and the corresponding results, both theoretical and experimental, can be found in Appendix J.

7.6.5 Results by the normal form method for the fundamental resonance

In the case of the *fundamental* parametric resonance, the results obtained experimentally were not convincing, mainly because the amplitudes were very small, so that it was difficult to distinguish between a stable system and one executing forced oscillation (e.g., such forced small-amplitude vibration could be induced if the pipe is not perfectly straight, or by transmission through the supports). For these reasons, such results are not presented here. It is, however, interesting to see how the results obtained with the normal form theory compare with those computed numerically. The parameters used are the same as before, and the approximation $N = 3$ is used in both cases. To find the normal form, it is necessary to first find the centre manifold. After putting the system in standard form and using the method developed in Section 7.3.2, the centre manifold is found to be

$$
\begin{aligned}
x_{2i+1} = &\ \epsilon\nu \left[\cos\omega\tau(C_1^{2i+1}x_1 + C_2^{2i+1}x_2) + \sin\omega\tau(C_3^{2i+1}x_1 + C_4^{2i+1}x_2)\right], \\
x_{2i+2} = &\ \epsilon\nu \left[\cos\omega\tau(C_5^{2i+1}x_1 + C_6^{2i+1}x_2) + \sin\omega\tau(C_7^{2i+1}x_1 + C_8^{2i+1}x_2)\right], \qquad i = 1, 2,
\end{aligned}
\tag{7.68}
$$

where $C^3 = \{C_1^3, ..., C_8^3\} = \{-0.149, 0.355, -0.159, -0.441, -0.092, -0.12, 0.171, 0.215\}$ and $C^5 = \{-0.016, -0.144, -0.442, -0.147, 0.187, 0.060, 0.115, -0.207\}$; the coordinates $x_{3,4}$ are associated with $\sigma_3 = -10.14$ and $\omega_3 = 7.5$ and $x_{5,6}$ with $\sigma_5 = -3.615$ and $\omega_5 = 53.51$, i.e. with the "first" and "third" mode respectively. It should be mentioned that the coefficients of C^3 and C^5 are rather small, so that the centre manifold is in fact close to the linear eigenspace. Once the centre manifold is found, it is easy to transform the equation of motion into complex form (7.30) and thereafter to identify the coefficients useful to compute the normal form (7.59). The detailed procedure can be found in Appendix K, while the different coefficients of the normal form are given in Table 7.3.

$a = -2.70110^{-4}, b = 1.20710^{-4}, c = -0.039, d = 0.138$
$C_r^1 = 0.017 C_i^1 = -0.025, C_r^2 = 0.283, C_i^2 = -0.732$
$V_r = -2.246, V_i = 2.099$

Table 7.3: Coefficients defining the normal form of the fundamental parametric resonance for $\beta = 0.131, \gamma = 26.1, \alpha = 0$ and $N = 3$; the subscripts r and i here indicate real and imaginary components

Because the normal form given by equations (7.59) has the same structure as that of (7.56), the interpretation of the results is the same. Most of the stability maps computed were *qualitatively* very similar to those obtained for the principal resonance, both in the (μ, ν)-plane and in the (σ, ν)-plane, so that again three different regions may be distinguished. In one of them, the system is stable, in the other it performs limit cycle motion with a frequency equal to the forcing frequency, and in the third it exhibits quasiperiodic oscillations.

From equations (7.59), it is straighforward to find the *linear* boundaries corresponding to the fundamental parametric resonance, the conditions for *nontrivial* solutions to exist, as well as the *stability* of these nontrivial solutions. Introducing $A_r = d\mu + C_r^1\mu^2 + C_r^2\nu^2$, $A_\phi = -\sigma + c\mu + C_i^1\mu^2 + C_i^2\nu^2$ and $\eta = \sqrt{V_r^2 + V_i^2}$, these conditions are:

(a) *loss of stability of the trivial solution through a Hopf bifurcation* [equivalent to (7.67a)]:

$$A_r = 0; \tag{7.69a}$$

(b) *loss of stability of the trivial solution through a pitchfork bifurcation* [equivalent to (7.67b)]:

$$A_r^2 + A_\phi^2 - (\eta\nu^2)^2 = 0; \tag{7.69b}$$

(c) *necessary condition for the existence of a nontrivial solution:*

$$\Delta = (a^2 + b^2)(\eta\nu^2)^2 - (aA_r - bA_\phi) \geq 0; \tag{7.69c}$$

(d) *sufficient condition:*

$$(\sqrt{a^2 + b^2})\, r_0^{\pm} = -(aA_r + bA_\phi) \pm \sqrt{\Delta} \geq 0, \tag{7.69d}$$

where $r_0^{\pm}$ represents the two non-zero fixed points. Again, it can be shown easily that r_0^- is always unstable, and

(e) r_0^+ *loses stability only by a Hopf bifurcation*, if

$$A_r + 2ar_0^+ \geq 0. \tag{7.69e}$$

In all the cases considered, the coefficient C_r^2 was found to be positive, which means that the flow perturbation tends to reduce slightly the flow velocity for which the Hopf bifurcation occurs. For example, for the parameters considered, $A_r = 0.138\mu + 0.0169\mu^2 + 0.284\nu^2$, so that the Hopf bifurcation occurs at $\mu = -0.02$ for $\nu = 0.1$ and at $\mu = -0.19$ for $\nu = 0.3$. For comparison with the results obtained numerically, we consider here only the case $\mu > 0$, which means that only periodic or quasiperiodic oscillations can occur. Choosing $\mu = 0.37$, the different conditions (7.69b,c,e) were computed and are shown in Figure 7.15(a). For comparison, the linear boundary corresponding to (7.69b) has been obtained on the full linear equations using AUTO, as well as some points from the full nonlinear equations using FDM. As can be seen, the comparison is good in some aspects, but rather poor in others.

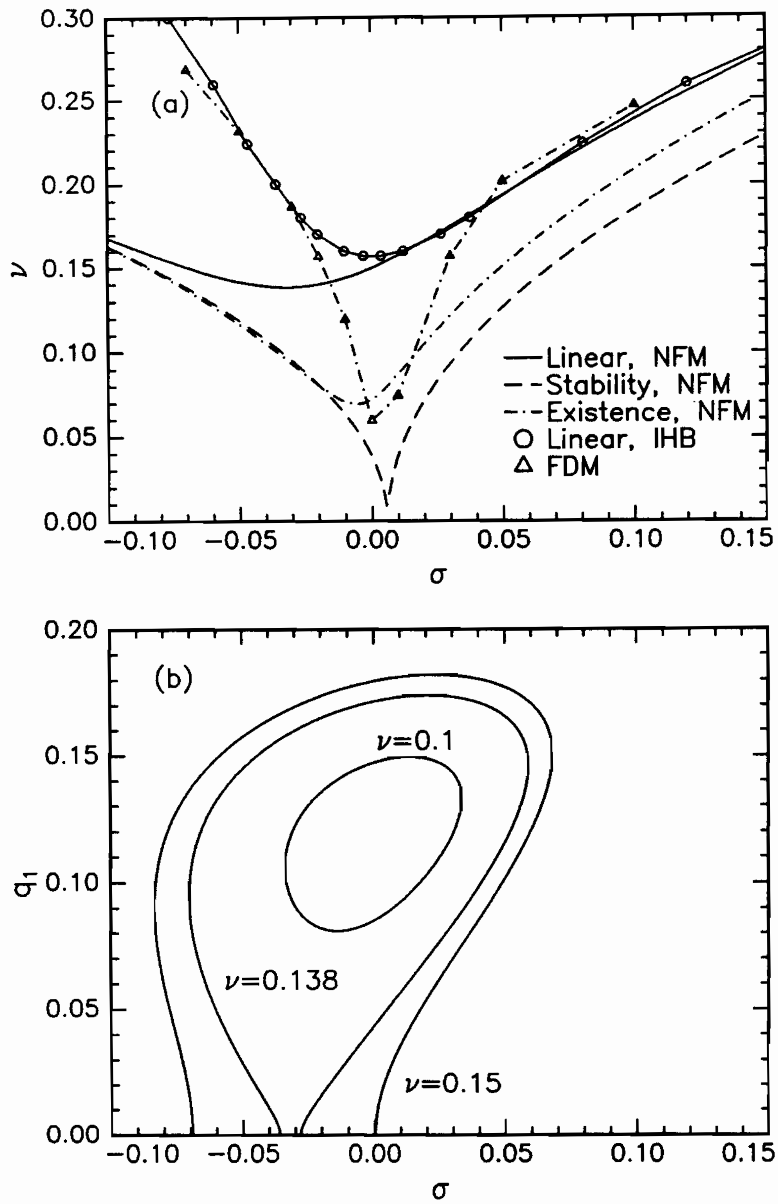

Figure 7.15: (a) Comparison between the results of the normal form method (NFM) and those obtained numerically for the fundamental parametric resonance in the (σ, ν) parameter space, for $\mu = 0.37$, $N = 3$ and the same parameters as in Figure 7.13: —, linear boundary, —·—, existence, and — — —, stability boundaries predicted by NFM; o, linear boundary using AUTO, Δ, appearance of a periodic solution in the original equation found by FDM; (b) response curves obtained by NFM for $\nu = 0.1$, $\nu = 0.138$ and $\nu = 0.15$.

This can be summarized as follows:

(i) The agreement between the normal form and the numerical methods for the *linear* boundaries is rather good when $\sigma \geq 0$, but fails completely when $\sigma < 0$.

(ii) The nonlinear analysis is very important here because non-zero solutions exist *outside* the linear boundaries.

(iii) It can be seen that the prediction of the normal form is accurate when $\sigma \to 0$: both numerical and theoretical calculations show that there exist periodic solutions for $\nu \simeq 0.07$ while the linear analysis predicts a value of $\nu = 0.16$ when $\sigma = 0$.

(iv) It is interesting to mention that the two non-zero solutions are in some cases "isolated" and are of the same type as already found by Bajaj (1986). To illustrate how these isolated solutions emerge, the evolution of the fixed points of the reduced system for three values of ν is shown in Figure 7.15(b).

The results discussed above are in fact to be expected: for the analysis of the fundamental resonance to be valid, the detuning parameter σ has to be of second order (Nayfeh 1986). In the case of the principal resonance, $\sigma = 0.15$ was shown to be the maximum admissible value for first-order, so that for the fundamental resonance this value becomes $\sigma = 0.15^2 \simeq 0.02$. Hence in practice, comparison is only possible for very small values of σ. Consequently, it can be said that for the cases considered, the normal form theory is of major importance only for the principal resonance while it is much more restricted for the fundamental resonance. Furthermore, it can be said that the fundamental resonance is considerably less important than the principal one. However, the normal form theory still gives some insight into the dynamics of the system, at least from the qualitative viewpoint. It should be mentioned that these remarks apply only for the cases considered here, and that the conclusion might be different for other parameter values, especially if the mass parameter β is larger ($\beta > 0.3$).

7.7 CONCLUSION

The nonlinear dynamics of a cantilevered pipe conveying fluid with a sinusoidally perturbed flow velocity has been studied analytically, numerically as well as experimentally. A major difficulty is the presence of generally large inertial nonlinearities, which hinders the reliable numerical integration of the equations of motion. When the nonlinearities are small, classical perturbation methods can be used to analyse the dynamics of the system and to overcome this difficulty. Here, the centre manifold and the normal form methods (NFM) have been applied to simplify the analysis as much as possible, yielding very simple equations that capture the essence of the dynamics. Two *numerical* methods were also found useful to solve the problem: the Finite Difference Method (FDM) and the Incremental Harmonic Balance (IHB) method, the latter being able to find also unstable branches of solutions.

The IHB method, in conjunction with AUTO, was used to study the dynamics of the system for flow velocities either below or above the critical (u_{cr}), in the latter case leading to self-exited flutter. In particular, the primary and secondary parametric resonance regions associated with the second mode were investigated and, broadly, the resonance bounds were found to agree well with those previously obtained by Païdoussis & Issid (1974) and Païdoussis & Sundararajan (1975). However, the amplitudes associated with these resonances were now also determined. Interestingly, it was found that the effect of inertial nonlinearities can be large, so that, if they are neglected or inadequately represented by assuming that they are small, the error can be significant. It was also found that if a perturbation method is used (in the sense of Section 7.4.1) to obtain an easily solvable equation, erroneous results may be obtained (unstable solutions in regions where the full equations show stable ones).

Comparison was made with some recently obtained experimental results, in terms of the extent in the (ν, ω)-plane of the principal resonance region in the case of $\mu = u_0 - u_{cr} < 0$. It was found that agreement in the upper resonance boundary was $\mathcal{O}(5\%)$, while the lower one was underestimated by $10 - 15\%$ (and hence the extent of the parametric resonance region overestimated). No explanation for this can be advanced as yet, because the nonlinear analysis does not reveal any subcritical bifurcation if $\mu < 0$. Experiments were also undertaken by keeping the frequency constant instead of the flow velocity u_0, yielding more accurate results in the (μ, ν)-plane. However, it should be recalled that agreement of the order of $5-10\%$ is the best one can reasonably expect in this type of fluid-structure interaction system (Païdoussis & Li 1993).

Some work was also done on combination resonances, yielding quasiperiodic solutions. Again, these were predicted analytically (NFM), numerically (FDM), as well as experimentally. Time traces and phase portraits were used to illustrate quasiperiodic responses, and stability boundaries were constructed in the (μ, ν)-plane. The agreement between the different methods of solution was very satisfactory. However, it was found that the regions previously found by Païdoussis & Sundararajan (1975) could not be reproduced for u_0 close to u_{cr}, whereas they could if u_0 was further removed from u_{cr}.

Finally, some results were also obtained numerically and by using the NFM in the case of the fundamental resonance ($\omega \simeq \omega_0$). For that purpose, it was necessary to compute first the centre manifold on which the equations were projected. The comparison showed that the NFM was able to give accurate results only if the detuning parameter σ was small, which is in fact a necessary condition for the NFM to be applicable. However, the NFM clearly demonstrated how solutions arise *outside* the linear stability boundaries, showing therefore why the nonlinear analysis is essential in this case. Unfortunately, comparison with experiment was difficult, not to say impossible, mainly because in the experiments the amplitude of the oscillations was very small. This leads to the conclusion that for the mass parameter considered ($\beta < 0.25$), the fundamental or secondary resonance might be of little practical importance.

Chapter 8

CONCLUSION

In this Thesis, the nonlinear dynamics of a cantilevered pipe conveying fluid has been examined analytically, numerically and experimentally. The study was cast in the light of modern nonlinear dynamics theory to show that the system under consideration displays a kaleidoscope of interesting dynamical behaviour.

8.1 OVERALL OVERVIEW

As mentioned in the Introduction, the main goal of the Thesis was to describe the fascinating behaviour of nonconservative fluid-conveying pipes and to discuss, clarify and illustrate the diversity of the possible responses. To this end,

(i) **a systematic *classification* and *clarification* of the dynamical response of the system was performed** (fixed points, periodic and quasiperiodic motions, etc.);

(ii) **the possibility of chaotic oscillations for the *autonomous* system was investigated;**

(iii) **the *nonlinear* dynamics of the pipe conveying *unsteady* flows was examined in detail.**

To achieve these goals, it was decided to conduct in parallel an analytical, numerical and experimental study, not only to evidence and illustrate a number of diverse nonlinear dynamics phenomena, but also to show how this system has become important in the development and testing of the tools of modern dynamics theory. This is why different methods of investigation were used throughout the Thesis.

From the numerical point of view, several "work horses" were developed and/or were extensively used: **Fourth and eighth-order Runge-Kutta methods, Houbolt Finite Difference Method, AUTO** and the **Incremental Harmonic Balance** method; with these tools, it was possible to:

- compute *time traces, power spectra* and *phase plane plots* to obtain a geometric picture of the dynamics;
- construct *bifurcation diagrams* to illustrate the qualitative change in the dynamics, when parameters are varied;
- find *Floquet multipliers* to detect and classify the various instability types;
- construct *Poincaré* and *Lorenz return maps* to extract the essence of the dynamics;
- compute *Lyapunov exponents* to characterize chaotic oscillations.

Similarly, from the analytical point of view, other methods were utilized:

- the *centre manifold theory* to reduce the dimension of the system by projection on the appropriate modes;
- the method of *averaging* and the *normal form theory* to simplify the equations to their simplest form;
- the *codimension-one and -two bifurcation theory* to characterize and understand the overall dynamics.

Finally, a thorough experimental program was undertaken to verify the results predicted theoretically.

Furthermore, to illustrate item (ii) in the first paragraph of the section (chaotic dynamics), it was decided to "unfold" the problem by tackling several configurations, namely:

♣ to determine the effects of a *spring support* of variable location and rigidity on the global dynamics;

♣ to include the *inherent nonlinearities of the pipe impacting on physical constraints* after the occurrence of the Hopf bifurcation, in order to improve the agreement between theoretical and existing experimental results;

♣ to add or remove a small *mass at the free end* and then study the system response, both theoretically and experimentally;

♣ to examine carefully the *possible existence of "special" orbits* such as heteroclinic orbits that may lead to chaos if perturbed.

To explore item (iii) of that same paragraph (unsteady flow), the following was undertaken:

♠ *the effects of the nonlinearities on parametric resonances* were studied in detail;

♠ the problem of the pipe conveying fluid having a sinusoidal component was reduced to that of a *periodically perturbed Hopf bifurcation*, which is particularly interesting;

♠ *small time-dependent perturbations* were applied on the autonomous system in the vicinity of heteroclinic orbits.

8.2 FROM A WIDER PERSPECTIVE

From the literature review and the various items above, it becomes clear that the study of the system of a fluid-conveying pipe is particularly interesting; from a *linear* point of view, it exemplifies nonconservative gyroscopic systems, while from the *nonlinear* viewpoint, it displays a wide variety of dynamical states and phenomena. Restricting our attention to the latter case, one may easily conclude that **diversity was omnipresent throughout the Thesis**, in particular with regard to (i) **the dynamical**

behaviour, which was very rich, (ii) **the approaches and methods of solution**, that were multifaceted, and (iii) **the variety of configurations** that were considered. This diversity is illustrated schematically in Figure 8.1, together with corresponding outcomes.

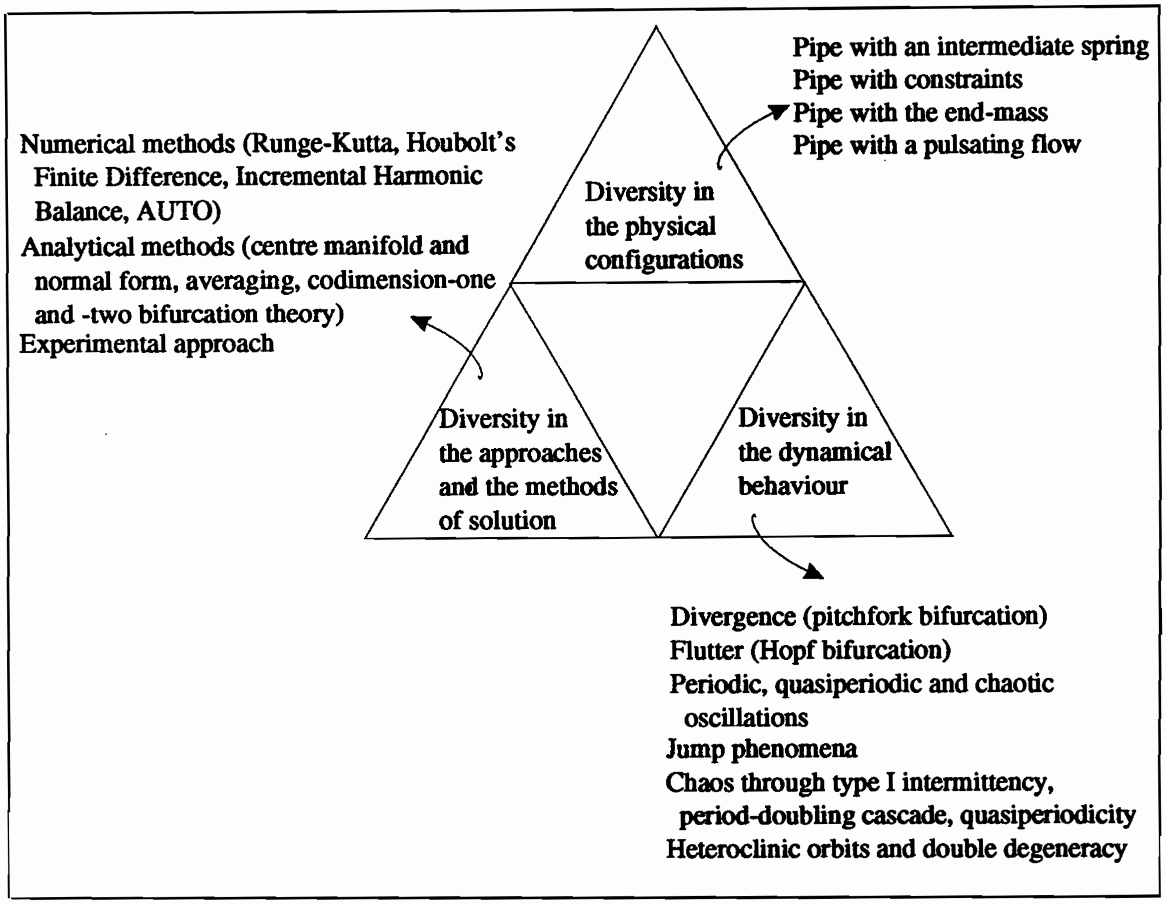

Figure 8.1: Illustration of the "diversity" in the Thesis

What is important to mention is the fact that all aspects had a lot of influence on one another: (a) the wide variety in behaviour could be obtained only by using numerous methods of solutions; (b) it was necessary to consider different variants of the system to reveal a large number of characteristics; (c) several methods of solution could be applied or adopted only because of the diversity in the physical configurations. Consequently, the three poles of the triangle in Figure 8.1 had a major impact one another, which explains why even the structure of the Thesis might be perceived as *nonlinear*.

A second aspect of the study of fluid-conveying pipes is that it bridges a gap between the field of nonlinear dynamics, usually restricted to the study of relatively simple systems of small dimension, and other fields of more practical concern. Indeed, in any problem in engineering, physiology, biology, chemistry or economics (the list should, in fact, be much longer), it seems more and more important and appropriate to include the effects of the nonlinearities in the analysis, i.e. to take into account the nonlinear interaction between the elements, within a same problem. For example, the wing of an airplane or an electrical cable subjected to wind may display characteristics similar that of a pipe conveying fluid (they can all be subject to divergence or flutter), so that if research or design is undertaken on such systems, one should be aware of the various possibilities in dynamical behaviour, as well as of all methods of solution available to obtain reliable predictions. On the other hand, complex systems often respond similarly to low-dimensional systems (for example the features observed in the eight-dimensional model were the same as in a trivial one-dimensional map), so that a good starting point for the nonlinear analysis of realistic situations may be a very simple model.

Before giving recommendations for further investigations, specific conclusions for each chapter of the Thesis are summarized in the next section.

8.3 THE SPECIFICS

In the previous two sections, our intention was to mention only the major results that have emerged throughout the course of the study, so that for a detailed enumeration, the reader is referred to the concluding remarks in the chapters. Nevertheless, for each of them, the following observations seem particularly important.

In Chapter 2, where a nonlinear model was developed, the nonlinear equations of motion were derived in a clear and simple manner using two methods, and were compared with those obtained previously. They were found to be identical and consistent with some of the previous derivations, while revealing a number of erroneous equations; **because of their completeness and relative simplicity, the equations derived constitute the theoretical basis of the present study.** For pipes with fixed ends, the equations derived were considered to be the only one correct to the same order as that for the cantilevered pipes, and it was shown that the origin of the terms in the equations, as well as the structure of the equations, were distinctly different for pipes with both ends fixed, as compared to cantilevered pipes. It also became evident subsequently in the Thesis that the nonlinear inertial terms present in the equations were very important and should therefore not be neglected, even if they introduce many difficulties in the numerical resolution of the problem.

In Chapter 3, the effect of a spring support was examined, mainly because it corresponds to an intermediate case between a cantilevered pipe and one having both ends fixed. Linear stability boundaries corresponding to *divergence, flutter*, and concurrent divergence and flutter (*double degeneracy*) were constructed, and the post-instability behaviour was explored from a nonlinear viewpoint. An analytical study was undertaken by using the centre manifold theory, the averaging method and the normal form theory, and the approximation of the simplified subsystem on the centre manifold was compared to the actual flow computed numerically; excellent agreement was obtained in all cases. A local bifurcation analysis near fixed points of higher degeneracy (*codimension-two*) was also performed, revealing the existence of heteroclinic orbits that led to chaos, if appropriately perturbed. **All the results proved that the addition of the intermediate spring tend to enrich the dynamics considerably.**

In Chapter 4, the case of a cantilevered pipe constrained by motion-limiting restraints was investigated, together with the effects of varying various system parameters. Phase portraits, bifurcation diagrams, power spectra and Lyapunov exponents were presented, and **the mechanism leading to chaos was well elucidated**, from a physical viewpoint (*interaction of limit-cycle motion and potential wells* associated with divergence of the pipe at the constraints), as well as from a dynamical point of view (*cascade of period-doubling bifurcations*). With the nonlinear model developed in Chapter 2, **excellent qualitative and quantitative agreement with experiment was achieved**, not only in terms of the threshold flow velocities corresponding to the key bifurcations, but also by capturing features of behaviour not hitherto predicted by theory, such as the sticking of the pipe on one of the restraints at sufficiently high flow velocities.

In Chapter 5, numerical solutions of second-order implicit nonlinear ordinary differential equations were proposed, mainly because the nonlinear inertial terms present in the equation of motion cannot be neglected or removed. Three specific methods were examined, two of them appearing particularly powerful: the *Houbolt method*, based on a fourth-order *finite difference* scheme, is an initial-value solver able to yield the time response of the system for any initial condition, and the *incremental harmonic balance* method, which yields bifurcation diagrams representing both stable and unstable periodic solutions. It was shown that **the combination of the two methods constitutes an effective tool in the study of systems represented by second-order *implicit* nonlinear equations.**

In Chapter 6, the dynamics of the pipe with an end-mass was explored analytically, numerically and experimentally. The study of the case of *an end-mass defect* showed that **chaotic oscillations occurred** via a *type I intermittency route*, and it was demonstrated through the construction of a Lorenz return map that the qualitative features of the eighth-order system could be captured by a very simple map. The period between "turbulent bursts" of nonperiodic oscillations and the Lyapunov exponents were found numerically, and it was demonstrated that they both vary as predicted by the normal form represented by a one-dimensional map. For the more realistic case of *a positive end-mass*, the agreement between theory and experiment was very good, and different types of motion — **periodic, quasiperiodic and chaotic** — together with **a very rich and complex bifurcational behaviour**, could be predicted and/or observed. For large end-masses, it was shown that a three-dimensional model was necessary.

In Chapter 7, a harmonic component was superposed to the constant mean flow velocity, $u_0(1+\nu\sin\omega\tau)$, so that the effects of the forcing frequency, ω, the perturbation amplitude, ν, and the constant flow velocity, u_0, were considered, using multiple approaches: analytical (centre manifold and normal form), semi-analytical (perturbation method), numerical (FDM and IHB) and experimental. Parametric and combination resonances were examined in detail, and **particular attention was paid to the effect of the nonlinearities**. It was shown that the effect of the nonlinear inertial terms may be large in some cases, and the amplitudes of oscillation within and sometimes outside the linear boundaries were predicted. Again, comparison with experiment was good, and it was concluded that, for the system considered, the fundamental or secondary resonance was of little practical importance.

8.4 SUGGESTIONS FOR FUTURE WORK

In this Thesis, the potential for the application of modern nonlinear dynamics techniques to the problem of a pipe conveying fluid has been demonstrated, but there are still many possible directions in which the present work could be extended. Basically, two different philosophies may be followed: one may either (i) use or improve the existing model on the same system, or (ii) apply the results and methods on other fluidelatic problems.

(i) First category

Even though the dynamics has been studied for a wide range of parameters, it seems obvious that a systematic parametric study might be useful. For example, it would be interesting to examine in detail the effect of varying the mass parameter β, especially for values of β larger than 0.3 or 0.4, where qualitative changes have been observed in several previous investigations (Lundgren *et al.* 1979; Rousselet & Herrmann 1981).

Because of the diversity of the dynamical response, especially if the physical system is slightly altered, it is not clear what would be the combined effect of several modifications. For example, it is not obvious to say, *a priori*, what would be the dynamical response if several springs or masses were added, not to say if the pipe was further subjected to a pulsating flow!

It would be interesting to investigate the dynamics of the system on the basis of the equations of motion derived *without* the assumption of the inextensibility condition, i.e. by keeping the lateral and longitudinal force components in their original form, equation (2.62).

Refinements could be made to the modeling of the fluid. The fluid forces could be formulated by means of ideal flow theory, rather than by considering the fluid as an infinitely flexible rod (plug flow). Moreover, even in the case where plug flow theory is used, nonlinearities of the flow components could be considered.

(ii) Second category

As already mentioned in Section 8.2, the techniques developed here could well be applied on a large variety of physical systems; for example, considering only the field of fluid-structure interactions and cylindrical structures, it seems that the *nonlinear dynamics of curved pipes and of shells* have not received much attention (Païdoussis & Li 1993; Païdoussis 1996), and thus deserve a better treatment.

Recently, the problem of the identification of system parameters has been studied extensively from the perspective of modern nonlinear dynamics (Abarbanel *et al.* 1993), and it would be particularly interesting to use the system of a pipe conveying fluid as a test case for these new techniques, since comparison between theory and experiment is rather easy.

Similarly, the domain of nonlinear control is one that is expanding very fast (Nijmeijer & van der Shaft 1990; Païdoussis & Namachchivaya 1992; Kolk & Lerman 1992; Isidori 1995), so that this system might be used again to try known techniques or to develop new ones.

REFERENCES

- ABARBANEL, H.D.I., BROWN, R., SIDOROWICH, J.J. & TSIMRING, L.S. 1993 The analysis of observed chaotic data in physical systems. *Reviews of Modern Physics* **65**, 1331-1392.

- ARIARATNAM, S.T. & NAMACHCHIVAYA, N.S. 1986 Dynamic stability of pipes conveying pulsating fluid. *Journal of Sound and Vibration* **107**, 215-230.

- ARNOLD, V.I. 1983 *Geometrical Methods in the Theory of Ordinary Differential Equations.* New York: Springer.

- ARONSON, V.I. 1991 CHAOS: a SUN based program for analysing chaotic systems. College Park, Maryland: Programmers Guide.

- ATLURI, S. 1973 Nonlinear vibrations of a hinged beam including nonlinear inertia effects. *Journal of Applied Mechanics* **40**, 121-126.

- BAJAJ, A.K. 1982 Bifurcating periodic solutions in rotationally symmetric systems. *SIAM Journal of Applied Mathematics* **42**, 1078-1098.

- BAJAJ, A.K. 1984 Interactions between self and parametrically excited motions in articulated tubes. *Journal of Applied Mechanics* **51**, 423-429. Bajaj, A.K. 1986 Resonant parametric perturbations of the Hopf bifurcation. *Journal of Mathematical Analysis and Applications* **115**, 214-224.

- BAJAJ, A.K. 1986 Resonant parametric perturbations of the Hopf bifurcation. *Journal of Mathematical Analysis and Applications* **115**, 214-224.

- BAJAJ, A.K. 1987 Nonlinear dynamics of tubes carrying a pulsatile flow. *Dynamics and Stability of Systems* **2**, 19-41.

- BAJAJ, A.K. & SETHNA, P.R. 1982 Bifurcations in three dimensional motions of articulated tubes. I: Linear systems and symmetry.

- BAJAJ, A.K. & SETHNA, P.R. 1991 Effect of symmetry-breaking perturbations on flow-induced oscillations in tubes. *Journal of Fluids and Structures* **5**, 651-679.

- BAJAJ, A.K., SETHNA, P.R. & LUNDGREN, T.S. 1980 Hopf bifurcation phenomena in tubes carrying fluid. *SIAM Journal of Applied Mathematics* **39**, 213-230.

- BECKER, M., HAUGER, W. & WINZEN, W. 1978 Exact stability analysis of uniform cantilevered pipes conveying fluid or gas. *Archives of Mechanics (Warsaw)* **30**, 757-768.

- BENJAMIN, T.B. 1961 Dynamics of a system of articulated pipes conveying fluid. I. Theory. II. Experiments. *Proceedings of the Royal Society (London)* Series A **261**, 457-486 and 487-499.

- BERGÉ, P., POMEAU, Y., AND VIDAL, C. 1984 *Order within Chaos.* New York: Wiley.

- BLEVINS, R.D. 1977 *Flow-Induced Vibration.* New York: Van Nostrand Publishing.

- BOLOTIN, V.V. 1963 *Nonconservative Problems of the Theory of Elastic Stability.* London: Pergamon.

- BOLOTIN, V.V. 1964 *The Dynamic Stability of Elastic Systems.* San Francisco: Holden Day.

- BOURRIÈRES, F.-J. 1939 Sur un phénomène d'oscillation auto-entretenue en mécanique des fluides réels. *Publications Scientifiques et Techniques du Ministère de l'Air*, No. 147.

- BRENAN, K.E., CAMPBELL, S.L., & PETZOLD, L.R. 1989 *Numerical Solution of Initial-Value Problems in Differential-Algebraic Equations.* New York: Elsevier Science Publishing.

- CAMERON, T.M. & GRIFFIN J.H. 1989 An alternating frequency/time domain method for calculating the steady state response of nonlinear dynamical systems. *Journal of Applied Mechanics*, **56**, 149-154.

- CARR, J. 1981 *Applications of Center Manifold Theory.* New York: Springer.

- CARTWRIGHT, J.H.E. & PIRO, O. 1992 The dynamics of Runge-Kutta methods. *International Journal of Bifurcation and Chaos* **2**, 427-449.

- CHAMPNEYS, A.R. 1991 Homoclinic orbits in the dynamics of articulated pipes conveying fluid. *Nonlinearity* **4**, 747-774.

- CHAMPNEYS, A.R. 1993 Homoclinic tangencies in the dynamics of articulated pipes conveying fluid. *Physica* **62**D, 347-359.

- CHEN, S.S. 1971 Flow-induced instability of an elastic tube. *ASME Paper* No. 71-Vibr.-39.

- CH'NG, E. 1978 A theoretical analysis of nonlinear effects on the flutter and divergence of a tube conveying fluid. Dept of Mechanical and Aerospace Engineering, Princeton University, AMS Report No. 1343 (revised).

- CH'NG, E. & DOWELL, E.H. 1979 A theoretical analysis of nonlinear effects on the flutter and divergence of a tube conveying fluid. In *Flow-Induced Vibrations* (eds S.S. Chen & M.D. Bernstein), pp. 65-81. New York: ASME.

- CHOW, S.N. & MALLET-PARET, J. 1977 Integral averaging and bifurcation. *Journal of Differential Equations* **26**, 112-159.

- CLENSHAW, C.W. & NORTON, H.J. 1963 The solution of nonlinear differential equation in Chebyshev series. *Computer Journal* **6**, 88-92.

- COPELAND, G.S. 1992 Flow-Induced Vibration and Chaotic Motion of a Slender Tube Conveying Fluid, Ph.D Thesis, Cornell University, Ithaca, New York.

- COPELAND, G.S. & MOON, F.C. 1992 Chaotic flow-induced vibration of a flexible tube with end mass. *Journal of Fluids and Structures* **6**, 705-718.

- DEVANEY, R.L. 1986 *An Introduction to Chaotic Dynamical Systems.* Menlo Park, California: Benjamin/Cummings.

- DODDS, H.L. JR. & RUNYAN, H.L. 1965 Effect of high velocity fluid flow on the bending vibrations and static divergence of a simply supported pipe. *NASA Technical Note* D-2870.

- DOEDEL, E. 1981 AUTO, a program for automatic bifurcation analysis of autonomous systems. *Congressus Numerantium* **30**, 265-284.

- DOEDEL, E.J. AND KERNÉVES, J.P. 1986 AUTO: software for continuation and bifurcation problems in ordinary differential equations, Applied Mathematics Report, Califonia Institute of Technology, Passadena, California, U.S.A. (This report can be obtained from doedel@cs.concordia.ca).

- EDELSTEIN, W.S. & CHEN, S.S. 1985 Flow-induced instability of an elastic tube with a variable support. *Nuclear Engineering and Design* **84**, 1-11.

- EDELSTEIN, W.S., CHEN, S.S. & JENDRZEJCZYK, J.A. 1986 A finite element computation of the flow-induced oscillations in a cantilevered tube. *Journal of Sound and Vibration* **107**, 121-129.

- Ekwaro-Osire, S. & Ertas, A. 1994 Response statistics of a beam-mass oscillator under combined harmonic and random excitation. *Symposium on Nonlinear and Stochastic Dynamics*, AMD-Vol. 192, 179-189. New-York: ASME.

- Eringen, A.C. 1987 *Mechanics of Continua.* New York: Wiley

- Feodos'ev, V.P. 1951 Vibrations and stability of a pipe when liquid flows through it. *Inzhenernyi Sbornik* **10**, 169-170.

- Feigenbaum, M.J. 1983 Universal behaviour in nonlinear system. In *Nonlinear Dynamics and Turbulence* (eds G. Barenblatt, G. Iooss & D.D. Joseph), pp. 101-138. Boston: Pitman.

- Ferri, A.A. 1986 On the equivalence of the incremental harmonic balance method and the harmonic balance Newton-Raphson method. *Journal of Applied Mechanics* **53**, 455-457.

- Fox, L. & Parker, I.B. 1968 *Polynomial in Numerical Analysis.* Toronto: Oxford University Press.

- Fung, Y.C. 1969 *A First Course in Continuum Mechanics.* New Jersey: Prentice Hall.

- Gear, C.W. 1971 *Numerical Initial Value Problems in Ordinary Differential Equations.* New Jersey: Prentice Hall.

- A. Gelb & W.E. Vander Velde 1968 *Multiple-Input Describing Functions and Nonlinear System Design.* New York: McGraw-Hill.

- Golubitsky, M. & Schaeffer, D. 1985 *Singularities and Groups in Bifurcation Theory.* New York: Springer.

- Gregory, R.W. & Païdoussis, M.P. 1966 Unstable oscillation of tubular cantilevers conveying fluid. I. Theory. II. Experiments. *Proceedings of the Royal Society (London)* A **293**, 512-527 and 528-542.

- GUCKENHEIMER, J. & HOLMES, P. 1983 *Nonlinear Oscillations, Dynamical Systems, and Bifurcations of Vector Fields.* New York: Springer.

- HAIRER, E., NORSETT, S.P. & WANNER, G. 1993 *Solving Ordinary Differential Equations.* Berlin: Springer.

- HALE, J.K. 1969 *Ordinary Differential Equations.* New York: Wiley.

- HANNOYER, M.J. & PAÏDOUSSIS, M.P. 1979 Dynamics of slender tapered beams with internal or external axial flow. I: Theory. II: Experiments. *Journal of Applied Mechanics* **46**, 45-51 and 52-57.

- HARTMAN, P. 1964, *Ordinary Differential Equations.* New York: Wiley.

- HERRMANN, G. 1967 Stability of equilibrium of elastic systems subjected to non-conservative forces. *Applied Mechanics Reviews* **20**, 103-108.

- HERRMANN, G. & NEMAT-NASSER, S. 1967 Instability modes of cantilevered bars induced by fluid flow through attached pipes. *International Journal of Solids and Structures* **3**, 39-52.

- HILL, J.L. & SWANSON, C.P. 1970 Effects of lumped masses on the stability of fluid conveying tubes. *Journal of Applied Mechanics* **37**, 494-497.

- HINDMARSH, A.C. 1983 *Scientific Computing* (eds. R.S. Stepleman et al.), 55-64. Amsterdam: North-Holland. ODEPACK, a systematized collection of ODE solvers (can be obtained by email at netlib@research.att.com).

- HOLMES, P.J. 1977 Bifurcations to divergence and flutter in flow-induced oscillations: a finite-dimensional analysis. *Journal of Sound and Vibration* **53**, 471-503.

- HOLMES, P.J. 1978 Pipes supported at both ends cannot flutter. *Journal of Applied Mechanics* **45**, 619-622.

- HOUBOLT, J.C. 1950 A recurrence matrix solution for the dynamic response of elastic aircraft. *Journal of Aeronautical Sciences* **17**, 540-550.

- HOUSNER, G.W. 1952 Bending vibrations of a pipe line containing flowing fluid. *Journal of Applied Mechanics* **19**, 205-208.

- IOOSS, G. AND JOSEPH, D.D. 1981 *Elementary Stability and Bifurcation Theory.* New York: Springer.

- ISIDORI, A. 1995 *Nonlinear Control Systems.* New York: Springer.

- JENDRZEJCZYK, J.A. & CHEN, S.S. 1985 Experiments on tubes conveying fluid. *Thin-Walled Structures* **3**, 109-134.

- JOHNSON, D.E. 1966 A proof of the stability of the Houbolt method. *AIAA Journal* **4**, 1450-1451.

- JONES, D.J. & LEE, B.H.K. 1985 Time marching numerical solutions of the dynamic response of nonlinear systems. National Research Council of Canada, Report NAE-AN-25, Ottawa, Canada.

- JOSEPH, D.D. & SATTINGER, D.H. 1972 Bifurcating time periodic solutions and their stability. *Archive for Rational Mechanics and Analysis* **45**, 79-109.

- KOLK, W.R. & LERMAN, R.A. 1992 *Nonlinear System Dynamics.* New York: Van Nostrand Reinhold.

- LAMBERT, J.D. 1973 *Computational Methods in Ordinary Differential Equations.* New York: Academic Press.

- LAU, S.L., CHEUNG, Y.K. & CHEN, S. 1989 An alternative perturbation procedure of multiple scales for nonlinear dynamics systems. *Journal of Applied Mechanics* **56**, 667-875.

- LAU, S.L., CHEUNG, Y. K. & WU, S.Y. 1982 A variable parameter incrementation method for dynamic instability of linear and nonlinear vibration of elastic systems. *Journal of Applied Mechanics* **49**, 849-853.

- LAU, S.L., CHEUNG, Y. K. & WU, S.Y. 1983 Incremental harmonic balance method with multiple time scales for aperiodic vibration of nonlinear systems. *Journal of Applied Mechanics* **50**, 871-876.

- LAU, S.L. & YUEN, S.W. 1993 Solution diagram of non-linear dynamic systems by the IHB method. *Journal of Sound and Vibration* **167**, 303-316.

- LI, G.X. & PAÏDOUSSIS, M.P. 1994 Stability, double degeneracy and chaos in cantilevered pipes conveying fluid. *International Journal of Non-Linear Mechanics* **29**, 83-107.

- LING, F.H. 1990 An alternating frequency/time domain method for calculating the steady-state response of nonlinear dynamic systems. *Journal of Applied Mechanics* **57**, 251-252.

- LING, F.H. & WU, X.X. 1987 Fast Galerkin method and its application to determine periodic solutions of non-linear oscillators. *International Journal of Non-Linear Mechanics* **22**, 88-89.

- LUNDGREN, T.S., SETHNA, P.R. & BAJAJ, A.K. 1979 Stability boundaries for flow induced motions of tubes with an inclined terminal nozzle. *Journal of Sound and Vibration* **64**, 553-571.

- MAKRIDES, G.A. & EDELSTEIN, W.S. 1992 Some numerical studies of chaotic motions in tubes conveying fluid. *Journal of Sound and Vibration* **152**, 517-530.

- MANDELBROT, B. 1983 *The Fractal Geometry of Nature.* San Francisco: Freeman.

- MANNEVILLE, P. & POMEAU, Y. 1980 Different Ways to Turbulence in Dissipative Dynamical Systems. *Physica 1D* **1**, 219-226.

- MARSDEN, J.E. & MCCRACKEN, M. *The Hopf Bifurcation and Its Applications.* New York: Springer. MCIVER, D.B. 1973 Hamilton's principle for systems of changing mass. *Journal of Engineering Mathematics* **7**, 249-261.

- MEIROVITCH, L. 1967 *Analytical Methods in Vibrations.* New York: Macmillan.

- MILES, W.H., PEZESHKI, C. & ELGAR, S. 1992 Bispectral analysis of a fluid elastic system: the cantilevered pipe. *Journal of Fluids and Structures* **6**, 633-640.

- MINORSKY, N. 1962 *Nonlinear Oscillations.* New York: Van Nostrand.

- MISRA, A.K., PAÏDOUSSIS, M.P. & VAN, K.S. 1988 On the dynamics of curved pipes transporting fluid. I: inextensible theory. II: extensible theory. *Journal of Fluids and Structures* **2**, 211-244 and 245-261.

- MOON, F.C. 1987 *Chaotic Vibrations: An Introduction for Applied Scientists and Engineers.* New York: Wiley.

- MOON, F.C. 1992 *Chaotic and Fractal Dynamics: an Introduction for applied Scientists and Engineers.* New York: Wiley.

- MOTE, C.D. JR. 1968 Dynamic stability of an axially moving band. *Journal of the Franklin Institute* **285**, 329-346.

- NAMACHCHIVAYA, N.S. 1989 Non-linear dynamics of supported pipe conveying pulsating fluid. 1. Subharmonic resonance. *International Journal of Non-Linear Mechanics* **24**, 185-196.

- NAMACHCHIVAYA, N.S. & ARIARATNAM, S.T. 1987 Periodically perturbed Hopf bifurcation. *Journal of Applied Mathematics* **47**, 15-39.

- NAMACHCHIVAYA, N.S. & TIEN, W.M. 1989 Bifurcation behavior of nonlinear pipes conveying pulsating flow. *Journal of Fluids and Structures* **3**, 609-629.

- NAMACHCHIVAYA, N.S. & TIEN, W.M. 1989b Non-linear dynamics of supported pipe conveying pulsating fluid. 2. Combination resonance. *International Journal of Non-Linear Mechanics* **24**, 197-208.

- NATH, Y. & SANDEEP, K. 1994 The stability of the Houbolt time marching scheme in non-linear systems. *Journal of Sound and Vibration* **175**, 565-569.

- NAYFEH, A. H. 1981 *Introduction to Perturbation Techniques.* New York: Wiley.

- NAYFEH, A.H. 1985 *Problems in Perturbation.* NewYork: Wiley.

- NAYFEH, A. H. 1986 Perturbation methods in nonlinear dynamics. In *Nonlinear Dynamics Aspects of Particle Accelerators*; Lecture Notes in Physics **247**, pp. 238-314. New York: Springer.

- NAYFEH, A.H. 1993 *Method of Normal Forms.* New York: Wiley.

- NAYFEH, A.H., BALACHANDRAN, B., COLBERT, M.A. & NAYFEH, M.A. 1989 An experimental investigation of complicated responses of a two-degree-of-freedom structure. *Journal of Applied Mechanics* **56**, 960-967.

- NAYFEH, A.H. & MOOK, D.T. 1979 *Nonlinear Oscillations.* New York: Wiley.

- NEMAT-NASSER, S., PRASAD, S.N. & HERRMANN, G. 1966 Destabilizing effect of velocity-dependent forces in non-conservative continuous systems. *AIAA Journal* **4**, 1276-1280.

- NIJMEIJER, H. & VAN DER SCHAFT, A.J. 1990 *Nonlinear Dynamical Control Systems.* New York: Springer.

- NIORDSON, F.I. 1953 Vibrations of a cylindrical tube containing flowing fluid. *Kungliga Tekniska Hogskolans Handlingar (Stockholm)* No. 73.

- NORTON, H.J. 1964 The iterative solution of non-linear ordinary differential equations in Chebyshev series. *Computer Journal* **7**, 76-85.

- PAÏDOUSSIS, M.P. 1966 Dynamics of flexible slender cylinders in axial flow — I. Theory. *Journal of Fluid Mechanics* **26**, 717-736.

- PAÏDOUSSIS, M.P. 1970 Dynamics of tubular cantilevers conveying fluid. *I. Mech. E. Journal of Mechanical Engineering Science* **12**, 85-103.

- PAÏDOUSSIS, M.P. 1980 Flow-induced vibrations in nuclear reactors and heat exchangers. Practical experiences and state of the knowledge. In *Practical Experiences with Flow-Induced Vibrations*, (eds E. Naudascher & D. Rockwell), pp. 1-81. Berlin: Springer.

- PAÏDOUSSIS, M.P. 1981 Fluidelastic vibration of cylinder arrays in axial and cross-flow: state of the art. *Journal of Sound and Vibration* **76**, 329-360.

- PAÏDOUSSIS, M.P. 1987 Flow-induced instabilities of cylindrical structures. *Applied Mechanics Reviews* **40**, 163-175.

- PAÏDOUSSIS, M.P. 1991 Pipes conveying fluid: a model dynamical problem. In *Proceedings of CANCAM'91 (Canadian Congress of Applied Mechanics)*, pp. 1-33, Winnipeg, Man. Canada.

- PAÏDOUSSIS, M.P. 1993 Calvin Rice Lecture: Some Curiosity-Driven Research in Fluid-Structure Interactions and Its Current Applications. *ASME Journal of Pressure Vessel Technology* **115**, 2-14.

- PAÏDOUSSIS, M.P. 1996 *Flow-induced vibrations of slender bodies in axial flow.* In preparation.

- PAÏDOUSSIS, M.P., CHAN, S.P. AND MISRA, A.K. 1984 Dynamics and stability of coaxial cylindrical shells containing flowing fluid. *Journal of Sound and Vibration* **97**, 201-235.

- PAÏDOUSSIS, M.P., CUSUMANO, J.P. & COPELAND, G.S. 1992 Low-dimensional chaos in a flexible tube conveying fluid. *Journal of Applied Mechanics* **59**, 196-205.

- PAÏDOUSSIS, M.P. & DEKSNIS, E.B. 1970 Articulated models of cantilevers conveying fluid: the study of a paradox. *Journal of Mechanical Engineering Science* **12**, 288-300.

- PAÏDOUSSIS, M.P. & ISSID, N.T. 1974 Dynamic stability of pipes conveying fluid. *Journal of Sound and Vibration* **33**, 267-294.

- PAÏDOUSSIS, M.P. & ISSID, N.T. 1976 Experiments on parametric resonance of pipes containing pulsatile flow. *Journal of Applied Mechanics* **43**, 198-202.

- PAÏDOUSSIS, M.P. & LAITHIER, B.E. 1976 Dynamics of Timoshenko beams conveying fluid. *Journal of Mechanical Engineering Science* **18**, 210-220.

- PAÏDOUSSIS, M.P. & LI, G.X. 1993 Pipes conveying fluid: a model dynamical problem. *Journal of Fluids and Structures* **7**, 137-204.

- PAÏDOUSSIS, M.P., LI, G.X. & MOON, F.C. 1989 Chaotic oscillations of the autonomous system of a constrained pipe conveying fluid. *Journal of Sound and Vibration* **135**, 1-19.

- PAÏDOUSSIS, M.P., LI, G.X. & RAND, R.H. 1991 Chaotic motions of a constrained pipe conveying fluid: comparison between simulation, analysis and experiment. *Journal of Applied Mechanics* **58**, 559-565.

- PAÏDOUSSIS, M.P. & MOON, F.C. 1988 Nonlinear and chaotic fluidelastic vibrations of a flexible pipe conveying fluid. *Journal of Fluids and Structures* **2**, 567-591.

- PAÏDOUSSIS, M.P. & NAMACHCHIVAYA, N.S. (editors) 1992 *Proceedings 3rd International Symposium on Flow-Induced Vibration and Noise; Volume 8: Stability and Control of Pipes Conveying Fluid.* New York: ASME.

- PAÏDOUSSIS, M.P. & SEMLER, C. 1993 Nonlinear and chaotic oscillations of a constrained cantilevered pipe conveying fluid: a full nonlinear analysis. *Nonlinear Dynamics* **4**, 655-670.

- PAÏDOUSSIS, M.P. & SEMLER, C. 1993 Nonlinear dynamics of a fluid-conveying cantilevered pipe with an intermediate spring support. *Journal of Fluids and Structures* **7**, 269-298.

- PAÏDOUSSIS, M.P. & SEMLER, C. 1996 Nonlinear dynamics of a fluid-conveying cantilevered pipe with a small mass attached at the free end. Submitted to the *International Journal of Non-Linear Mechanics.*

- PAÏDOUSSIS, M.P. & SUNDARARAJAN, C. 1975 Parametric and combination resonances of a pipe conveying pulsating fluid. *Journal of Applied Mechanics* **42**, 780-784.

- PARK, K.C. 1975 An improved stiffly stable method for direct integration of nonlinear structural dynamic equations. *Journal of Applied Mechanics* **42**, 464-470.

- PARKER, T.S. & CHUA, L.O. 1989 *Practical Numerical Algorithms for Chaotic Systems.* New York: Springer.

- PIERRE, C. & DOWELL, E.H. 1985 A study of dynamic instability of plates by an extended incremental harmonic balance method. *Journal of Applied Mechanics* **52**, 693-697.

- PIERRE, C., FERRI, A.A. & DOWELL, E.H. 1985 Multi-harmonic analysis of dry friction damped systems using an incremental harmonic balance method. *Journal of Applied Mechanics* **52**, 958-964.

- PRESS, W.H., TEUKOLSKY, S.A., VETTERLING, W.T. & FLANNERY, B.P. 1992 *Numerical Recipes in FORTRAN, 2nd edition.* Cambridge: Cambridge University Press.

- RAND, R.H. 1984 *Computer Algebra in Applied Mathematics: An Introduction to MACSYMA*. Boston: Pitman.

- RAND, R.H. & ARMBRUSTER, D. 1987 *Perturbation Methods, Bifurcation Theory, and Computer Algebra.* New York: Springer.

- ROTH, W. 1964 Instabilität durchströmter Rohre. *Ingenieur-Archiv* **33**, 236-263.

- ROUSSELET, J. 1975 *Dynamic behavior of pipes conveying fluid near critical velocities.* Ph.D. Dissertation, Stanford University, California, U.S.A.

- ROUSSELET, J. & HERRMANN, G. 1977 Flutter of articulated pipes at finite amplitude. *Journal of Applied Mechanics* **44**, 154-158.

- ROUSSELET, J. & HERRMANN, G. 1981 Dynamic behaviour of continuous cantilevered pipes conveying fluid near critical velocities. *Journal of Applied Mechanics* **48**, 943-947.

- ROUTH, E.J. 1960 *Dynamics of System of Rigid Bodies. Part II. Articles*, pp. 290–301. New York: Dover.

- SANDERS, J.A. & VERHULST, F. 1985 *Averaging Methods in Nonlinear Dynamical Systems.* New York: Springer.

- SEKAR, P. & NARAYANAN, S. 1994 Periodic and chaotic motions of a square prism in cross-flow. *Journal of Sound and Vibration* **170**, 1-24.

- SEMLER, C. 1991 *Nonlinear Dynamics and Chaos of a Pipe Conveying Fluid.* Master's Thesis, Faculty of Engineering, McGill University, Montréal, Canada.

- SEMLER, C., GENTLEMAN, W.C. & PAÏDOUSSIS, M.P. 1996 Numerical solutions of second-order implicit ordinary differential equations. *Journal of Sound and Vibration* (accepted for publication).

- SEMLER, C., LI, G.X. & PAÏDOUSSIS, M.P. 1994 The nonlinear equations of motion of pipes conveying fluid. *Journal of Sound and Vibration* **169**, 577-599.

- SEMLER, C. & PAÏDOUSSIS, M.P. 1995 Intermittency route to chaos of a cantilevered pipe conveying fluid fitted with a buoyant end-mass. *Journal of Applied Mechanics* **62**, 903-908.

- SEMLER, C. & PAÏDOUSSIS, M.P. 1995b Parametric resonances of a cantilevered pipe conveying fluid: a nonlinear analysis, ASME Design Engineering Technical Conferences, Boston, Ma.; in *Proceedings, Vol.3, Part A, Vibration of Nonlinear, Random, and Time-Varying Systems*, Section on Time Varying Systems and Structures (eds S.C. Sinha, J.P. Cusumano and F. Pfeiffer), DE-Vol. 84-1, 325-335.

- SEMLER, C. & PAÏDOUSSIS, M.P. 1996 Nonlinear analysis of the parametric resonances of a planar fluid-conveying cantilevered pipe. Submitted to the *Journal of Fluids and Structures.*

- SETHNA, P.R. & GU, X.M. 1985 On global motions of articulated tubes carrying fluid. *International Journal of Non-Linear Mechanics* **20**, 453-469.

- SETHNA, P.R. & SHAW, S.W. 1987 On codimension-three bifurcations in the motion of articulated tubes conveying a fluid. *Physica* **24**D, 305-327.

- SEYDEL, R. 1988, *From Equilibrium to Chaos: Practical Bifurcation and Stability Analysis.* New York: Elsevier.

- SINHA, S.C. 1994 Personal communication.

- SINHA, S.C., SENTHILNATHAN, N.R. & PANDIYAN, R. 1993 A new technique for the analysis of parametrically excited systems. *Nonlinear Dynamics* **4**, 483-489.

- SINHA, S.C. & WU, D.-H. 1991 An efficient computational scheme for the analysis of periodic systems. *Journal of Sound and Vibration* **151**, 91-117.

- SMALE, S. 1963 Diffeomorphisms with many periodic points. In *Differential and Combinatorial Topology* (ed. S.S. Cairns), pp. 63-80. Princeton: Princeton University Press.
- SMALE, S. 1967 Differentiable dynamical systems. *Bulletin of the American Mathematical Society* **73**, 747-817.
- SNOWDON, J.C. 1968 *Vibration and Shock in Damped Mechanical Systems.* New York: Wiley.
- STEINDL, A. & TROGER, H. 1988 Flow induced bifurcations to 3-dimensional motions of tubes with an elastic support. In *Trends in Applications of Mathematics to Mechanics* (eds J.F. Besserling & W. Eckhaus), pp. 128-138. Berlin: Springer.
- STOKER, J.J. 1968 *Nonlinear elasticity.* New York: Gordon and Breach.
- SUGIYAMA, Y., TANAKA, Y., KISHI, T. & KAWAGOE, H. 1985 Effect of a spring support on the stability of pipes conveying fluid. *Journal of Sound and Vibration* **100**, 257-270.
- SZEMPLINSKA-STUPNICKA, W., PLAUT, R.H. & HSIEH, J.-C. 1989 Period doubling and chaos in unsymmetric structures under parametric excitation. *Journal of Applied Mechanics* **56**, 947-952.
- TAKENS, F. 1974 Singularities of Vector Fields. *Publications Mathématiques* (Institut des Hautes Etudes Scientifiques), **43**, 47–100.
- TANG, D.M. & DOWELL, E.H. 1988 Chaotic oscillations of a cantilevered pipe conveying fluid. *Journal of Fluids and Structures* **2**, 263-283.
- THOMPSON, J.M.T. 1982 'Paradoxial' mechanics under fluid flow. *Nature* **296**, 135-137.

- THURMAN, A.L. & MOTE, C.D. JR. 1969 Non-linear oscillation of a cylinder containing flowing fluid. *ASME Journal of Engineering for Industry* **91**, 1147-1155.

- TILLERSON, J.R. & STRICKLIN, J.A. 1970 Numerical methods of integration applied in the nonlinear dynamic analysis of shells of revolution. *Report NASA-CR-108639.* Washington, D.C., U.S.A.: National Aeronautics and Space Administration.

- TIMOSHENKO, S.P. & GERE, J.M.1961 *Theory of Elastic Stability.* New York: McGraw-Hill.

- TOUSI, S. & BAJAJ, A.K. 1985 Period-doubling bifurcations and modulated motions in forced mechanical systems. *Journal of Applied Mechanics* **57**, 446–452.

- URABE, M. 1965 Galerkin's procedure for nonlinear periodic systems. *Archive for Rational Mechanics and Analysis* **20**, 120-152.

- WEAVER, H.J. 1989 *Theory of Discrete and Continuous Fourier Analysis.* Toronto: John Wiley.

- WIGGINS, S. 1988 *Global Bifurcations and Chaos: Analytical Methods.* New York: Springer.

- WILEY, J.C. & FURKERT, R.E. 1972 Stability of beams subjected to a follower force within the span. *ASCE National Structural Engineering Meeting*, Reprint 1641.

- WRIGHT, K. 1963 Chebyshev collocation methods for ordinary differential equations. *Computer Journal* **6**, 358-365.

- WU, R.W.H. & WITMER, E.A. 1973 Nonlinear transient responses of structures by the spatial finite-element method. *AIAA Journal* **11**, 1110-1117.

- YOSHIZAWA, M., NAO, H., HASEGAWA, E. & TSUJIOKA, Y. 1986 Lateral vibration of a flexible pipe conveying fluid with pulsating flow. *Bulletin of JSME* **29**, 2243-2250.

- ZIEGLER, H. 1968 *Principles of Structural Stability.* Waltham, Mass: Blaisdell.

Appendix A

Derivation of Equation (2.22)

Let us find the quantity A defined by

$$A = \int_0^L g(s) \left(\int_0^s f(s)\, \delta y \, \mathrm{d}s \right) \mathrm{d}s. \tag{A.1}$$

Integrating by parts leads to

$$\begin{aligned}
A &= \left[\left(\int_0^s g(s)\mathrm{d}s \right) \left(\int_0^s f(s)\, \delta y \, \mathrm{d}s \right) \right]_0^L - \int_0^L f(s)\, \delta y \left(\int_0^s g(s)\mathrm{d}s \right) \mathrm{d}s \\
&= \left(\int_0^L g(s)\mathrm{d}s \right) \left(\int_0^L f(s)\, \delta y \, \mathrm{d}s \right) - \int_0^L \left(\int_0^s g(s)\mathrm{d}s \right) f(s)\, \delta y \, \mathrm{d}s \\
&= \int_0^L \left(\int_0^L g(s)\mathrm{d}s \right) f(s)\, \delta y \, \mathrm{d}s - \int_0^L \left(\int_0^s g(s)\mathrm{d}s \right) f(s)\, \delta y \, \mathrm{d}s \\
&= \int_0^L \left(\int_0^L g(s)\mathrm{d}s - \int_0^s g(s)\mathrm{d}s \right) f(s)\, \delta y \, \mathrm{d}s \\
&= \int_0^L \left(\int_s^L g(s)\mathrm{d}s \right) f(s)\, \delta y \, \mathrm{d}s.
\end{aligned} \tag{A.2}$$

This proves the validity of equation (2.22).

Appendix B

Interesting Properties of the Curvature κ and the Unit Vector $\boldsymbol{\tau}$

Let the location of a material point be given by

$$\mathbf{r} = x\,\mathbf{i} + y\,\mathbf{j} + z\,\mathbf{k} \tag{B.1}$$

where $\mathbf{i}, \mathbf{j}, \mathbf{k}$ are fixed orthogonal unit vectors. As it was proved for an inextensible pipe in Chapter 2, the arc length s can be used as the material variable. Hence,

$$\boldsymbol{\tau} = \partial \mathbf{r}/\partial s = \partial x/\partial s\,\mathbf{i} + \partial y/\partial s\,\mathbf{j} + \partial z/\partial s\,\mathbf{k}, \tag{B.2}$$

and the normal and the binormal vectors, $\mathbf{n}$ and $\mathbf{b}$, are given by

$$\partial \boldsymbol{\tau}/\partial s = \kappa\,\mathbf{n}, \quad \mathbf{b} = \boldsymbol{\tau} \times \mathbf{n}, \tag{B.3}$$

where κ is the curvature of the centreline.

By definition, because $\boldsymbol{\tau}$, $\mathbf{n}, \mathbf{b}$ represent orthogonal vectors, one has

$$\boldsymbol{\tau} \cdot \frac{\partial \boldsymbol{\tau}}{\partial s} = 0, \quad \boldsymbol{\tau} \cdot \mathbf{b} = 0, \tag{B.4}$$

For a two-dimensional problem, $\boldsymbol{\tau}$ being a unit vector,

$$||\boldsymbol{\tau}|| = (\partial x/\partial s)^2 + (\partial y/\partial s)^2 = 1. \tag{B.5}$$

Using (B.3) through (B.5) and Frenet-Serret formulae yields

$$\frac{\partial \boldsymbol{\tau}}{\partial s} \cdot \frac{\partial^2 \boldsymbol{\tau}}{\partial s^2} = \mathbf{b} \cdot \frac{\partial \mathbf{b}}{\partial s} = \frac{1}{2} \frac{\partial \kappa^2}{\partial s}, \tag{B.6}$$

$$\boldsymbol{\tau} \cdot \frac{\partial^2 \boldsymbol{\tau}}{\partial s^2} = -\kappa^2, \tag{B.7}$$

$$\boldsymbol{\tau} \cdot \frac{\partial^3 \boldsymbol{\tau}}{\partial s^3} = -\frac{1}{2} \frac{\partial \kappa^2}{\partial s}. \tag{B.8}$$

Appendix C

Nonlinear Coefficients of the Discretized Equation (3.11)

The fourth-order tensors in equation (3.11) are computed numerically from the integrals of the eigenfunctions $\phi_i(\xi)$. They are defined as follows.

$$
\begin{aligned}
\alpha_{ijkl} &= u^2 a_{ijkl} + \gamma\, b_{ijkl} + c_{ijkl}, \\
\beta_{ijkl} &= 2\,u\,\sqrt{\beta}\, d_{ijkl}, \\
\gamma_{ijkl} &= \int_0^1 \phi_i \phi_j' \left(\int_0^\xi \phi_k' \phi_l' \,\mathrm{d}\xi \right) \mathrm{d}\xi \;-\; \int_0^1 \phi_i \phi_j'' \left(\int_\xi^1 \int_0^\xi \phi_k' \phi_l' \,\mathrm{d}\xi \mathrm{d}\xi \right) \mathrm{d}\xi,
\end{aligned}
$$

where

$$
\begin{aligned}
a_{ijkl} &= \int_0^1 \phi_i \phi_j'' \phi_k' \phi_l' \,\mathrm{d}\xi - \int_0^1 \phi_i \phi_j' \left\{ \int_0^\xi \phi_k' \phi_l''' \mathrm{d}\xi \right\} \mathrm{d}\xi \\
&+ \int_0^1 \phi_i \phi_j'' \left\{ \int_\xi^1 \int_0^\xi \phi_k' \phi_l''') \,\mathrm{d}\xi \mathrm{d}\xi \right\} \mathrm{d}\xi - \int_0^\xi \phi_i \phi_j'' \left\{ \int_0^\xi \phi_k' \phi_l'' \,\mathrm{d}\xi \right\} \,\mathrm{d}\xi, \\
b_{ijkl} &= -\tfrac{3}{2} \int_0^1 \phi_i \phi_j'' \phi_k' \phi_l' (1-\xi) \,\mathrm{d}\xi - \tfrac{1}{2} \int_0^1 \phi_i \phi_j' \phi_k' \phi_l' \,\mathrm{d}\xi \\
&+ \int_0^1 \phi_i \phi_j' \left\{ \int_0^\xi \phi_k' \phi_l''' (1-\xi) \,\mathrm{d}\xi \right\} \mathrm{d}\xi \\
&- \int_0^1 \phi_i \phi_j'' \left\{ \int_\xi^1 \int_0^\xi \phi_k' \phi_l''' (1-\xi) \,\mathrm{d}\xi \mathrm{d}\xi \right\} \mathrm{d}\xi \\
&+ \int_0^1 \phi_i \phi_j'' \left\{ \int_\xi^1 \phi_k' \phi_l' \,\mathrm{d}\xi \right\} \mathrm{d}\xi,
\end{aligned}
$$

$$
\begin{aligned}
c_{ijkl} &= 3\int_0^1 \phi_i\phi_j'\phi_k''\phi_l''' \, \mathrm{d}\xi + \int_0^1 \phi_i\phi_j''\phi_k''\phi_l'' \, \mathrm{d}\xi \\
&- \int_0^1 \phi_i\phi_j'' \left\{ \int_\xi^1 \int_0^\xi \phi_k''\phi_l'''' \mathrm{d}\xi \mathrm{d}\xi \right\} \mathrm{d}\xi \\
&+ \int_0^1 \phi_i\phi_j' \left\{ \int_0^\xi \phi_k''\phi_l'''' \mathrm{d}\xi \right\} \mathrm{d}\xi - \int_0^1 \phi_i\phi_j'' \left\{ \int_\xi^1 \phi_k''\phi_l''' \mathrm{d}\xi \right\} \mathrm{d}\xi, \\
d_{ijkl} &= \int_0^1 \phi_i\phi_j'\phi_k'\phi_l' \, \mathrm{d}\xi - \int_0^1 \phi_i\phi_j' \left\{ \int_0^\xi \phi_k'\phi_l'' \mathrm{d}\xi \right\} \mathrm{d}\xi \\
&+ \int_0^1 \phi_i\phi_j'' \left\{ \int_\xi^1 \int_0^\xi \phi_k'\phi_l'' \, \mathrm{d}\xi \mathrm{d}\xi \right\} \mathrm{d}\xi - \int_0^1 \phi_i\phi_j'' \left\{ \int_\xi^1 \phi_k'\phi_l' \, \mathrm{d}\xi \right\} \mathrm{d}\xi.
\end{aligned}
$$

Appendix D

Analytical Computation of Matrix [A] Defined in Equation (3.14) and Routh's Criteria

This is an output file generated by Mathematica. The matrix [A] and the coefficients of the characteristic polynomial are computed as a function of u, γ, β, and k. The viscous damping $\alpha = 0.005$ and the location of the spring $\xi_s = 0.8$ are kept constant. The number of mode is equal to $N = 2$. The solution corresponding to the static instability for $k = 100$ is also shown graphically.

(Local B) In[12]:=

```
nmode = 2; (* Corresponds to the number of modes *)
xspring = 0.8;  (* Position of the spring *)
ar = 0.005;     (* Damping coefficient alpha *)

(* EIGENVALUES *)

rl[1] = 1.875104043341462;
rl[2] = 4.694091054370627;

(* SIGMA COEFFICIENTS *)

Do [{si[i] = (Sinh[rl[i]]-Sin[rl[i]])/
                           (Cosh[rl[i]]+Cos[rl[i]]),
   tm = rl[i]*1,
   ph[i] = Cosh[tm]-Cos[tm]-si[i]*(Sinh[tm]-Sin[tm]),
   tm = rl[i]*xspring,
   phsp[i] = Cosh[tm]-Cos[tm]-si[i]*(Sinh[tm]-Sin[tm])
},{i,nmode}]

(* COEFFICIENTS OF EIGENFUNCTIONS *)

Do [ Do [{
    tau[i,j] = (rl[i]/rl[j])^2,
    one[i,j] = (-1)^(i+j),
    If [i==j, delta[i,j] = 1, delta[i,j] = 0],
    If [j==i,bb[i,j] = 2.0,
             bb[i,j] = 4.0/(tau[i,j]+one[i,j])],
    If [j==i,cc[i,j] = rl[j]*si[j]*(2.0-rl[j]*si[j]),
             cc[i,j] = 4.0*(rl[j]*si[j]-rl[i]*si[i])/
                             (one[i,j]-tau[i,j])],
    If [j==i,ee[i,j] = 2.0 - 0.5*cc[i,j],
           ee[i,j] = (4.0*(rl[j]*si[j]-rl[i]*si[i]+2.0
             *one[i,j]-2.0*(1.0+tau[i,j]^2)*bb[i,j])
                          /(1.0-tau[i,j]^2)-cc[i,j]],
    ff[i,j] = bb[i,j] - ee[i,j]},
{j,nmode}],{i,nmode}];

(* THE DAMPING AND STIFFNESS MATRICES*)

 Do [ Do [{
    rc[i,j] = -(ar*rl[j]^4*delta[i,j]
                        + 2.0*Sqrt[ba]*u*bb[i,j]),
    rk[i,j] = -(rl[j]^4*delta[i,j] +u^2*cc[i,j]
             + gama*ee[i,j] + ksp*phsp[i]*phsp[j])},
{j,nmode}],{i,nmode}];
```

(Local B) In[16]:=

```
(* LINEAR MATRIX A *)

Do [ Do [{
  r[i,j] = 0,
  r[i,j+nmode] = delta[i,j],
  r[i+nmode,j] = rk[i,j],
  r[i+nmode,j+nmode] = rc[i,j]},
{j,nmode}],{i,nmode}]
Do [ Do [Print["a[",i,",",j,"]=",r[i,j]],{i,2*nmode}],
                                           {j,2*nmode}]
a = Table[r[i,j],{i,2*nmode},{j,2*nmode}];
```

```
a[1,1]=0
a[2,1]=0
a[3,1]=-12.3624 - 1.57088 gama - 2.10527 ksp -

             2
   0.858244 u
                                                2
a[4,1]=0.42232 gama + 0.203238 ksp - 1.87385 u
a[1,2]=0
a[2,2]=0
                                                2
a[3,2]=0.42232 gama + 0.203238 ksp + 11.7432 u
a[4,2]=-485.519 - 8.64714 gama - 0.0196201 ksp +

            2
   13.2943 u
a[1,3]=1
a[2,3]=0
a[3,3]=-0.0618118 - 4. Sqrt[ba] u
a[4,3]=-1.51892 Sqrt[ba] u
a[1,4]=0
a[2,4]=1
a[3,4]=9.51892 Sqrt[ba] u
a[4,4]=-2.42759 - 4. Sqrt[ba] u
```

(Local B) In[18]:=

```
(* Find the characteristic polynomial *)
charpoly = Det[a-x*IdentityMatrix[4]];
```

(Local B) In[20]:=

```
(* Compute the coefficients of the characteristic
   equation --- see equation (3.15)  *)

a0 = Coefficient[charpoly,x,0]
```

(Local B) Out[20]=

```
                                   2
6002.16 + 869.59 gama + 13.4053 gama  + 1022.39 ksp +

                                  2                 2
  18.0637 gama ksp + 252.345 u  - 17.6304 gama u  -

                2             4
  29.9771 ksp u  + 10.5954 u
```

(Local B) In[21]:=

```
a1 = Coefficient[charpoly,x,1]
```

(Local B) Out[21]=

```
60.0216 + 4.34795 gama + 5.11196 ksp +
  1991.52 Sqrt[ba] u + 37.4935 Sqrt[ba] gama u +
                                      2
  6.87366 Sqrt[ba] ksp u + 1.26172 u  - 14.07 Sqrt[ba]
```

(Local B) In[22]:=

```
a2 = Coefficient[charpoly,x,2]
```

(Local B) Out[22]=

```
498.031 + 10.218 gama + 2.12489 ksp +
                                2                 2
  9.95762 Sqrt[ba] u - 12.436 u  + 30.4585 ba u
```

(Local B) In[23]:=

```
a3 = Coefficient[charpoly,x,3]
```

(Local B) Out[23]=

```
2.48941 + 8. Sqrt[ba] u
```

(Local B) In[24]:=

```
a4 = Coefficient[charpoly,x,4]
```

(Local B) Out[24]=

```
1.
```

(Local B) In[25]:=

(Local B) In[27]:=

```
(* Set the spring constant and the value of beta *)

ksp = 100;
ba = 0.18;
```

(Local B) In[31]:=

```
(* To simplify, define a new variable for velocity
   and solve a0 = 0 for the boundary for divergence;
   this boundary is plotted for the same parameters
   as in Figure 3.15, the spring stiffness k = 100 *)

u = Sqrt[v];
a0bis = a0;
solu = Solve[a0bis==0,v];
```

(Local B) In[34]:=

```
firstu = Sqrt[v] /. solu[[1]]
seconu = Sqrt[v] /. solu[[2]]
Plot[{firstu,seconu},{gama,-100,100},
        Frame->True,
        FrameLabel->{Gravity parameter,Flow velocity},
        PlotRange -> {{-100, 100},{0,20}}]
```

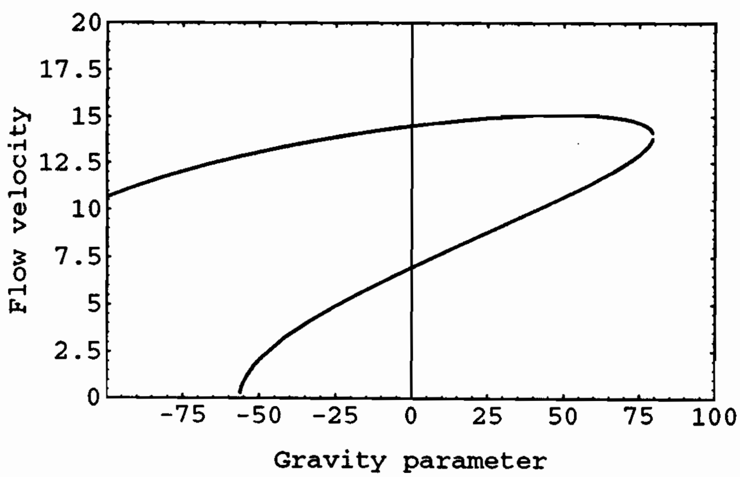

(Local B) Out[34]=

```
-Graphics-
```

Appendix E

Revision of the Bifurcation Diagram of Figure 3.7(c)[§]

Because of the emergence of new software packages dealing with nonlinear systems of ordinary differential equations (Doedel 1981; Aronson 1991), it was decided to confirm the numerical results of Section 3.4.2 using AUTO (Doedel 1981), the software permitting the investigation of stability of fixed points as well as the computation of stable and unstable limit cycles. In this manner, panels (a), (b) and (d) of Figure 3.7 were obtained easily. However, some differences were observed in the case of Figure 3.7(c): the Hopf bifurcation occurring at point A, for $u = 13.23$, was *subcritical*, giving rise to an unstable limit cycle which is restabilized at the limit point B ($u = 12.09$), as shown in Figure E.1(a) below.

Of more interest is the behaviour of the unstable limit cycle emerging from the subcritical Hopf bifurcation occurring at point C for the new stable fixed point ($u = 13.81$). In fact, as shown in expanded form in Figure E.1(b), the unstable limit cycle *is restabilized* at point D, for $u = 11.72$, where a first limit point is obtained; the amplitude of the limit cycle is diminished as u is increased, and it becomes unstable again at

[§]This corresponds to the letter to the editor by Païdoussis & Semler 1993 Nonlinear dynamics of a fluid-conveying cantilevered pipe with an intermediate spring support: addendum. *Journal of Fluids and Structures* 7, 565-566.

point E, for $u = 12.24$, by undergoing a secondary Hopf bifurcation (two complex conjugate Floquet multipliers cross the unit circle, $\lambda = 0.787 \pm i0.618$). Theoretically, in the neighbourhood of that point (in fact on the branch E–E′), it should be possible to observe quasiperiodic oscillations. The limit cycle remains unstable until $u = 12.24$, where stabilization reoccurs. Of course, after point D′ ($u = 11.72$), the "cycle" is complete (see the arrows).

Therefore, the dynamics is much more complicated than supposed in Section 3.4.2. This was found only by "following" the unstable limit cycle. It was decided to integrate numerically the equations of motion in the neighbourhood of $u = 12.3$, and all qualitative dynamics could indeed be obtained, i.e. symmetric, asymmetric, quasiperiodic oscillations and stable fixed points.

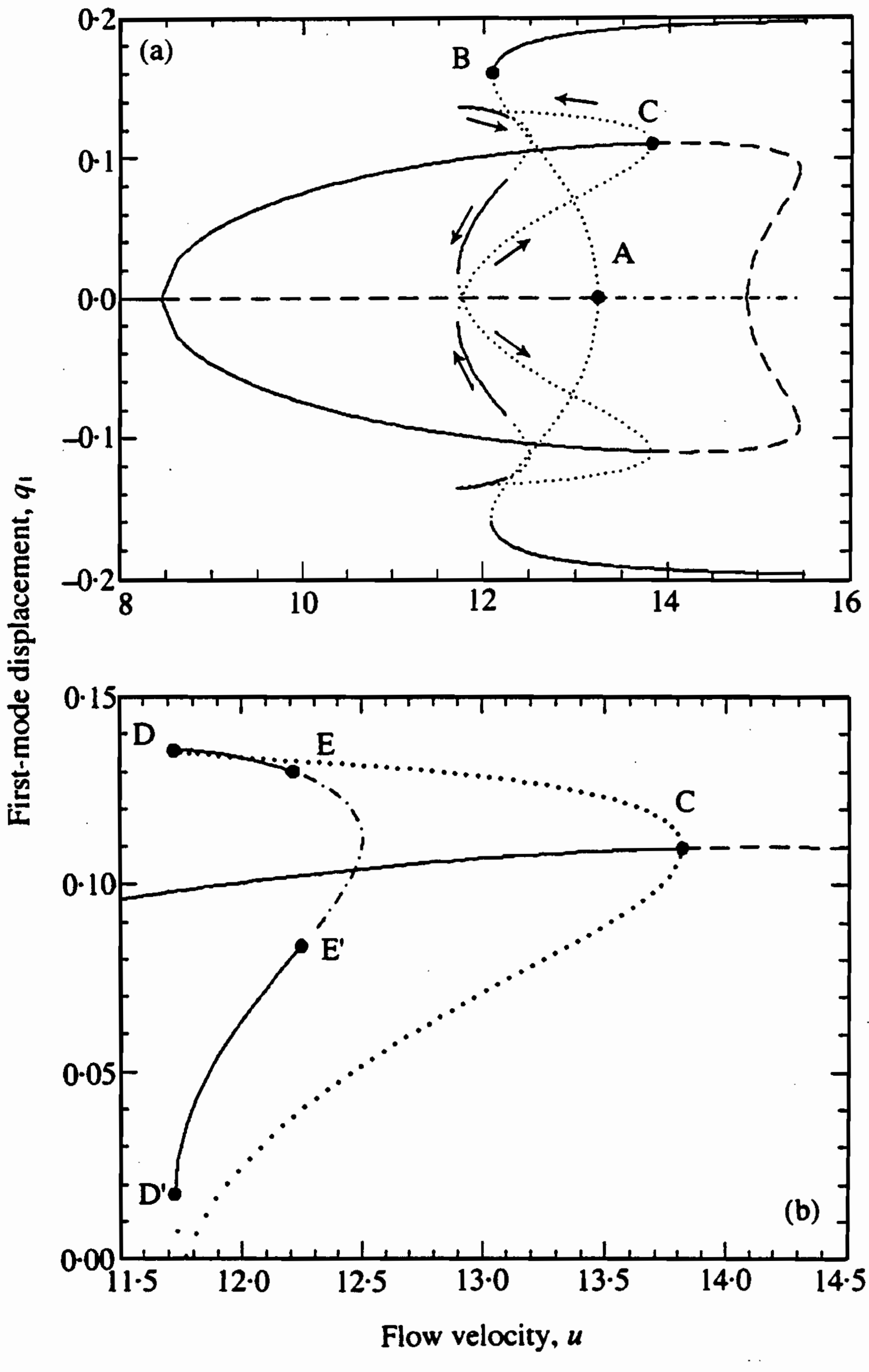

Figure E.1: Bifurcation diagrams for the same parameters as in Figure 3.7(c): (a) the "whole" bifurcation diagram; (b) blown–up portion of the upper part of the bifurcation diagram for $11.5 \leq u \leq 14.5$.

Appendix F

Construction of the Unfolding for the Case VIII

The subsystem may be written as

$$\begin{aligned} \dot{r} &= r\,(\mu_1 + r^2 + b\,z^2)\;, \\ \dot{z} &= z\,(\mu_2 + cr^2 + d\,z^2)\;, \quad d=-1, \quad \alpha = d - bc < 0\,. \end{aligned} \tag{F.1}$$

F.1 Determination of the Fixed Points

$$\begin{aligned} r\,[\mu_1 + r^2 + b\,z^2] &= 0, \\ z\,[\mu_2 + cr^2 + d\,z^2] &= 0. \end{aligned} \tag{F.2}$$

The origin $(r,z) = (0,0)$ is always an equilibrium point. Depending on μ_1 and μ_2, three other equilibrium may exist

$$\begin{aligned} (r,z) =&\ \ (0, \sqrt{\mu_2}, \mu_2 > 0, \\ (r,z) =&\ \ (\sqrt{-\mu_1}, 0, \mu_1 < 0, \\ (r,z) =&\ \ \left(\sqrt{\tfrac{b\mu_2+\mu_1}{\alpha}}, \sqrt{\tfrac{c\mu_1-\mu_2}{\alpha}}\right), \tfrac{b\mu_2+\mu_1}{\alpha} > 0, \tfrac{c\mu_1-\mu_2}{\alpha} > 0. \end{aligned} \tag{F.3}$$

F.2 Stability Analysis

The characteristics of the flow are determined by the eigenvalues of the matrix $[A_0]$ of the linearized system at the equilibrium points denoted (r_0, z_0). $[A_0]$ can be determined from the original subsystem (F.1),

$$[A_0] = \begin{bmatrix} \mu_1 + 3r_0^2 + bz_0^2 & 2br_0 z_0 \\ 2cr_0 z_0 & \mu_2 + cr_0^2 - 3z_0^2 \end{bmatrix}. \tag{F.4}$$

Hence, for $(0,0)$,

$$[A_0] = \begin{bmatrix} \mu_1 & 0 \\ 0 & \mu_2 \end{bmatrix}, \tag{F.5}$$

a pithfork bifurcation occurs if $\mu_1 = 0$ or $\mu_2 = 0$.

For $(0, \sqrt{\mu_2}), \mu_2 > 0$,

$$[A_0] = \begin{bmatrix} \mu_1 + b\mu_2 & 0 \\ 0 & -2\mu_2 \end{bmatrix}, \tag{F.6}$$

a new pithfork bifurcation occurs if $\mu_1 + b\mu_2 = 0$.

For $(\sqrt{-\mu_1}, 0), \mu_1 < 0$,

$$[A_0] = \begin{bmatrix} -2\mu_1 & 0 \\ 0 & \mu_2 - c\mu_1 \end{bmatrix}, \tag{F.7}$$

another pithfork bifurcation occurs if $\mu_2 - c\mu_1 = 0$.

In the three cases, the stability of all the fixed points is determined very easily.

Finally, for the last fixed point (with $\alpha < 0$),

$$[A_0] = \frac{2}{\alpha} \begin{bmatrix} \mu_1 + b\mu_2 & b\sqrt{(b\mu_2 + \mu_1)(c\mu_1 - \mu_2)} \\ c\sqrt{(b\mu_2 + \mu_1)(c\mu_1 - \mu_2)} & \mu_2 - c\mu_1 \end{bmatrix}. \tag{F.8}$$

Since $\alpha < 0$, no bifurcation can occur for this fixed point. Hence, without loss of information, one can set $\mu_1 = 0$, and the eigenvalues of $[A_0]$ can be found. It appears that one eigenvalue is always positive and the other one negative, the fixed point is a saddle; the complete bifurcation set can be drawn easily [Figure 3.11(b)].

Appendix G

Coefficients Arising from the Galerkin Discretization

The stationary damping and stiffness matrices are defined by[§]

$$\begin{aligned} c_{ij} &= \alpha\lambda_j^4\delta_{ij} + 2\sqrt{\beta}u_0 b_{ij}, \\ k_{ij} &= \lambda_j^4\delta_{ij} + (u_0^2-\gamma)c_{ij} + \gamma(d_{ij} + b_{ij}); \end{aligned} \tag{G.1}$$

δ_{ij} is Kroneker's delta, λ_j are the dimensionless eigenvalues of a cantilever beam and the constants b_{ij}, c_{ij}, d_{ij}, introduced by Païdoussis & Issid (1974), are given by

$$b_{ij} = \int_0^1 \phi_i\phi_j'\,d\xi\ ,\ c_{ij} = \int_0^1 \phi_i\phi_j''\,d\xi\ ,\ d_{ij} = \int_0^1 \xi\phi_i\phi_j''\,d\xi. \tag{G.2}$$

α_{ijkl}, β_{ijkl} and γ_{ijkl} are coefficients computed numerically from the integrals of the eigenfunctions $\phi_i(\xi)$.[†] Their definition is more complicated:

$$\begin{aligned} \alpha_{ijkl} &= \int_0^1 \phi_i(\phi_j''''\phi_k'\phi_l' + 4\phi_j'\phi_k''\phi_l''' + \phi_j''\phi_k''\phi_l'')\mathrm{d}\xi + u_0^2\int_0^1 \phi_i\phi_j''\left(\phi_k'\phi_l' - \int_\xi^1 \phi_k'\phi_l''\mathrm{d}\xi\right)\mathrm{d}\xi \\ &+ \gamma\int_0^1 \phi_i\left(\tfrac{1}{2}\phi_j'\phi_k'\phi_l' - \tfrac{3}{2}(1-\xi)\phi_j''\phi_k'\phi_l'\right)\,\mathrm{d}\xi, \\ \beta_{ijkl} &= 2\,u_0\sqrt{\beta}\int_0^1 \phi_i\left(\phi_j'\phi_k'\phi_l' - \phi_j''\int_\xi^1 \phi_k'\,\phi_l'\,\mathrm{d}\xi\right)\mathrm{d}\xi, \\ \gamma_{ijkl} &= \int_0^1 \phi_i\phi_j'\left(\int_0^\xi \phi_k'\phi_l'\,d\xi\right)\,\mathrm{d}\xi - \int_0^1 \phi_i\phi_j''\left(\int_\xi^1\int_0^\xi \phi_k'\phi_l'\,\mathrm{d}\xi\mathrm{d}\xi\right)\mathrm{d}\xi. \end{aligned}$$

[§]In Chapter 7, the two linear matrices are represented by capital letters, C_{ij}, K_{ij}.

[†]Note that these definitions are different in Chapters 3 and 4 — see Appendix C.

Appendix H

Instruction for the Construction of the Pipes[§]

H.1 Introduction

The purpose of this appendix is to describe the fabrication procedure for uniform tubular pipes with a steel strip centrally moulded inside. This is not an easy task, and as a result, the procedure was slightly modified after each attempt. The "optimal" one is presented here.

H.2 Instructions

The procedure described here consists of two phases: phase I, consisting of steps 1-5 is preliminary to casting the pipe itself and is required to seal the edges of the metal strip/mould edges; phase II is related to casting the pipe itself and then removal of the mould.

1. Prepare a small quantity of elastomer by thoroughly mixing about 50 gram of **Silastic E RTV** with one tenth its weight of catalyzer.

[§] **Based on Milcent and Petermann's 1993 Experimental study of a cantilevered pipe conveying fluid Mech Lab II report. McGill University, Department of Mechanical Engineering.**

2. Put the uniform mixture in the plexiglas injector and close it after sealing the cover. Connect the vacuum pump to the upper region of the injector, so that the bubbles trapped in the elastomer can go up and escape at the surface. The fact that the mixture is air-free makes the pipe more robust, as well as uniform.

3. Inject the mixture in a small syringe (be careful not to put air inside).

4. Put some glue on the parts of the strip that are not covered by the two half-cylinders. Use the syringe and put the air-free mixture in small amounts on the glued surfaces.

The reason for performing step 4 (and not moulding the complete system at once) is that the most important problem came from moulds that could not be removed after curing. This was due to the elastomer which was sticking to the moulds. Indeed, when the two half-cylinders were positioned, a small space did still exist between them and the steel strip, and hence, the elastomer could spread between them.

To improve the procedure, the two moulds with the steel strip in-between are also clamped together. As the metal strip is smaller than the two half-cylinders, small pieces of metal are positioned at each end to ensure the same thickness all along the length of the system.

5. To accelerate the process of drying, which takes usually about 3 days at room temperature, it is best to use an oven (preferably programmable). With a constant temperature of 160°C, the process then takes only half an hour. It is also advised to dry all the parts that have to be used a second time in the oven (simultaneously), because they can then be cleaned more easily.

6. Repeat steps 1 and 2 with 150 gram of Silastic E RTV and 15 gram of curing agent (catalyst).

7. Clean the moulds with acetone and spray all surfaces of the plexigas mould with the releaser. Put the steel strip and the two half-cylinders inside and clamp them at their ends.

8. Turn the wheel of the injector to push the air-free mixture to the top. Then, connect the injector to the plexiglas mould and fix the complete system in a vertical

position, as shown on the Picture 1. Rotate carefully the wheel so that the elastomer moves upwards slowly around the metal mould, without mixing with air. Do it until some mixture appears at the top of the plexiglas mould.

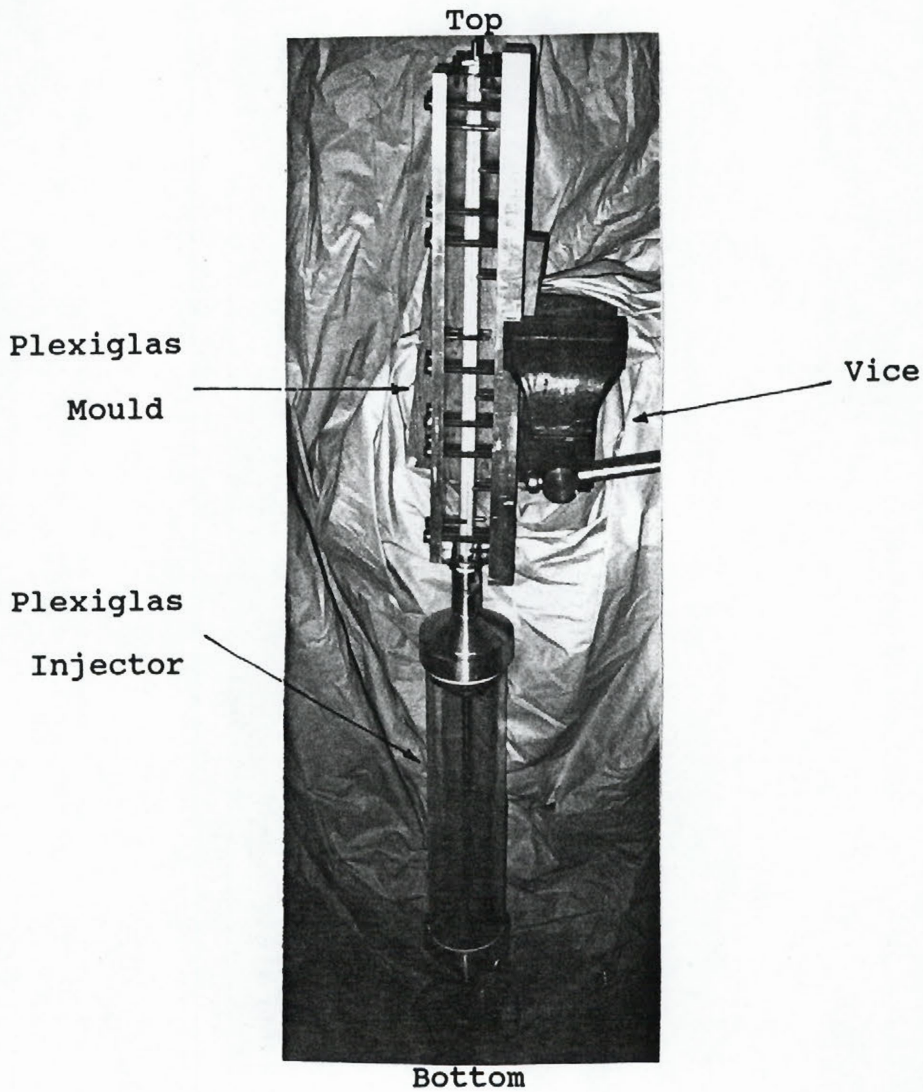

Picture 1: Pipe drying after elastomer injection

9. Let the whole system dry for the appropriate period of time.

10. Take the pipe out of the plexiglas mould. Different methods have been tested to remove the two half-cylinders. The best is a combination of hammering one half-cylinder and blowing pressurized air inside the pipe. The danger of the first method is to cause buckling of the metal mould, while the second one tends to unglue the metal strip.

10(a). Use compressed air (maximum 10 bars), and inject it between the metal moulds and the pipe. To prevent the pipe from enlarging (due to air effects), two planks of wood are used, the pipe being maintained between them. Air leakage is reduced by installing clamps at the connection.

10(b). Put the pipe in the plexiglas mould. Hammer out the metal half-cylinders one after the other.

11. Repeat steps 10(a) and 10(b) until success is achieved. Once one half-cylinder has been removed, the second one can only be taken out with the hammer, because air injection becomes useless as most of the air flows into the empty part. If the half-cylinder is driven in too far, a beam of smaller diameter permits to push and remove the second half- cylinder.

H.3 Troubleshooting

On the next page, Table H.1 lists a certain number of problems encountered during the construction of the pipes, possible reasons, and the corresponding steps to refer to.

List of problems	Reasons	See step
Air bubbles in the pipe	The mixture did not spend enough time in the vacuum pump	6
	The elastomer was injected too fast	8
Difficulty to remove the two half-cylinders	Glue or Silastic stuck the metal cylinders to the strip	4
	Unsufficient releaser	7
Unstuck strip	Bad glueing	4
	Air injection too strong	10a
	Hammering too violent	10b
Releaser on the steel strip	The metal moulds were not positioned horizontally	7

Table H.1: Typical problems encountered.

Appendix I

Transformation of Equation (7.27) into Complex Form

To transform equation (7.27) into equation (7.30), the change of coordinates (7.28b) is used. To obtain a relationship between the complex coefficients and the original real coefficients, a identification process is undertaken: the right-hand side of (7.30) is obtained automatically using symbolic software such as Mathematica through

$$\dot{\zeta} = 0.5\omega_0(\dot{x}_2 - \mathrm{i}\dot{x}_1),$$

simply by identifying the desired coefficients. In practice, this is a straighforward procedure. For example, it can be shown that

$$\begin{aligned}
\alpha_1 &= 0.5\left(A^1_{1,1} - \mathrm{i}\,A^1_{1,2} + \mathrm{i}\,A^1_{2,1} + A^1_{2,2}\right), \\
\alpha_4 &= 0.25\left(-A^2_{1,1} - \mathrm{i}\,A^2_{1,2} - \mathrm{i}\,A^2_{2,1} + A^2_{2,2}\right), \\
\alpha_6 &= 0.25\,\mathrm{i}\left(A^3_{1,1} + \mathrm{i}\,A^3_{1,2} + \mathrm{i}\,A^3_{2,1} - A^3_{2,2}\right).
\end{aligned}$$

Appendix J

Principal Parametric Resonance: Experimental Results and Computer Programs

J.1 Experiments

The complete experimental results corresponding to Figure 7.14 are shown in the following two figures. The different regions of dynamical behaviour can be identified, and it can be seen that the results are better for $\sigma = -4\%$ than for $\sigma = +8\%$.

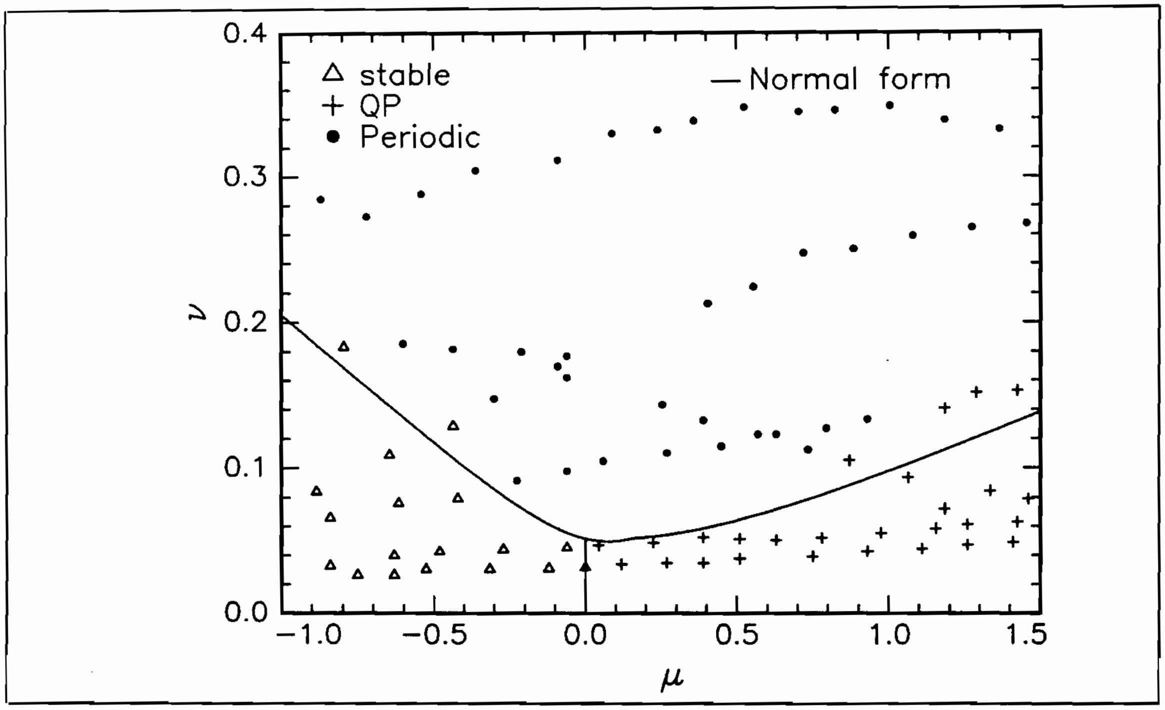

Figure J.1: Experimental results for the principal parametric resonance in the (μ, ν) parameter space for $\sigma = -0.04$, $\beta = 0.131$ and $\gamma = 26.1$. Three regions of dynamical behaviour can be identified: Δ, the system is stable, $\bullet$, the response is periodic; $+$, the response is quasiperiodic

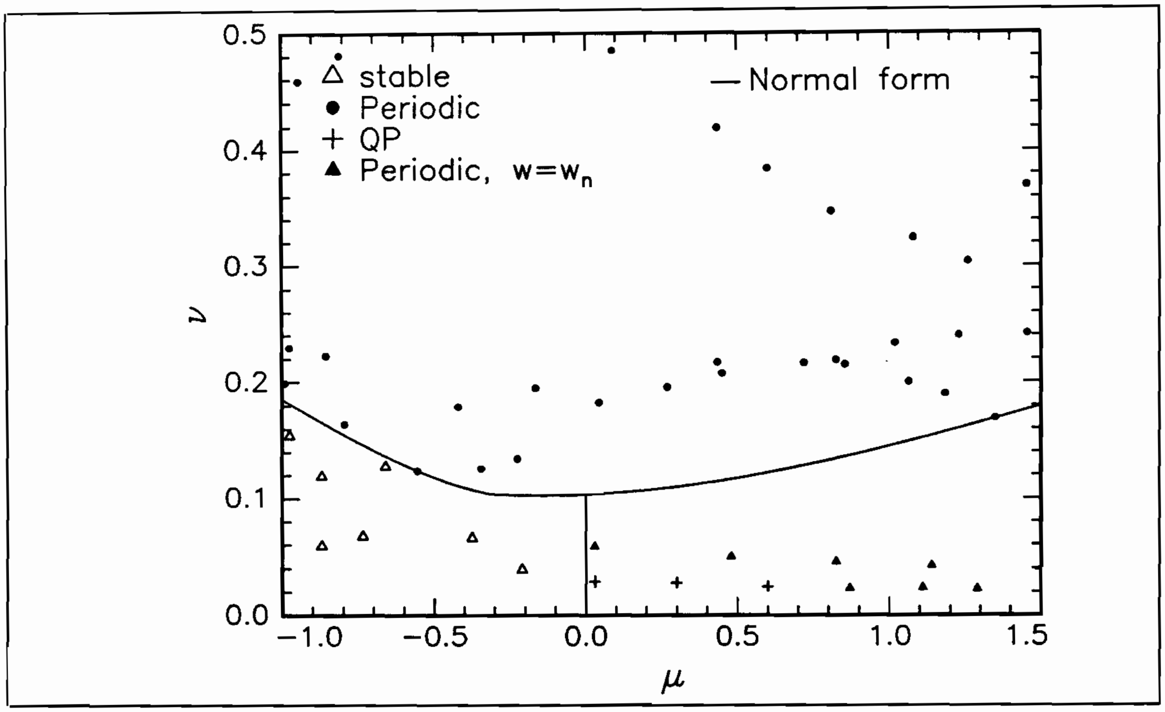

Figure J.2: Experimental results for the principal parametric resonance in the (μ, ν) parameter space for $\sigma = -0.04$, $\beta = 0.131$ and $\gamma = 26.1$. Three regions of dynamical behaviour can be identified: Δ, the system is stable, $\bullet$, the response is periodic; $+$, the response is quasiperiodic

J.2 Theory

In the next 18 pages is the output file generated by Mathematica and corresponding to the computation of the normal form for the case of the principal parametric resonance. The most interesting results are presented, but it is obvious that it becomes very easy to investigate the effect of any parameter. The nomenclature for the program is given in the output file.

```
nmode = 3;          (* Number of modes *)
ar = 0.00;          (* Damping coefficient alpha *)
ba = 0.131;          (* Mass parameter beta *)
gama = 26.1;         (* Gravity parameter *)
uhb = 6.334915;     (* Critical flow velocity Hopf
                       bifurcation (calculated by linear.:
u = uhb + eps*mu;

(* EIGENVALUES *)

rl[1] = 1.875104043341462;
rl[2] = 4.694091054370627;
rl[3] = 7.854757438237613;

(* SIGMA COEFFICIENTS AND EIGENFUNCTIONS OF THE BEAM*)

xb = 1.0;
Do [{
 si[i] = (Sinh[rl[i]]-Sin[rl[i]])/
                          (Cosh[rl[i]]+Cos[rl[i]]),
 ph[i] = Cosh[rl[i]*xb]-Cos[rl[i]*xb]-
          si[i]*(Sinh[rl[i]*xb]-Sin[rl[i]*xb])
    },{i,nmode}]

(* LINEAR COEFFICIENTS -- See Appendix G *)

Do [ Do [{
  tau[i,j] = (rl[i]/rl[j])^2,
  one[i,j] = (-1)^(i+j),
  If [j==i,
    bb[i,j] = 2.0,
    bb[i,j] = 4.0/(tau[i,j]+one[i,j])],
  If [j==i,
    cc[i,j] = rl[j]*si[j]*(2.0-rl[j]*si[j]),
    cc[i,j] = 4.0*(rl[j]*si[j]-rl[i]*si[i])/
                  (one[i,j]-tau[i,j])],
  If [j==i,
    ee[i,j] = 2.0 - 0.5*cc[i,j],
    ee[i,j] = (4.0*(rl[j]*si[j]-rl[i]*si[i]+2.0)*
                                         one[i,j]-
      +2.0*(1.0+tau[i,j]^2)*bb[i,j])/
           (1.0-tau[i,j]^2)-cc[i,j]],
    ff[i,j] = bb[i,j] - ee[i,j]},
{j,nmode}],{i,nmode}];

(* THE DAMPING AND STIFFNESS MATRICES*)

 Do [ Do [{
   If [i==j,
```

```
      rc[i,j] = -(ar*rl[j]^4 + 2.0*Sqrt[ba]*u*bb[i,j]),
      rc[i,j] = -(2.0*Sqrt[ba]*u*bb[i,j])],
   If [i==j,
      rk[i,j] = -(rl[j]^4 +u^2*cc[i,j] + gama*ee[i,j]),
      rk[i,j] = -(u^2*cc[i,j] + gama*ee[i,j])]},
{j,nmode}],{i,nmode}];

(* LINEAR MATRIX A *)

Do [ Do [{
If [i==j, delta[i,j] = 1, delta[i,j] = 0],
r[i,j] = 0,
r[i,j+nmode] = delta[i,j],
r[i+nmode,j] = rk[i,j],
r[i+nmode,j+nmode] = rc[i,j]},{j,nmode}],{i,nmode}]

a = Table[r[i,j],{i,2*nmode},{j,2*nmode}];
mu = 0;

(* This matrix transforms the nonlinear inertial
   terms *)

Do [ Do [{jord[i,j] = 0},{j,2*nmode}],{i,2*nmode}]
jord[1,2] = -w0;
jord[2,1] = w0;
jordan = Table[jord[i,j],{i,2*nmode},{j,2*nmode}];

(* FORCING TERMS; amplitude defined by :
                      nu Sin(Omega t) *)

Do [ Do [{
 rfs[i,j] = 0,
 rfc[i,j] = 0,
 rfs[i,j+nmode] = 0,
 rfc[i,j+nmode] = 0,
 rfc[i+nmode,j] = -Sqrt[ba]*u*eps*nu*Omega*ff[i,j],
 rfs[i+nmode,j] = -2*u^2*nu*eps*cc[i,j],
 rfc[i+nmode,j+nmode] = 0,
 rfs[i+nmode,j+nmode] = -2*Sqrt[ba]*u*eps*nu*bb[i,j]},
{j,nmode}],{i,nmode}]

fs = Sin[Omega*t]*Table[rfs[i,j],{i,2*nmode},
                                       {j,2*nmode}];
fc = Cos[Omega*t]*Table[rfc[i,j],{i,2*nmode},
                                       {j,2*nmode}];

(* EIGENVALUES AND TRANSFORMATION MATRIX P *)
(* mu is set to zero to calculate the eigenvalues *)
```

```
{lam,vecs} = Eigensystem[a];
Clear[mu];
Do [Print[lam[[i]]],{i,2*nmode}]
ptp[1] = Re[vecs[[3]]];
ptp[2] = Im[vecs[[4]]];
ptp[3] = Re[vecs[[1]]];
ptp[4] = Im[vecs[[2]]];
ptp[5] = Re[vecs[[5]]];
ptp[6] = Im[vecs[[6]]];
ptem = Table[ptp[i],{i,2*nmode}];
p = Transpose[ptem];
aa = Chop[Inverse[p].a.p,0.0001];

-3.61532 + 53.5113 I
-3.61532 - 53.5113 I
           -6
-1.71714 10   + 17.3427 I
           -6
-1.71714 10   - 17.3427 I
-10.1418 + 7.49941 I
-10.1418 - 7.49941 I

(* NONLINEAR COEFFICIENTS *)

nonlinear = 1;

toto1 = ReadList["/u/chris/coefficient/rmuu3.dat",
                                          Number];
toto2 = ReadList["/u/chris/coefficient/rmgrav3.dat",
                                          Number];
toto3 = ReadList["/u/chris/coefficient/rmstif3.dat",
                                          Number];
toto4 = ReadList["/u/chris/coefficient/rmbeta3.dat",
                                          Number];
toto5 = ReadList["/u/chris/coefficient/rminer3.dat",
                                          Number];

Do [rm10[i]=Part[toto1,i],{i,Length[toto1]}];
Do [rm20[i]=Part[toto2,i],{i,Length[toto2]}];
Do [rm30[i]=Part[toto3,i],{i,Length[toto3]}];
Do [rm40[i]=Part[toto4,i],{i,Length[toto4]}];
Do [rm50[i]=Part[toto5,i],{i,Length[toto5]}];
```

```
(* u IS SET TO THE uhb VALUE IN THE NONLINEAR TERMS *)

it = 1;
Do [ Do [ Do [ Do [ {
 al[i,j,k,l]=-(uhb^2*rm10[it]+gama*rm20[it]+rm30[it]),
 be[i,j,k,l]=-(2.0*uhb*Sqrt[ba]*rm40[it]),
 ga[i,j,k,l]=-rm50[it],
 it = it + 1},
{l,nmode}],{k,nmode}],{j,nmode}],{i,nmode}]

(* To the order considered, the nonlinear inertial
   terms are simply represented by I w0 zdot *)

xx = Table[x[i],{i,2*nmode}];
z = p.xx;
Do [x[i] = 0,{i,3,2*nmode,1}]
zdot = (p.jordan).xx;
Do [tp[i] = 0, {i,nmode}];
Do [ Do [ Do [ Do [{
  tp[i] = tp[i] +
          al[i,j,k,l]*z[[j]]*z[[k]]*z[[l]]+
        be[i,j,k,l]*z[[j]]*z[[k]]*z[[l+nmode]]+
      ga[i,j,k,l]*(z[[j]]*z[[k+nmode]]*z[[l+nmode]]+
                  z[[j]]*z[[k]]*zdot[[l+nmode]])},
{l,nmode}],{k,nmode}],{j,nmode}],{i,nmode}]
Do [{f[i] = 0,
     f[i+nmode] = Expand[tp[i]]},{i,nmode}]


(* STANDART FORM : Xdot = aa.X + Inverse[p].f *)
(* where f represents the nonlinear terms     *)

ff = Array[f,{2*nmode}];
xx = Array[x,{2*nmode}];

aafsin = Expand[Inverse[p].fs.p];
aafcos = Expand[Inverse[p].fc.p];
equnl = eps*nonlinear Expand[Inverse[p].ff];

equfinal = Chop[Normal[Series[aa.xx +aafsin.xx +
            aafcos.xx + equnl,{eps,0,1}]],0.0001];
```

(Local B) In[85]:=

```
w0 =  Im[lam[[3]]]
x[1] = I/w0*(zeta-zetabar)
x[2] = 1/w0*(zeta+zetabar)

zetadot = Chop[Simplify[
0.5*w0*(equfinal[[2]]-I*equfinal[[1]])],0.0000001]
```

(Local B) Out[82]=

```
17.3427
```

(Local B) Out[83]=

```
0.057661 I (zeta - zetabar)
```

(Local B) Out[84]=

```
0.057661 (zeta + zetabar)
```

(Local B) Out[85]=

```
17.3427 I zeta + (2.39475 - 0.682004 I) eps mu zeta +
                                            3
   (-0.00111443 + 0.00341739 I) eps zeta  +
   (-3.49112 - 0.520007 I) eps mu zetabar +
                                            2
   (-0.00468452 + 0.00209354 I) eps zeta  zetabar +
                                                   2
   (0.00250663 - 0.00266522 I) eps zeta zetabar  +
                                                3
   (0.00322478 + 0.000351549 I) eps zetabar  +
   (0.334808 - 0.0922188 I) eps nu Omega zeta
    Cos[Omega t] + (-0.323725 + 0.0152576 I) eps nu Ome
    zetabar Cos[Omega t] +
   (15.1706 - 4.32044 I) eps nu zeta Sin[Omega t] +
   (-22.1159 - 3.2942 I) eps nu zetabar Sin[Omega t]
```

(Local B) In[87]:=

```
(* See equation (7.55) for the definitions *)

alpha[1] = Coefficient[zetadot,
    eps*mu*zeta]
```

(Local B) Out[87]=

```
2.39475 - 0.682004 I
```

(Local B) In[88]:=

```
alpha[4] = Coefficient[zetadot,
    eps*nu*Omega*zetabar*Cos[Omega*t]]/2
```

(Local B) Out[88]=

```
-0.161862 + 0.00762882 I
```

(Local B) In[89]:=

```
alpha[6] = Coefficient[zetadot,
    eps*nu*zetabar*Sin[Omega*t]]/(2*I)
```

(Local B) Out[89]=

```
-1.6471 + 11.058 I
```

(Local B) In[90]:=

```
betanl[2] = Coefficient[zetadot,
    eps*zeta^2*zetabar]
```

(Local B) Out[90]=

```
-0.00468452 + 0.00209354 I
```

```
(* Principal resonance *)

etadotzero = Normal[Series[zetadot,{eps,0,0}]]
etadotone = eps*mu*alpha[1]*eta +
       eps*nu*(alpha[6] + Omega*alpha[4])*etabarzz
```

(Local B) Out[92]=

```
17.3427 I zeta
```

(Local B) Out[93]=

```
(2.39475 - 0.682004 I) eps eta mu +
  eps etabarzz nu (-1.6471 + 11.058 I +
     (-0.161862 + 0.00762882 I) Omega)
```

(Local B) In[99]:=

```
(* See equation (7.56) for the definitions *)

Omega = 2*w0
Ur = Im[alpha[6]+Omega*alpha[4]];
Vr = Re[alpha[6]+Omega*alpha[4]];
rdot = mu*Re[alpha[1]]*r + Re[betanl[2]]*r^3 +
       nu*r*(Ur*Sin[2*phi]+Vr*Cos[2*phi])
rphidot = mu*Im[alpha[1]]*r + Im[betanl[2]]*r^3 +
       nu*r*(Ur*Cos[2*phi]-Vr*Sin[2*phi])
```

(Local B) Out[95]=

```
34.6855
```

(Local B) Out[98]=

$$2.39475 \text{ mu r} - 0.00468452 \text{ r}^3 + \text{nu r } (-7.26137 \text{ Cos}[2 \text{ phi}] + 11.3226 \text{ Sin}[2 \text{ phi}])$$

(Local B) Out[99]=

$$-0.682004 \text{ mu r} + 0.00209354 \text{ r}^3 + \text{nu r } (11.3226 \text{ Cos}[2 \text{ phi}] + 7.26137 \text{ Sin}[2 \text{ phi}])$$

(Local B) In[102]:=

```
(* Check if same as averaging : OK *)

Expand[rdot/w0/2]
Expand[rphidot/w0/2]
```

(Local B) Out[101]=

```
0.069042 mu r - 0.000135057 r^3 -
  0.209349 nu r Cos[2 phi] + 0.326436 nu r Sin[2 phi]
```

(Local B) Out[102]=

```
-0.0196625 mu r + 0.0000603579 r^3 +
  0.326436 nu r Cos[2 phi] + 0.209349 nu r Sin[2 phi]
```

(Local B) In[109]:=

```
(* See equation (7.57a) for the definitions *)

eta = Sqrt[Ur^2 + Vr^2]/(2*w0);
teta = .5 ArcTan[Ur/Vr];
ar = Coefficient[rdot,r^3]/(2*w0);
br = Coefficient[rphidot,r^3]/(2*w0);
cr = Coefficient[rphidot,mu r]/(2*w0);
dr = Coefficient[rdot,mu r]/(2*w0);

rdot = dr mu r + ar r^3 + nu r eta Sin[2(phi+teta)]
phidot =-sig/2+cr mu+br r^2+nu eta Cos[2(phi+teta)]
```

(Local B) Out[110]=

```
0.069042 mu r - 0.000135057 r^3 +
  0.387798 nu r Sin[2 (-0.500274 + phi)]
```

(Local B) Out[111]=

$$-0.0196625\ mu + 0.0000603579\ r^2 - \frac{sig}{2} +$$
$$0.387798\ nu\ Cos[2\ (-0.500274 + phi)]$$

```
(* Transformation needed to find the fixed point
   in the original coordinate *)

zeta = rad*Exp[I*tau];
zetabar = rad*Exp[-I*tau];
final = ComplexExpand[p.xx];
q1 = final[[1]]
modulus = Sqrt[Coefficient[q1,rad*Cos[tau]]^2+
               Coefficient[q1,rad*Sin[tau]]^2]
Clear[q1]
```

(Local B) Out[116]=

```
0.00561769 rad Cos[tau] + 0.00614929 rad Sin[tau]
```

(Local B) Out[117]=

```
0.008329
```

```
(* Trivial solution : see equation (7.67a) *)

trivstable=(dr mu)^2-((nu eta)^2-(-sig/2 + cr mu)^2)

(* Find the solution : nu is the "y-coordinate" *)

tototriv = Solve[trivstable == 0,nu];

(* Find the solution : sigma is the "y-coordinate" *)

tototrivsig = Solve[trivstable == 0,sig];
```

(Local B) Out[120]=

$$0.0047668\ mu^2 - 0.150387\ nu^2 + (-0.0196625\ mu - \frac{sig}{2})^2$$

(Local B) In[129]:=

```
(* Show the stability boundary in the (mu,nu)-plane
   for a constant value of sigma  *)

nutriv = nu /. tototriv[[1]]
sig = -0.11;
p12=Plot[nutriv,{mu,-1,1},
         Frame->True,
         FrameLabel -> {FontForm["m",{"Symbol",14}],
                        FontForm["n",{"Symbol",14}]},
         PlotRange -> {{-1, 1},{0,1.2/uhb}}]
```

(Local B) Out[127]=

```
1.28933 Sqrt[0.0206137 mu^2 + 0.0786502 mu sig + 1. sig
```

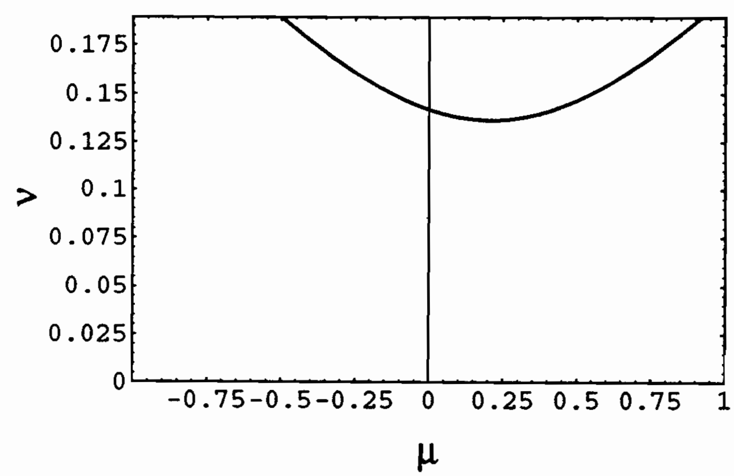

```
(* From equation (7.57b), the characteristic polynomia
   can be found; the characteristic equation is of
   second order, and the following function correspond
   to the zero of the discriminant; hence the discrimi
   nant is positive "above" the curve, which explains
   that the Hopf occurs "below" the curve (and mu = 0)
   and the pitchfork bifurcation above *)

plcn1 = Plot[(-sig/2 + cr mu)/eta,{mu,-1,1},
        Frame->True,
        FrameLabel -> {FontForm["m",{"Symbol",14}],
                       FontForm["n",{"Symbol",14}]},
        PlotRange -> {{-1, 1},{0,1.2/uhb}}]
```

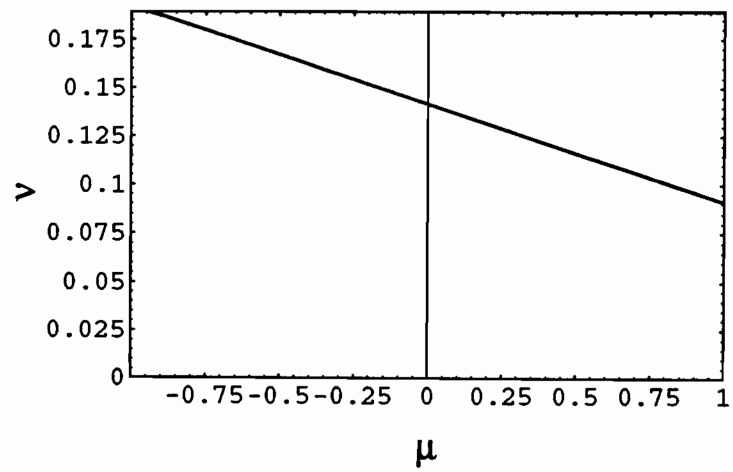

(Local B) In[133]:=

```
(* Show the two graphs together *)

Show[plcn1,pl2]
```

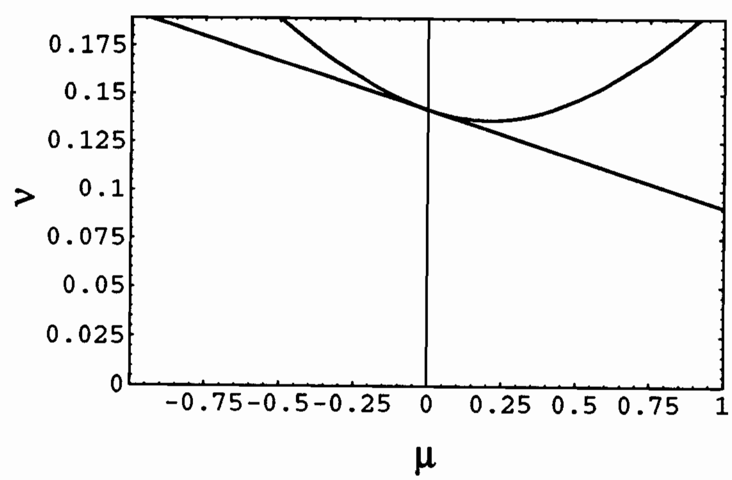

```
(* Nontrivial solution *)

Clear[mu]
Clear[sig]
delta = (ar^2+br^2) (nu eta)^2 -
        (ar(-sig/2+cr mu)-br dr mu)^2;
soldelta = Solve[delta == 0,nu];
```

(Local B) In[141]:=

```
nunontriv = nu /. soldelta[[1]]
sig = -0.11;
pldel1 = Plot[nunontriv,{mu,-1,1},
         Frame->True,
         FrameLabel -> {FontForm["m",{"Symbol",14}],
                        FontForm["n",{"Symbol",14}]},
         PlotRange -> {{-1, 1},{0,1.2/uhb}}]
```

(Local B) Out[139]=

$$1.17713 \text{ Sqrt}[0.000501115 \text{ mu}^2 - 0.0447712 \text{ mu sig} + 1. \text{ sig}^2]$$

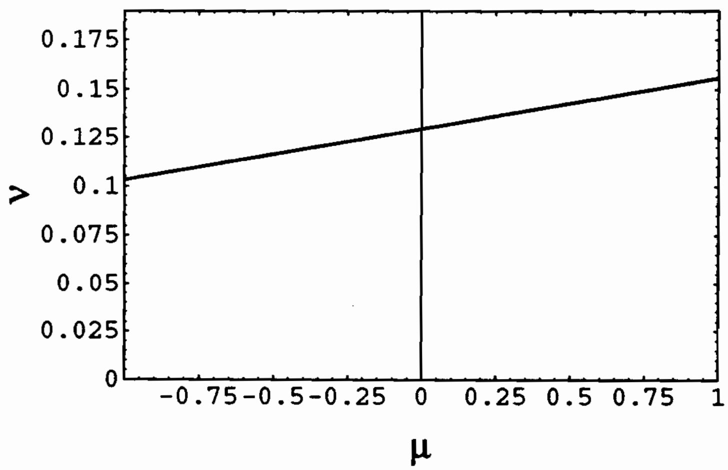

(Local B) In[143]:=

```
Clear[sig]
toto = -((ar dr + br cr) mu - br sig/2)
```

(Local B) Out[143]=

```
0.0000105114 mu + 0.000030179 sig
```

(Local B) In[144]:=

```
Solve[toto == 0, mu]
```

(Local B) Out[144]=

```
{{mu -> -2.87107 sig}}
```

(Local B) In[145]:=

```
Show[plcn1,pl2,pldel1,
        PlotRange -> {{-0.8, 0.8},{0,1.2/uhb}}]
```

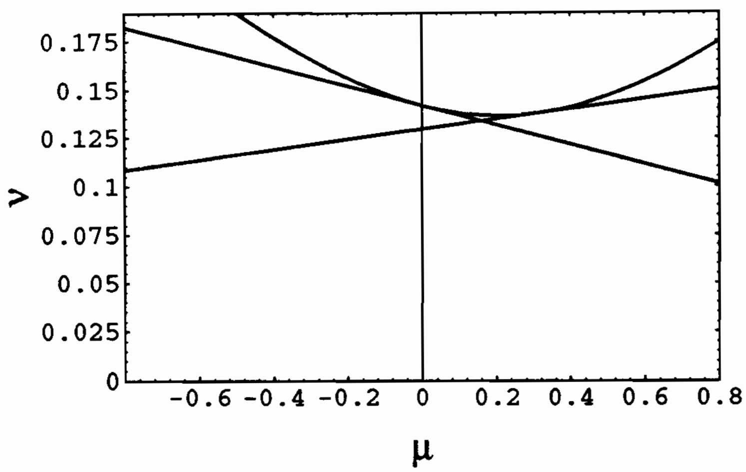

(Local B) In[149]:=

```
(* Find the nontrivial solutions *)

Clear[sig]
ntrivradius2 =   (toto + Sqrt[delta])/(ar^2 + br^2);
ntrivradius2mi = (toto - Sqrt[delta])/(ar^2 + br^2);
```

(Local B) In[152]:=

```
(* Find the stability of the positive solution *)

test3 = dr*mu + 2*ar*ntrivradius2;
nontrivstab = Solve[test3 == 0,nu]
```

(Local B) Out[152]=

```
                                     2
{{nu -> 1.28933 Sqrt[0.00483854 mu  + 0.0169395 mu sig
           2
       1. sig ]}, {nu ->
                                    2
    -1.28933 Sqrt[0.00483854 mu  + 0.0169395 mu sig +
           2
       1. sig ]}}
```

(Local B) In[155]:=

```
sig = -0.11;
nunontrivstab = nu /. nontrivstab[[1]]
plnunontrivstab = Plot[nunontrivstab,{mu,-1,1},
 PlotStyle -> {Dashing[{0.02,0.02}]}]
```

(Local B) Out[154]=

```
                                                        2
1.28933 Sqrt[0.0121 - 0.00186334 mu + 0.00483854 mu ]
```

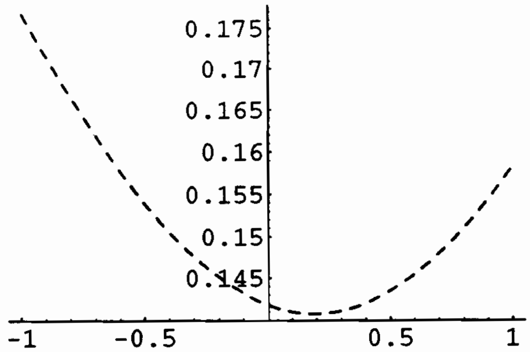

(Local B) In[156]:=

```
Show[{plnunontrivstab,pl2,pldel1},
        Frame->True,
        FrameLabel -> {FontForm["m",{"Symbol",14}],
                   FontForm["n",{"Symbol",14}]},
        PlotRange -> {{-1,1},{0,1.4/uhb}}]
```

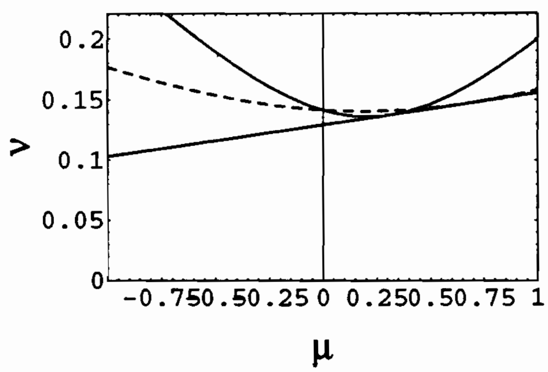

(Local B) In[159]:=

```
(* Plot the amplitude of the nontrivial solutions *)

nu = 0.2;
plotnu02 = Plot[{Sqrt[ntrivradius2]*modulus,
                 Sqrt[ntrivradius2mi]*modulus},
        {mu,-2,2},
        Frame->True,
        FrameLabel -> {FontForm["m",{"Symbol",14}],
                                  q1},
        PlotRange -> {{-2, 2},{0,0.3}}]
```

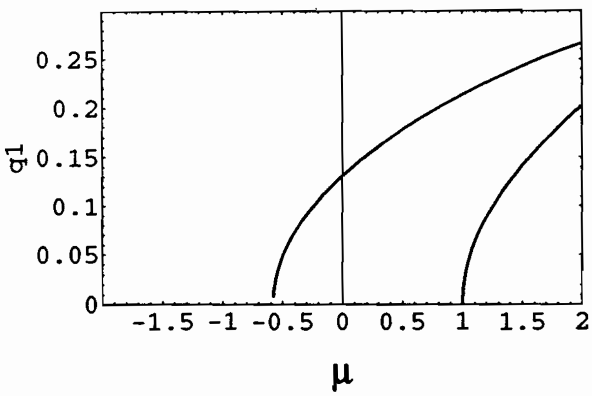


```
(*  Plot r0+ for a given sigma and several value of
    mu; see Figure 7.11 *)

mu =  0.25;
Clear[nu];
plro025 = Plot[{Sqrt[ntrivradius2]*modulus,
                Sqrt[ntrivradius2mi]*modulus},
          {nu,0,0.3},
          Frame->True,
          FrameLabel -> {FontForm["n",{"Symbol",14}],
                          q1max},
          PlotRange -> {{0, 0.3},{0,0.2}}]
```

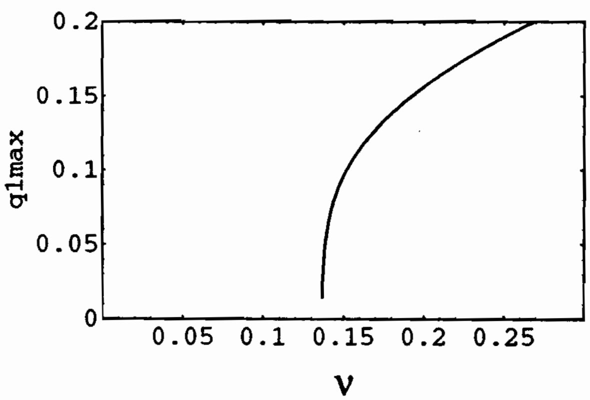

(Local B) In[166]:=

```
mu =  1.0;
Clear[nu];
plro010 = Plot[{Sqrt[ntrivradius2]*modulus,
                Sqrt[ntrivradius2mi]*modulus},
          {nu,0.1,0.3},
          Frame->True,
          FrameLabel -> {FontForm["n",{"Symbol",14}],
                          q1max},
          PlotRange -> {{0,0.3},{0,0.2}}];
```

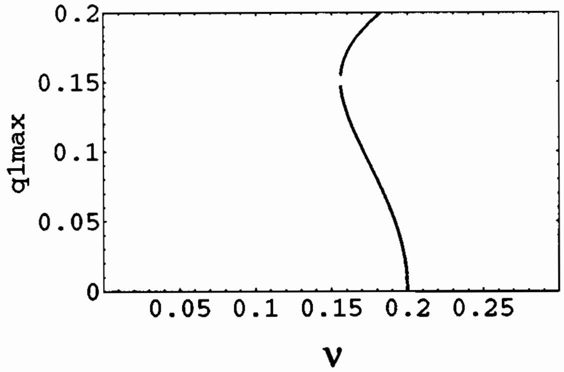

(Local B) In[169]:=

```
mu =  -0.50;
Clear[nu];
plro050mi = Plot[{Sqrt[ntrivradius2]*modulus,
                 Sqrt[ntrivradius2mi]*modulus},
        {nu,0,0.3},
        Frame->True,
        FrameLabel -> {FontForm["n",{"Symbol",14}],
                       q1max},
        PlotRange -> {{0,0.3},{0,0.2}}]
```

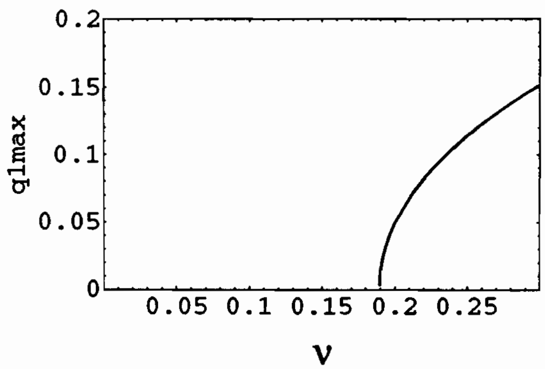

(Local B) In[171]:=

```
(* Plot them on the same graph *)

Show[plro025,plro010,plro050mi]
```

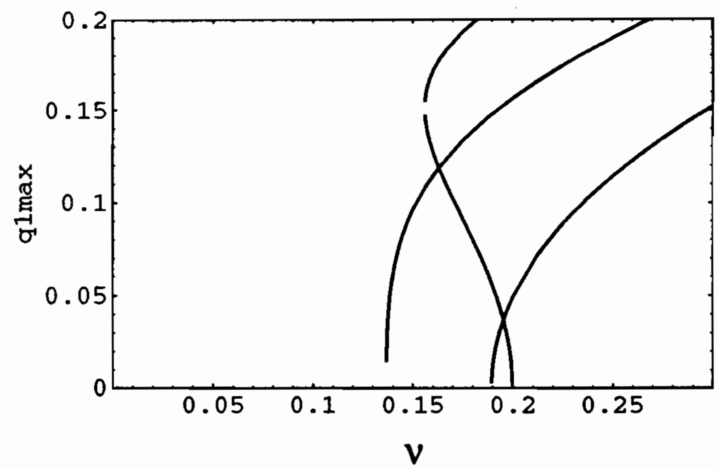

(Local B) In[183]:=

```
(* The same procedure can be undertaken keeping
   mu constant, and finding the linear boundaries
   in the (sigma,nu)-plane; here only the combined
   figure is presented: the curves "lift" when
   mu decreases, as expected *)

Clear[nu]
Clear[mu]
Clear[sig]
mu = 0.0;
pl00 = Plot[nutriv,{sig,-0.2,0.2},
    Frame->True,
    FrameLabel -> {FontForm["s",{"Symbol",14}],
                   FontForm["n",{"Symbol",14}]}]
mu = -0.1;
pl01m = Plot[nutriv,{sig,-0.2,0.2},
            Frame->True,
            FrameLabel->{sig,nu}]
mu = -0.2;
pl02m = Plot[nutriv,{sig,-0.2,0.2},
            Frame->True,
            FrameLabel->{sig,nu}]
mu = -0.3;
pl03m = Plot[nutriv,{sig,-0.2,0.2},
            Frame->True,
            FrameLabel->{sig,nu}]
```

(Local B) In[184]:=

```
Show[pl00,pl01m,pl02m,pl03m]
```

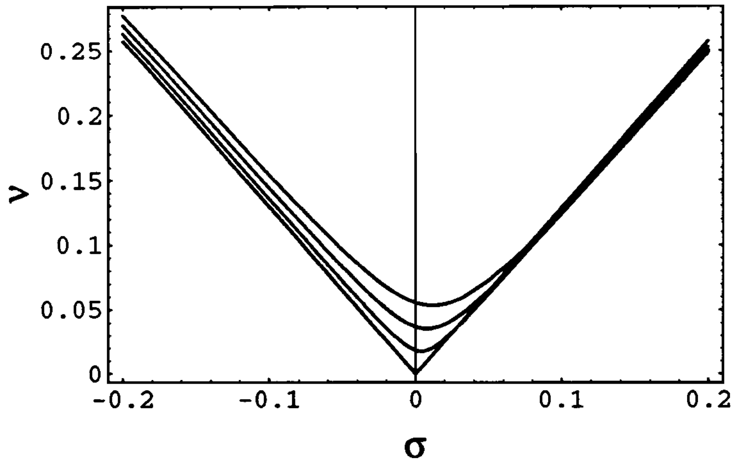

(Local B) In[186]:=

```
(* The evolution of the nontrivial solutions can be
   found also, for example if nu increases; again,
   the complete figure is presented (the curves are
   not connected because of the weak resolution) *)
mu=-0.31;
```

(Local B) In[189]:=

```
Clear[nu];
nu = .20;
plnu20 = Plot[{Sqrt[ntrivradius2]*modulus,
               Sqrt[ntrivradius2mi]*modulus},
         {sig,-0.2,0.2},
          PlotRange -> {{-0.3,0.3},{0,0.3}},
          Frame->True,
     FrameLabel -> {FontForm["s",{"Symbol",14}],
                    q1max}]
```

(Local B) In[192]:=

```
nu = .30;
plnu30po = Plot[Sqrt[ntrivradius2]*modulus,
          {sig,-0.3,0.3},
          PlotRange -> {{-0.3,0.3},{0,0.3}},
          Frame->True,
          FrameLabel->{sig,radius}]

plnu30mi = Plot[Sqrt[ntrivradius2mi]*modulus,
         {sig,0.2,0.25},
          PlotStyle -> {Dashing[{0.02,0.02}]},
          PlotRange -> {{-0.3,0.3},{0,0.3}},
          PlotPoints -> 1000,
          Frame->True,
          FrameLabel->{sig,radius}]
```

(Local B) In[195]:=

```
Clear[nu];
nu = .095;
plnu10 = Plot[{Sqrt[ntrivradius2]*modulus,
               Sqrt[ntrivradius2mi]*modulus},
         {sig,-0.3,0.3},
          PlotRange -> {{-0.3,0.3},{0,0.3}},
          Frame->True,
      FrameLabel -> {FontForm["s",{"Symbol",14}],
                     q1max}]
```

(Local B) In[196]:=

```
Show[{plnu10,plnu20,plnu30po,plnu30mi},{Axes->False}]
```

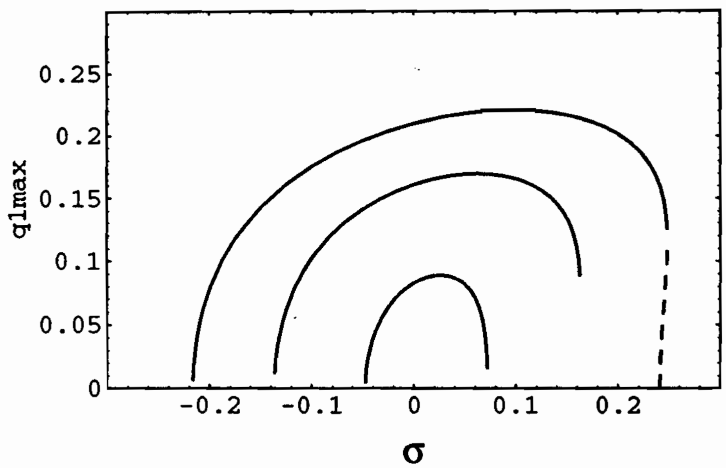


```
Clear[nu]
Clear[mu]
Clear[sig]
sig = -0.05;
limitmu = Solve[-((ar dr + br cr) mu - br sig/2) ==0,
lim = mu /. limitmu;
nunontrivstab = nu /. nontrivstab[[1]];
mu = 0;
limithopf = nunontrivstab;
Clear[mu]
plnunontrivstab = Plot[nunontrivstab,
         {mu,lim[[1]],1},
         PlotStyle -> {Dashing[{0.02,0.02}]},
         Frame->True,
         FrameLabel->{mu,nu},
         PlotRange->{{-1,1},{0,.18}}]

pl0511 = Plot[nutriv,
             {mu,-1,1},
             Frame->True,
             FrameLabel->{mu,nu}]
```

```
pl0522 = Plot[nunontriv,
             {mu,lim[[1]],1},
             Frame->True,
             FrameLabel->{mu,nu}]

sh005mi = Show[plnunontrivstab,pl0511,pl0522,
     Graphics[Circle[{-0.75,.075},{.05,.007}],
              Text[1,{-0.75,0.075}],
              Circle[{-0.25,.15},{.05,.007}],
              Text[2,{-0.25,0.15}],
              Circle[{ 0.80,.125},{.05,.007}],
              Text[3,{ 0.80,.125}],
              Circle[{ 0.80,.09},{.05,.007}],
              Text[4,{ 0.80,.09}],
              Circle[{ 0.60,.04},{.05,.007}],
              Text[5,{ 0.60,.04}],
              Line[{{0,0},{0,limithopf}}]],
     FrameLabel -> {FontForm["m",{"Symbol",14}],
                    FontForm["n",{"Symbol",14}]},
     Axes->False]
```

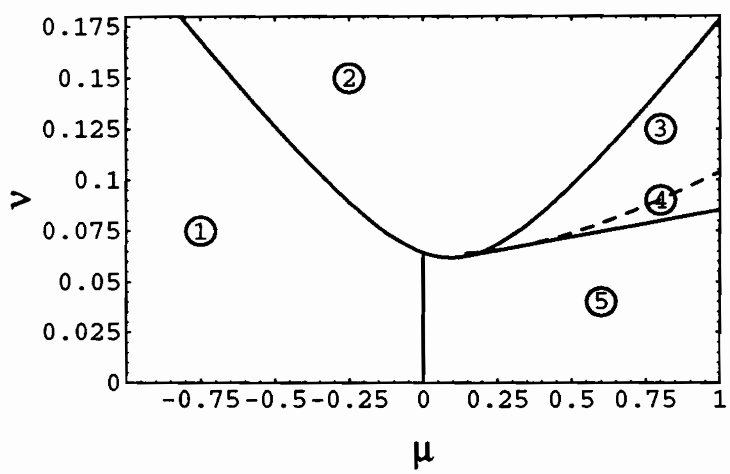


```
(* Finally, the following two functions were used to
   plot Figure 7.13 and 7.14; they correspond to the
   linear boundaries and the stability of the nontrivi
   solution *)

Clear[mu]
nutriv  nu /. nontrivstab[[1]]
```

(Local B) Out[213]=

```
1.28933 Sqrt[0.0025 - 0.00393251 mu + 0.0206137 mu^2]
```

(Local B) Out[214]=

```
1.28933 Sqrt[0.0025 - 0.000846974 mu + 0.00483854 mu^2]
```

Appendix K

Fundamental Parametric Resonance: Detailed Procedure

In the next 13 pages is the output file generated by Mathematica and corresponding to the computation of the normal form for the case of the fundamental parametric resonance. To reduce the number of pages, the first commands, similar to those for the principal resonance, are not shown (see app.princ.ma, pp.1-4). Particular attention is paid to the computation of the centre manifold.

```
ff = Array[f,{2*nmode}];

equnl = eps^2*nonlinear*Expand[Inverse[p].ff];

(* STANDART FORM : Xdot = aa.X + Inverse[p].f   *)
(* where f represents the nonlinear terms       *)

xx = Array[x,{2*nmode}];

aafsin = Expand[Inverse[p].fs.p];
aafsinu2 = Expand[Inverse[p].f2s.p];
aafcos = Expand[Inverse[p].fc.p];

(* Centre manifold *)
(* Transform the eigenvalues into real form *)

w0 =  Im[lam[[3]]];
sigma[3] =  Re[lam[[5]]];
freqy[3] =  Im[lam[[5]]];
sigma[5] =  Re[lam[[1]]];
freqy[5] =  Im[lam[[1]]];
Print["w0 = ",w0]
Do[Print["sigma[",i,"] = ",sigma[i],
           "  w[",i,"] = ",freqy[i]],
{i,3,2*nmode-1,2}];

Print[" "]
(* Construct the matrix composed by Jp and wp I4 *)
(* See equation 7.24 and 7.25 *)

Do [J[i] =
       {{-sigma[i],w0,Omega,0  , freqy[i],0,0,0},
       {-w0,-sigma[i],0,Omega , 0,freqy[i],0,0},
       {-Omega,0,-sigma[i],w0 , 0,0,freqy[i],0},
       {0,-Omega,-w0,-sigma[i], 0,0,0,freqy[i]},
       {-freqy[i],0,0,0,  -sigma[i],w0,Omega,0},
       {0,-freqy[i],0,0, -w0,-sigma[i],0,Omega},
       {0,0,-freqy[i],0, -Omega,0,-sigma[i],w0},
       {0,0,0,-freqy[i],0,-Omega,-w0,-sigma[i]}},
{i,3,2*nmode-1,2}];

(* Construct the vector b *)
(* The matrices tmpcos and tmpsin are first
   transformed into their "standard form" *)

costrans = Inverse[p].tmpcos.p;
sintrans = Inverse[p].tmpsin.p;

Do [vectorb[i] =
```

```
  {costrans[[i,1]],  costrans[[i,2]],
   sintrans[[i,1]],  sintrans[[i,2]],
   costrans[[i+1,1]],costrans[[i+1,2]],
   sintrans[[i+1,1]],sintrans[[i+1,2]]},
{i,3,2*nmode-1,2}];


(* For the fundamental resonance *)

Omega = w0;
Do[centre[i] = Inverse[J[i]].vectorb[i],
                                {i,3,2*nmode+1,2}];

Do[{Print["CM[",i,"] = ",centre[i]],
    Print[" "]},
{i,3,2*nmode-1,2}];


Clear[Omega];

Do[{x[i] = eps*nu*Cos[Omega*t]*
     (centre[i][[1]]*x[1] + centre[i][[2]]*x[2])+
      eps*nu*Sin[Omega*t]*
     (centre[i][[3]]*x[1] + centre[i][[4]]*x[2]),

  x[i+1] = eps*nu*Cos[Omega*t]*
     (centre[i][[5]]*x[1] + centre[i][[6]]*x[2])+
      eps*nu*Sin[Omega*t]*
     (centre[i][[7]]*x[1] + centre[i][[8]]*x[2])},
{i,3,2*nmode-1,2}];


Do[{Print["x[",i,"] = ",x[i]],
    Print[" "]},
{i,3,2*nmode,1}];
```

```
w0 = 17.3427
sigma[3] = -10.1418  w[3] = 7.49941
sigma[5] = -3.61532  w[5] = 53.5113

CM[3] = {-0.148871, 0.35538, -0.159557, -0.441632,

   -0.0922069, -0.11992, 0.170528, 0.214836}

CM[5] = {-0.0162864, -0.143754, -0.441585, -0.147318,

   0.186846, 0.0600356, 0.115157, -0.207303}

x[3] = eps nu Sin[Omega t]

    (-0.159557 x[1] - 0.441632 x[2]) +

   eps nu Cos[Omega t] (-0.148871 x[1] + 0.35538 x[2])

x[4] = eps nu Cos[Omega t]

    (-0.0922069 x[1] - 0.11992 x[2]) +

   eps nu Sin[Omega t] (0.170528 x[1] + 0.214836 x[2])

x[5] = eps nu Sin[Omega t]

    (-0.441585 x[1] - 0.147318 x[2]) +

   eps nu Cos[Omega t] (-0.0162864 x[1] - 0.143754 x[2

x[6] = eps nu Sin[Omega t]

    (0.115157 x[1] - 0.207303 x[2]) +

   eps nu Cos[Omega t] (0.186846 x[1] + 0.0600356 x[2]
```

```
(* The final equation defined on the centre manifold *

equfinal = Normal[Series[Chop[Expand[
    aa.xx + aafsin.xx + aafcos.xx + aafsinu2.xx + equn
               0.0001],{eps,0,2}]];

(* Change of coordinates -- see equation 7.28b *)

x[1] = I/w0*(zeta-zetabar);
x[2] = 1/w0*(zeta+zetabar);

(* Equation in complex form *)

zetadot = Chop[Simplify[
0.5*w0*(equfinal[[2]]-I*equfinal[[1]])],0.0000001]
```

```
(* Identification of the coefficients of interest
   See equation 7.30 *)

alpha[1] = Coefficient[zetadot,
    eps*mu*zeta];
alpha[2] = Coefficient[zetadot,
    eps*mu*zetabar];
alpha[3] = Coefficient[zetadot,
    eps*nu*Omega*zeta*Cos[Omega*t]]/2;
alpha[4] = Coefficient[zetadot,
    eps*nu*Omega*zetabar*Cos[Omega*t]]/2;
alpha[5] = Coefficient[zetadot,
    eps*nu*zeta*Sin[Omega*t]]/(2*I);
alpha[6] = Coefficient[zetadot,
    eps*nu*zetabar*Sin[Omega*t]]/(2*I);
betanl[2] = Coefficient[zetadot,
    eps^2*zeta^2*zetabar];
tmp[1] = Coefficient[zetadot,
    eps^2*nu^2*zeta];
tmp[2] = Coefficient[tmp[1],
    Cos[2*Omega*t]];
tmp[3] = Coefficient[tmp[1],
    Sin[2*Omega*t]];
coefgama[1] = Simplify[tmp[1]-tmp[2]*Cos[2*Omega*t]
                                  -tmp[3]*Sin[2*Omega*t]];
coefgama[4] = Simplify[Coefficient[zetadot,
    eps^2*nu^2*zetabar*Cos[2*Omega*t]]/2];
coefgama[6] = Simplify[Coefficient[zetadot,
    eps^2*nu^2*zetabar*Sin[2*Omega*t]]/(2*I)];
coefdelta[5] = Coefficient[zetadot,
    eps^2*mu^2*zeta];


Print["(",alpha[1],")   eps mu zeta"]
Print[" "]
Print["(",alpha[2],")   eps mu zetabar"]
Print[" "]
Print["(",Simplify[2*alpha[3]],")",
   "  eps nu Omega zeta Cos(Omega*t)"]
Print[" "]
Print["(",Simplify[2*alpha[4]],")",
   "  eps nu Omega zetabar Cos(Omega*t)"]
Print[" "]
Print["(",Simplify[2*I*alpha[5]],")",
   "  eps nu zeta Sin(Omega*t)"]
Print[" "]
Print["(",Simplify[2*I*alpha[6]],")",
   "  eps nu zetabar Sin(Omega*t)"]
Print[" "]
```

```
Print["(",betanl[2],")   eps^2 zeta^2 zetabar"]
Print[" "]
Print["(",coefgama[1],")   eps^2 nu^2 zeta"]
Print[" "]
Print["(",Simplify[2*coefgama[4]],")",
   "  eps^2 nu^2 zetabar Cos(2 Omega t)"]
Print[" "]
Print["(",Simplify[2*I*coefgama[4]],")",
   "  eps^2 nu^2 zetabar Sin(2 Omega t)"]
Print[" "]
Print["(",coefdelta[5],")   eps^2 mu^2 zeta"]

coefetazzbar = Simplify[-2*I/(3*w0)*
    (2*w0^2*alpha[4]*Conjugate[alpha[4]] +
     w0*alpha[4]*Conjugate[alpha[6]] +
     w0*alpha[6]*Conjugate[alpha[4]] +
     2*alpha[6]*Conjugate[alpha[6]])]

coefetabarz2 = Simplify[I/w0*
 (-(coefgama[4]+coefgama[6])*I*w0) +
  (w0*alpha[4]+alpha[6])*
  (w0*(alpha[3]-Conjugate[alpha[3]]) +
   alpha[5]+Conjugate[alpha[5]])]

coefmu2 = coefdelta[5]-I*alpha[2]*Conjugate[alpha[2]]/
```

```
(2.39475 - 0.682004 I)   eps mu zeta

(-3.49112 - 0.520007 I)   eps mu zetabar

(0.334808 - 0.0922188 I)  eps nu Omega zeta Cos(Omega*

(-0.323725 + 0.0152576 I)

    eps nu Omega zetabar Cos(Omega*t)

(15.1706 - 4.32044 I)  eps nu zeta Sin(Omega*t)

(-22.1159 - 3.2942 I)  eps nu zetabar Sin(Omega*t)

(-0.00468452 + 0.00209354 I)   eps^2 zeta^2 zetabar

(6.50026 - 3.4049 I + (-0.0914743 + 0.080505 I) Omega

  )   eps^2 nu^2 zeta

(2.05418 + 9.40566 I + (0.111097 + 0.0214307 I) Omega)

    eps^2 nu^2 zetabar Cos(2 Omega t)

(-9.40566 + 2.05418 I + (-0.0214307 + 0.111097 I) Omeg

    eps^2 nu^2 zetabar Sin(2 Omega t)

(0.292491 - 0.0794995 I)   eps^2 mu^2 zeta
0. - 10.6846 I
36.5986 - 38.951 I + (-0.0116054 - 0.000160055 I) Omeg
0.292491 - 0.438679 I
```

```
(* Fundamental resonance : see equation 7.47 and 7.59

Omega = w0;
Ur = Im[coefetabarz2]
Vr = Re[coefetabarz2]
realnu2 = Re[coefetazzbar + coefgama[1]]
imagnu2 = Im[coefetazzbar + coefgama[1]]
mu2real = Re[coefmu2]
mu2imag = Im[coefmu2]

rdot = mu*Re[alpha[1]]*r + realnu2*nu^2*r + mu2real*mu
    Re[betanl[2]]*r^3 + nu^2*r*(Ur*Sin[2*phi]+Vr*Cos[2

phidot = mu*Im[alpha[1]] + imagnu2*nu^2 + mu2imag*mu^2
    Im[betanl[2]]*r^2 + nu^2*(Ur*Cos[2*phi]-Vr*Sin[2*p
```

```
-38.9537

36.3973

4.91384

-12.6934

0.292491

-0.438679

                     2                2
2.39475 mu r + 0.292491 mu  r + 4.91384 nu  r -

             3     2
  0.00468452 r  + nu  r
   (36.3973 Cos[2 phi] - 38.9537 Sin[2 phi])

                             2             2
-0.682004 mu - 0.438679 mu  - 12.6934 nu  +

             2     2
  0.00209354 r  + nu  (-38.9537 Cos[2 phi] -
     36.3973 Sin[2 phi])
```

```
(* For simplicity, nu^2 is replaced by nu2 *)

eta = Sqrt[Ur^2 + Vr^2]/w0;
teta = .5 ArcTan[Ur/Vr];

ar = Coefficient[rdot,r^3]/w0
br = Coefficient[phidot,r^2]/w0

Alinr = Simplify[
    (mu*Re[alpha[1]] + realnu2*nu2 + mu2real*mu^2)/w0]
Aphi = Simplify[-sig +
    (mu*Im[alpha[1]] + imagnu2*nu2 + mu2imag*mu^2)/w0]

rdot = Alinr*r + ar*r^3 + nu2*r*eta*Sin[2(phi+teta)]
phidot = Aphi + br*r^2 + nu2 * eta*Cos[2(phi+teta)]
```

```
-0.000270114

0.000120716

                             2
0.138084 mu + 0.0168654 mu  + 0.283337 nu2

                               2
-0.0393251 mu - 0.0252947 mu  - 0.731913 nu2 - sig

                              2
(0.138084 mu + 0.0168654 mu  + 0.283337 nu2) r -

               3
  0.000270114 r  + 3.07402 nu2 r Sin[2 (-0.409656 + ph
```

```
-0.0393251 mu - 0.0252947 mu^2 - 0.731913 nu2 +
  0.000120716 r^2 - sig +
  3.07402 nu2 Cos[2 (-0.409656 + phi)]
```

```
zeta = rad*Exp[I*tau];
zetabar = rad*Exp[-I*tau];
final = ComplexExpand[p.xx];
q1 = final[[1]];
modulus = Sqrt[Coefficient[q1,rad*Cos[tau]]^2+
               Coefficient[q1,rad*Sin[tau]]^2]
Clear[q1]
```

```
0.008329
```

```
(* Trivial solution : see equation 7.69b*)
Clear[sig]
Clear[nu2]

trivstable = Expand[Alinr^2 - ((nu2*eta)^2 - Aphi^2)]
```

```
0.0206137 mu^2 + 0.0066471 mu^3 + 0.000924261 mu^4 +
  0.135814 mu nu2 + 0.0465842 mu^2 nu2 - 8.83363 nu2^2 +
  0.0786502 mu sig + 0.0505894 mu^2 sig +
  1.46383 nu2 sig + sig^2
```

```
(* Solve the equation 7.69b as a function of nu
   and plot the result in the (mu,nu)-plane for
   a constant sigma *)

tototriv = Solve[trivstable == 0,nu2];

Clear[mu]
Clear[sig]
nutriv = nu2 /. tototriv[[1]]
sig = 0.05;
pltriv05=Plot[Sqrt[nutriv],{mu,-1,1},
         Frame->True,
         FrameLabel->{mu,nu}]
```

```
0.5 (0.0153746 mu + 0.0052735 mu^2 + 0.165711 sig +
    0.0211265 Sqrt[21.4428 mu^2 + 7.10701 mu^3 + 1. mu^4 ·
       91.2095 mu sig + 55.2403 mu^2 sig + 1076.06 sig^2
```

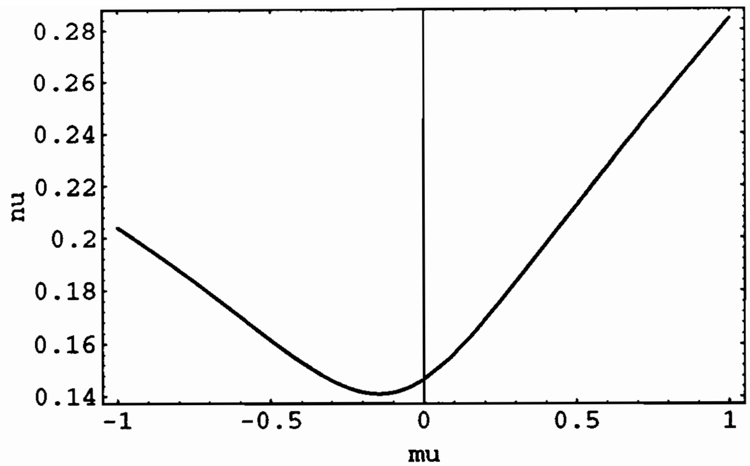


```
-Graphics-

(* Nontrivial solution : see equation 7.69c *)

Clear[nu2]
Clear[mu]
Clear[sig]
delta = Expand[(ar^2+br^2) (nu2 eta)^2 -
             (ar*Aphi-br*Alinr)^2];
soldelta = Solve[delta == 0,nu2]

                                               2
{{nu2 -> 0.5 (-0.0024702 mu + 0.00195949 mu  +
       0.110348 sig + 0.0109001
                    2            3        4
        Sqrt[1.5892 mu  - 2.52127 mu  + 1. mu  -
                                    2
          141.984 mu sig + 112.629 mu  sig + 3171.32 s
          ])}, {nu2 ->
                                          2
    0.5 (-0.0024702 mu + 0.00195949 mu  + 0.110348 sig
                             2             3
       0.0109001 Sqrt[1.5892 mu  - 2.52127 mu  +
              4                               2
          1. mu  - 141.984 mu sig + 112.629 mu  sig +
                     2
          3171.32 sig ])}}

nunontriv = nu2 /. soldelta[[1]]
sig = 0.05;
pldel05 = Plot[Sqrt[nunontriv],{mu,-1,1},
         Frame->True,
         FrameLabel->{mu,nu}]
```

```
0.5 (-0.0024702 mu + 0.00195949 mu^2 + 0.110348 sig +
    0.0109001 Sqrt[1.5892 mu^2 - 2.52127 mu^3 + 1. mu^4 -
      141.984 mu sig + 112.629 mu^2 sig + 3171.32 sig^2
```

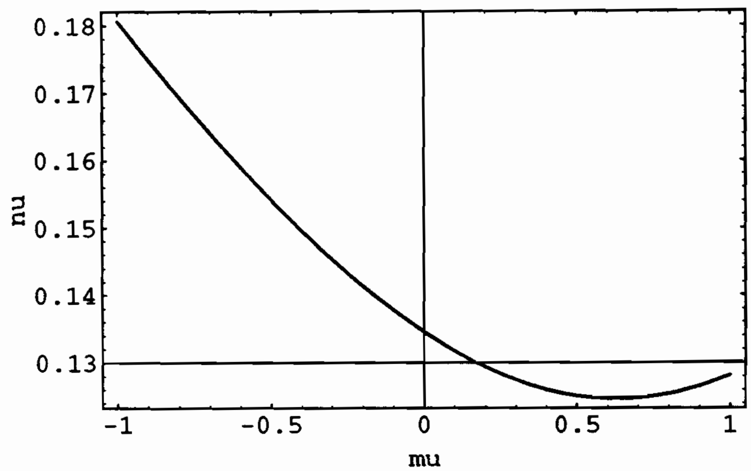


```
-Graphics-
```

```
(* Find the nontrivial solutions : see equation 7.69d
Clear[sig]
toto = -(ar*Alinr + br*Aphi)
ntrivradius2 =   (toto + Sqrt[delta])/(ar^2 + br^2);
ntrivradius2mi = (toto - Sqrt[delta])/(ar^2 + br^2);
```

```
0.000270114 (0.138084 mu + 0.0168654 mu^2 +
     0.283337 nu2) - 0.000120716
   (-0.0393251 mu - 0.0252947 mu^2 - 0.731913 nu2 - sig
```

```
(* Find the stability of the positive solution :
   see equation 7.69e *)

test3 = Alinr + 2*ar*ntrivradius2;
nontrivstab = Solve[test3 == 0,nu2];


sig = 0.05;
nunontrivstab = nu2 /. nontrivstab[[1]]
plnunontrivstab = Plot[Sqrt[nunontrivstab],{mu,-1,1},
PlotStyle -> {Dashing[{0.02,0.02}]}]
```

```
0.5 (0.00744336 + 0.00343867 mu + 0.00347052 mu^2 +
    0.0158131 Sqrt[4.6737 + 1.71305 mu + 12.7041 mu^2 +
      2.81848 mu^3 + 1. mu^4])
```

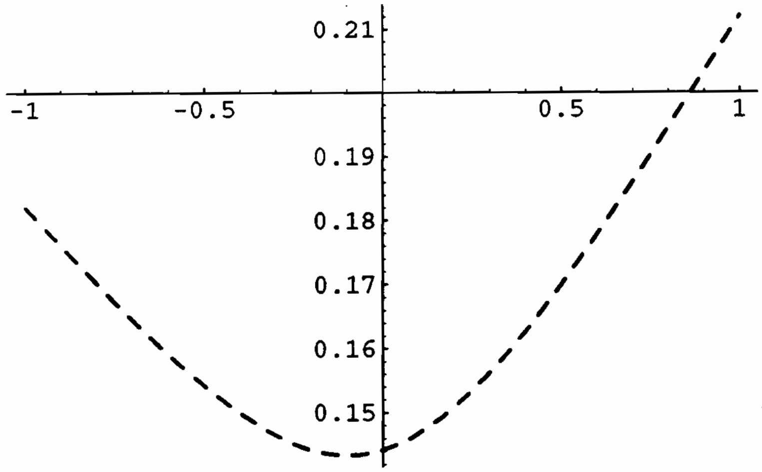

-Graphics-

```
Show[pltriv05,pldel05,plnunontrivstab]
```

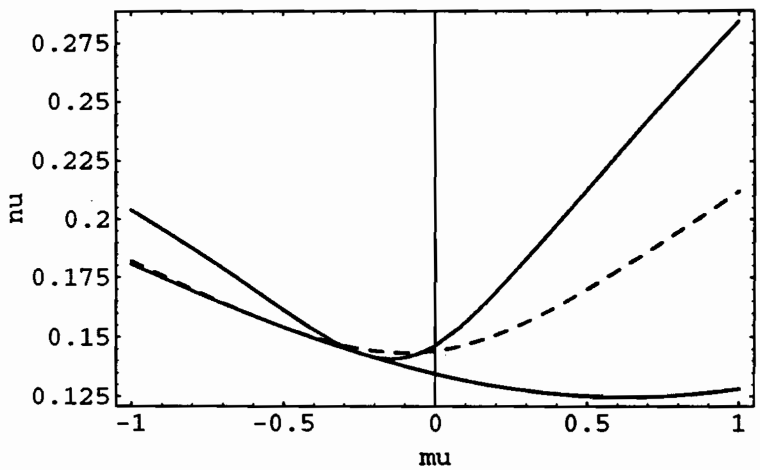

-Graphics-

```
(* Find the nontrivial solutions using (7.69d)
   for a constant nu and a constant sigma *)

nu2 = 0.2^2;
sig = 0.05;
plotnu008 = Plot[{Sqrt[ntrivradius2]*modulus,
                  Sqrt[ntrivradius2mi]*modulus},
         {mu,-1,5},
         Frame->True,
         FrameLabel->{mu,q1}]
```

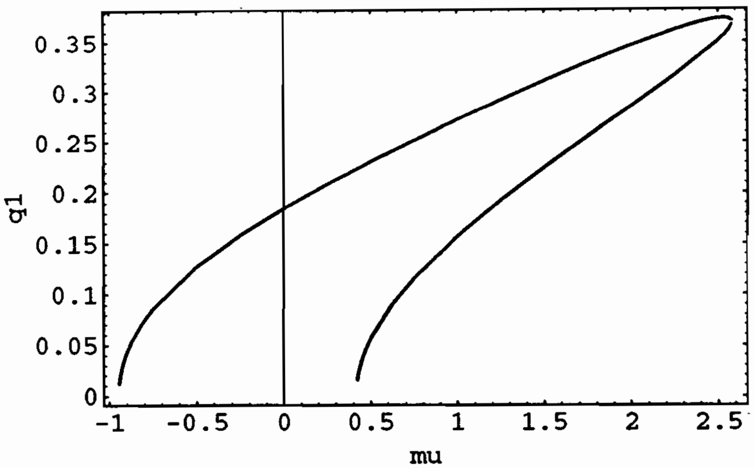

-Graphics-

```
(* The stability map shown on Figure 7.15(a) *)

Clear[nu2,mu,sig]
mu = 0.37;
pl037 = Plot[{Sqrt[nutriv],Sqrt[nunontriv],
              Sqrt[nunontrivstab]},
            {sig,-0.15,0.15},
            Frame->True,
            FrameLabel->{sig,nu}]
```

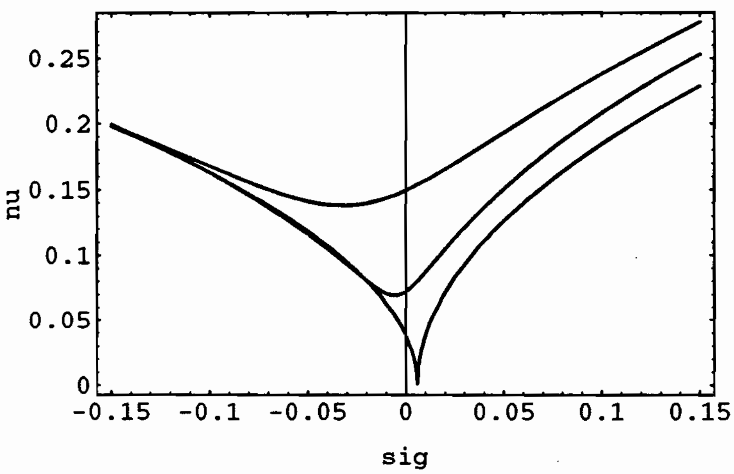

-Graphics-

```
(* Computation of the nontrivial solution for
   mu = 0.37 and nu = 0.1, as in Figure 7.15(b) *)

Clear[nu2,mu,sig]
mu = 0.37;
nu2 = 0.1^2;
plro02 = Plot[{Sqrt[ntrivradius2]*modulus,
                Sqrt[ntrivradius2mi]*modulus},
               {sig,-.2,0.2},
               Frame->True,
               FrameLabel->{sig,q1}];
```